Estimation of photochemical degradation rates of pesticides in outdoor cosm water

Guidance for inclusion in higher tier exposure assessments of the registration procedure in The Netherlands or at EU level, using the TOXSWA model

P.I. Adriaanse, J.J.T.I. Boesten, M.M.S. ter Horst, C.M.J. Jacobs and C. van Griethuysen

WAGENINGEN
UNIVERSITY & RESEARCH

ctgb

Estimation of photochemical degradation rates of pesticides in outdoor cosm water

Guidance for inclusion in higher tier exposure assessments of the registration procedure in The Netherlands or at EU level, using the TOXSWA model

P.I. Adriaanse[1], J.J.T.I. Boesten[1], M.M.S. ter Horst[1], C.M.J. Jacobs[1,2] and C. van Griethuysen[3]

1 Wageningen Environmental Research, Wageningen University and Research (WUR)
2 National Institute for Public Health and the Environment (RIVM, from 1 March 2021 onwards)
3 Board for the Authorisation of Plant Protection Products and Biocides

Wageningen Environmental Research
Wageningen, May 2021

Reviewed by:
This report is a product of and has been approved by the working group on the developed estimation method for photolytical degradation rate in water and the proposed guidance for risk assessors presented in this report

Approved for publication:
Bram de Vos, managing Director Environmental Sciences Group of WUR

WAGENINGEN
UNIVERSITY & RESEARCH

ctgb

Estimation of the degradation rate of plant protection products in water under realistic conditions may be important for correct estimation of exposure concentrations for regulatory purposes. Standardized tests for degradation in water and in water-sediment systems in the laboratory exist, but these do not reflect degradation under field conditions. This is especially true for studies on photolytic degradation; therefore, generally photolytic degradation is not accounted for in the lower tiers of the exposure assessment. The aim of this study is to develop a procedure for the estimation of photochemical degradation rates from outdoor cosm experiments for use in the higher tiers of the exposure assessment. Observations in outdoor ponds or cosms are regularly used as a higher-tier risk assessment to evaluate the ecotoxicological effects on the aquatic ecosystem in a more realistic way. By means of inverse modelling of the behaviour of the compound in the cosm we determined the degradation rate in water, $DegT_{50}$, for three compounds which are known to degrade photolytically. We did so by coupling the fate model TOXSWA to the optimisation tool PEST and determined the $DegT_{50}$ for a daily reference UV radiation, weighed with a vitamin-D action spectrum, assuming that the degradation rate was directly proportional to the amount of weighed UV radiation. The UV radiation data were derived from satellite-based observations accounting for the effects of the thickness of the ozone layer and the cloud cover. For cosm studies with metribuzin, imidacloprid and metamitron we obtained satisfactory estimates of $DegT_{50}$ values. After correcting these for effects of water depth, coverage of water surface by plants and the skyview factor on the UV radiation in the water, the variation between the $DegT_{50}$ values of metribuzin and imidacloprid was smaller than the variation between $DegT_{50}$ values derived (in an earlier study) by assuming that the degradation rate depended on water temperature and not on UV radiation. This indicates that for photolabile compounds assuming a radiation-dependent degradation rate will probably lead to a more realistic exposure in the regulatory surface water scenarios.

Keywords: photolysis, outdoor cosm, TOXSWA model.

Het bepalen van afbraaksnelheden van gewasbeschermingsmiddelen in water onder realistische omstandigheden kan belangrijk zijn voor een correcte bepaling van blootstellingsconcentraties in de toelating. Er zijn standaard laboratorium testen voor afbraak in water en in water-sediment systemen, maar deze weerspiegelen niet de afbraak onder realistische omstandigheden in het veld. Dit geldt m.n. voor studies over fotochemische afbraak; dit is de reden dat fotochemische afbraak in het algemeen niet wordt meegenomen in de lagere treden van de blootstellingsbepaling. Het doel van deze studie is om een procedure te ontwikkelen voor de bepaling van fotochemische afbraaksnelheden met behulp van cosm experimenten in de buitenlucht, voor gebruik in de hogere treden van de blootstellingsbepaling. Waarnemingen in vijvers of cosms in de buitenlucht worden regelmatig gebruikt als hogere trede in de risicobeoordeling om ecotoxicologische effecten op het aquatisch ecosysteem op een realistischere manier te bepalen. Met behulp van een inverse modellering van het gedrag van een middel in de cosm hebben we de afbraaksnelheid in water, $DegT_{50}$, bepaald voor drie middelen, waarvan het bekend is dat ze fotochemisch afbreken. Dit deden we door het model TOXSWA te koppelen aan het optimalisatie instrument PEST en de $DegT_{50}$ te bepalen voor een dagelijkse referentie UV stralingsdosis, gewogen voor het vitamine D actiespectrum; hierbij werd aangenomen dat de afbraaksnelheid recht evenredig is met de gewogen UV straling. De UV stralingsdata waren afgeleid uit satelliet waarnemingen die rekening hielden met de dikte van de ozonlaag en de bewolkingsgraad. Voor de cosm studies met metribuzin, imidacloprid en metamitron verkregen we zo toereikend geschatte $DegT_{50}$ waarden. Na een correctie voor de effecten van waterdiepte, bedekkingsgraad van het wateroppervlak door planten en de 'hemelzicht' factor op de UV straling in het water, was de variatie in $DegT_{50}$ waarden van metribuzin en imidacloprid kleiner dan de variatie tussen de $DegT_{50}$ waarden uit een eerdere studie, waarin was aangenomen dat de afbraaksnelheid van de watertemperatuur afhing en niet de UV straling. Dit geeft aan dat voor fotolabiele middelen een afbraaksnelheid als functie van straling waarschijnlijk leidt tot een realistischere blootstelling in oppervlaktewaterscenario's van de toelating.

In 2003 Wageningen Environmental Research implemented the ISO 9001 certified quality management system.
Since 2006 Wageningen Environmental Research has been working with the ISO 14001 certified environmental care system.
By implementing the ISO 26000 guideline, Wageningen Environmental Research can manage and deliver its social responsibility.

Photo cover: Floris Bijlsma

Contents

Verification

Wageningen Environmental Research (WENR) values the quality of our end products greatly. A review of the reports on scientific quality by a reviewer is a standard part of our quality policy.

This report is a product of and has been approved by the working group on the developed estimation method for photolytical degradation rate in water and the proposed guidance for risk assessors presented in this report.

Approved team leader responsible for the contents,

name: Bram de Vos

date: 30-04-2021

Preface

This report is the third report of a series. The first report is the report 'Estimation of degradation rates in cosm water. Guidance for inverse modelling using TOXSWA.' by J.W. Deneer, P.I. Adriaanse, C. van Griethuysen and J.J.T.I. Boesten of 2015, and estimates the degradation rate in outdoor cosms of ecotoxicological experiments for compounds that are mainly present in the water layer. The second report is 'Estimation of degradation rates in water of outdoor cosms with measured concentrations in water and sediment. Guidance for inverse modelling using TOXSWA.' by P.I. Adriaanse, J.W. Deneer, J.J.T.I. Boesten and C. van Griethuysen of 2017, and and estimates the degradation rate in outdoor cosms of ecotoxicological experiments for compounds that are present both in the sediment and the water layer. In these two reports overall degradation rates in water are determined as a function of the water temperature.

The current report focusses on degradation rates in water for compounds that are known to undergo photolytic degradation; often photolytic degradation may be fast with half-lives in the order of hours or a couple of days. So, for photo-degradable compounds this may be a dominant process. Thus including photolytic degradation for such compounds may lead to a more realistic exposure assessment and thus to a more realistic aquatic risk assessment.

Summary

Estimation of the degradation rate of pesticides in water under realistic conditions is important for correct estimation of exposure concentrations for regulatory purposes. Standardized tests for degradation in water and in water-sediment systems in the laboratory exist, but these do not reflect degradation under field conditions. This is especially true for studies on photolytic degradation; therefore, generally photolytic degradation is not accounted for in the exposure assessment. There are indications that photolysis is an important degradation mechanism in water for a large percentage of the registered pesticides. Thus the aim of this study was to develop guidance for including photolysis in the regulatory exposure assessment and to test this guidance for a few compounds.

Usually, a distinction is made between direct and indirect photolysis: (i) for direct photolysis the reacting pesticide molecule absorbs light and the excited molecule reacts, while (ii) for indirect (or 'sensitized') photolysis light is absorbed by another molecule, which then transfers its energy to the acceptor pesticide molecule, causing the latter to react. For many compounds, the rate of indirect photolysis may be much faster than the rate of direct photolysis. Both direct and indirect photolysis are likely to be proportional to UV radiation.

Experiments on direct photolysis based on an OECD protocol are part of the standard data requirements. However, there are no standard data requirements for indirect photolysis. So photolysis rates can best be derived from outdoor experiments in which both degradation mechanisms may occur simultaneously.

Observations in outdoor ponds or cosms are regulatory used as a higher-tier risk assessment to evaluate the ecotoxicological effects on the aquatic ecosystem in a more realistic way. By means of inverse modelling of the behaviour of the compound in the cosm we determined the degradation rate in water, $DegT_{50}$, for three compounds which are known to degrade photolytically in three or two outdoor cosms. We did so by coupling the fate model TOXSWA to the optimisation tool PEST and determined the $DegT_{50}$, assuming that the degradation rate was directly proportional to UV radiation weighed with a vitamin-D action spectrum. The UV radiation data were derived from satellite-based observations accounting for the effects of the thickness of the ozone layer and the cloud cover.

The outdoor cosms differed not only with respect to incoming radiation at the water level, but also with respect to radiation in the water column, due to extinction of radiation with depth, shadow effects by floating water plants or a limited skyview. So, in order to be able to compare the estimated $DegT_{50}$ values, we standardized the obtained values not only for the incoming radiation, but also to a water depth of 30 cm, no coverage by water plants and full skyview. Now, the variation between the $DegT_{50}$ values of metribuzin and imidacloprid was smaller than the variation between $DegT_{50}$ values derived (in an earlier study) by assuming that the degradation rate depended on water temperature and not on UV radiation. For metamitron this comparison was not possible but the variation between the radiation-based $DegT_{50}$ values of metamitron was considerably smaller than the variation between the radiation-based $DegT_{50}$ values of either metribuzin or imidacloprid.

We designed a flow chart to help risk assessors decide whether photodegradation is the dominant degradation process in water and thus whether it is useful to determine a higher-tier, more realistic degradation rate caused by photolysis by using the inverse modelling methodology for outdoor cosm experiments of this report. We tested the flow chart using the three compounds studied.

We calculated multi-year time series of UV Vitamin-D radiation sums for the surface water scenarios of The Netherlands as well as for the EU-FOCUS surface water scenarios (accounting for temporal fluctuations of the thickness of the ozone layer and for the effect of cloud coverage), thus allowing for a scenario-specific correction of photolytic degradation rates. For photolabile compounds, the combination of these time series with $DegT_{50}$ estimates derived from cosm experiments as described above is likely to result in an improved calculation of the PEC_{sw} in these scenarios, thus leading to an improved aquatic risk assessment for regulatory purposes.

Samenvatting

Het bepalen van de afbraaksnelheid van gewasbeschermingsmiddelen in water onder realistische omstandigheden is van belang voor een correcte bepaling van blootstellingsconcentraties voor de toelating. Er zijn standaard laboratorium testen voor afbraak in water en water-sediment systemen, maar deze weerspiegelen niet de afbraak onder realistische omstandigheden in het veld. Dit geldt m.n. voor studies over fotochemische afbraak; dit is de reden dat fotochemische afbraak in het algemeen niet wordt meegenomen in de blootstellingsbepaling. Er zijn echter aanwijzingen dat fotolyse een belangrijk afbraakmechanisme in water is voor een groot percentage van de geregistreerde gewasbeschermingsmiddelen. Daarom was het doel van deze studie om een methodiek te ontwikkelen dat fotolyse meeneemt in de blootstellingsbepaling voor de toelating én om het methodiek te testen voor een paar middelen.

In het algemeen wordt een onderscheid gemaakt in directe en indirecte fotolyse: (i) bij directe fotolyse absorbeert het reagerende molecuul licht en het aangeslagen molecuul valt uiteen, terwijl (ii) bij indirecte fotolyse licht wordt geabsorbeerd door een ander molecuul, dat vervolgens zijn energie overdraagt naar het acceptor (bestrijdingsmiddel) molecuul, en dit laatste valt dan uiteen. Voor veel middelen is de snelheid van indirecte fotolyse veel groter dan die van directe fotolyse. Zowel directe als indirecte fotolyse worden geacht een functie te zijn van UV straling.

Experimenten over directe fotolyse zijn gebaseerd op een OECD protocol en vormen onderdeel van de standaard data vereisten bij de toelating. Daarentegen zijn er geen standaard data vereisten voor indirecte fotolyse. Daarom kunnen fotolyse snelheden het beste worden afgeleid in experimenten in de buitenlucht, waar beide typen fotolyse gelijktijdig plaatsvinden.

Waarnemingen in vijvers of cosms in de buitenlucht worden regelmatig gebruikt als hogere trede in de risicobeoordeling om ecotoxicologische effecten op het aquatisch ecosysteem op een realistischere manier te bepalen. Met behulp van inverse modellering van het gedrag in de cosm hebben we de afbraaksnelheid in water, $DegT_{50}$, voor drie middelen in twee of drie cosms bepaald, waarvan het bekend is dat ze fotochemisch afbreken. Dit deden we door het model TOXSWA te koppelen aan het optimalisatie instrument PEST en de $DegT_{50}$ te bepalen voor een dagelijkse referentie UV stralingsdosis; hierbij werd aangenomen dat de afbraaksnelheid recht evenredig is met de UV straling gewogen naar het vitamine D actiespectrum. De UV stralingsdata waren afgeleid uit satelliet waarnemingen die rekening hielden met de dikte van de ozonlaag en de bewolkingsgraad.

De cosms verschilden niet alleen in hoeveelheid inkomende straling op het wateroppervlak, maar ook wat betreft de straling in de waterkolom door het optreden van uitdoving van straling met de diepte, beschaduwing door drijvende waterplanten of een beperkt zicht op de hemel boven de cosm. Dus om de geschatte $DegT_{50}$ waarden te kunnen vergelijken, zijn de verkregen waarden voor de cosms niet alleen voor de inkomende straling gestandariseerd, maar ook voor een waterdiepte van 30 cm, geen bedekking door waterplanten en een vrij zicht op de hemel. De variatie in $DegT_{50}$ waarden van metribuzin en imidacloprid was nu kleiner dan de variatie tussen de $DegT_{50}$ waarden uit een eerdere studie, waarin was aangenomen dat de afbraaksnelheid van de watertemperatuur afhing en niet de UV vitamine-D straling. Voor metamitron kon deze vergelijking niet worden gemaakt, maar de variatie in UV vitamine-D gebaseerde $DegT_{50}$ waarden was duidelijk kleiner dan de variatie in UV vitamine-D gebaseerde $DegT_{50}$ waarden van zowel metribuzin als van imidacloprid.

We ontwierpen een stroomschema om risico beoordelaars te helpen bij hun beslissing of fotochemische afbraak het overheersende afbraakproces in water is en of het dus zinvol is om een hogere trede, realistischere fotolytische afbraaksnelheid te bepalen met behulp van de inverse modelleringstechniek beschreven in dit rapport. We testten het stroomschema voor de drie middelen uit deze studie.

We berekenden meerjarige tijdreeksen van UV vitamine-D stralingssommen voor oppervlaktewaterscenario's in Nederland, maar ook voor de EU FOCUS scenario's (waarbij we rekening hielden met fluctuaties in de dikte van de ozonlaag alsmede het effect van bewolkingsgraad). Zo kunnen fotolytische afbraaksnelheden per scenario worden gecorrigeerd. Voor fotolabiele middelen is de verwachting dat de combinatie van deze tijdreeksen met de *DegT$_{50}$* waarden berekend voor de cosm experimenten leidt tot een verbeterde berekening van de blootstelling in de oppervlaktewaterscenario's, en dus tot een verbeterde aquatische risicobeoordeling in de toelating.

1 Introduction

1.1 Available guidance for degradation rates in surface water

The aquatic risk assessment of pesticides requires the assessment of exposure of aquatic ecosystems in small surface waters adjacent to agricultural fields treated with pesticides. Exposure is predicted using simulation models, in which the degradation rate in water is an important input parameter. The rate of degradation may strongly affect the course of the concentration of the pesticide over time or the peak concentration, especially in scenarios with low water flow velocities and/or multiple applications. At present, there are a number of standard tests to determine different degradation rates in water: hydrolysis (OECD 111) and photolysis (OECD 316) studies, degradation studies in surface water in the dark (OECD 309) or degradation studies in systems containing both water and sediment in the dark (OECD 308). However, there is no adequate procedure to use these for estimating degradation rates in the surface water under realistic conditions. In view of the importance of model calculations in the aquatic risk assessment in authorisation procedures, it is important to estimate the degradation rate in water of a compound in a realistic way.

Guidance at EU-level for the derivation of DT_{50} values (kinetic endpoints) was developed by the Workgroup on Degradation Kinetics of FOCUS DG SANTE - the FOrum for Co-ordination of pesticide fate models and their USe within the European Commission's (EC's) Directorate General for Health and Food Safety (2006). However, this guidance provides an estimation of degradation rates in laboratory water-sediment studies and does not address the estimation of degradation rates under more realistic (field) conditions. The estimation procedure described in this report addresses this gap for photo-labile compounds and provides guidance on the estimation of degradation rates in water using data from outdoor cosm studies primarily performed for higher-tier ecotoxicological effect assessments. It is limited to parent compounds.

Differences with the approach of FOCUS (2006) are as follows. Firstly, for surface water, FOCUS (2006) was limited to developing: *'guidance about how to estimate and use the disappearance times (kinetic endpoints) that describe the various aspects of parent and metabolite fate in water-sediment studies'* (FOCUS, 2006). In this report, the emphasis is not on water-sediment studies, but on outdoor cosm studies, performed in the framework of higher-tier ecotoxicological effect assessment.

Secondly, FOCUS (2006) relied on compartmental approaches, rather than more detailed, mechanistic approaches. A distinction was made between two levels: Level P-I for a one-compartmental approach and Level P-II for a two-compartmental approach, combined with several types of kinetics. As an alternative to this approach, FOCUS (2006) suggested to use the TOXic substances in Surface WAters (TOXSWA) model to fit the water-sediment system data using inverse modelling. This report only focuses on this alternative approach for photo-labile compounds. Compartmental approaches do not consider processes, such as volatilisation and sorption, whilst the mechanistic TOXSWA model includes these processes. In outdoor cosms, these processes may play an important role in the disappearance of the compound from the water. Since the aim was to find a generic, broadly-applicable approach, it should be possible to include these processes in the estimation procedure.

In their guidance, FOCUS (2006) made a distinction between two general types of kinetic endpoints: (i) persistence endpoints, used as trigger to determine whether various aquatic ecotoxicology studies are needed and (ii) modelling endpoints, needed for calculating Predicted Environmental Concentrations, as part of an aquatic risk assessment. This report focuses on the estimation of the degradation rate in water as a modelling endpoint only. The refined estimation of this endpoint, as presented in this report, may be useful for more refined exposure assessments at EU level, as well as at national level (illustrated in this report for The Netherlands).

The estimation procedure in this report uses the TOXSWA model coupled to the PEST (Parameter ESTimation) optimisation tool. Degradation rates are estimated by inverse modelling of fate data taken from a cosm study. In the first report on this topic by Deneer et al. (2015), the estimation procedure was limited to compounds with a relatively high water solubility for which penetration into sediment is negligible. In the second report by Adriaanse et al. (2017) the estimation procedure was extended to include also compounds that penetrate to a significant extent into the sediment. In this report the estimation procedure focuses on compounds for which photolytic degradation is known to be important, with the aim of developing an estimation procedure for degradation rates in water. While the estimated degradation half-lives in the first two reports are a function of the water temperature, the estimated photolytic degradation half-life of this report is a function of radiation intensity and independent of water temperature.

More recent guidance on the estimation of $DT_{50, degradation}$ ($DegT_{50}$) values for surface water was written by Boesten et al. (2014). They proposed a stepped approach for the estimation of $DegT_{50, water}$ values for application in the Dutch surface water scenarios currently under development for use in the pesticide authorisation procedure in The Netherlands. The procedure described in the current report covers the estimation procedure described in the box '*Outdoor studies with algae and possibly macrophytes*' of Chapter 2.10 of Boesten et al. (2014). The studies in this box represent the highest (and most realistic) tier of the proposed stepped approach, with lower tiers that include photolysis studies in pure, buffered water, hydrolysis or photolysis studies in fresh surface water, aerobic water-sediment studies in light or indoor studies with algae and possibly macrophytes in light. The estimate of the degradation in water ($DegT_{50,water}$) in Boesten et al. (2014) represents the overall degradation rate in water and thus in principle it includes photolysis, hydrolysis and microbial degradation.

1.2   Background and aim of this study

The background for this study is that many pesticides are known to degrade under the influence of light, i.e. (solar) radiation, but this degradation is not taken into account in the environmental risk assessment during pesticide registration. In the registration dossiers information is available on direct (and occasionally indirect) photochemical degradation rates, that have been measured under standardized light conditions (OECD, 2008; EPA 1998 a and b, see Chapter 6). However, these rates have limited value for photochemical degradation rates in surface water under outdoor conditions. Therefore, it is common practice not to take the process of photochemical degradation into account in the lower tiers of exposure estimations for the aquatic risk assessment. For higher-tier exposure estimations that should reflect realistic conditions, it may be useful to account for faster degradation occurring by existing radiation and, in this way, estimate more realistic exposures.

The aim of this study is
  i. To develop a method to determine photochemical degradation rates in outdoor surface water as a function of the ambient radiation conditions;
 ii. To implement this method in the TOXSWA model and test it for a number of compounds and studies;
iii. To test the proposed tiered approach of Boesten et al. (2014) for estimating $DegT_{50}$ values for surface water to be used in surface water scenarios for the obtained $DegT_{50,water}$ values in this report;
 iv. To supplement the surface water scenarios used in the pesticide registration procedure of The Netherlands and at EU level with appropriately selected radiation data, and
  v. To develop guidance on how to use the photochemical degradation rates in higher tiers of the aquatic exposure assessment procedure in The Netherlands and at EU level.

The final products we aim for are:
  i. A TOXSWA version that is able to account for degradation as a function of daily doses of radiation in the relevant wavelength (distributing the daily doses into hourly doses),
 ii. Surface water scenarios for The Netherlands and the EU that include time series of daily radiation doses, and
iii. A flow chart to determine whether photolysis is the dominant degradation process in the water layer.

Considering product (ii), the time series, we expect that it will be developed in a different way for the Dutch and EU registration. The reason is that the philosophy behind the scenario development has been quite different: for the FOCUS surface water scenarios in the EU (1997-2003) and their 'FOCUS Repair' update (2020) no well-designed probabilities of occurrence in space of the PEC values were defined, while for the Dutch scenarios (developed since 2007, not yet implemented) clear exposure assessment goals with well-defined spatio-temporal populations of concentrations were defined following the concepts of Boesten (2017). However, both for the Dutch and the EU scenarios the exposure concentrations in the refined, higher tier will be based upon the analysis of the spatial variability of sums of daily radiation doses across the Netherlands or the EU (assuming that sums of daily radiation doses are a good predictor of concentration declines in surface water by photochemical degradation). Next, time series of daily radiation doses will be defined for e.g. each of the ten FOCUS surface water scenarios.

Considering product (iii), the flow chart, this has been developed to help risk assessors decide whether it is useful to determine a higher-tier, more realistic degradation rate caused by photolysis by using the inverse modelling methodology for outdoor cosm experiments of this report. The flow chart can be applied by risk assessors in The Netherlands, as well as at EU level (Chapter 15). Note that the minimal requirements for outdoor cosms to be suitable for the inverse modelling exercise remain valid; i.e. at least five measured concentrations in the water phase as a function of time, as well as the water depth should be available (see also Deneer et al., 2015).

Chapter 2 of this report gives an introduction to solar radiation and Chapter 3 focusses on UV radiation, its measurement and the exact procedure used to obtain the wished type of UV radiation. In Chapter 4 the radiation series gathered for the surface water scenarios of The Netherlands and the EU are explained. Chapter 5 provides a short introduction to the process of direct and indirect photolysis in water, an overview of their importance and how the photolysis rates are lowered by attenuation of UV radiation by penetration into the water column. Chapter 6 describes the existing requirements for registration dossiers on photochemical degradation in surface water in the EU and USA. Chapter 7 describes next how the $DegT_{50,water}$ value of the cosm can be standardised to a reference daily, actual UV Vitamin-D radiation, no coverage of the surface water by water plants and no full skyview, i.e. the fraction of the overlying sky to which the water surface area of the cosm is exposed, while Chapter 8 describes the principles of the estimation procedure, including the quality criteria for minimising the differences between simulated and measured concentrations. Chapter 9 specifies more in detail how the cosm studies must be parameterised for TOXSWA and PEST, whilst in Chapter 10, the selection of suitable compounds and cosm studies for testing the estimation procedure is described. The Chapters 11, 12 and 13 summarize the results of the estimation procedure when applied to cosm studies for metribuzin, imidacloprid and metamitron, respectively. The estimated degradation rates in cosm water are compared to the corresponding values found in laboratory studies, and checks the validity of the proposed stepped approach of Boesten et al. (2014) for estimating $DegT_{50}$ values for surface water to be used in surface water scenarios. Chapter 14 gives an overview of the 4 factors for standardising the $DegT_{50,cosm,water}$, determines these and next, calculates the final $DegT_{50,water}$, standardised to (i) a reference daily UV-Vitamin-D radiation of 5 kJ m^{-2}, (ii) water depth of 30 cm, (iii) no coverage of the water surface by water plants and (iv) full skyview. It also gives the conclusions on the usefulness of the designed inverse modelling methodology. Chapter 15 presents the flow chart to decide upon the estimation of a higher-tier photochemical degradation rate and finally, Chapter 16 presents the discussion, conclusions and provides some recommendations.

2 Introduction to solar radiation

2.1 Brief overview of solar radiation

2.1.1 Terminology

Any object with a temperature higher than 0 K (-273.15°C) emits electromagnetic radiation. Total energy emitted and the distribution of the energy over the wavelength spectrum depend on the temperature of the object.

Solar radiation received at the Earth's surface is emitted by the Sun. The Sun's temperature is such that over 99% of the radiation energy is emitted in the wavelength band between 150 and 4000 nm, with a peak intensity at about 500 nm (American Meteorological Society, 2016). This peak intensity is in the visible part of the electromagnetic spectrum (from 400 to 700 nm). By contrast, objects in the Earth-atmosphere system are much cooler than the Sun. They not only emit less radiation, but also at different, longer wavelengths. The emission occurs mainly in the far infrared part of the spectrum, between 3000 and 100000 nm, with a peak at about 10000 nm (Oke, 1987). Because of this difference in spectral characteristics solar radiation is often called short-wave radiation while radiation from objects in the Earth-atmosphere system (including the atmosphere itself) is called terrestrial or long-wave radiation (Monteith and Unsworth, 2013; Oke, 1987). In the context of photochemical degradation longwave radiation plays no role and will not be considered anymore.

Here, we are considering the ultraviolet (UV) wavelength band (200-400 nm), which is part of the solar radiation. The UV band usually is subdivided in three main bands. Following Monteith and Unsworth (2013), we define:
- UVA: 320-400 nm
- UVB: 280-320 nm
- UVC: 200-280 nm

It is important to note that the classification is not a universally accepted one. Although in the scientific literature the wavelength of 320 nm is often taken to be the boundary between UVB and UVA, most international agencies and consortia dealing with human health issues seem to agree on the value of 315 nm to distinguish between UVB and UVA (Calbó et al., 2005). Note also that radiation with wavelength up to 290 nm does not reach the earth's surface as it is absorbed in the atmosphere (e.g. OECD, 2008).

Shortwave radiation may be defined as the energy in the visible and near-infrared portion of the electromagnetic spectrum (wavelength 400–1000 nm). In practice, the term is often used to distinguish radiation in the visible and near-infrared portions of the electromagnetic spectrum (wavelengths 400–4000 nm), usually of solar origin, from that at longer wavelengths, the longwave radiation (>3000 nm), usually of terrestrial origin.

According to the definitions given above, solar radiation can be regarded as the sum of UV radiation and shortwave radiation. In many applications, the total incoming solar radiation received at a horizontal surface at or near the Earth's surface is relevant. This quantity is also called global radiation, formally defined as the solar radiation received from a solid angle of 2π steradians (one half of a globe) on a horizontal surface. It consists of the sum of direct solar radiation, the portion of the solar radiation that has not been scattered or absorbed, and diffuse radiation, the "downward scattered and reflected solar radiation coming from the whole hemisphere of the sky with the exception of the solid angle subtended by the sun's disk." (American Meteorological Society, 2016). Global radiation is measured at the main Dutch meteorological stations and in a growing number of meteorological stations around the world. The measuring device is an upward facing pyranometer, which is able to measure the amount of energy contained in the solar radiation wavelengths between

–typically- 300 and 2800 nm. Henceforth, we stick to the term 'solar radiation' because this term is often used in the scientific literature on UV radiation.

2.1.2 Photochemical degradation and light

It is generally assumed that photodegradation of chemicals in outdoor surface water is mainly driven by UV radiation (e.g. Burrows et al., 2002), especially UVB radiation (e.g. Wanatabe et al., 2006). The reason is that UVC radiation does not reach the Earth's surface and UVB radiation contains more energy than UVA radiation.

Boesten et al. (2014) propose that photochemical degradation in outdoor surface water is proportional to daily solar radiation, thus enabling a standardization of photochemical degradation rates: "It is generally assumed that the rate coefficient for direct and indirect photochemical degradation is proportional to the product of the molar absorption coefficient and the light intensity at a certain wavelength (e.g. OECD, 2008). Usually meteorological stations provide only daily global radiation. As an approximation we consider it defensible to assume that the rate coefficient for photochemical degradation:

$$k = k_{ref} \left(\frac{G}{G_{ref}} \right)$$ (2.1)

where k is the rate coefficient for photochemical degradation (d^{-1}), k_{ref} is the k at a reference global radiation G_{ref} (J cm^{-2}) and G is the daily global radiation (J cm^{-2}). Eqn 2.1 gives for the *DegT50:*

$$DegT50 = DegT50_{ref} \left(\frac{G_{ref}}{G} \right)$$ (2.2)

where *DegT50$_{ref}$* is the *DegT50* at the reference daily global radiation. Daily global radiation varies in the Netherlands typically from 200 J cm^{-2} in winter to 2000 J cm^{-2} in summer (Velds, 1992). Therefore we propose to use a G_{ref} of 1000 J cm^{-2}. This reference value of the global radiation is an arbitrary value needed to standardize *DegT50* values obtained from different outdoor experiments (e.g. a *DegT50* of 10 d at G = 1000 J cm^{-2} is identical to a *DegT50* of 5 d at G = 2000 J cm^{-2}, so if different *DegT50* values have to be averaged, they have to be calculated back first to the same reference G value)."

With UVB radiation determining photochemical degradation Eqs. 2.1-2.2 would provide a convenient method to standardize photochemical degradation rates using solar radiation (called global radiation in the quote given above) measured at meteorological stations. However, applicability of Eqs 2.1 and 2.2 depends on the implicit assumption that the proportion of UVB in the solar radiation is approximately constant. Given the strong dependency of the interaction between solar radiation and the atmosphere on the wavelength (see next section, Figure 2.1), the broadband total solar radiation may be expected to behave differently than the UV radiation in general, and UVB in particular. In the next sections we therefore further investigate the proportion of UVB in the solar radiation at the Earth's surface. To that end, we start with a brief description of attenuation processes in the atmosphere, which are highly wavelength dependent.

2.1.3 Attenuation of radiation in the atmosphere

Before reaching the Earth's surface radiation interacts with the atmosphere, which affects the spectral composition of the solar radiation reaching the surface. There are two main mechanisms of interaction or attenuation in the atmosphere: *absorption* and *scattering*.

Absorption takes energy out of the radiation beam, thereby heating the atmosphere. Rather well-known is the absorption of UV radiation by ozone. Water vapour, carbon dioxide and oxygen mainly absorb radiation in the near-infrared part of the spectrum, at wavelengths over 700 nm. This is shown in Figure 2.1, taken from Monteith and Unsworth (2013). The figure shows that a relatively large portion of near-infrared radiation is filtered out by water vapour, oxygen and CO_2. The spectral composition at the Earth's surface will to some extent be influenced by the air mass and therefore by

the actual weather conditions. This effect is relatively small, however in the present context (compare D and E in the figure). Far more important in the present context is the absorption of UV radiation by ozone (A versus B in Figure 2.1). We will come back to this issue below. First, we explain the effect of scattering, which is revealed by comparing B versus C and C versus D in Figure 2.1.
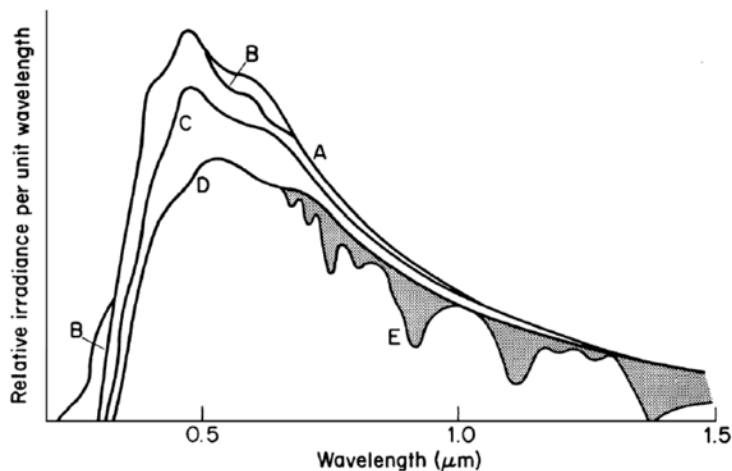
Figure 2.1   *Effect of absorption and scattering of electromagnetic radiation on the spectral composition of down welling radiation. The figure has been taken from Monteith and Unsworth (2013). Curve A denotes the extra-terrestrial solar radiation; B after absorption by ozone; C after molecular scattering; D after aerosol scattering; E after absorption by water vapour, oxygen and CO_2.*

Scattering only changes direction of the photons. In the atmosphere, there are two main mechanisms of scattering. The first one is Rayleigh scattering, which occurs if individual photons hit gaseous molecules in the atmosphere. Shorter wavelengths are affected much stronger than longer ones: the effectiveness of Rayleigh scattering is inversely proportional to the fourth power of the wavelength. Rayleigh scattering therefore causes the sky to look blue and the sun to look yellow/red: while the shorter wavelengths (blue) are easily spread all over the sky, more of the longer wavelength photons (red) continue their travel in their original direction. The second main scattering mechanism is Mie scattering which occurs when radiation hits particles with diameters much larger than the wavelength, such as dust, smoke and pollen. The large range of aerosol diameters present in the atmosphere causes Mie scattering to be much less sensitive to the wavelength of the radiation than Rayleigh scattering. Furthermore, in the case of Mie scattering much of the scattering may be forward, that is, in the direction of the propagation of the beam (Monteith and Unsworth, 2013). Yet, both mechanisms cause a significant part of backward scattering. Hence, the loss that is made visible in the comparison of curve C versus curve B and curve D versus C in Figure 2.1.

2.1.4   Direct and diffuse radiation

Whereas the solar radiation at the top of the atmosphere can be considered to consist of parallel radiation beams, the aforementioned interactions with the atmosphere may cause a change of direction of the photons. The solar radiation therefore consists of the so-called direct radiation and diffuse radiation, respectively. Direct solar radiation comes from the direction of the solar disc and can still be regarded as a bundle of parallel beams. Direct radiation may be zero under completely cloudy conditions. Diffuse radiation results from the scattering of solar radiation and may arrive at the Earth's surface from all directions. The actual distribution of diffuse radiation over the sky needs not be uniform, depending on the atmospheric conditions, notably the amount and type of clouds (Monteith and Unsworth, 2013).

2.2 UV radiation

2.2.1 General

Solar elevation (the angle between the centre of the solar disc and the horizon, or solar altitude), which determines the length of atmospheric path of the solar beam, and several atmospheric factors such as cloudiness and the amount of aerosol determine the total amount of scattering and absorption in the atmosphere and therefore the amount of UV radiation that ultimately reaches the Earth's surface (e.g., Calbó et al., 2005; Fioletov et al., 2010). Initially, at the top of the atmosphere, about 8% of the solar radiation is UV radiation (Frederick et al., 1989). UVC radiation is effectively absorbed by ozone in the stratosphere and does not reach the Earth's surface (Calbó et al., 2005). By far the largest part of the UVB is absorbed as well, especially the smaller wavelengths (Fioletov et al., 2010). UV radiation is very sensitive to Rayleigh scattering because of its small wavelength, resulting in some reflection (back-scattering) as well. As a result of the interactions of UV radiation with the atmosphere, a maximum of only about half of the initial UV radiation in the solar beam, 4%, arrives at the Earth's surface (Goudriaan, 1977; Oke, 1987) and by far the largest part is UVA. In typical midday summer sunlight conditions and at the equator, about 95% of the UV radiation near the ground is UVA and 5% is UVB (NTP, 2000). Thus, in general only ~1-2‰ of the energy contained in the solar radiation is UVB. Since the atmospheric interaction with UV light is different from that with longer wavelengths in the solar radiation the fraction of (total) UV light in the solar radiation may be expected to differ considerably as well. Fractions varying between 0.2‰ and 8‰ have been reported (Adam, 2015).

Rayleigh scattering causes another important characteristic of the UV radiation arriving at the Earth surface: it is predominantly diffuse. This is different from radiation in other parts of the solar spectrum, notably the longer wavelengths, of which under clear conditions a significant part is received as direct radiation.

2.2.2 Proportion of UV radiation in solar radiation at the Earth's surface

Because of the biological importance of UV(B) radiation many studies have attempted to measure and predict its intensity at the Earth's surface. An important source of information are the studies in support of the development and prediction of the so-called UV-index, developed to inform the general public about safe exposure times to sunlight, thereby preventing sunburn and skin cancer. A disadvantage of this source of information in the context of photochemical degradation of chemicals in water is the fact that these studies often weigh the reported UV radiation levels with a so-called erythemal or sunburning action spectrum (describing the sensitivity of the skin to given UV wavelengths; Calbó et al., 2005; Fiolotov et al., 2010), which may clearly differ from 'photolysis action spectra.' Also, information on the specific contribution of UVB may be lacking, with results reported for the combined UVB and UVA parts in the solar radiation. Nevertheless, useful information regarding the behavior of UV radiation in the atmosphere may be obtained.

Results of such studies show that one of the main factors determining the relation between UV and solar radiation intensities at the Earth's surface are the cloud cover and the cloud type. Many studies have been devoted to determination of the so-called Cloud Modification Factor (CMF). This factor may be defined as the ratio of the actual (measured) radiation intensity (I_{actual}) to the one expected under a clear sky (I_{clear}):

$$CMF_X = I_{actual,X}/I_{clear,X} \tag{2.3}$$

(Calbó et al., 2005). The CMF is sometimes called reduction factor (R_X). It can be computed both for UV radiation (subscript X=UV) and for total solar radiation (subscript X=TS), to evaluate the effect of clouds in radiation intensity for UV and total solar radiation separately.

To compute the CMF, clear-sky irradiation $I_{clear,X}$ is first predicted from astronomical computations that evaluate the solar elevation as a function of time of day, season and geographical position (Oke, 1987). The actual (observed) radiation levels $I_{actual,X}$ are then divided by $I_{clear,X}$ to obtain CMF_X. When estimating $I_{clear,X}$ at a specific location typical atmospheric conditions for that location are assumed.

The clear-sky value of UVB radiation is also determined by the depth of the (stratospheric) ozone column (Allaart et al., 2004).

If UV irradiance is a fixed fraction of total solar radiation, the CMF for UV and total solar radiation should remain approximately equal since the *relative* effect of the clouds on both radiation intensities would be similar. However, because of the differing behavior regarding atmospheric absorption and scattering, deviations may be expected, in clear-sky as well as cloudy conditions. Indeed, the proportion of UV radiation in the solar radiation may already show a seasonal trend, depending on the location. This portion is further modulated by weather conditions, notably clouds (see below), depending on the relationship between CMF_{UV} and CMF_{TS}.
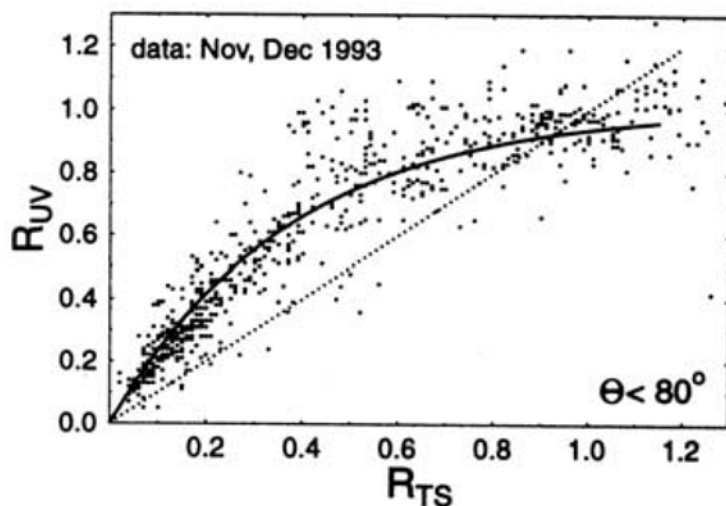
Figure 2.2 *Reduction factor (i.e., CMF) for UV doses versus the same ratio for total solar radiation. From Bordewijk et al. (1995), as reproduced in Calbó et al. (2005). The results are valid for solar zenith angles (Θ or the difference between zenith and solar elevation) of less than 80 degrees. In this case, UV irradiance refers to wavelengths between 285 and 345 nm, weighed with the action spectrum for carcinogenesis in albino mice.*

Calbó et al. (2005) reviewed studies on the relationship between CMF_{UV} and CMF_{TS}. A typical result from a study based on observed UV and solar radiation is depicted in Figure 2.2 (from Bordewijk et al., 1995), showing CMF_{UV} (R_{UV} in the figure) versus CMF_{TS} (R_{TS} in the figure). The figure reveals a non-linear relationship between R_{TS} and R_{UV}, with the largest deviations in the mid-range of the CMF values for total solar radiation (R_{TS}). The deviation in the mid-range (R_{TS} = 0.4 – 0.6, say) may be in the order of 50% on average or more in specific cases. However, the scatter is quite large.

UV intensity used in Figure 2.2 refers to wavelengths between 285 and 345 nm and has been weighed using an action spectrum for carcinogenesis in albino mice. Nevertheless, similar relationships have been found in studies using other wavelength bands and action spectra. This is shown in another figure from Calbó et al. (2005), in which several relationships from radiation observations are compared (Figure 2.3). Note that the CMF or reduction factor has been plotted in reverse order and that CMF_{TS} is denoted as CMF(total) in the figure and CMF_{UV} as CMF(UV). The relationships are computed using the statistical regression functions from the original papers, most of which apply a weighing with a so-called erythemal action spectrum (related to sunburn of human skin). It can be seen that deviations between CMF(UV) and CMF(total) of up to 30% are possible. It can also be seen that differences between the curves can be considerable, in spite of some similarity, reflecting effects of season, location, atmospheric composition, cloud type and other factors. Based on the observed relationships between CMF_{UV} and CMF_{TS} it can be concluded that the ratio of the radiation intensity of UV and total solar radiation is not necessarily constant.
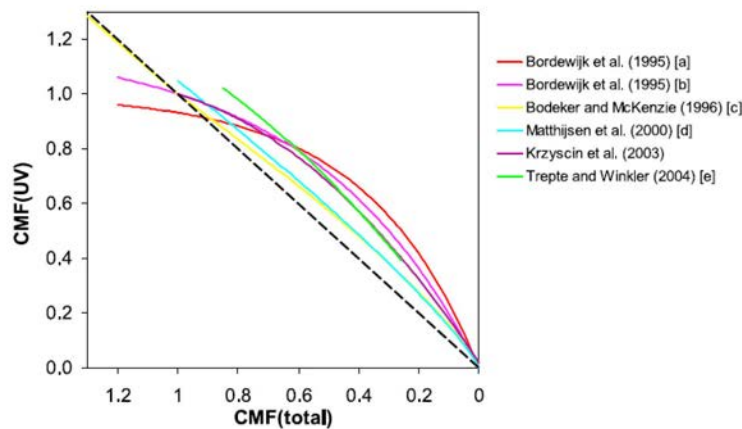
Figure 2.3 *Cloud modification factors for UV radiation against the equivalent for total solar radiation, as given by several papers reviewed by Calbó et al. (2005). Note that the values in the abscissa have been plotted in the reverse sense. All works but one (Bordewijk et al.[1995] use an action spectrum for carcinogenesis in albino mice) use erythemal UV when defining CMF(UV). The dashed line corresponds to CMF(UV) = CMF(total).*

2.2.3 Important measurement data portals

At the following sites data on UV radiation and related quantities such as ozone layer depth collected globally can be accessed.

www.temis.nl
TEMIS (Tropospheric Emission Monitoring Internet Service) started as part of the data user program of the European Space Agency (ESA) and has become a portal for *satellite-based* observations on air quality, ozone depletion, climate change, volcanic activity, surface reflectivity and UV radiation. Satellite instruments used for the various measurements include GOME, GOME-2, SCIAMACHY and OMI. Various satellite-based UV products are available, including cloud-free UV Index (effective, erythemally weighted UV irradiance reaching the Earth's surface; 1 unit equals 25 mW/m^2) clear-sky daily dose weighted with differing action spectra (see Section 3.2.2) and ozone layer depth. These data are provided as global fields, at a spatial resolution of 0.25 degree in both latitude and longitude. Corresponding cloud modified UV dose is computed using cloud observations from Meteosat Second Generation (MSG) and are therefore only available for the MSG data area (Zempila et al., 2017). Data quality is checked on a regular basis and data sets are reprocessed in accordance with important new insights and developments.

www.woudc.org
The World Ozone and Ultraviolet Radiation Data Centre (WOUDC) is a WMO (World Meteorological Organization) portal allowing visualization of and access to *ground-based* ozone and UV radiation observations worldwide. Thus, data are obtained at specific locations using upward facing instruments that probe the atmospheric column at specific locations. At present, data from 474 sites are available. Different instruments are used at the sites. In the case of UV radiation, a distinction is made between broadband instruments (providing UV intensity integrated UV-A, UV-B, or erythemally weighted UV radiation), multiband instruments (measuring UV radiation with a number (typically 3-10) of discrete passband filters, with a resolution of 2-10 nm) and spectral measurements (measured in a continuous spectral band, with a resolution of 2 nm or better and therefore giving detailed information on the UV radiation intensity in a specified band, e.g. UV-B). Often, an erythemal weighting filter is applied in the instruments. Therefore, data are often also provided as the UV Index. Contributors to WOUDC must follow WMO standards regarding (meta-)data description, quality assessment and quality control and file structure and content. The availability of data depends on the activity of the contributors and may vary from year to year.

3 Estimation of UV radiation intensity

3.1 Introduction

Based on the discussion in the previous chapter it can be concluded that estimation of UV radiation intensity at the Earth's surface is not a straightforward task. Here, we require an estimate of this quantity with the purpose to determine photochemical degradation rates in surface water as a function of the ambient radiation conditions. Various attempts to empirically model UV intensity at the Earth's surface have been reported (e.g., Wang et al., 2014). Such simple modelling attempts are probably valid for specific regions only. Since our spatial domain involves the European Union methods that are more generally applicable are required. Radiative transfer modelling approaches are applicable globally, but need much more information to be used (see, e.g., Den Outer et al., 2010) and this seems not to be an appropriate choice in the present context. Two reasonable options remain:

Option 1) Using measured solar radiation and a simple radiation model combined with a parameterization of the relationship between CMF$_{UV}$ and CMF$_{TS}$
The relationship between CMF$_{UV}$ and CMF$_{TS}$ is reasonably well established (Den Outer, personal communication). Clear-sky values of radiation intensities can be estimated with reasonable accuracy as well, in particular if the ozone layer depth and its effect on UV can be included. This allows computing UV intensity from observed solar radiation and then application of [1] and [2] with $I_{actual,UV}$ instead of with G or $I_{actual,TS}$. This method to estimate $I_{actual,UV}$ from the CMF's, using $I_{actual,TS}$, $I_{clear,TS}$ and $I_{clear,UV}$ was considered first because it is globally applicable in principle and would allow reconstruction of past UV intensities to some extent. A description of the method including calculation examples and an evaluation for two sites in Europe is described in Annex 1. Since this method still requires considerable effort from the user and the uncertainty of the result can be quite large it was decided to switch to the alternative option.

Option 2) Using UV observations provided at *www.temis.nl*
At the TEMIS website, clear sky and actual, cloud-modified UV radiation at the surface is made available for major parts of the EU. Data can be obtained in a quasi-operational mode and forecasts of the UV index are made as well. Data quality is checked on a regular basis and data sets are reprocessed in accordance with important new insights and developments. The disadvantage of this data source is that cloud modified actual UV radiation are only available as of January 2004, while we needed data from 1975 onwards. Therefore, we decided to use the TEMIS clear sky data in combination with a cloud modification factor. The next section will give a brief overview of the methodology that underlies the production of the TEMIS UV radiation products.

3.2 Description of UV data products from TEMIS

3.2.1 Background

Climate change, air pollution, and risk of enhanced exposure to UV radiation because of ozone depletion in the stratosphere are phenomena related to changes in atmospheric composition. In response to such problems several international agreements and protocols have emerged, such as the Montreal protocol and the so-called Paris Agreement on Climate Change. In this context, quantification of the concentrations of atmospheric trace gases is important. TEMIS (Tropospheric Emission Monitoring Internet Service) started as part of the data user program of the European Space Agency (ESA) and has become a portal for *satellite-based* observations on air quality, ozone depletion, climate change, volcanic activity, surface reflectivity and UV radiation (www.temis.nl).

Various satellite-based UV products are available from TEMIS, including cloud-free UV Index (effective, erythemally weighted UV irradiance reaching the Earth's surface; 1 unit equals 25 mW/m^2) clear-sky daily dose weighted with differing action spectra (in kJ/m^2; see below for action spectra) and ozone layer depth (in Dobson Units). The amount of UV radiation reaching the Earth's surface is largely related to the thickness of the UV absorbing ozone layer (atmospheric layer between 10 and 40 km altitude). As such, satellite-based observations of the ozone layer are the basis of diagnostic UV products from TEMIS and UV index forecasts that can also be obtained from TEMIS.

At the TEMIS portal UV radiation products are made available in near-real time. The most recent product version is 2.0, which contains data on a latitude-longitude grid of 0.25° x 0.25°. Daily UV dose [kJ/m^2] can be downloaded as maps, time series or data sets at specific locations. Clear-sky UV radiation data are provided for the entire globe. Corresponding cloud modified UV dose is computed using cloud observations from Meteosat Second Generation (MSG) and are therefore only available for the MSG spatial data domain (www.temis.nl; Zempila et al., 2017). An example illustrating the spatial domains of the clear-sky versus the cloud-modified dose is given in Figure 3.
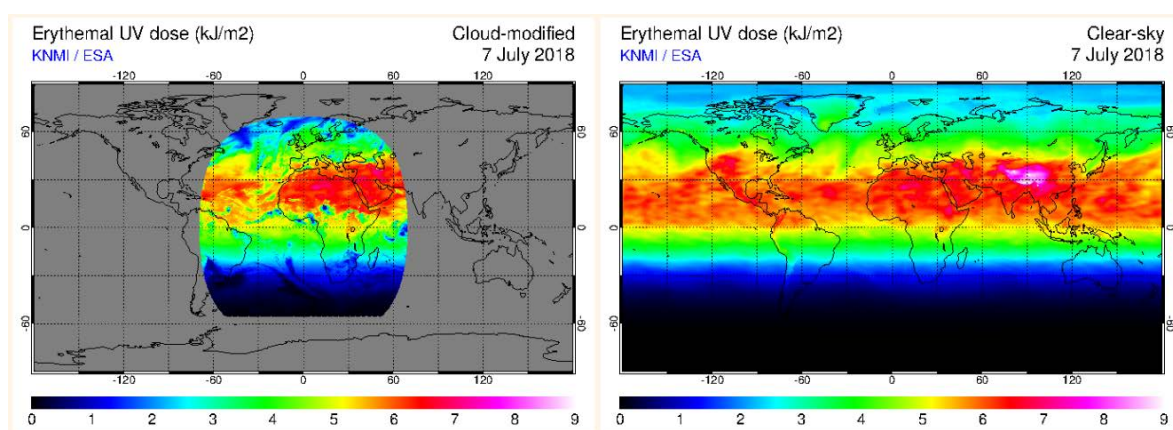
Figure 3.1   *Illustration of the spatial domain of clear-sky UV dose (right) versus cloud-modified dose (left). Obtained from www.temis.nl. The colour bar with numbers 0 to 9 indicates that the erythemal UV dose ranges from 0 to 9 kJ/m^2.*

3.2.2   Production of TEMIS UV fields

The TEMIS UV products are based on the parametrization proposed by Allaart et al. (2004), which describes the UV radiation intensity at the Earth's surface as a function of the total ozone column depth and solar zenith angle. Wavelength-dependent responses to UV radiation are taken into account via specific action spectra.

The parameterization of Allaart et al. (2004) is essentially a fit of the clear-sky UV Index on ozone column depth, taking into account the solar zenith angle and the Sun-Earth distance. Other relevant atmospheric parameters and surface albedo are ignored. The error involved in ignoring these parameters is estimated to be less than 10%, except over a snow cover with very high albedo (Allaart et al., 2004). In contrast with using a radiation transfer model to obtain UV intensity at the Earth's surface this is a computationally efficient method, which can be important in a near real-time setting, like TEMIS.

For the derivation of the fit, UV Index and ozone column depth were observed at two stations - one mid-latitude station, De Bilt (Netherlands), and one tropical station, Paramaribo (Suriname). In fact, the fitting procedure and subsequent parameterisation involves two steps.

First, an ozone-free atmosphere is considered. Because the amount of UVA radiation is nearly independent of ozone, observations of this quantity are taken to be the starting point. UVA is estimated as a function of solar zenith angle, Sun-Earth distance and atmospheric extinction and

scattering. This part of the fit accounts for variations in light intensity because of astronomical parameters:

$$UVA = \left(\frac{D_0}{D}\right)^2 \cdot S \cdot \mu_x \cdot \exp\left(-\frac{\tau}{\mu_x}\right) \qquad (3.1)$$

where D_0 [km or Astronomical Unit] is the average distance between the Sun and the Earth and D [km or Astronomical Unit] is the actual distance, S [W m^{-2} nm^{-1}] is the extra-terrestrial value for UVA radiation intensity, depending on D, τ [$-$] is the atmospheric extinction coefficient and

$$\mu_x = \mu_0(1 - \varepsilon) + \varepsilon \qquad (3.2)$$

[-] is the cosine of the solar zenith angle (SZA [radians]), μ_o = cos(SZA) [-], but modified to take into account effects of atmospheric scattering on UVA, which results in an offset ε.

Second, effects of ozone layer depth on UV absorption are taken into account. To this end, the ratio of UV Index (UVI, [-]) to UVA is used, assuming that the extinction of UV radiation will depend on the total amount of ozone (TO [Dobson Units]) on a straight line between the location of interest and the Sun's disc. This idea is represented by the empirical fit:

$$\frac{UVI}{UVA} = F \cdot (1000\frac{\mu_0}{TO})^G + \frac{H}{TO} + J \qquad (3.3)$$

with F, G, H and J fitting parameters. Values derived by Allaart et al. are F = 2.0, G = 1.62, H = 280.0 and J = 1.4, respectively. (Please note that the empirical fitting equation Eqn 3.3 is not based on consistent use of units.) The parameterization performs very well for estimation of clear-sky UV index (Allaart et al., 2004).

Improvements of the fit implemented later include corrections for the surface elevation, for the ground albedo and for the varying distance between the Sun and the Earth (Van Geffen et al., 2005, Zempila et al., 2017). Furthermore, correction methods have been implemented to account for location specific effects of atmospheric aerosols (Bodesa and Van Weele, 2002).

An important development has been the inclusion of a cloud modification factor for UV radiation (see Eq. 2.3). In one of the product versions available from TEMIS (Version 1.4), attenuation factor A_f [-] is used. This factor is related directly to cloud cover (*Cc*, a fraction between 0 (cloudless), and 1 (completely overcast), sometimes given in percentage). It takes into account absorption of UV radiation by clouds without recourse to cloud physical properties. The factor A_f has been derived from measurements of cloud cover and UV radiation at De Bilt (NL). By definition $A_f = 1$ if there are no clouds (*Cc* = 0). UV intensity is then equal to the clear-sky value. The maximum attenuation of UV by clouds occurs at a completely overcast sky and turned out to be 50%, that is, $A_f = 0.5$ if *Cc* = 1. These two cases are treated as special cases. For other values of *Cc* (thus excluding *Cc*=0 *and Cc*=1), linear fit of A_f on *Cc* was found to describe the measurements quite well (Van Geffen et al., 2005). The resulting description of A_f [-] as a function of *Cc* [-] reads:

$$A_f = \begin{cases} 1 & Cc = 0 \\ 0.9651 - 0.2555Cc & 0 < Cc < 1 \\ 0.5 & Cc = 1 \end{cases} \qquad (3.4)$$

Using A_f, the actual, instead of potential or clear-sky dose of UV received at the Earth's surface can be estimated. A_f is computed using Meteosat satellite cloud cover data (Meteosat Second Generation, MSG). Hence, the cloud modified UV dose is available in the MSG domain only (see Figure 3.1); outside that domain, only clear-sky values are produced at present. The daily UV dose UV_d is obtained by integrating the cloud modified UV intensity from a 15-minute step integration between sunset and sunrise (Van Geffen et al., 2005; Zempila et al., 2017):

$$UV_d = \int_{sunrise}^{sunset} UV(\mu_0(t), TO) \cdot A_f(t) \cdot dt \qquad (3.5)$$

[J m^{-2}] where t [s] is time. Note that in Eqn (3.5) the solar zenith angle has become time dependent, so that clear-sky UV intensity is also time dependent. However, the depth of the ozone column, *TO*, is evaluated at local noon only. This is defensible since ozone layer depth variations typically occur at daily timescales.

Zempila et al. (2017) validated TEMIS daily-dose UV products, Version 1.4, and found that the satellite estimates were strongly correlated with ground-based reference measurements for Thessaloniki (Greece) with an r^2 between 0.92 and 0.95. However, on average TEMIS UV products were found to overestimate the observed doses by 13%.

At the time of writing, Version 2.0 of the TEMIS UV products had been made available, alongside product version 1.4 (www.temis.nl)[1] and Version 1.4 cannot be accessed anymore. Version 2.0 utilizes a cloud modification factor, Af_2, based on the ratio, x, of actual solar irradiation at the surface on a horizontal plane, S_{act}, and the clear-sky solar radiation S_{clear}. So, $x=S_{act}/S_{clear}$, with S_{act} the actual solar radiation received at the surface (horizontal plane) and S_{clear} the clear-sky solar radiation (Wiegant, 2016) and Af_2, the new cloud modification factor equals:

$$Af_2 = -0.435\ x^2 + 1.348\ x + 0.095 \qquad (3.6)$$

In contrast with Eq. 3.4, which yields cloud modification factors between 0.5 and 1, the new parameterization allows cloud modification factors down to 0.095 and over 1 (see also Section 2.2). It takes into account cloud-physical properties and is therefore expected to agree better with observations. A comparison between results based on cloud effects according to Eqs 3.4 and 3.6, respectively, is provided by Wiegant (2016) for the 2nd of September 2012. This comparison is reproduced in Figure 3.2. The cut-off implied in A_f computed using Eq. 3.4 can clearly be seen in the right figure panel, which essentially compares A_f (Eq. 3.4) and y (Eq. 3.6). However, the total UV daily radiation, which is compared in the left panel, does not show this behaviour because total UV intensity depends on other factors as well. Although differences are clearly visible, the majority of the data shows reasonably consistent behaviour, in spite of the limitations of using Eq. 3.4.
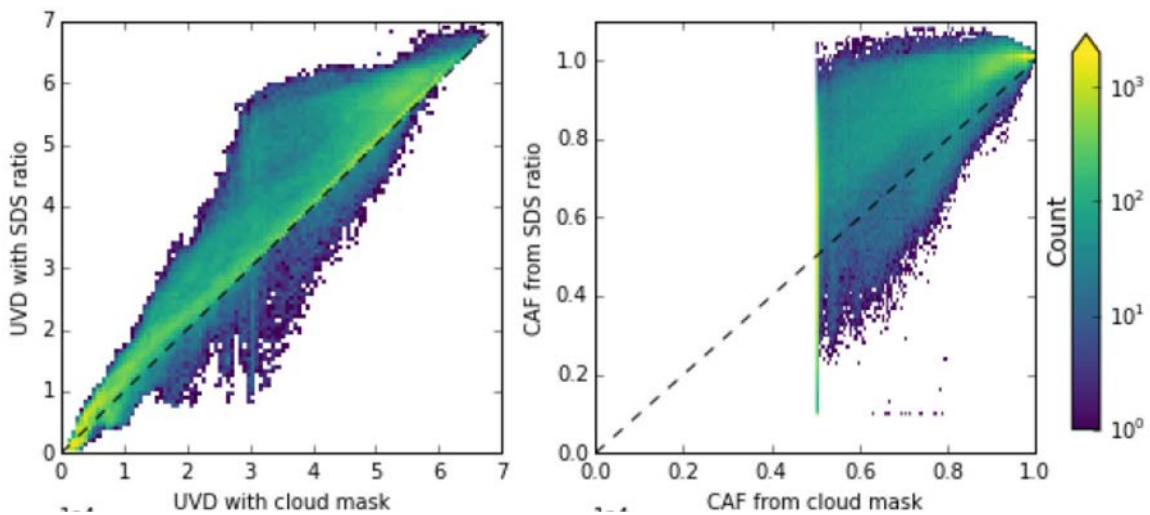
Figure 3.2   *Comparison of UVD (daily UV radiation) estimates on 2 September 2012 (left) and underlying cloud modification factor, here called Cloud Attenuation Factor (CAF) (right). From Wiegant (2016). A so-called cloud mask has been used to estimate cloud cover from remote sensing images (as used in Eq. 3.4). SDS ratio refers to estimates of global radiation at the surface and the corresponding clear-sky value (as used in Eq. 3.6).*

In the context of the present report, we decided to compute the cloud modification factor according to A_f in Eq. 3.4. The method has a clear practical advantage, since it is based on one parameter only,

---

[1] At present, version 2.1 of TEMIS products has been made available and version 1.4 cannot be accessed anymore.

cloud cover, which is usually more readily available than the combination of clear-sky solar radiation and actual surface solar radiation. The approach has been applied in Version 1.4 of the TEMIS products, which has been extensively used until 2017 (www.temis.nl) and has been evaluated in the scientific literature (Sempila et al., 2017). The evaluation shows that this product version is suitable for use in the present context. Due to differences in the cloud modification, the relative deviations between the two approaches are expected to be the largest at high cloud cover. This is judged acceptable here, since this is also when UV radiation is attenuated, and thus its effect on photochemical degradation is relatively weak (see Figure 3.2). For future applications in a similar context, a (gradual) development towards the use of the method in Version 2.0 of the TEMIS UV products is recommended, depending on the availability of solar radiation data.

3.2.3   Action spectra used in TEMIS UV products

The parameterisation of UV Index by Allaart et al. (2004) is based on the action spectrum for erythema issued by the International Committee on Illumination (CIE), described by McKinlay and Diffey (1987). Similar parametrisations have been derived and are used for the generalized DNA-damage UV dose and the vitamin-D UV dose (Zempila et al., 2017). DNA-damage UV dose is based on the action spectrum from Setlow (1974), but normalized at 300 nm (Bernhard and Seckmeyer, 1997). The vitamin-D UV dose spectrum is based on Holick et al. (2005). A graphical representation of these action spectra is given in Figure 3.3. See Zempila et al. (2017) for more details.
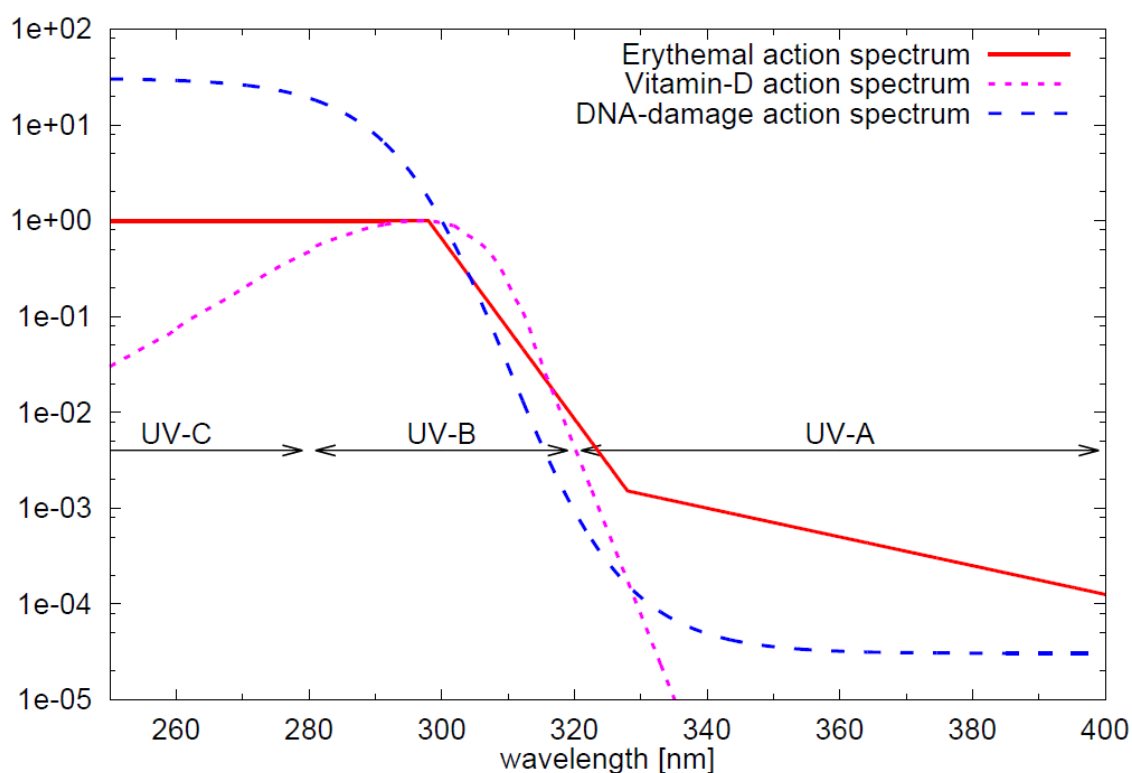
Figure 3.3   *Erythemal, Vitamin-D and DNA damage action spectra applied in TEMIS UV products.*

The use of these three action spectra leads to three essentially different UV products, all of which contain clear-sky values with global coverage as well as actual cloud modified values covering the MSG (Meteosat Second Generation) domain (see Figure 3.1). The selection of these action spectra used in TEMIS derives from the idea that the resulting combination of products serves a broad range of purposes, from health to atmospheric chemistry.

In the present context of photodegradation we will use UV data products based on the Vitamin-D action spectrum since this spectrum represents effects of UV on many larger organic molecules, with the main contribution from UVB, but also taking into account some contribution from UVA (Van Weele, 2018, personal communication). In the remainder of this report we will use the UV radiation data

based on the vitamin-D action spectrum to estimate the effect of radiation on the degradation rate of pesticides in surface water and indicate this by UV-VitD radiation.

3.3 Selection procedure of $I_{actual,UV-VitD}$ values

As argued in Section 3.2 we will use values of actual UV radiation based upon the Vitamin-D action spectrum, $I_{actual,UV-VitD}$, for the calculation of photochemical pesticide degradation rates in surface water. Such $I_{actual,UV-VitD}$ values will serve two purposes:

1. test the method developed in this report to estimate $DegT_{50,water,photo}$ values using data from outdoor cosm experiments
2. application in the NL surface water scenario location of De Bilt and the 10 EU FOCUS surface water scenarios at locations throughout Europe.

Often, photochemical degradation of pesticides is rapid in surface waters, with half-lives of less than a couple of days, e.g. fluazinam – 2.5 d, imidacloprid – 0.2 d, lufenuron – 0.75 d, metamitron – 0.02 d, metiram – 0.3 d, metribuzin - 0.2 d (Deneer et al., Table 3.1, 2015). Because this implies that a daily resolution of radiation values may not be appropriate to calculate the behaviour of pesticides we decided to work with hourly $I_{actual,UV-VitD}$ values. The hourly resolution also corresponds well with the hourly resolution for output of the TOXSWA model, which will be used for calculating the pesticide behaviour in surface water.

The selected cosm experiments of which data are used to test the method described in this report lasted several weeks to months and were performed in the period from 1999 to 2009. The NL surface water scenario spans 15 years from 1991 up to 2005, while the EU FOCUS surface water scenarios are based upon weather years starting from 1975 up to 2000 (depending on their availability for each location). For consistency, we wanted to use the same type of radiation data in all cases and applications.

Daily $I_{actual,UV-VitD}$ for the MSG domain can readily be obtained from TEMIS (www.temis.nl), as of the year 2004. However, this would exclude some of the cosm experiments and (large parts of) the aforementioned scenarios. However, worldwide clear-sky UV data for the period 1970-2017 are available for all action spectra, from a so-called Multi-Sensor Reanalysis (MSR). This is a merger from various sources of satellite data, using the most recent methods for the computation of UV radiation data during the (re-)processing of the raw data (Van Geffen et al., 2017). Because of the spatial and temporal coverage of this product we decided to take the most recent TEMIS clear-sky MSR product (v2.0) based on the Vitamin D action spectrum as a starting point to obtain the required $I_{actual,UBV-VitD}$.

Note that this clear-sky product does not depend on the cloud modification factor (taken from version 1.4).

The TEMIS MSR data represent daily dose for clear-sky conditions. Thus, they have to be post-processed in order to obtain hourly values for actual cloud conditions. The conversion from daily clear-sky values to hourly clear-sky values can be achieved using astronomical functions to evaluate solar elevation as a function of time. Next, these hourly clear-sky values need to be converted to actual values using A_f, which requires cloud cover as input. For this purpose, we also need global fields of cloud cover. To this end, we decided to use so-called meteorological reanalysis data, which have recently become freely available from the European Copernicus program, at the Copernicus data store. This dataset will be further described below, as part of a more detailed description of the procedure followed here.

In summary, we proceed as follows:
1. Download the TEMIS MSR(2.0) daily UV dose weighed with the Vitamin D action spectrum ($I_{clearl,UV-VitD}$)
2. Convert the daily clear-sky dose into hourly values using astronomical functions

3. Estimate cloud cover using meteorological reanalyses available at the Copernicus climate data store and compute attenuation factor A_f, using (3.4), so corresponding to the old v1.4 of the cloud-modified TEMIS product as described in Section 3.2.2.
4. Multiply A_f with the hourly clear-sky values for UV from step 1) and 2), to obtain $I_{actual, UV-VitD}$ on an hourly basis.

Below, these steps will be detailed further.

3.3.1 Procedure to extract and convert the required radiation data

In this section, the procedure to obtain $I_{actual, UV-VitD}$ on an hourly basis is described in detail. The target quantity is $I_{actual, UV-VitD}$ given as an hourly dose, in kJ m^{-2}. It is derived from a daily clear-sky value for UV dose, also given in kJ m^{-2}. Note that (strictly speaking) time is not in the unit because the definition of the target quantity defines the corresponding time period.

The principle of the procedure is valid for any location on Earth, for any period in time. However, in practice, specific datasets will be restricted to specific regions and periods, simply because of availability of data. Here, we focus on a number of specific locations and periods relevant at those locations in the present context. An overview over locations and periods considered here is given in Table 3.1, along with some other information relevant for the procedure (more details given in Annex 3). All locations, except one, are located within the EU. One cosm was located in Columbia in the state of Missouri of the USA. In the latter case, we need to refer to another database of cloud cover than used for the European locations. This difference will be detailed below.

Table 3.1 *Overview of compiled UV$_{actual, UV-VitD}$ radiation data and locations of the EU FOCUS surface water scenarios, the meteorological station for the Dutch surface water scenarios and the outdoor cosms (for which DegT$_{50, water, photo}$ have been determined in this report). The acronyms D and R of the FOCUS scenarios refer to drainage, respectively runoff scenarios, (FOCUS, 2001).*

FOCUS or NL scenario / cosm	Location	Longitude (decimal notation)	Latitude (decimal notation)	Time series $UV_{actual, UV-VitD}$ start or selected years	end
FOCUS D1	Lanna (S)	13.050	58.333	1980#	2000#
FOCUS D2	Brimstone (UK)	-1.633	51.650	1975	1994
FOCUS D3	Vredepeel (NL)	5.867	51.533	1975	1994
FOCUS D4	Skousbo (DK)	12.083	55.617	1975	1994
FOCUS D5	La Jailliere (F)	0.967	47.450	1975	1994
FOCUS D6	Thiva (GR)	23.100	38.383	1977	1996
FOCUS R1	Weiherbach (D)	8.667	49.000	1975	1994
FOCUS R2	Porto (P)	-8.631*	41.096*	1975	1994
FOCUS R3	Bologna (I)	11.400	44.500	1975	1994
FOCUS R4	Roujan (F)	3.317	43.500	1975	1994
NL	De Bilt (NL)	5.180	52.100	1991	2005
Cosm	Renkum (NL)	5.754	51.990	1999, 2002	
Cosm	Berlin (D)	13.283	52.493	2009, 2012	
Cosm	Monheim (D)	6.901	51.074	2000	
Cosm	Itingen (CH)	7.785	47.467	2000, 2001	
Cosm	Columbia (MO, USA)	-92.334	38.952	2001	

* coordinates of Valdares which is close to R2 scenario (coordinates -8.640, 41.183)

should be 1980-1993 plus 1995-2000 added as 1994-1999. (In order to account for leap years the 29th of February should be deleted in 1995 and 1999, in 1996 the 29th of February should be added with average properties from the day before and the day after.)

Objective
The objective of the procedure is to determine $I_{actual, UV-VitD}$ on an hourly basis for a location at longitude Λ (in radians, positive West) and latitude Φ (in radians, positive North); the target period is 1-Jan-1975 – 31-Dec-2005, the period covered by the EU FOCUS and NL scenarios (Table 3.1). as well

as the periods during which the outdoor cosm studies were performed (More details are provided in Annex 3).

Step 1

We downloaded daily clear-sky, vitamin-D weighted dose ($I_{clear,UV-VitD}$ [kJ m^{-2}]*)* for the period 1975-2005 and for 2009, via www.temis.nl/uvradiation/UVarchive/uvdvc_msr2.php. Files for download contain global fields of daily dose, with a spatial resolution of 0.25° x 0.25°, packed as self-descriptive hdf5 files. There is one folder per year, containing 365 or 366 files for normal years and leap years, respectively. Naming convention of the files is: uvdvcYYYYMMDD_msr.hdf with YYYY the year, MM the month and DD day in the month. The string "uvdvc" indicates the variable contained in the files, which is clear-sky UV dose weighted with the Vitamin D action spectrum (see Section 3.2.3). The string "MSR" indicates multi-sensor reanalysis. The unit is kJ/m^2 (dosage per day), but a so-called scaling factor of 1000 has been applied for storage efficiency. So in fact, the numbers in the source files can also be interpreted as dosages in J m^{-2}. This means that extracted numbers have to be multiplied with 0.001 to arrive at the more conventional magnitude in kJ m^{-2}, which also corresponds to the description of the database. $I_{clear,UV-VitD}$ is extracted for each location of interest, taking the value in the gridbox containing coordinates Λ and Φ, This results in time series of $I_{clear,UV-VitD}$ at each of the locations of interest.

Step 2

Convert $I_{clear,UVB-VvitD}$ to hourly values assuming that the distribution of irradiation under clear skies follows the solar elevation. We applied the following practical estimate of the sine of solar elevation (Stull, 1988):

$$\sin\varphi = \sin\delta \sin\Phi + \cos t_h \cos\delta \cos\Phi \tag{3.7}$$

where δ (in radians) = $0.409\cos(2\pi(D-d_s)/365.25)$ is the declination of the sun (with D the day of year and $d_s = 171$ is the day of the summer solstice). Furthermore, t_h (in radians) is the hour angle, approximated as $t_h = (\pi t_d/12 - \Lambda - \pi)$ (with t_d (in hours) the time of day in UTC).

For each day of the year an hourly weight W (dimensionless) is determined using Eq. 3.8, assuming a zero weight if the centre of the solar disc is below the horizon, that is, if $\sin\varphi < 0$:

$$W_h^d = \frac{\max{(sin\varphi,\ 0)}_h^d}{\sum_{h=1}^{h=24} \max{(sin\varphi,\ 0)}_h^d} \tag{3.8}$$

Where superscript d indicates day number and subscript h the hour of the day.

The hourly dose of clear-sky, Vitamin-D weighted UV radiation is then

$$I_{clear,UV-VitD}{}^{d,h} = W_h^d \cdot I_{clear,UV-VitD,}{}^{d} \tag{3.9}$$

Note that in the present framework the values will formally be valid from h-1/2 to h+1/2.

Step 3

Cloud cover is estimated using meteorological reanalysis data available from the EU Copernicus climate data store. The EU Copernicus programme (www.copernicus.eu) stimulates use of Earth observation data by making freely available data from various sources, ranging from remote sensing data to data from weather and climate models. The Climate Change Service of the program provides a rapidly growing amount of data on the past, present and future climate, made available via the so-called Climate Data Store (cds.climate.copernicus.eu). An important source of information are the so-called reanalysis data, which are a merger of observations and model calculations with an advanced weather forecast models. By combining model data with observations, sets of physically consistent high-quality meteorological data are obtained.

Recently, the Copernicus Climate Data Store has made available high-resolution reanalysis data for the European domain, at a resolution of 11x11 km. The so-called UERRA (Uncertainties in Ensembles

of Regional Reanalyses) reanalysis database at single level (that is, computed at or observed at a height of 2m) contains total cloud cover [%] at 6-hourly resolution. Because of the excellent spatial resolution and because of the complete temporal coverage of the periods of interest at each location we decided to use this data source for the European locations. Data are available for the period 1961 – present, from which data between 1975 and 2005 are extracted. The data source is made available as one file in the self-descriptive GRIB format, but efforts to provide the data in files according to the more familiar netcdf protocol as well are ongoing. From the downloaded file, cloud cover is extracted for each of the European locations of interest (Table 3.1), taking the cloud cover (Cc, [%]) value of the box that corresponds to longitude Λ and latitude Φ, which results in time series of Cc at these locations. In the UERRA database, cc is given six-hourly as instantaneous values. We have assumed these values to apply between t and $t+6$ hours, with t the time for which cc is formally valid.

For the location at Columbia, Missouri, USA, the UERRA database cannot be used and therefore we decided to use the ERA5 (fifth generation ECMWF reanalysis; ECMWF = European Centre for Medium-Range Weather Forecasts) global reanalysis data, which is very much akin to the UERRA reanalysis. The disadvantage is the somewhat coarser spatial resolution of 0.25° x 0.25° (roughly corresponding to about 25 by 25 km at lower to mid-latitudes, including the position of interest), but the cloud cover in this database has a temporal resolution of 1 hour and is given as a fraction between 0 and 1 instead of percentage. Data at single level are available as of 1979, from which only data for the year 2009 are extracted for our purpose. The data are made available as files in the self-descriptive GRIB format, but efforts to provide the data in files according to the more familiar 'netcdf' protocol as well are ongoing. From the downloaded data, cloud cover is extracted for the location of interest (Columbia, Missouri, USA, Table 3.1), taking the cloud cover (Cc) value of the box that corresponds to Λ and Φ, which results in time series of cc at this location. Since the Cc is given hourly, no further assumption was made on the period of validity.

In the next step, these Cc time series and those of $I_{clear,UV\text{-}VitD}$ are combined to obtain time series of $I_{actual,UV\text{-}VitD}$.

Step 4
We apply the parameterization proposed by Geffen et al. (2005) (Eq. 3.4) to compute A_f from Cc that was obtained in Step 3. We assume that the effect of clouds is similar for each action spectrum (Fioletov et al., 2009) hence,

$$I_{actual,UV\text{-}VitD}\,^d{}_h = A_f \cdot I_{clear,UV\text{-}VitD}\,^d{}_h \qquad\qquad (3.10)$$

This is our desired result, namely a time series of hourly, actual UV dose weighed with the vitamin D action spectrum in kJ m^{-2}.

3.3.2 Comparison between actual daily UV-VitD radiation and measured UVB radiation

For one of the studies we obtained UVB radiation data measured during the study. Below we compare these data to our UV-VitD data obtained from the TEMIS database as described above in section 3.3.1.

Figure 3.5 presents the same data set as Figure 3.4, but the radiation date have been converted from kJ/(m^{2}h) to µW/cm^2. (Note that an hourly dose of 1 kJ/m^2 corresponds to an hourly dose of $10^5/3600=28$ µW/cm^2.) In Figure 3.5 and 3.6 $I_{actual,UV\text{-}VitD}$ of Berlin as obtained from the TEMIS database is compared to the UVB radiation recorded during the experiment and reported by the authors of Colombo et al. (2013) in the student report obtained (see Annex 5). The $I_{actual,UV\text{-}VitD}$ is approximately a factor 2 higher than the radiation measured by Colombo (2009) and the fluctuations are clearly smaller than the fluctuations measured by Colombo (2009). The differences may be due to e.g. the different action spectra (UV-VitD vs UVB), the difference in measurement instruments, or the post-processing done in the TEMIS data set. Moreover, given the large scatter in the relationship between the different cloud modification estimation procedures for even a single day as shown in Figure 3.2, no high accuracy of the UV estimates could be expected.
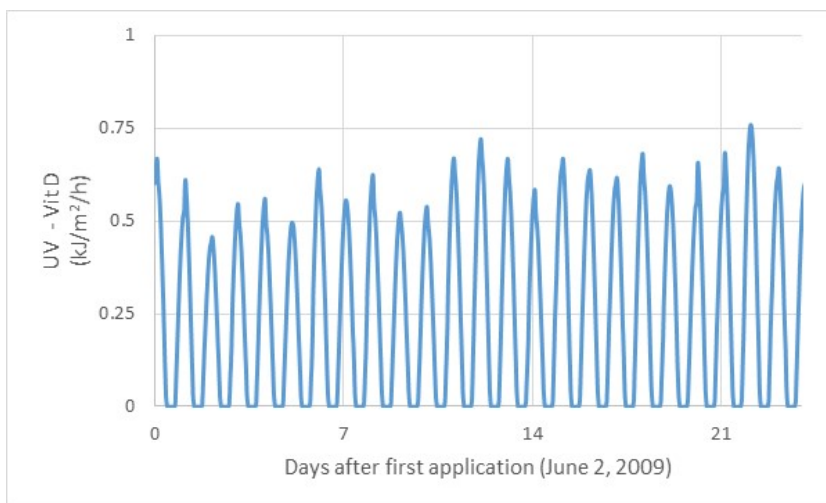
Figure 3.4   *Hourly UV-VitD data (kJ/m²) in Berlin for the study period of Colombo et al. (2013) derived from the TEMIS database (Geodesk WUR).*
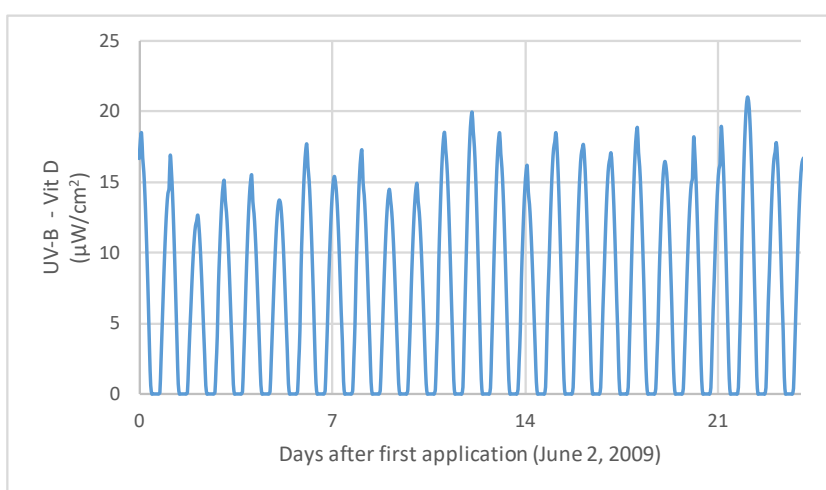
Figure 3.5   *Hourly UV-VitD data (µW/cm²) in Berlin for the study period of Colombo et al. (2013) derived from the TEMIS-database (Geodesk WUR).*
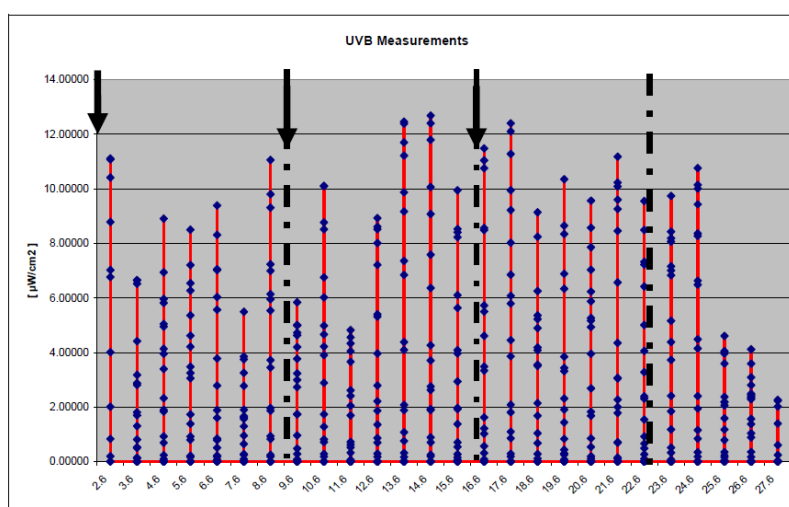
Fig. 15 UVB levels recorded during the three pulses. The arrows indicate the three pulse days; the black dotted lines indicate the interval of time after an application, during which imidacloprid degradation was measured.

Figure 3.6   *Measured UVB radiation data for the imidacloprid cosm study performed in Berlin in June 2009 (reproduced from the students report by Colombo, 2009 mentioned in Annex 5).*

4 Selection of time series of daily UV-VitD radiation doses for surface water scenarios of The Netherlands and the EU

4.1 Introduction

Since approximately 2008 risk assessments of organisms at EU level are based on a specific protection goal, consisting of two parts: an ecotoxicological effect assessment goal and an exposure assessment goal (e.g. EFSA (2013a and b), EFSA (2015) and EFSA (2016)). The exposure assessment goal for aquatic organisms consists of seven elements (Figure 4.1 from Boesten, 2017):
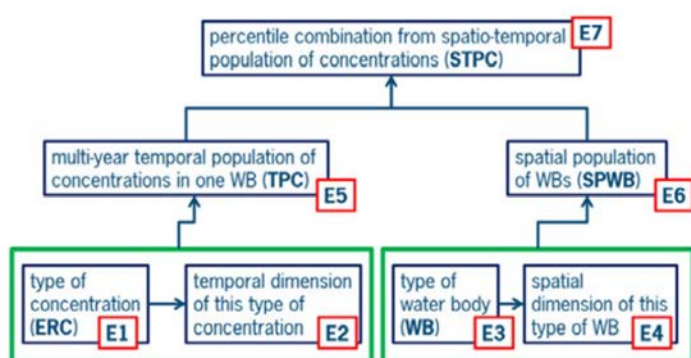
Figure 4.1   *Schematic overview of the seven elements defining the exposure assessment goal for aquatic risks of pesticides (reproduced from Boesten, 2017).*

The relevant elements for this chapter are:
The spatial population of water bodies (E6), and
The multi-year temporal population of concentrations in one water body (E5); note that every year has been reduced to one concentration (e.g. the annual peak) in each of the water bodies of E6.

Examples of E6 are: all permanent watercourses adjacent to arable land or all permanent watercourses adjacent to fruit orchards in The Netherlands.

Combining E5 and E6 results in a spatio-temporal population of concentrations, that can be ranked to select the wished percentile, i.e. the final result of the exposure assessment. Usually a 90th overall percentile of occurrence in time and space is selected to represent the "realistic worst case' situation, mentioned in the EU Regulation 1107/2009. Figure 4.2 is a fictitious example of the contour plot of exposure concentration percentiles. Note that the selection of the overall 90th percentile implies that all points at the 90th percentile line in the contour plot are acceptable, indifferent whether this percentile concentration is exceeded in 95% of the years or in 15% of the years.
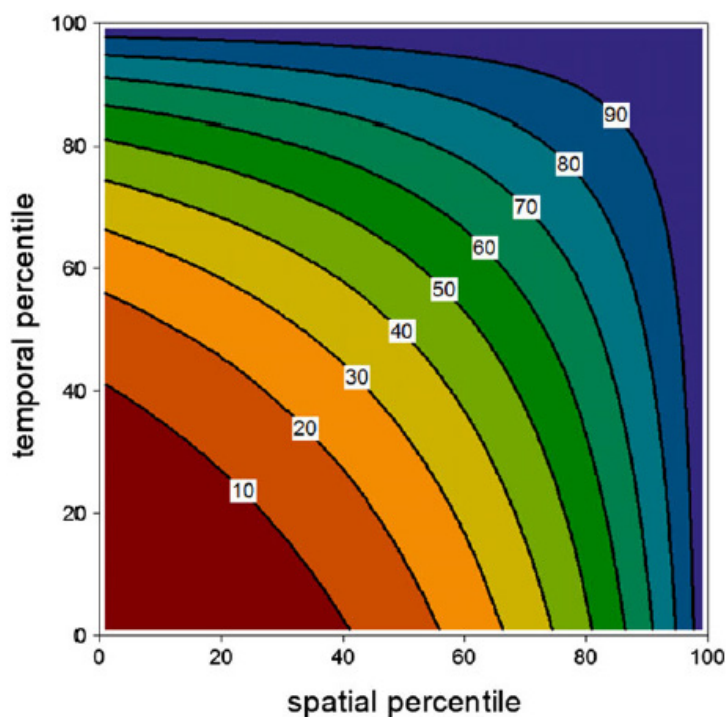
Figure 4.2 *Simplified example of a contour plot of percentiles of the spatio-temporal population of concentrations (E7 in Figure 4.1), as a function of the spatial and temporal percentiles. The label of each line indicates the corresponding percentile (reproduced from Boesten, 2017).*

In the EU as well as in The Netherlands exposure of aquatic organisms is assessed with the aid of a tiered approach. In a higher tier of the assessment it would be ideal to calculate exposure concentrations by a spatial model for the relevant area, that incorporates photochemical degradation in the watercourse, next to e.g. soil, crop development, other agro-environmental conditions and the pesticide entry routes, such as spray drift deposition, drainage or runoff/erosion. Doing this for a time series of e.g. 20 or 30 years, the model can, in a simple way, determine the overall 90th percentile of occurrence in time and space of the PEC_{sw}, representing the 'realistic worst case' exposure. Such an approach is for example being followed for the assessment of leaching in The Netherlands with the aid of the GeoPEARL model. By following such an approach the importance of the spatial and temporal distribution of the $I_{act,UV-VitD}$ on the exposure concentrations in the watercourse would be automatically weighed in a correct way. However, such a geographically distributed model does not exist at EU level or for The Netherlands. Therefore we need to design another approach. As the philosophy behind the scenario development at EU level and in The Netherlands has been different the approach will be different as well.

4.2   Exposure assessment in The Netherlands

For The Netherlands new surface water scenarios are being developed since 2007, following the EU approach of defining first specific protection goals. So, clear exposure assessment goals with well-defined spatio-temporal populations of concentrations were defined for watercourses adjacent to arable fields treated by downward spraying (Tiktak et al., 2012) and for watercourses adjacent to fruit orchards treated by sideward and upward spraying (Boesten et al., 2018). Both types of watercourses receive drainage water as well. The scenarios, aimed at obtaining 90th percentile exposure concentrations were selected combining results of geographically distributed models for either pesticide entries via spray drift or via drainage into the ditch. To additionally take photochemical degradation into account in the assessment we see the following options.

Option 1. Simple watercourse model
Feed a simple first-order degradation model for concentration as f(time) with daily doses of $I_{act,UV-VitD}$ that are distributed across The Netherlands. The degradation rate coefficient depends on $I_{act,UV-VitD}$ only. The

model calculates concentrations in e.g. watercourses adjacent to fruit orchards, starting from a fictitious concentration level at a relevant date for pesticide applications, e.g. 1 June, and evaluates the relative concentration decline at a relevant moment, i.e. after 3 or 7 days (depending on the ecotoxicological relevant concentration for effects on water organisms). The model can be parameterised for the spatially distributed, various types of watercourses e.g. those adjacent to fruit orchards. For reasons of simplicity it is assumed to be stagnant. The combination of the modelled watercourses with the spatially distributed $I_{act,UV-VitD}$ values over a series of years results in a spatio-temporal distribution of relative concentration declines. The concentration declines can be weighed according to watercourse length. These calculations should be repeated for various relevant dates and evaluation moments.

The population of concentration declines can be analysed with the aid of a contour plot (see e.g. Figure 4.2). For the area of The Netherlands we expect that the temporal variation between the years is much larger than the spatial variation across such a small country as The Netherlands. This is based upon the observation that daily global radiation doses fluctuate strongly in The Netherlands, e.g. between 1 May and 30 June the daily doses ranged from approximately 5000 to 30000 kJ m^{-2} at the weather station in Wageningen for the years 1954, 1975 and 1999 (Boesten et al., 2014). Therefore, it is then defensible to opt for a simple solution and use the time series of concentration declines for the scenario location, not taking the spatial variation into account. We will need to confirm that also for UV-VitD radiation the temporal variation is significantly more important than the spatial variation.

Option 2. Consider only sums of daily doses of $I_{act,UV-VitD}$
This option is comparable to Option 1, but instead of considering concentration declines we look at a direct characteristic of $I_{act,UV-VitD}$, because probably this is a good measure for the concentration decline, e.g. the sum of daily doses for 1-3 June or 1-7 June. (This could be demonstrated with the aid of the simple model of Option 1.)

Option 3. Simple watercourse model including water flow
In this option the simple watercourse model of Option 1 is used but now inflow and outflow of water are taken into account, e.g. by incorporating a distribution of probability of hydraulic residence times in the watercourse. As soon as hydraulic residence times are low (below e.g. 5-10 days) concentration declines by flow will be equally important as declines by photochemical degradation (half-lives often couple of days) and thus the influence of $I_{act,UV-VitD}$ will be difficult to trace. So, this option is only valuable for watercourses with relatively long hydraulic residence times (above approx. 10 days) during the application season.
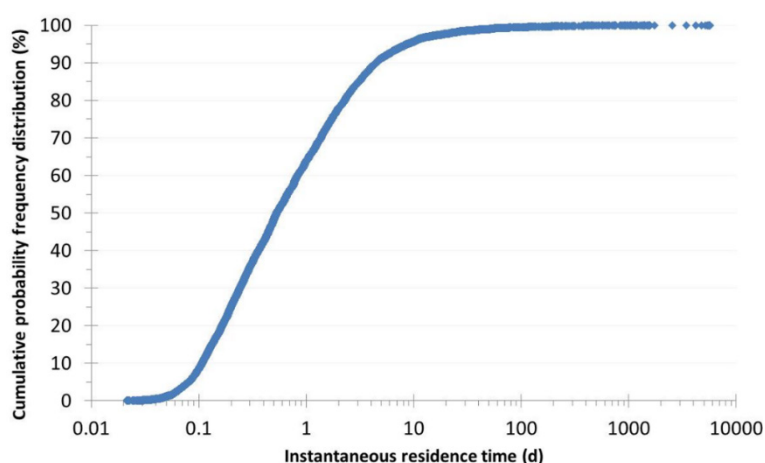
Figure 4.3 *Frequency distribution of instantaneous hydraulic residence times of the ditch of the Dutch fruit orchard scenario (Boesten et al., 2018).*

Option 3 described above for The Netherlands indicates that photochemical degradation is only important if it dominates other decline processes in the watercourse, such as inflow and outflow. This is valid both for surface water scenarios developed for The Netherlands as the EU FOCUS surface water scenarios, discussed in section 4.3. Figure 4.3 presents the frequency distribution of

instantaneous hydraulic residence times for the ditch of the Dutch fruit orchards scenario. It indicates that approximately 90% of the time the residence time is shorter than 5 days. So, we expect a limited build-up of concentrations of subsequent applications and only in a limited number of cases the peak concentration will be influenced by build-up. However, time-weighted average (TWA) concentrations will be influenced by the photochemical degradation rate, but these are decreasingly used to refine the ecotoxicological risk assessment[2].

Therefore, we wanted to assess the spatio-temporal population of sums of daily UV-VitD radiation data. As explained in Chapter 3.2.3 we present UV radiation weighted according to the Vitamin D action spectrum, judged to represent best the action spectrum for photochemical degradation of organic compounds such as pesticides. Below we first consider the temporal variation, and next the spatial variation.

We focus on the distribution of sums of daily radiation doses over a series of years across The Netherlands. A comprehensive analysis might consider 3-d sums and 7-d sums of daily radiation, starting at 1 April, 1 May, 1 June, 1 August and 1 October, for a series of 15 years, 2004-2018. However, we limited ourselves to considering 3-d sums, starting at 1 June. The radiation data were obtained from www.temis.nl, the Tropospheric Emission Monitoring Internet Service, a web-based service containing near real-time satellite data products of the atmospheric composition, which is part of the Data User Programme (DUP) of the European Space Agency (ESA) and hosted by the KNMI, the Royal Netherlands Meteorological Institute. The $I_{act,UV-VitD}$ radiation data originate from Meteosat and their resolution is 0.25 x 0.25º.

So, concerning the spatial variation of the UV VitD radiation data, the TEMIS database consists of data at a resolution of 0.25×0.25º, with pixel centres at 0.125, 0.375, 0.625 and 0.825 degrees (in decimal units). So there are 16 pixel centres within a surface area of 1×1º. This gives 83 pixels for the Netherlands and 54 pixels for the area containing most fruit crops as indicated in Figure 4.4. For these pixels the sum of the daily UV radiation (Vitamin-D spectrum) from 1 to 3 June over a period of 13 years (2005-2017) was derived.
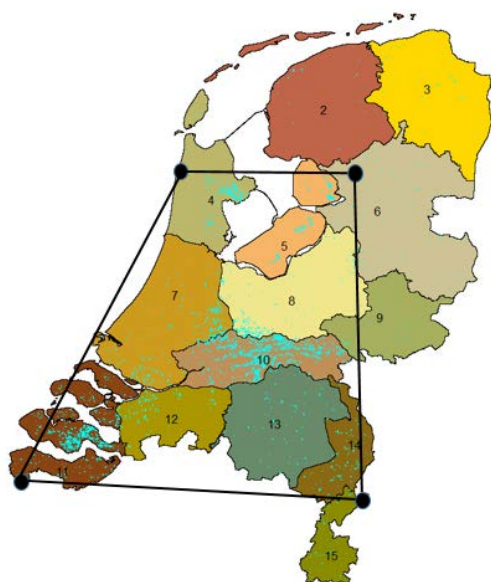
Figure 4.4 *Distribution of fruit crops in the Netherlands (indicated by the light blue areas). The quadrangle contains most of the fruit crop areas and contains 54 of the 83 pixels with UV-VitD-data available for the Netherlands.*

---

[2] See the aquatic guidance document by EFSA (2013a).

We generated contour diagrams of the spatio-temporal distribution of these 54 pixels (see Boesten, 2017, for the description of the procedure). Figure 4.5 shows a somewhat irregular pattern; this is probably caused by the relatively small number of data points (13 years and 54 locations). However, the variation in the vertical direction (i.e. in time) is much larger than in the horizontal direction (i.e. in space). This is was expected because daily radiation differences between locations in the Netherlands are likely to be quite small.
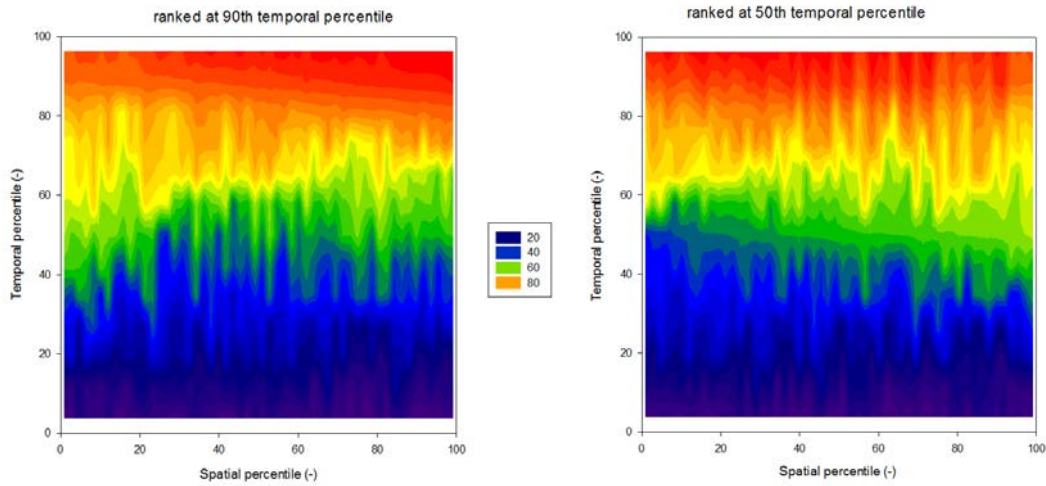
Figure 4.5   *Contour diagrams of the percentiles of the three-day sums (1-3 June) of the UV-VitD radiation data for 54 pixels of the UV-VitD-database in the quadrangle of Figure 4.4. In the left graph spatial percentiles are ranked based on the 90th temporal percentile and in the right graph based on the 50th temporal percentile.*

The small differences between different locations in the Netherlands are confirmed by Figure 4.6: the cumulative frequency at one selected location (i.e. the pixel closest to the Dutch fruit scenario located in Andelst) almost exactly coincides with the cumulative frequency of the quadrangle of Figure 4.4 and both coincide also almost exactly with the cumulative frequency of the whole of the Netherlands. So it can be concluded that the spatio-temporal population of the UV-VitD-data can be approximated well by the temporal population at one single point (e.g. that at meteo station de Bilt). Figure 4.6 shows further that differences between years are limited to about a factor of two.
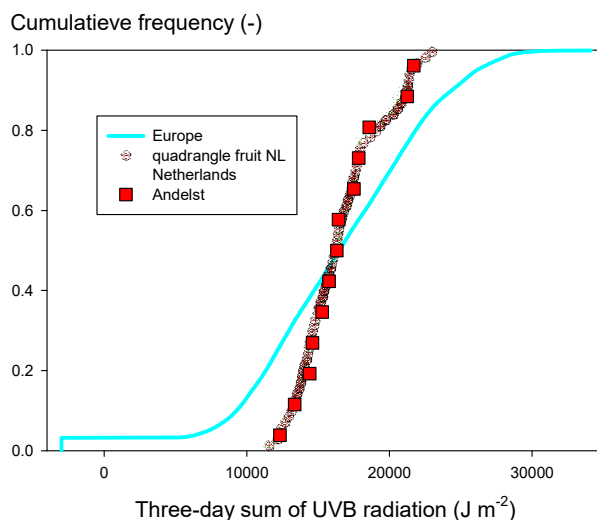
Figure 4.6   *Cumulative frequency of three-day sums (1-3 June) of UVB radiation. The 'quadrangle fruit NL' refers to the quadrangle in (Figure 4.4) and Andelst is the pixel closest to the location of the fruit scenario for the Netherlands. The line for Europe starts at -3000 J m-2 because this value was used to indicate missing data.*

The selection of the temporal percentile to be used depends on the overall approach used for the exposure assessment: the concentrations are determined not only by photochemical degradation but also by e.g. the amounts entering the system by spray drift and drainpipe leaching. Given the relatively small temporal variation in the Netherlands as shown in Figure 4.6 we expect that the photochemical radiation data will usually play a minor role in the selection of the temporal percentile to be used (this selection procedure is beyond the scope of this report). This minor role does not mean that photochemical degradation has a small influence on the results of the exposure assessment because rapid photochemical degradation may lead to strong decreases in e.g. TWA exposure concentrations.

So, finally daily values of UV-VitD-data for a series of years were compiled for the meteorological station De Bilt, used in the future Dutch surface water scenarios (Tiktak et al.,2012; Boesten et al., 2018). Clear sky, UV-vitamin D weighed daily radiation doses were extracted from the TEMIS data and combined with cloud cover data, according to the procedure of Chapter 3.3.1. The multi-year daily radiation series in De Bilt for the future Dutch surface water scenarios, are available upon request (see Annex 3 for more details on the exact procedure).

4.3 Exposure assessment in the EU

For the EU the FOCUS surface water scenarios were developed from 1997 up to 2003, so before the concepts of specific protection goals were developed. Consequently, probabilities of occurrence of the PEC values were rudimentarily defined, mainly with regards to the pesticide entry routes of either spray drift deposition and drainage or spray drift deposition and runoff/erosion (the so-called D and R FOCUS scenarios, see also Table 4.1). Currently the EFSA has 'repaired' the FOCUS surface water scenarios in a pragmatic way, it did not redesign EU scenarios by starting with the definition of an exposure assessment goal, fitting the defined specific protection goals in the Aquatic Guidance document (EFSA, 2013). This implies that there is no scientifically state-of-the-art exposure assessment at EU level available and therefore, in this report we also selected a pragmatic solution. We opted for the use of time series of $I_{act,UV-VitD}$ at the ten FOCUS surface water scenario locations to account for photochemical degradation in a tier 4 aquatic risk assessment.

Table 4.1 *The locations of the FOCUS surface water scenarios and the longitude and latitude of the centre of the grid cells in the TEMIS database that are closest to these locations. See FOCUS (2001) for explanation of the acronyms of the ten locations ('D' refers to drainage scenarios and 'R' refers to runoff scenarios).*

Scenario	FOCUS longitude		Longitude of grid cell (decimal)	FOCUS latitude		Latitude of grid cell (decimal)
	Conventional notation	Decimal notation		Conventional notation	Decimal notation	
D1	13 03 E	13.050	13.125	58 20 N	58.333	58.375
D2	01 38 W	-1.633	-1.625	51 39 N	51.650	51.625
D3	05 52 E	5.867	5.875	51 32 N	51.533	51.625
D4	12 05 E	12.083	12.125	55 37 N	55.617	55.625
D5	00 58 E	0.967	0.875	47 27 N	47.450	47.375
D6	23 06 E	23.100	23.125	38 23 N	38.383	38.375
R1	08 40 E	8.667	8.625	49 00 N	49.000	49.125
R2		-8.640	-8.625	41 11 N	41.183	41.125
R3	11 24 E	11.400	11.375	44 30 N	44.500	44.375
R4	03 19 E	3.317	3.375	43 30 N	43.500	43.375

Option 3 described above in section 4.2 for The Netherlands indicates that photochemical degradation is only important if it dominates other decline processes in the watercourse, such as inflow and outflow. This is also valid for FOCUS surface water scenarios developed for the EU. For the FOCUS scenarios so-called hydrological response curves exist, that give an overview of the hydraulic residence times (Appendix F of EFSA, 2001, Appendix B of EFSA, 2020). Examples are Figure 4.7 for

the D2 stream, Figure 4.8 for the R1 stream and Figure 4.9 for the R1 pond; they indicate that adding photochemical degradation with a half-life of a few days will not influence the concentration in the R1 stream with its residence times of less than 0.2 d, not even the TWA concentrations. However, for the R1 pond (residence times above 20 d, but mostly around 150 d) adding photochemical degradation will drastically lower the concentrations, so TWA concentrations will be influenced. Depending on the photochemical degradation rate and the application interval a build-up of peak concentrations might also occur.
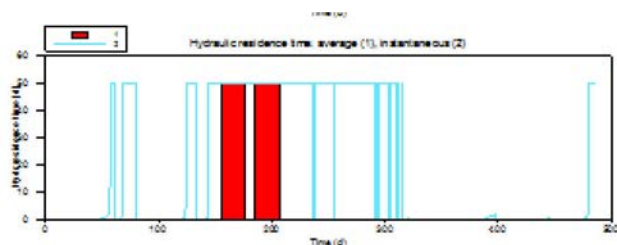
Figure 4.7   *Instantaneous and monthly average hydraulic residence times for the D2 stream of the FOCUS surface water scenarios (Appendix F, FOCUS, 2001).*
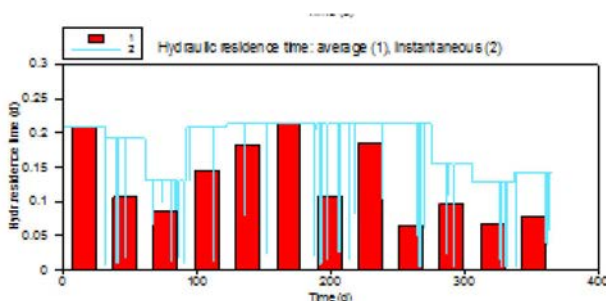
Figure 4.8   *Instantaneous and monthly average hydraulic residence times for the R1 stream (spring applications) of the FOCUS surface water scenarios (Appendix F, FOCUS, 2001).*
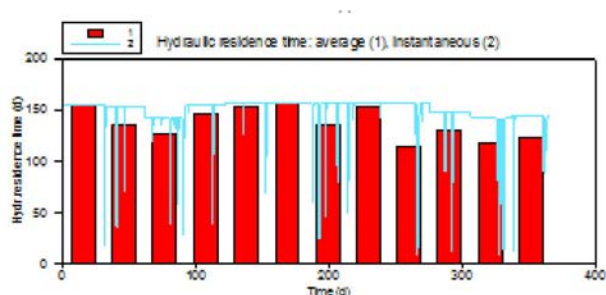
Figure 4.9   *Instantaneous and monthly average hydraulic residence times for the R1 pond of the FOCUS surface water scenarios (Appendix F, FOCUS, 2001).*

The FOCUS surface water scenarios used at EU level are based on ten locations with a fixed temporal percentile used for all locations. The time series of UV-VitD-data can be seen as an extension of the time series of the weather data. These weather data were based on the data in the MARS meteorological database which contains data for 50×50 km^2 grid cells. The grid cell of a scenario was selected based on its relevance to the 10 representative field sites on which the FOCUS-SW scenarios were based (FOCUS, 2001, p. 70). So consistent with this approach, the UV-VitD time series should be selected using the grids that are closest to these ten locations.

Figure 4.10 shows that the differences between the locations are remarkably small (considering that they include e.g. Swedish and Greek scenarios). This is consistent with the cumulative frequency of

the whole of Europe in Figure 4.6 which also shows comparatively small differences. In Figure 4.6 data for Europe are shown, for which the EU was considered to be a rectangle and grids covering water (seas only) were left out.

So, for the EU FOCUS surface water scenarios daily values of UV-VitD-data for a series of 20 years were compiled for the 10 EU FOCUS scenario locations. The 20 years periods cover the same period as the one used for the other meteorological data of the scenario locations. Clear sky, UV-vitamin D weighed daily radiation doses were extracted from the TEMIS data and combined with cloud cover data, according to the procedure of Chapter 3.3.1. The multi-year daily radiation series are available upon request (see Annex 3 for more details on the exact procedure).
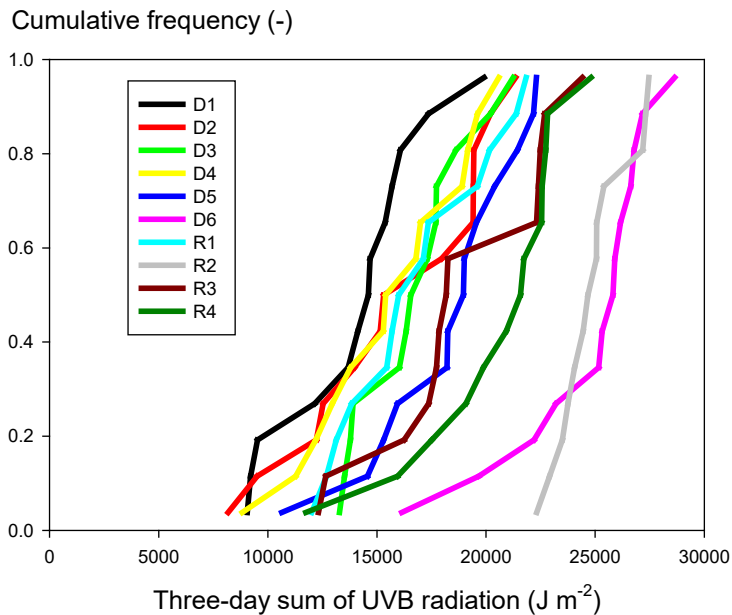
Figure 4.10 *Cumulative frequency of three-day sums (1-3 June) of UV-VitD radiation at the ten FOCUS surface water locations. See FOCUS (2001) for explanation of the acronyms of the ten locations ('D' refers to drainage scenarios and 'R' refers to runoff scenarios).*

5 Photochemical degradation in water

5.1 Introduction

Transformation of pesticides in surface waters is generally considered as three separate processes: hydrolysis, photolysis and biotic transformation, described by separate rate constants. Hydrolysis is the process of chemical degradation by reactions with [H3O$^+$] or [OH$^-$] ions. Biotransformation is degradation by microorganisms, while photolysis, or photochemical degradation is the degradation of a pesticide under influence of radiation. It is generally assumed that photolysis is mainly driven by UV radiation, especially the UVB radiation (e.g. Burrows et al., 2002; Wanatabe et al., 2006).

Concerning photolysis a distinction between two types of photochemical degradation is usually made: (i) direct photolysis, in which the reacting pesticide molecule absorbs light and the excited molecule reacts, and (ii) indirect (or 'sensitized') photolysis, where light is absorbed by a molecule, which then transfers its energy to the acceptor molecule, causing the latter to react. For many substances the rate of indirect photolysis is much larger than the rate of direct photolysis (Deneer et al., 2010, p 19, but also Burrows et al., 2002 and Apell et al., 2019). In section 5.2 below indirect and direct photolysis of pesticides is considered in more detail; also the likely difference between indirect photolysis rates of pesticides found in cosm studies versus rates in real-life edge-of-field watercourses has been evaluated. In section 5.3 the effect of the penetration depth of UVB radiation into water on the estimated size of the degradation rate coefficient is established.

In pesticide registration dossiers the three types of transformation are evaluated by three different types of studies, aimed at obtaining transformation rates. For hydrolysis experiments at three different pH levels are performed in the laboratory, which next allows for the estimation of a hydrolysis rate at any given pH using a set of equations. The biotic transformation rate is evaluated in minimally two types of water-sediment test systems in the laboratory, containing sediment and an overlying water layer in which the decline is measured as a function of time. The water-sediment systems are kept in the dark, to exclude degradation by light. For photolysis various studies are required in the registration procedure, which will be described in Chapter 6.

5.2 Indirect and direct photolysis

Mechanisms causing indirect photolysis
Indirect photolysis of a pesticide is caused by photoreactions of other compounds ('photosensitizers') that generate reactive species (e.g. OH radicals) which can degrade the pesticide. Indirect photolysis of pesticides that are not susceptible to direct photolysis may occur because indirect photolysis may involve reaction mechanisms that are completely different from those of direct photolysis; e.g. OH radicals produced by the photolysis of NO_3 may lead to oxidation of pesticide molecules that are not susceptible to direct photolysis. The main photosensitizers in agricultural surface waters are DOM and nitrate (Lam et al., 2003; Katagi, 2018). DOM produces a range of species including triplet DOM, H_2O_2, superoxide radical anion, hydroxyl radicals and singlet oxygen whereas nitrate produces only hydroxyl radicals (Remucal, 2014). These photoreactions require also photons with high radiation energies so it seems defensible to assume that also indirect photolysis is directly proportional to the UVB irradiance. E.g. nitrate has absorption maxima at 200 and 300 nm (Vione et al., 2005); the maximum at 200 nm is not relevant because such photons do not reach the surface of the earth.

So we can conclude that:
Indirect photolysis has no relationship with the absorption spectrum of the pesticide
The indirect photolysis rate can be assumed directly proportional to UVB irradiance.

Mechanisms causing direct photolysis
Direct photolysis in natural waters involves the transformation of a chemical resulting from the direct absorption of a solar photon. It is a complex process depending on a number a factors, such as (i) the chemical structure and electronic absorption spectrum of the chemical, (ii) the quantum yield of the photochemical reaction (i.e. fraction of amount of reactant consumed or product formed and the amount of photons absorbed) and (iii) the solar photon irradiance to which the chemical is exposed (OECD 316, 2008).

Relative importance of indirect and direct photolysis
Remucal (2014) reviewed the role of indirect photolysis for pesticides. The review was based on about 400 references, so there is a very large amount of literature available. Main generic conclusions were: (i) DOM may both increase and decrease the photolysis rate, (ii) in many photolysis studies with natural waters the concentration of DOM and nitrate are not reported, (iii) in many studies direct photolysis controls (i.e. experiments in pure water) are not included. The review includes statements for individual pesticides on whether they undergo direct and/or indirect photolysis: we found statements for in total 90 pesticides of which 57 (so about 60%) showed direct photolysis. For 77 pesticides statements were found on whether they undergo indirect photolysis and this was the case for 64 pesticides (so about 80%). The population of pesticides that shows direct photolysis does not overlap completely with the population that shows indirect photolysis: there are pesticides that show direct photolysis but no indirect photolysis and vice versa. The combination yes-direct & no-indirect applied to 13 pesticides while the combination no-direct & yes-indirect applied to 32 pesticides; furthermore the yes-yes combination applied also to 32 pesticides (see Table 5.1). For 17 of the pesticides statements were found on the effect of adding nitrate: in all cases this led to higher photolysis rates. The population of these 90 pesticides is of course not representative of all pesticides because the review did not consider publications on pesticides that show no photolysis at all (which are of course scarce). So we cannot draw conclusions for the population of all pesticides. The data indicate that if a pesticide shows direct photolysis the probability that it also shows indirect photolysis is 32/(13+32) so about 70%. Furthermore they indicate that if a pesticide shows indirect photolysis, the probability that it also shows direct photolysis is 32/(32+32), so about 50%. These percentages may be somewhat biased because they may be influenced by the incentive to perform and publish a photolysis study with a certain pesticide. It would be interesting to know what the probability is that indirect photolysis occurs if there is no direct photolysis (because the dossier contains information on direct photolysis but usually not on indirect photolysis). This is impossible because the review did not consider pesticides that show no photolysis at all. In view of the fact that 64 of the 77 pesticides studied show indirect photolysis whereas only 45 show direct photolysis, the review gives the impression that indirect photolysis is at least as important as direct photolysis when estimating photolysis rates of pesticides in surface water.

With respect to our example pesticides, the review indicated that imidacloprid and metribuzin showed direct photolysis and that information on indirect photolysis was not available while metamitron showed both direct and indirect photolysis.

Table 5.1   *Numbers of pesticides that showed combinations of occurrence of direct and indirect photolysis derived from the review by Remucal (2014).*

		Indirect		Sum
		Yes	**No**	
Direct	Yes	32	13	45
	No	32		
Sum		64		

Indirect photolysis rates in outdoor cosms versus rates in edge-of-field watercourses
Outdoor mesocosm studies are performed to assess ecotoxicological effects in a more realistic way than is done in the laboratory lower-tier assessments. Mesocosms intend to represent the aquatic ecosystem in edge-of-field watercourses. These watercourses receive nitrogen and phosphorus from the adjacent agricultural fields and therefore tend to be eutrophic (or sometimes even hypertrophic).

Outdoor mesocosms generally represent a mesotrophic to eutrophic system having favourable conditions for sustaining the wished type of aquatic ecosystem. Note that the trophic state defines the nutrient content of the ecosystem (mainly determined by nitrogen and phosphorus): eutrophic systems are characterised by a relatively high availability of inorganic nutrients and may support a high biomass of rooted aquatic plants, particularly if the availability of nutrients from sediment is relatively high compared to that in the water column. Hypertrophic systems are (very) nutrient-rich in both the sediment and water compartments and frequently have algal blooms, a situation not favoured in outdoor cosm studies. Mesotrophic systems have an intermediate nutrient status and support a diverse aquatic community, as wished in cosm studies. One of the reasons that the cosms generally are mesotrophic in the water layer, and not eutrophic, is that the cosm experiments are often performed during spring and early summer, so during periods that rooted vascular plants by their growth trap most of the available inorganic N and/or P in the cosms, thus lowering their concentration in the water column in particular.

Indirect photolysis rates are higher for increased nitrate concentrations (section 5.1). This implies that the indirect photolysis rates determined from mesotrophic to eutrophic outdoor cosm studies generally are lower than the indirect photolysis rates in more nutrient-rich edge-of-field watercourses. So the rates estimated for the outdoor cosms are likely to be on the conservative side. So, when using the $DegT_{50}$ values obtained by inverse modelling of the behaviour in the cosms, risks for the aquatic ecosystems in real-life watercourses tend to be overestimated, which is good practice in risk assessment procedures for registration of pesticides.

5.3 Effect of penetration depth of UVB on estimated degradation rate coefficient

It is commonly observed that the attenuation of UVB radiation in surface water can be described with an exponential function (de Lange, 1999):

$$I_z = I_0 \exp\left(-\alpha z\right)$$

(5.1)

where z is the water depth (m), I_z and I_0 are the daily irradiances at depth z and at the water surface (J m^{-2}), and a is the vertical attenuation coefficient for downward irradiance (m^{-1}).

De Lange (1999) measured the attenuation of UVB light with depth in a number of Dutch surface waters including seven ditches in spring 1998. The attenuation was characterised by the depth at which still 1% of the UVB light intensity at the water surface was measured (i.e. ln(100)/a). The seven ditches were from three distinctly different locations and included three experimental ditches from one location. This 1%-depth of the seven ditches ranged between 7 and 46 cm (corresponding with a range of a from 0.10 to 0.66 cm^{-1}, so 10 to 66 m^{-1}) and the median and average 1%-depths were 12 and 21 cm (corresponding with a values of 38 and 22 m^{-1} respectively). The 1%-depths for two ponds were found to be 21 and 29 cm. The 1%-depths for nine lakes or canals ranged between 9 and 51 cm with a median of 37 cm and an average of 31 cm. So considering the median and average depths, the ditches showed the strongest extinction but the range for the ditches was almost as wide as that for the other systems.

De Lange (1999) developed a number of regression equations to predict a based on properties of the water systems that are usually measured (such as pH, DOC, chlorophyll-a, ash mass etc.). Considering all systems, a was influenced by the concentrations of (i) humic substances, (ii) organic particulate matter, and (iii) inorganic particulate matter. They obtained a correlation coefficient of 0.78 with a regression equation that used absorbance at 250 nm and the concentrations of chlorophyll-a and ash mass. However, absorbance measurements are usually not available (e.g. Arts et al., 2006). Using only quantities that are mostly available, they found a maximum correlation coefficient of 0.38 for an equation that used only TOC. So estimating a for studies that are currently available in the dossiers is likely to result in considerable uncertainty. As described before, later research showed that also nitrate contributes significantly to the absorption of UVB light.

Let us now consider the effect of a on the overall degradation rate coefficient of a water system. TOXSWA assumes perfect mixing in the vertical direction so we are interested in the depth-averaged rate coefficient $k_{z,av}$:

$$k_{z,av} = \frac{\int_0^d k_z \, dz}{d} \tag{5.2}$$

where d is the depth of the water system (m). This equation can be understood intuitively by its consequence that a constant k_z over $x\%$ of the depth and a zero k_z for the remaining $(100-x)\%$ gives a $k_{z,av}$ that is $x\%$ of k_z; e.g. if k_z is non-zero and constant over e.g. 30% of the depth and zero for the remaining 70%, $k_{z,av}$ equals 30% of k_z.

We distinguish two options: direct and indirect photolysis. Pesticide concentrations are usually orders of magnitude lower than concentrations of photosensitizers such as nitrate and dissolved organic matter. So the depth-dependency of the irradiance (so a) will not be influenced by the pesticide concentration. In case of direct photolysis we assume that the photodegradation rate coefficient is directly proportional to I_z (e.g. OECD, 2008).

The assumption of a photodegradation rate coefficient that is directly proportional to I_z gives the following relationship:

$$k_z = \varphi I_0 \exp(-\alpha z) \tag{5.3}$$

where k_z is the photodegradation rate coefficient at depth z (d^{-1}) and φ is a proportionality factor ($J^{-1} m^2 d^{-1}$). So

$$k_{z,av} = \varphi I_0 \frac{1 - \exp(-\alpha d)}{\alpha d} \tag{5.4}$$

We define $f_{red,dir}$ as the reduction factor (-) for the rate coefficient due to the vertical attenuation in the water system, so

$$f_{red,dir} = \frac{k_{z,av}}{k_{av,max}} \tag{5.5}$$

where $k_{av,max}$ is the maximum possible $k_{z,av}$. This maximum is found if $a = 0$, i.e. no attenuation at all, so $k_{max} = \varphi I_0$. This gives:

$$f_{red,dir} = \frac{1 - \exp(-\alpha d)}{\alpha d} \tag{5.6}$$

Figure 5.1 shows that $f_{red,dir}$ decreases strongly with increasing a and also that this decrease slows down. As described above a of seven Dutch ditches ranged from 10 to 66 m^{-1}. Figure 5.1 shows that $f_{red,dir}$ then ranges from 0.03 to 0.2 for a water depth of 50 cm, i.e. about a factor 7 difference. This indicate that for direct photolysis the reduction of the rate coefficient due to the vertical attenuation of the UVB irradiance is usually considerable and also that the expected uncertainty in a may lead to a large uncertainty in the overall degradation rate coefficient of the water system.

If we would assume that the vertical attenuation is completely determined by the concentration of the pesticide (which is unlikely as described above), then the parameter a would become proportional to the pesticide concentration. This will give the same equation for $k_{z,av}$ because this concentration is assumed constant with depth. However, then a will decrease with time if the pesticide concentration

decreases with time; so then $k_{z,av}$ will increase with time (probably resulting in an approximately zero-order overall degradation rate because a given daily irradiance can degrade a given mass of pesticide per surface area). We will not consider this option because it is considered unlikely.

In case of indirect photolysis we assume that the rate coefficient is proportional to the absorption rate of the UVB irradiance:

$$k_z = \chi \left| \frac{dI_z}{dz} \right| = \chi I_0 \, \alpha \exp\left(-\alpha z\right) \tag{5.7}$$

where χ is a proportionality factor (J^{-1} m^3 d^{-1}). The background of this assumption is that the rate coefficient is assumed directly proportional to the concentration of reactive species (e.g. OH radicals, singlet oxygen) generated by photosensitizers. All of these reactive species except H_2O_2 have probably a very short lifetime (e.g. in the order of microseconds for OH radicals in water; Attri et al., 2015). The concentration of the reactive species (c_r, mg m^{-3}) can then be approximated by the steady state value that follows from:

$$\frac{dc_r}{dt} = +p - k_r \, c_r = 0 \tag{5.8}$$

where p is the production rate (mg m^{-3} d^{-1}) and k_r is the dissipation rate coefficient of the species (d^{-1}). The steady state value of c_r equals then p / k_r. So the rate coefficient for indirect photolysis then is directly proportional to the production rate p which in turn is directly proportional to the absorption rate of the photons at a given depth, i.e. the derivative of I_z with depth. This steady-state approach will not hold for less reactive species such as H_2O_2 whose concentration may build up during a day. However, it is also unlikely that a less reactive species contributes strongly to the degradation of a pesticide so we will not consider this possibility any further.

We obtain then the following expression for $k_{z,av}$

$$k_{z,av} = \chi I_0 \frac{1 - \exp(-\alpha d)}{d} \tag{5.9}$$

In this case $k_{av,max}$ corresponds with the case that all UVB irradiance is absorbed in the water, so $a = \infty$ and $k_{max} = \chi I_0 / d$. This gives:

$$f_{red,ind} = 1 - \exp\left(-\alpha d\right) \tag{5.10}$$

Figure 5.1 shows that there is only reduction at a values below 10 m^{-1} for a water depth of 50 cm. The background of this phenomenon is that the reduction is caused by the irradiance that is not absorbed and thus reaches the bottom of the ditch. For a water depth of 20 cm, the range of a from 10 to 66 m^{-1} gives an $f_{red,ind}$ range from 0.86 to 1.0. So in case of indirect photolysis the effect of a on the observed overall degradation rate coefficient is expected to be small.
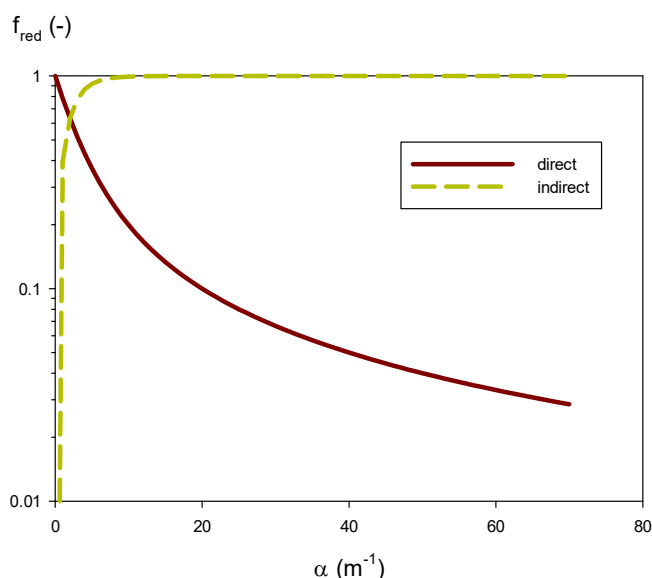
Figure 5.1 *The reduction factor f_{red} as a function of the attenuation coefficient a for a water depth d of 50 cm considering both direct and indirect photolysis.*

Please note that the equations for $k_{z,av}$ both for direct and indirect photolysis are decreasing functions of the water depth d. For a fixed value of a, both equations indicate that the effect is directly proportional to the factor $[1-exp(-ad)]/d$. Figure 5.2 shows that a may have a considerable effect for water depths shallower than 0.3 m; however, for larger water depths the lines coincide almost exactly. They coincide almost exactly with the line for $1/d$ (not shown) because the exponential functions then generate values close to zero. Mesocosms will almost always have water depths of at least 0.3 m, so for all practical purposes the effect of depth on $k_{z,av}$ can be described by assuming that $k_{z,av}$ is directly proportional to $1/d$. The background of this is as follows: if a cosm has a water depth that is deep enough to ensure that all UVB has been absorbed, then enlarging the water depth does not increase the total amount that is transformed (both for direct and indirect photolysis) and thus $k_{z,av}$ is proportional to $1/d$. The a value of 10 m^{-1} corresponds with a 1% penetration depth of UVB of 46 cm which corresponds with 5% penetration at 30 cm.
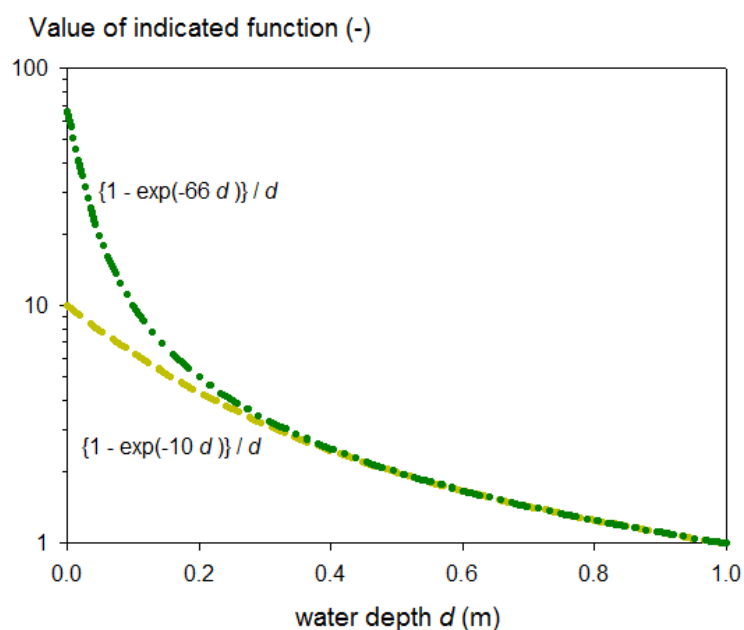
Figure 5.2 *Proportionality factor for effect of depth on average degradation rate coefficient for $a = 10$ m^{-1} and $a = 66$ m^{-1}.*

Conclusions

In case of direct photolysis, uncertainty in the attenuation of UVB light with depth (expressed in the factor *a*) leads for systems with water depths smaller than 0.3 m to considerable uncertainty in extrapolating an observed degradation rate coefficient to other systems. In case of indirect photolysis, the effect of this uncertainty is small. For water depths larger than 0.3 m, it can be assumed that the average degradation rate coefficient is proportional to the inverse of the water depth (both for direct and indirect photolysis).

6 Existing requirements for registration dossiers on photochemical degradation in surface water in the EU and USA

6.1 Introduction

In this chapter we summarize the information with respect to photochemical degradation in water that needs to be included in the registration dossiers. The exact relevant data requirements for active substances are specified in the EU Regulation 283/2013, in section 2 'Physical and chemical properties of the active substance' and in section 7 'Fate and behaviour in the environment' information with respect to radiation or degradation in the presence of light. Section 2.4 specifies that information on the ultraviolet-visible (UV-VIS) absorption spectra of the compound is required (Figure 6.1). Section 7.2 'Fate and behaviour in water and sediment' specifies that information on the direct photochemical degradation (OECD 316) and an irradiated water-sediment study (section 7.2.2.4 below, OECD 308) are required (Figure 6.2). Below we summarize these three types of study and conclude whether or how we can use the information of the study for the estimation of photochemical degradation in surface water in The Netherlands or the EU.

| 2.4. | Spectra (UV/VIS, IR, NMR, MS), molar extinction at relevant wavelengths, optical purity | OECD Test Guideline 101: UV-VIS Absorption Spectra | — |

Figure 6.1 *Excerpt of Commission Communication in the framework of the implementation of Commission Regulation (EU) No 283/2013 of 1 March 2013 setting out the data requirements for active substances, section 2 'Physical and chemical properties of the active substance'. The first column states the 'Reference to Part A of the Annex to Regulation (EU) No 283/2013', in the second and third column the relevant 'Test methods' and 'Guidance documents' are mentioned (see https://eur-lex.europa.eu/legal-content/EN/TXT/PDF/?uri=CELEX:52013XC0403(02)&from=EN for more details).*

7.2.	Fate and behaviour in water and sediment	—	—
7.2.1.	Route and rate of degradation in aquatic systems (chemical and photo-chemical degradation)	—	—
7.2.1.1.	Hydrolytic degradation	OECD Test Guideline 111: Hydrolysis as a Function of pH	—
7.2.1.2.	Direct photochemical degradation	OECD Test Guideline 316: Photo-transformation of Chemicals in Water - Direct Photolysis	—
7.2.1.3.	Indirect photochemical degradation	—	—
7.2.2.	Route and rate of biological degradation in aquatic systems	—	—
7.2.2.1.	"Ready biodegradability"	Method C.4 Determination of "ready" biodegradability (Annex to Regulation (EC) No 440/2008). OECD Guideline Test 301: Ready Biodegradability (301 A - F)	—
7.2.2.2.	Aerobic mineralisation in surface water	OECD Test Guideline 309: Aerobic Mineralisation in Surface Water - Simulation Biodegradation Test	ECHA Guidance on information requirements and chemical safety assessment Chapter R 11: PBT Assessment
7.2.2.3.	Water/sediment study	OECD Test Guideline 308: Aerobic and Anaerobic Transformation in Aquatic Sediment Systems	FOCUS Surface Water FOCUS Degradation Kinetics
7.2.2.4.	Irradiated water/sediment study	OECD Test Guideline 308: Aerobic and Anaerobic Transformation in Aquatic Sediment Systems	—
7.2.3.	Degradation in the saturated zone	—	—
7.3.	Fate and behaviour in air		FOCUS Air

Figure 6.2 *Excerpt of Commission Communication in the framework of the implementation of Commission Regulation (EU) No 283/2013 of 1 March 2013 setting out the data requirements for active substances, section 7 'Fate and behaviour in the environment' The first column states the 'Reference to Part A of the Annex to Regulation (EU) No 283/2013', in the second and third column the relevant 'Test methods' and 'Guidance documents' are mentioned (see https://eur-lex.europa.eu/legal-content/EN/TXT/PDF/?uri=CELEX:52013XC0403(02)&from=EN for more details).*

6.2 Ultraviolet-visible (UV-VIS) absorption spectra (OECD 101, 1981)

OECD Guideline 101 'UV-VIS absorption spectra (spectrophotometric method)' of 1981 provides guidance on the measurement of absorption of radiation in the ultraviolet-visible range. The primary environmental purpose of the measurements is to have 'some indication of the wavelengths at which

the compounds may be susceptible to photochemical degradation' (OECD 101, 1981). These spectra are assumed to be informative concerning the need for further persistence testing. Degradation will depend upon the total energy absorbed in specific wavelengths, characterised by both molar absorption coefficient (molar extinction coefficient) and band width. However, the guideline also states: 'the absence of measurable absorption does not preclude the possibility of photodegradation'.

Absorbance is measured in the ultraviolet-visible range, 200-750 nm, with a wavelength accuracy of ± 0.5 nm under three pH conditions, namely acidic (pH < 2), basic (pH > 10) and neutral. The latter is needed, because the absorption of a compound is due to its particular chemical form and different forms are present, depending on whether the test solution is acidic, basic or neutral. Absorption is measured in a spectrophotometer cell with a path length of usually between 0.1 and 10 cm and molar absorption coefficients are calculated for all absorbance maxima.

E.g. the Pesticides Properties DataBase (PPDB) of the University of Hertfordshire presents maximum UV-vis absorption coefficients (L mol^{-1} cm^{-1}) for its listed active ingredients. It gives as explanation for the Max UV-vis absorption (L mol-1 cm-1): 'Different compounds may have very different absorption maxima and intensities. The wavelength of the maximum absorbance is a characteristic value and so can be used for identification purposes'. Four example compounds give absorption maxima of 294 nm (metribuzin), 227 and 228 nm, 228 and 283 nm and 229 and 283 nm (pH of 1.16, 7.0 and 11.3, 2-4D with its pK_a of 3.40), no maximum (prosulfocarb) and 238, 310 and 390 nm (aclinofen) (Figure 6.3).

Max UV-Vis absorption L/mol cm	Different compounds may have very different absorption maxima and intensities. The wavelength of maximum absorbance is a characteristic value and so can be used for identification purposes.

Metribuzin

Maximum UV-vis absorption L mol^{-1} cm^{-1}	294nm = 8175 (mean)

2,4-D

Maximum UV-vis absorption L mol^{-1} cm^{-1}	pH 1.16: 227nm=7344.4, 228nm=1448.9 pH 7.0: 228nm=8815.6, 283nm=1940 pH 11.3: 229nm=8984.5nm, 283nm=1977.5

Prosulfocarb

Maximum UV-vis absorption L mol^{-1} cm^{-1}	>=295nm < 10, no absorbance maxima >210nm

Aclonifen

Maximum UV-vis absorption L mol^{-1} cm^{-1}	Neutral solution: 238nm = 18987, 310nm = 8431, 390nm = 6143

Figure 6.3 *Maximum absorption coefficients (L mol^{-1} cm^{-1}) for the ultraviolet-visible light range (200-750 nm) for four example compounds from the Pesticides Properties DataBase (PPDB) of the University of Hertfordshire (https://sitem.herts.ac.uk/aeru/ppdb/en/, accessed 24 May 2018).*

Concluding the information on the maximum UV-visible absorption coefficients are standardly available and they do give an indication whether the compound 'may be susceptible to photochemical degradation'. However, OECD (1981) also states: 'the absence of measurable absorption does not preclude the possibility of photodegradation', so the absence of absorption is no guarantee that photochemical degradation may not happen. This refers probably to the possibility of indirect photodegradation.

Besides, note that coefficients for wavelengths below 290 nm are not relevant for our purpose of degradation in surface water, because radiation of wavelength below 290 nm is already absorbed in the stratosphere and does not arrive at the earth's surface. Also absorption coefficients measured for the different chemical form of the compound at pH < 2 or pH > 10 are probably less relevant for degradation in natural surface waters, e.g. in Dutch surface waters the large majority of measured pH values were between 7 and 9.5 (Boesten et al., 2014).

6.3 Direct photochemical degradation in buffered pure water (OECD 316, 2008)

OECD Guideline 316 'Phototransformation of Chemicals in Water – Direct Photolysis' of 2008 provides guidance for conducting phototransformation in water studies to determine the potential effects of solar irradiation on chemical pollutants in surface water. So, as the studies are done in buffered, pure water, indirect aqueous photolysis, by photosensitizing or reaction with oxidizing transients, is not considered in this guideline.

In brief this guideline offers a tiered approach to determine direct photolysis. In a first tier the maximum possible direct photolysis rate constant is estimated based upon measured absorption coefficients from 290-800 nm for the chemical, tabulated solar irradiance for summer and 40º to 50º latitude and assuming the quantum yield is maximal, i.e. 1. In the second tier the rate of decline is measured in buffered, pure water exposed to a filtered Xenon arc lamp or sunlight. In the third tier the quantum yield for direct photolysis is experimentally determined, which can then be used to improve the estimation of the rate constant made in the first tier. The computations in tier 1 and 3 can be performed with the aid of existing computer programs, GCSOLAR from Zepp and Cline (1977), or ABIWAS from Frank and Klöpffer (1989), that both account for seasons, latitude and depth and light attenuation. However, they consider only long-term averages of the solar irradiance (See Annex 2).

In the second tier direct photolysis is measured in buffered pure water in photolysis cells in the laboratory for wavelengths between 290 and 800 nm, so for UV and the visible light spectrum with 290 nm being the cutoff of solar UV irradiation reaching the earth's surface. Used buffers or co-solvents should not absorb between 290 and 800 nm or be photosensitizers (paragraphs 34 and 38 of OECD 316). For non-ionisable test chemicals the tests should be conducted at a pH at which the test chemical is hydrolytically most stable in the pH range 4-9 (paragraph 39 of OECD 316). The guideline (paragraph 78) specifies how to convert the direct photolysis rate constant in a photolysis cell exposed to constant photon irradiances from a filtered Xenon arc lamp into the estimated direct photolysis rate constant for the test chemical in near surface clear natural water exposed to 24 hour average 290-800 nm daily solar photon irradiances (photon irradiance on amount basis, mmol cm^{-2} d^{-1}).

The study of the second tier can also be used to identify the major phototransformation products (>10% of applied radioactivity), to estimate their formation fractions and if possible, their formation and decline rates.

So, following OECD 316 and based upon the direct photolysis rate obtained in photolysis cells, a direct photolysis rate constant in near surface clear natural water for average daily solar radiation can be computed. In the absence of readily available daily $I_{act,UV-VitD}$ data we here use daily global radiation data to show that daily fluctuations are high, e.g. for Wageningen, The Netherlands in spring fluctuations range between approximately 5000 and 30000 kJ m^{-2} in the years 1954, 1975 and 1999 (Figure 6.4). So, $I_{act,UV-VitD}$ will probably also fluctuate strongly and any higher tier exposure estimate will need to take the daily fluctuations into account in order to estimate realistic direct photolysis rates for near surface clear natural waters.
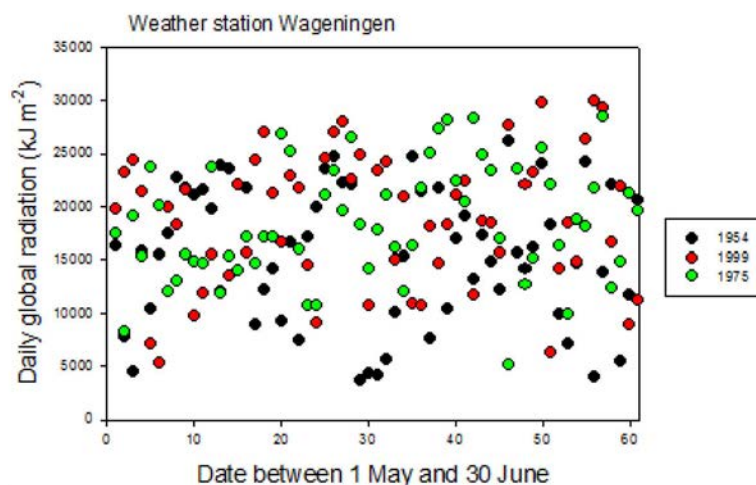
Figure 6.4 *Daily global radiation in spring as measured at weather station Wageningen in three different years. Note that 10000 kJ/m^2 corresponds with 1000 J/cm^2 (Boesten et al., 2014).*

For many substances the rate of indirect, or sensitised photolysis is much larger than the rate of direct photolysis (see Section 5.1). So, the direct photolysis rate determined following the OECD Guideline 316 does not represent the total photolysis rate in natural waters and the direct photolysis rate will be lower than the total photolysis rate.

To conclude on the usefulness for higher tier exposure estimates we have to evaluate whether the direct photolysis rate represents photochemical degradation in natural surface waters in a realistic or realistic worst case manner. On one hand, we have seen above that the direct photolysis rate of OECD 316 is overestimated because it represents direct photolysis in near surface clear natural waters, and does not account for extinction of light with depth. On the other hand the direct photolysis rate of OECD 316 underestimates the total photolysis rate, simply because indirect aqueous photolysis is not included. So, it is not possible to state whether concentrations in the higher tiers will be overestimated or underestimated. Therefore, our conclusion is that the direct photolysis rate according to OECD Guideline 316 is no good basis for higher tier exposure estimates for the aquatic risk assessment in The Netherlands or at EU level.

The photolysis test of the second tier is however useful to identify the major phototransformation products (>10% of applied radioactivity), to estimate their formation fractions and if possible, their formation and decline rates.

6.4 Irradiated aerobic and anaerobic degradation in aquatic sediment systems (OECD 308, 2002)

OECD Guideline 308 'Aerobic and anaerobic transformation in aquatic sediment systems' of 2002 describes a laboratory test method to assess aerobic and anaerobic transformation in aquatic sediment systems. The method permits the measurement of transformation rates as well as identification and quantification of transformation products and their distribution between water and sediment. At least two sediments different with respect to organic matter content and texture should be used.

Although section 7.2.2.4 of EU Regulation 283/2013 mentions 'irradiated water-sediment studies' and refers to OECD Test Guideline 308 on 'Aerobic and anaerobic degradation in aquatic sediment systems, (Figure 6.2) the guideline itself states that 'The test should be performed in the dark at ...' and makes no reference to irradiation in any part of the text. Therefore, no degradation rates of irradiated water-sediment systems are standardly measured and thus these are not standardly available as part of the registration dossiers.

6.5 Direct and indirect photolysis in water (OPPTS 835.2210 and 835.5270, US-EPA, 1998)

OPPTS 835.2210 (EPA, 1998a)

Ten years before the OECD, EPA (1998a) published a guideline for assessing the direct photolysis rate in water. This guideline can be considered as a precursor of OECD-316 (2008). So we limit ourselves here to a short description. The first tier is identical to OECD-316: the upper limit of the photochemical rate coefficient for exposure to sunlight is calculated from the absorption as a function of the wavelength of the light assuming that the quantum yield is 1 (i.e. the maximum possible value). The second tier consists of two sub-tiers (called 'phases'): (1) measurement of the decline of the concentration of the chemical in quartz tubes exposed to sunlight, and (2) measurement of this decline parallel to measurement of the decline of the concentration of p-nitroacetophenone (PNAP) in quartz tubes which is used as an actinometer. The principle is that the reaction quantum yield of PNAP (φ_a) is known and that the reaction quantum yield of the chemical φ_c can be estimated from (OECD-316, Eqn 19):

$$\varphi_c = \frac{k_c}{k_a} \frac{\sum \varepsilon_{a,\lambda} \, L_\lambda}{\sum \varepsilon_{c,\lambda} \, L_\lambda} \varphi_a \qquad\qquad (6.1)$$

where k_c and k_a are the observed rate coefficients for decline of the chemical and PNAP, respectively, $\varepsilon_{c,\lambda}$ and $\varepsilon_{a,\lambda}$ are molar absorption coefficients at wavelength λ of the chemical and PNAP, respectively, L_λ is irradiance at wavelength λ to which the systems are exposed and where the summations are over the range of λ from 290 to 800 nm.

The main differences between OECD (2008) and EPA (1998a) are:
\# OECD prefers exposure to a Xenon lamp in the laboratory instead of exposure to sunlight
\# OECD prefers use of spectral radiometers to measure the irradiance instead of chemical actinometers (paragraph 60) but acknowledges that these are expensive and not always readily available
\# OECD includes identification of photometabolites whereas EPA does not consider metabolites.

OPPTS 835.5270 (EPA, 1998b)

Introduction
Photolysis is assumed to occur by direct absorption of sunlight or indirectly by chemical or electronic excitation transfer from light-absorbing humic species in natural water. The aim of the test is to determine whether indirect photolysis is significant compared to direct photolysis (step 1) and if yes, to estimate a rate coefficient that includes both indirect and direct photolysis for a surface water with an approximately average concentration of humic acids (step 2).

Step 1: screening test
The principle of this test is comparison of the degradation rates of the chemical in synthetical humic water (SHW) and pure water (PW). The SHW is prepared by dissolving humic acid in pure water which is diluted to give an absorbance of 0.05 at 370 nm. A phosphate buffer is added to keep the pH at 7. This procedure gives a DOC of about 5 mg/L. This combination of absorbance, pH and DOC is considered characteristic of many surface fresh waters in the USA. The PW also contains this buffer.

The solutions are transferred into quartz tubes which are exposed to natural sunlight outdoors for 1 to 16 d (preferably warm clear-sky weather). Dark control tubes are included both for SHW and PW. If losses occur in the dark controls, more detailed experiments are needed (no further guidance provided).

If less than 20% photoreaction occurs in SHW after 16 d, then step 2 is not needed: the chemical is considered 'photoinert'. If more than 80% photoreaction occurs in SHW after 1 d, then step 2 is not needed as well: the chemical is considered 'photolabile'.

Otherwise the ratio *R* of the photolysis rate coefficient in SHW divided by this rate coefficient in PW is calculated. If *R*<1, the photoreaction is inhibited by the SHW so step 2 is not needed. If 1<*R*<2, moving to step 2 is optional and if *R*>2 step 2 has to be performed.

The criterion *R*>2 is considered to be conservative because SHW is subject to 'photobleaching' meaning that the concentration of the humic acids decreases by exposure to sunlight.

Step 2: indirect photoreaction including actinometer measurements
The aim of step 2 is to obtain a more accurate estimate of the photolysis rate coefficient in SHW by including an actinometer to measure the fluctuations in the radiation and by including a SHW-solution without test chemical to correct for the decline of the humic acid concentration in the SHW-solution due to photobleaching during the experiment.

The actinometer measures the decline of the concentration of p-nitroacetophenone (PNAP) by exposure to sunlight. The background is that the relationship between the rate coefficient for this decline and the sunlight intensity is well known as a function of the concentration of pyridine that is added. By choosing an appropriate pyridine concentration, a decline rate of PNAP can be generated that is suitable for the time period of the experiment. The measured decline of PNAP is then used to transform the measured decline of the test substance in SHW to clear-sky conditions.

Four types of solutions are prepared in quartz sample tubes:
1. the PNAP actinometer solution
2. test chemical in pH-7 buffer of PW
3. test chemical in pH-7 buffer of SHW
4. pH-7 buffer of SHW.

The tubes are exposed to natural sunlight outdoors (including dark controls) for periods ranging between 1 h and 32 d. The dark controls are assumed to show no losses of PNAP and test chemical and no changes in properties of the SHW.

Solution 4 is used to determine the decline of the rate coefficient in SHW due to degradation of humic acids (photobleaching). This is done by measuring the decline in absorbance at 370 nm. Solution 1 is used to correct for fluctuations in light intensity.

The endpoint of the study is the 'net environmental photoreaction' rate coefficient that applies to clear-sky conditions and water bodies with an average concentration of humic acids. The guideline states (p. 14) that it is valid only for the experimental latitude and season. The background of this limitation is probably that the quantum yield of the chemical cannot be derived from the parallel measurement of the declines of the chemical and PNAP because indirect photolysis is not related to the absorption spectrum of the chemical.

To the best of our knowledge this is the only guideline for assessing indirect photolysis. It is based on the assumption that indirect photolysis is caused by humic acids. However, Lam et al. (2003) showed that high nitrate concentrations may result in faster indirect photolysis than DOM and mechanisms of degradation induced by DOM and nitrate are different. So this guideline can only give an indication of the susceptibility of the molecule to indirect photolysis. It seems not useful for our purpose because it generates information that cannot be extrapolated to the range of environmental conditions in the EU.

6.6 Conclusions on relevance of existing guidelines for this guidance

The OECD Guideline 101 'UV-VIS absorption spectra (spectrophotometric method)' of 1981 provides an indication whether the compound 'may be susceptible to photochemical degradation', but at the same time 'the absence of measurable absorption does not preclude the possibility of photodegradation', so the absence of absorption is no guarantee that photochemical degradation may

not happen. So, its usefulness with respect to evaluating whether a compound may undergo photochemical degradation is limited. Thus this test is not useful for the purpose of higher-tier exposure estimates in the framework of regulatory risk assessment.

OECD Guideline 316 'Phototransformation of Chemicals in Water – Direct Photolysis' of 2008 provides guidance for conducting phototransformation in water studies to determine the potential effects of solar irradiation on chemical pollutants in surface water. The studies are done in buffered, pure water, and thus indirect aqueous photolysis, by photosensitizing or reaction with oxidizing transients, is not considered in this guideline. Moreover, because the degradation is measured in photolysis cells used in the laboratory, photolytic degradation in near surface clear natural water is represented that thus overestimates the photolytic degradation in surface water bodies where light extinguishes with depth. So, we do not know whether the photolytic degradation in water is over- or underestimated in this test, and thus its degradation rates cannot be used in higher-tier exposure estimates in the framework of regulatory risk assessment.

OECD Guideline 308 'Aerobic and anaerobic transformation in aquatic sediment systems' of 2002 describes a laboratory test method to assess aerobic and anaerobic transformation in aquatic sediment systems. However, no reference is made to the irradiation in the text and moreover, the studies are not standardly available in registration dossiers (only water-sediment studies *in the dark* are an actual data requirement). So, they are of no use for the estimation of higher tier photolytic degradation rates in water.

The EPA OPPTS 835.2210 guideline (1998a) for assessing the direct photolysis rate in water, was published ten years before the OECD 316 guideline. Thus the EPA guideline can be considered as a precursor of OECD-316 (2008) and therefore we do not evaluate the EPA guideline here.

The EPA OPPTS 835.5270 (1998b) assumes photolysis to occur by direct absorption of sunlight or indirectly by chemical or electronic excitation transfer from light-absorbing humic species in natural water. The aim of the test is to determine whether indirect photolysis is significant compared to direct photolysis and if yes, to estimate a rate coefficient that includes both indirect and direct photolysis for a surface water with an approximately average concentration of humic acids. However, Lam et al. (2003) showed that high nitrate concentrations may result in faster indirect photolysis than DOM and mechanisms of degradation induced by DOM and nitrate are different. So the EPA guideline can only give an indication of the susceptibility of the molecule to indirect photolysis. Therefore, it seems not useful for our purpose because it generates information that cannot be extrapolated to the range of environmental conditions in the EU.

So, the overall conclusion is that at present there are no useful guidelines to determine the photolysis rates in natural surface waters, that can be used for the purpose of higher-tier exposure estimates in the framework of regulatory risk assessment.

7 Standardisation of measured DegT$_{50,photo}$

7.1 Introduction

In the aquatic risk assessment of the pesticide registration procedure a tiered approach is followed going from simple and conservative lower tiers to more sophisticated and realistic higher tiers. Generally in the lower tiers laboratory studies are used to characterise the behaviour of the pesticide in the environment, while in higher tier parameters obtained in more realistic studies may be used, e.g. performed in the field. This is especially true for photolysis studies, which in the laboratory are performed with artificial light, differing in absorption spectra from the natural light in outdoor experiments, such as outdoor cosm studies where the decline of the pesticide has been measured in the water layer as a function of time.

As argued in Chapters 2 and 3 we propose to assume that the rate coefficient for photolysis is proportional to the intensity of the daily incoming actual UV-VitD radiation. This represents the incoming daily UV radiation at the earth surface with the Vitamin-D action spectrum; this spectrum represents effects of UV on many larger organic molecules, of which pesticides may be representations. Its main contribution is from UVB, but it also takes some contribution from UVA (section 3.2.3).

So,

$$k_{photo} = k_{ref,photo} \left(\frac{I_{actual,UVB-VitD}}{I_{ref,actual,UVB-VitD}} \right) \tag{7.1}$$

where k_{photo} is the rate coefficient for photochemical degradation (d^{-1}), $k_{ref,photo}$ is the k at reference daily actual UV-VitD radiation $I_{ref,actual,UV-VitD}$ (J.m^{-2}) and $I_{actual,UV-VitD}$ is the daily actual UV-VitD radiation (J.m^{-2}). Note that this radiation refers to a daily <u>dose</u>, so an amount of radiation summed up over a period in time, here a day. For the $DegT_{50,photo}$ the equation reads:

$$DegT_{50,water,photo} = DegT_{50,water,photo,ref} \left(\frac{I_{ref,actual,UVB-VitD}}{I_{actual,UVB-VitD}} \right) \tag{7.2}$$

where $DegT_{50,water,photo,ref}$ is the half-life $DegT_{50,water,photo}$ (d) at the reference daily actual UV-VitD radiation. Daily actual UV-VitD radiation varies in the Central Zone of the EU typically from approximately 2000 J.m^{-2} to 8000 J.m^{-2} in the period April to October, which is the period when most pesticide applications are done (Data Geodesk WUR, May 2019). Therefore we propose to use a reference daily actual UV-VitD radiation $I_{ref,actual,UV-VitD}$ of 5000 J.m^{-2}. This reference value is an arbitrary value needed to standardize $DegT_{50,water,photo}$ values obtained from different outdoor experiments. E.g. a $DegT_{50,water,photo}$ of 10 d at $I_{actual,UV-VitD}$ = 5000 J.m^{-2} is identical to a $DegT_{50,water,photo}$ of 5 d at $I_{actual,UV-VitD}$ = 10 000 J.m^{-2}. So, if different $DegT_{50,water,photo}$ values have to be averaged, they have to be calculated back first to the same reference value $I_{ref,actual,UV-VitD}$.

Note that the $I_{actual,UV-VitD}$ time series to be used in the surface water scenarios of the aquatic risk assessment represent daily values that characterise the scenarios. So, they are not related to the reference value $I_{ref,actual,UV-VitD}$. The $DegT_{50,water,photo}$ for the scenarios ($DegT_{50,water,photo,scen}$) can be calculated with

$$DegT_{50,water,photo,scen} = DegT_{50,water,photo,ref} \left(\frac{I_{ref,actual,UVB-VitD}}{I_{scen,actual,UVB-VitD}} \right) \tag{7.3}$$

where $I_{scen,actual,UV-VitD}$ is the daily actual UV-VitD radiation of the scenario. These have been determined in Chapter 4, both for the Dutch scenarios as the EU FOCUS surface water scenarios.

In addition to a dependence on the incoming daily actual UV-VitD radiation, the half-lives for photochemical degradation in outdoor cosms, $DegT_{50,water,photo}$, also vary as function of the water depth, due to extinction of UV radiation with depth in the water column (section 5.3), and the radiation actually entering the cosm water. Therefore, to be able to compare photolytic degradation half-lives observed in different outdoor waters we consider the following four factors to standardize the rates found:

1. The amount of incoming UV-VitD radiation, by using a reference daily incoming actual UV-VitD radiation, $I_{act,UV-VitD}$, of 5000 J/m^2;
2. The water depth to account for extinction of UV radiation with depth, by standardizing the degradation rate to the rate in a 30-cm deep water layer (section 5.3);
3. The coverage of the water surface area by water plants blocking the incoming radiation, by standardizing to a rate for no coverage, and
4. The skyview factor to account for parts of the surface area that are shaded by the rim of the outdoor cosm, by standardizing to a rate for a skyview factor of 1.

In sections 7.2 and 7.3 we describe how the standardisation on coverage of the surface water area by water plants and by use of the skyview factor can be done.

Note that the approach above implicitly assumes that photolysis is the main process for degradation in the outdoor cosm and the role of hydrolysis and biotransformation can be neglected. So, in the equation below k_{hydr} and k_{bio} are negligible compared to k_{photo}.

$$k_{total} = k_{photo} + k_{hydr} + k_{bio}$$ (7.4)

So, only when photolysis is the dominant degradation process standardisation on basis of the radiation intensity is defensible. This should be evaluated by e.g. considering the dossier data on hydrolysis rates or on dissipation rates in water-sediment studies in the dark (see also the flow chart in Chapter 15).

7.2   Coverage of water surface by water plants

Photolytic degradation in surface water is a function of the available UV-VitD radiation within the water column. In the outdoor cosm studies water plants may be present and they may block the incoming radiation, i.e. part of the water column may be shaded. In order to be able to standardise the estimated $DegT_{50,water,photo}$ of the cosms it is necessary to quantify the water plants present.

For each cosm study the available information on macrophyte (water plant) data was scrutinized concerning the type, amount and coverage of the cosms. The coverage percentage was not always determined, and moreover, in the ecotoxicological literature the coverage is related to the percentage of macrophytes covering the bottom of the cosm generally without mentioning where in the water column the macrophytes are present. As we are interested in the amount of radiation that cannot enter the water column, we are interested in macrophytes that cover water surface area. Thus we considered only macrophytes that float on the water or emerge above the water surface. So, we did not consider macrophytes below the water surface, which is defensible in view of the generally fast extinction with depth (section 5.3). So, we finally deduced the surface area coverage percentage from the type of macrophytes, the amount and month of the experiment (determining the growth stage of the macrophytes).

Most pesticide mass in the water is degraded in the beginning of the experiment. After a lapse of time equal to $2*DT_{50,water}$, i.e. two dissipation half-lives in water, only 25% of the pesticide mass is present, and after $3*DT_{50,water}$ only approx. 10% of the mass is still present in the water layer. This implies that the coverage percentage should be determined for the period immediately after the application of the pesticide up to approximately 3 $DT_{50,water}$ days later.

7.3 Procedure for calculation of skyview factors for cosm experiments

Introduction
Cosm experiments are conducted in different types of systems. This section describes the procedures for the calculation of the skyview factor for the most common systems.

As most of the UV radiation is diffuse, we calculated the skyview factor based on the fraction of the hemisphere that is seen from a certain point (so without considering the direction of the beam of the sunlight).

Procedure for a cylinder
We consider first a cylinder that is impervious to UVB light and with a water level that is at a certain depth below the rim of the cylinder (e.g. the study by Brock et al., 2004).

The calculation is done in two steps: first the skyview factor is calculated for a certain point C on the water surface at distance r from the centre Figure 7.1 and thereafter the average skyview factor is calculated from the relationship between the skyview factor and the distance r.
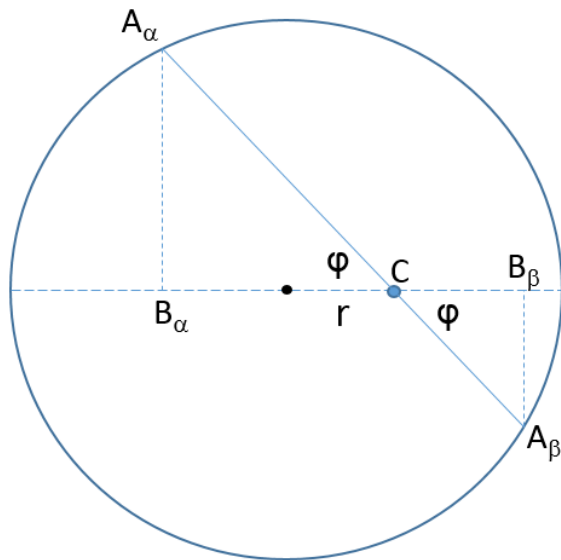
Figure 7.1 *The horizontal plane of the cylinder showing the line Aα Aβ that passes through a point C at a distance r from the centre and that makes an arbitrary angle φ with the horizontal line passing through the centre of the circle.*

At this point C we can define angles α, β and γ as shown in Figure 7.2. The skyview factor Ψ_s at this point C then equals then γ / p with $p = \pi$ rad and γ can be calculated as

$$\gamma = p - \alpha - \beta \tag{7.5}$$

We have to average Ψ_s considering all directions for diffuse radiation, so considering all possible angles φ in Figure 7.1. Because of symmetry we can limit φ to the range between 0 and π/2. The angles α and β can be calculated from the distances $A_\alpha C$ and $A_\beta C$ as their tangens equals $h / A_\alpha C$ and $h / A_\beta C$, respectively (Figure 7.2). Considering the triangle $A_\alpha B_\alpha C$ it follows from Figure 7.1 that:

$$A_\alpha B_\alpha^{\,2} + B_\alpha C^2 = A_\alpha C^2 \tag{7.6}$$

$$\tan(\varphi) = \frac{A_\alpha B_\alpha}{B_\alpha C} \tag{7.7}$$

$$A_\alpha B_\alpha^{\ 2} + \left(B_\alpha C - r\right)^2 = R^2 \tag{7.8}$$

where R is the radius of the cylinder (m) and r is the distance to the centre of the cylinder (m). This is a set of three equations with three unknowns ($A_\alpha B_\alpha$, $B_\alpha C$ and $A_\alpha C$) which can be solved straightforward to obtain $A_\alpha C$ (first derive $A_\alpha B_\alpha$ and $B_\alpha C$ from the last two equations and insert in the first equation). For the triangle $A_\beta B_\beta C$ a similar set of equations can be defined.
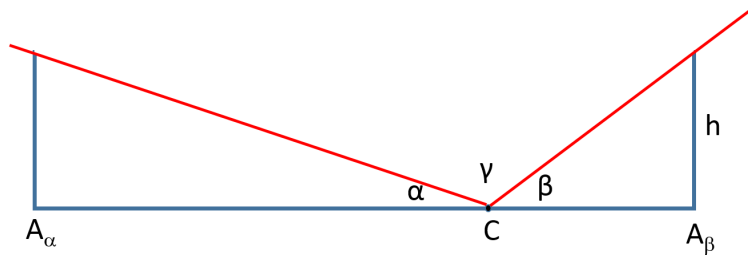
Figure 7.2   *Vertical plane through the line A_α A_β as shown in Figure 7.1 showing the angles α, β and γ needed to calculate the skyview factor at point C; h is the height of the rim above the water surface.*

The point C was varied in steps between the midpoint of the circle and the circumference. For each point C calculations were made using 100 φ values ranging from 0.5 to 99.5% of π/2 and the average value was taken. As an example we consider a cylinder with a radius of 0.525 m diameter whose rim is 25 cm above the water surface. This gives Ψ_s as a function of the distance r from the centre of the mesocosm as shown in Figure 7.3. The average Ψ_s over the surface of the circle was calculated as

$$\frac{\displaystyle\int_0^R \Psi_s \; r \; dr}{\displaystyle\int_0^R r \; dr} \tag{7.9}$$

This gives the horizontal line in the graph, i.e. 0.58.
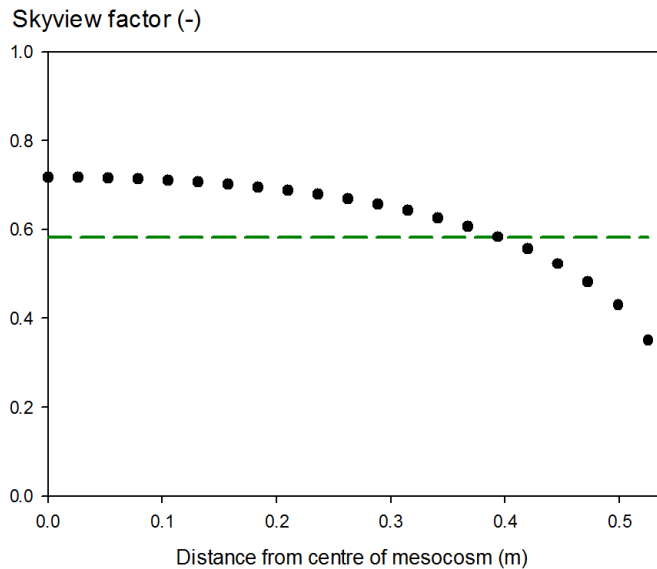
Figure 7.3 *The skyview factor as a function of the distance from the centre of the water surface within a cylinder with radius of 0.525 m whose rim is 25 cm above the water surface. The dashed line is the average for the cylinder surface.*

The level of the water surface of a mesocosm is of course not constant at exactly 25 cm below the rim. Figure 7.4 shows that the average Ψ_s is moderately sensitive to the height of the rim.
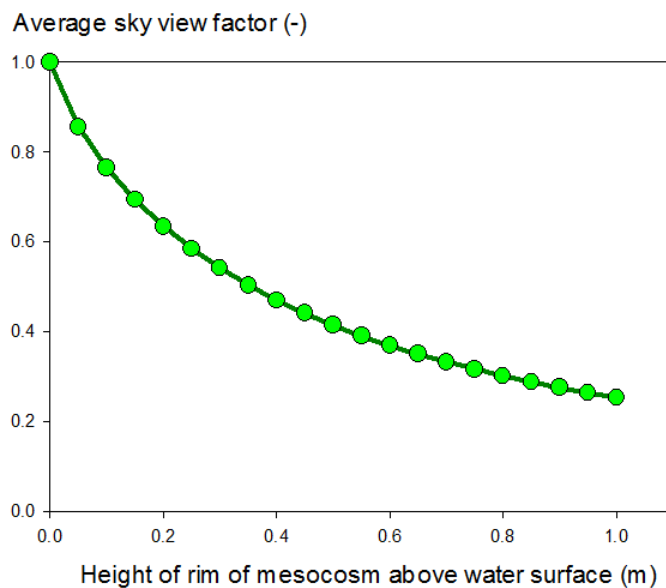
Figure 7.4 *The average skyview factor of the water surface within a cylinder with radius of 0.525 m as a function of the height of the rim above the water surface.*

Procedure for a rectangular

Finally we consider a rectangular water surface within a tank.

The procedure for the calculation of the skyview factor was as follows:
A regular rectangular grid was defined consisting of 100 points x_i-y_i covering one quarter of the water surface (for symmetry reasons the skyview factor of all four quarters has to be equal)
For each point x_i-y_i 100 lines were defined in the plane of the water surface passing through this point with angles increasing in equal steps from 0.5 to 99.5% of п rad

Each line has then two intersection points with the walls of the tank and the locations of these points were calculated

So we know then the two distances between the point x_i-y_i and the walls of the tank along this line

From these distances (AB and AC in Figure 7.5) and the distance between the water surface and the rim of the tank (h in Figure 7.5) the skyview factor along this line can be calculated as γ/π (see Figure 7.5)

The results for the 100 lines are then averaged to give the skyview factor for this point x_i-y_i

The final step is then to average the factors of all 100 points x_i-y_i.

We consider as example a study by Wendt-Rasch et al. (2004). The study was conducted in concrete outdoor tanks with a length of 1.2 m, a width of 1.4 m and a rim of about 30 cm above the water surface. The factor of each of the 100 points ranged between 0.32 to 0.76 and the average of all points was 0.62. Increasing the number of points into 196 did not change this 0.62.

We consider as another example a square with a size of 93 cm and a rim 25 cm above the water surface. This square has the same surface area as the example cylinder so it should give about the same result. The skyview factor was 0.58 so very close to that of the cylinder.
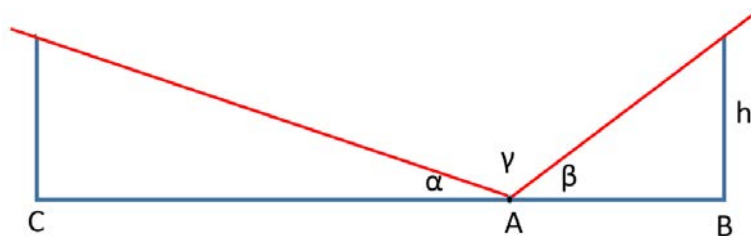
Figure 7.5   *Schematic representation of the calculation of the skyview factor along a line passing through a point xi-yi at the water surface of a tank. A is this point and B and C are intersection points with the wall of the tank; h is the distance between the water surface and the rim of the tank.*

Procedure for a ditch
Next we consider a ditch with a certain side slope (as e.g. used by Arts et al., 2006).

Figure 7.6 gives a schematic representation of the skyview of such a water surface in the direction perpendicular to the direction of the ditch.
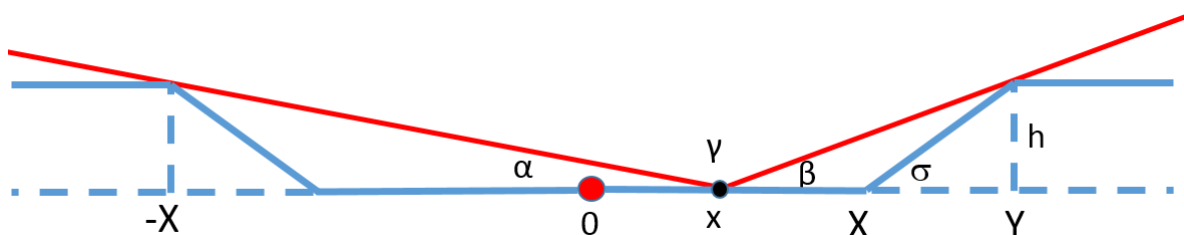
Figure 7.6   *Schematic representation of the skyview of the water surface of a ditch with a width of 2X, a side slope σ and a bank that is a distance h above the water surface, considering the vertical plane perpendicular to the direction of the ditch.*

The skyview reduction factor for this system was based on a similar procedure as for the cylinder using the schematic representation in Figure 7.7. The angles α and β can again be calculated from the distances $A_\alpha C$ and $A_\beta C$ as their tangens equals $h / A_\alpha C$ and $h / A_\beta C$, respectively where h is now the distance between the level of the top of the bank and the water surface. The distance $A_\alpha C$ can be calculated from the distances $A_\alpha B_\alpha$ and $B_\alpha C$ using the theorem of Pythagoras and considering that $B_\alpha C$

equals $A_\alpha B_\alpha$ / tan(φ). Similarly the distance $A_\beta C$ can be calculated. Calculations were made for 100 points x regularly distributed between the centre of the ditch and the right border of the ditch. For each point x, calculations were made for 100 φ values ranging from 0.5 to 99.5% of $\pi/2$ and the average value of the skyview factor was taken. Then the average of the 100 points x was taken.

We consider as an example the experimental ditches used by Arts et al. (2006) which had a water surface of 3.3 m wide and 40 m long and a water depth of 0.5 m. The side slope was 2/3 (i.e. the tangens of the angle σ in Figure 7.7) and the bank was about 0.4 m above the water surface (so h = 0.4 m). The resulting skyview factor was 0.92, 0.91, 0.90 and 0.89 for h values of 0.3, 0.4, 0.5 and 0.6 m, respectively. So the factor is for such a ditch rather unsensitive to h.
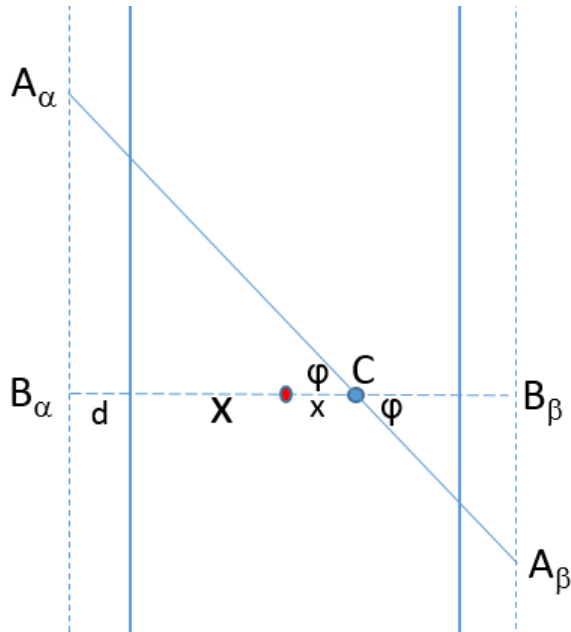
Figure 7.7   *Schematic representation of the ditch in a horizontal plane showing the line $A_\alpha A_\beta$ that passes through a point C at a distance x from the centre and that makes an arbitrary angle φ with the horizontal line perpendicular to the direction of the ditch; d is the distance between the water surface and the top of the bank in horizontal direction (i.e. the distance XY in Figure 7.6).*

8 Procedure to estimate $DegT_{50,water}$ in outdoor cosm water by radiation, using inverse modelling with TOXSWA

8.1 Introduction

In regulatory dossiers information is available on (direct and indirect) photochemical degradation rates, that have been measured under standardized light conditions (OECD, 1981, 2002 and 2008; EPA 1998 a and b). However, these rates have limited value for photochemical degradation rates in surface water under outdoor conditions (see previous chapter). Sometimes, in these regulatory dossiers, outdoor cosm studies used for estimating the decline rate in water are available. These outdoor cosm studies can potentially be used for estimating photochemical degradation rates in surface water.

Adriaanse et al. (2012) designed a procedure to estimate the degradation rate in water that is suitable for cosm studies with limited data sets, e.g. lacking site-specific sorption coefficients and relevant sediment properties. In this report this procedure (somewhat adapted) was applied to a number of selected compounds for which it is likely that photochemical degradation in water is the main route of degradation and for which cosm studies were available. However, most of these studies were performed to evaluate the ecotoxicological effects and, therefore, they had limited data sets of the fate of the compound.

This report is limited to compounds for which there is evidence that degradation is mainly dominated by the process of photolysis and that are predominantly present in the water phase, i.e. compounds with a sorption coefficient (K_{oc}) of up to approximately 1,000 L/kg. As the compound is mainly present in the water phase, concentrations in the sediment were not considered in the optimisation procedure. Even if concentrations in the sediment were available, which was seldom the case for the selected compounds, only aqueous concentrations were used in the estimation procedures.

8.2 Brief description of the TOXSWA model

8.2.1 General

The TOXSWA model was selected for the inverse modelling, because it is a process-oriented, deterministic model. It has been used in the pesticide registration procedure of the Netherlands since 1996 and at EU-level since 2003. This carries the advantage that process descriptions in the inverse modelling procedure are fully consistent with process descriptions in the exposure assessments used in registration.

The TOXSWA model describes the behaviour of pesticides in edge-of-field watercourses (Adriaanse, 1997; Adriaanse et al., 2012). It assumes that pesticides can enter the watercourse by various routes, such as spray drift deposition, drain flow or runoff. It models these entries as being either instantaneous or distributed over a certain period, and as a point-source type or distributed over a certain length of the watercourse.

TOXSWA considers four processes: (i) transport, (ii) degradation, (iii) sorption and (iv) volatilisation. Its simulated watercourse is two-dimensional and consists of a water layer containing suspended solids and macrophytes, and a sediment layer, which properties (bulk density, porosity and organic matter content) may vary with depth. In the water layer, the pesticide concentration may vary in horizontal direction, x, but is assumed to be uniform within vertical cross-sections. In the sediment, the pesticide concentration varies in the x direction, as well as in the z direction, i.e. with depth.
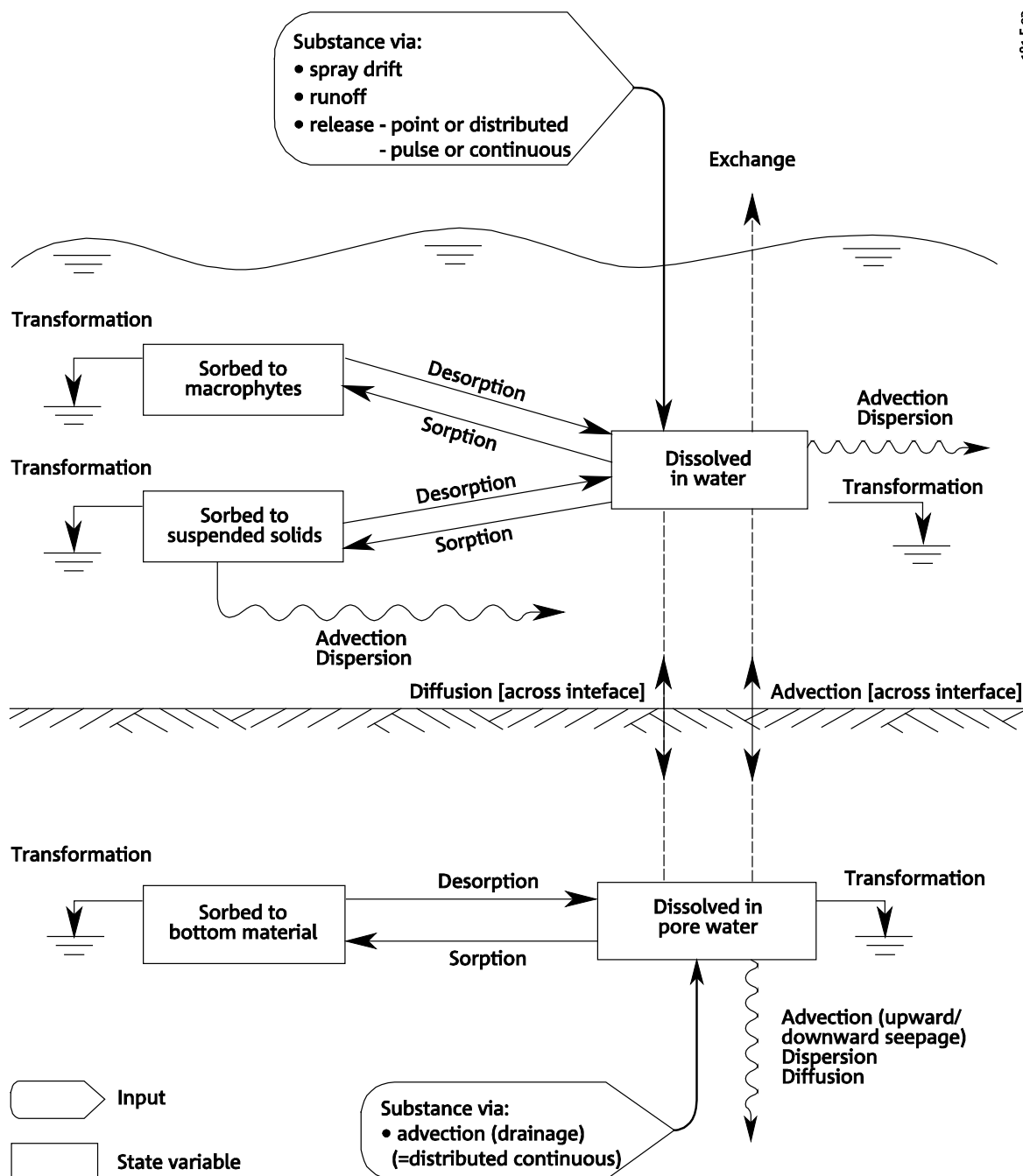
Figure 8.1 *Diagram of the processes in TOXSWA for describing the behaviour in watercourses (taken from Adriaanse, 1996).*

Figure 8.1 shows the processes included in TOXSWA. In the water layer, pesticides are transported by advection and dispersion, whilst in the sediment, diffusion also occurs. Their overall degradation rate is dependent upon temperature. Pesticides are sorbed to suspended solids, macrophytes and sediment. They are transported across the water-sediment interface by advection (i.e. upward- or downward seepage) and diffusion. In all the cosm studies, the cosm water was stagnant and there was no seepage into sediment, so both horizontal- and vertical advection and dispersion were zero.

A detailed description of the processes in the TOXSWA model is provided by Adriaanse et al. (2012).

The model is based upon two mass conservation equations: one for the water layer and one for the sediment. These are solved with an explicit central finite difference method. For the numerical solution, the water layer and sediment are divided into a number of nodes. Since there is no concentration gradient in the horizontal direction in the cosm studies, only one node is used for the water layer. For the sediment, an array of nodes can be defined below the water layer node. The

FOCUS default array was used in this study, consisting of a segment size increasing in six steps from 1 mm at the water-sediment interface to 30 mm at 7-10 cm depth, for 14 segments in total. The time step for the substance simulation was calculated by the model. A maximum time frame of 600 s for both water and sediment was used.

Sediment segmentation for compounds with K_{oc} value above 30000 L/kg
For compounds with a relatively high sorption coefficient a finer segmentation than the standard sediment segmentation (14 segments ranging from 1 mm at the water-sediment interface to 3 cm at 10 cm depth) may be needed to obtain an accurate numerical solution. As long as no convergent numerical solution for the mass balance equation of the sediment is used, the concentrations in the sediment change with other segmentations, which may affect the water concentrations and thus the estimated $DegT_{50, photo,ref}$ by the optimisation procedure used in this report. This is an undesirable situation: the solution of the mass balance equation should not depend on the selected segment sizes in the numerical solution. In the FOCUS surface water scenarios the so-called 'FOCUS_highKoc sediment segmentation' (27 segments ranging from 0.03 mm at the water-sediment interface to 3 cm at 10 cm depth) is suggested for compounds with K_{oc} values above 30000 L/kg to obtain a stable and convergent numerical solution (Beltman et al., 2014, section 4.4.3). Thus, for compounds with K_{oc} values above approximately 30000 L kg^{-1}, the accuracy of the estimated $DegT_{50, photo,ref}$ may be improved by applying a finer sediment segmentation.

8.2.2 Concept for simulating photolysis in water

Beltman et al. (2015) describe the implementation of a concept for simulating photolysis in water in the TOXSWA model. The concept is based on modelling photolysis as a first-order process, where the transformation rate is considered to be linearly proportional to global radiation and not to depend on the water temperature.

As described in previous chapters, it was concluded that for estimating the effect of radiation on the degradation rate of pesticides in surface water, it is more opportune to use the UV radiation data based on the vitamin-D action spectrum. This type of radiation is indicated as UV-VitD radiation: $I_{act,UV-VitD}$.

The photolysis concept in TOXSWA is therefore slightly adapted. Photolysis is still modelled as a first-order process. However, the transformation rate is considered to be linearly proportional to the UV radiation based on the vitamin-D action spectrum instead of the global radiation.

This slightly adapted concept and its implementation in the TOXSWA model are described in this section. This research version of the TOXSWA model has the version number of 3.4.0, latest updated on 19 October 2019.

The photochemical degradation rate coefficient is considered to be linearly proportional to the daily UV radiation based on the vitamin-D action spectrum:

$$k_{photo} = k_{photo,ref} \frac{I_{act,UV-vitD}}{I_{act,UV-vitD,ref}} \tag{8.1}$$

with
k_{photo}	= photochemical degradation rate coefficient (d^{-1})
$k_{photo,ref}$	= photochemical degradation rate coefficient at reference radiation $I_{act,UV-vitD}$ (d^{-1})
$I_{act,UV-vitD}$	= daily UV-vitD radiation $I_{act,UV-vitD}$ (kJ m^{-2} d^{-1})
$I_{act,UV-vitD,ref}$	= reference daily UV-vitD radiation $I_{act,UV-vitD}$ (kJ m^{-2} d^{-1})

Note that the photolysis rate is negligibly influenced by temperature (Beltman et al., 2015). Hence, the reference rate constant, $k_{photo,ref}$, is assumed to be temperature-independent, contrary to the degradation rates determined in Deneer et al. (2015) and Adriaanse et al. (2017), where the degradation rate was a function of temperature and thus the k_{ref} obtained by inverse modelling in those reports represented a degradation rate standardized to temperature (of 20°C). In this report

however, the obtained degradation rate at reference conditions, $k_{photo,ref}$, refers to a standardization to a reference UV-VitD radiation, as explained above.

Below we summarize the exact implementation of the photolytical degradation in the TOXSWA model version 3.4.0 (repeating parts of section 3.3.1).

In TOXSWA, aggregated daily values of $I_{act,UV-vitD}$ are read from an input file (*.IUV) and these values are distributed over the number of hours in a day that the sun remains above the horizon. This distribution is based on the de solar elevation[3]. The solar elevation, φ, is calculated according Eqs (8.2), (8.3) and (8.4) in radians.

Solar elevation φ is obtained via:

$$sin(\varphi) = sin(\delta)sin(\phi) - cos(t_h)cos(\delta)cos(\phi) \tag{8.2}$$

where
Φ = latitude (positive north) (radians)
δ = declination of the sun (radians)
t_h = the hour angle (radians)

The declination of the sun, δ, is calculated as

$$\delta = 0.409 \, cos\left[\frac{2\pi \, (D - d_s)}{365.25}\right] \tag{8.3}$$

where
D = day of year (-)
d_s = day of the summer solstice, = 172[4] (-)

The hour angle t_h is approximated by:

$$t_h = \frac{\pi \, (t_d+0.5)}{12} - \Lambda - \pi \tag{8.4}$$

where
t_d = time of day in UTC (h)
Λ = longitude (positive west) (radians)

Note that the hour angle (t_h; Eqn 8.4) is calculated at the middle of the hour.

To distribute the daily sum of van $I_{act,UV-vitD}$, a relative distribution of the solar elevation in one day is calculated first. This is done by calculating the daily sum of hourly values of the sinus of the solar elevation over the hours that the sun remains above the horizon (φ > 0):

$$\varphi_{d,pos} = \sum_{h=1}^{h=24} sin(\varphi_{h,pos}) \tag{8.5}$$

With
$\varphi_{d,pos}$ = sum of positive hourly solar elevation values (rad)
$\varphi_{h,pos}$ = positive hourly solar elevation value (rad)
h = hour in day (-)

---

[3] The solar zenith angle is the angle between the zenith and the center of the Sun's disc. The solar elevation angle is the altitude of the Sun, the angle between the horizon and the center of the Sun's disc. These two angles are complementary. (Wikipedia)

[4] TOXSWA uses a value of 172 for non-leap years and 173 for leap years. Since the start of summer is commonly set on June 21st, we use this date as the day of summer solstice, which results in values of ds of 172 for non-leap years and 173 for leap years.

Aggregated daily values of $I_{act,UV\text{-}vitD}$ are distributed over the hours according:

$$\varphi_h \leq 0 \qquad I_{act,UV\text{-}vitD} = 0 \qquad\qquad (8.6a)$$

$$\varphi_h > 0 \qquad I_{act,UV-vitD} = \frac{\sin(\varphi_{h,pos})}{\varphi_{d,pos}}\; I_{act,UV-vitD,d} \qquad\qquad (8.6b)$$

8.3 Overview of the model optimisation procedure

In this section, the optimisation procedure for estimating the photochemical degradation rate in water of the cosm is described. The procedure was based on inverse modelling of the behaviour of the compound in the cosm by TOXSWA. As stated in Deneer et al. (2015) the minimal requirements for outdoor cosms to be suitable for the inverse modelling exercise is that:
At least five measured concentrations in the water phase as a function of time and
The water depth
are available.

For each cosm, the TOXSWA model was parameterised as far as possible, i.e. reflecting the conditions in the cosm as well as possible, using all available, relevant, reported parameters. However, for all cosms, the degradation input parameters were unknown, for the water layer, as well as for the sediment. For the cosms selected for this study, it is implicitly assumed that photolysis is the main process for degradation in the water of the cosm and that hydrolysis and biotransformation are negligible. The half-life of photochemical degradation in water at a daily reference UV radiation of 5 kJ m^{-2} was estimated. A first estimate of the photochemical degradation rate in water for the different compounds was loosely based on estimates of the decline rate in water. Generally, in the sediment there are no or too few measured concentrations available, and the decline rate is unknown. For the purpose of this study it was assumed that degradation in the sediment is negligible. To implement this assumption in TOXSWA a very high default value for the sediment half-life of 1,000 days was used. This corresponded to the worst case default value given in the guidance of FOCUS (2006) for the estimation of degradation rates in water-sediment studies, and was based on the observation that in water-sediment studies, the degradation rate in sediment is often low. Moreover, as only compounds with a relatively low sorption coefficient were considered in this study (K_{oc} value of below approximately 1,000 L kg^{-1}), relatively few mass will enter the sediment and thus, the degradation rate in the sediment is relatively unimportant for the simulation of the compound behaviour in the cosm.

After parameterisation, the TOXSWA model was run and the concentration of the cosm was simulated. To mimic the behaviour of the compound in the cosm as well as possible, two input parameters of TOXSWA had to be optimised: (i) the photochemical degradation rate in water - $DegT_{50,\,photo,ref}$, and (ii) the (first) loading in to the water (which is an indirect way of optimising the initial concentration in water - c_0). These two parameters were selected according to the following considerations: Neglecting the behaviour in the sediment and assuming that photolysis is the main degradation route, the process parameter $DegT_{50,\,photo,ref}$ is the only remaining process parameter controlling the behaviour in the cosm for compounds with relatively low volatilisation and low sorption (to sediment, suspended solids and macrophytes) (Adriaanse et al., 2012). So, for compounds that are only slightly volatile (saturated vapour pressure at 20-25°C less than 10 mPa; Mensink et al., 1995) with a K_{oc} smaller than 1,000 L/kg, it is justified to optimise only the process parameter $DegT_{50,\,photo,ref}$. The first loading was included in the curve-fitting procedure, in accordance with the general recommendations on data issues of FOCUS (2006) concerning time zero samples. Optimisation of the (first) loading in to the water was preferred over optimising the initial concentration (as done by Deneer et al., 2015 and Adriaanse et al., 2017) for the following reason. The starting time of the simulation in TOXSWA can only be entered on a daily basis. Consequence is that the model assumes that the initial concentration occurs at the specified starting day at 00:00 hour (i.e. at the beginning of the day). However, for simulating photolysis the exact timing of the application of the compound is very relevant as degradation is highly influenced by UV radiation in the hours following the application event. TOXSWA version 3.4.1. is able to read the timing of the loadings on an hourly basis. It was therefore decided to optimise the first loading in TOXSWA as in this way it is possible to simulate the real timing of the

application of the compound in the cosm experiment with the accuracy of an hour. The initial estimate of the first loading (i.e. the deposition in mg compound per m^2 of area of water surface) was derived from the data reported for the cosm experiment.

The optimisation procedure focused on the correspondence between the measured and model-generated concentrations in the water layer of the cosm. It consisted of PEST (Parameter ESTimation; Doherty, 2005), version 13.0 running TOXSWA (TOXSWA version 3.4.1 of 14 October 2019) many times with chosen parameters values, but varying $DegT_{50, photo,ref}$ and the first loading (mg m^{-2}), whilst minimising the sum of squared differences between model-generated and measured values. The sum is called the objective function phi. PEST uses a non-linear estimation technique, the Gauss-Marquardt-Levenberg method, for minimisation of the objective function.

Minimising the objective function phi and choice of initial values
The inverse modelling procedure attempts to identify the values for the parameters to be fitted that result in the best correspondence between measured and simulated values for the experimental quantities under consideration, i.e. the concentrations of the test compound in water.

PEST requires that each of the parameters to be fitted is given an initial value, which is used as the starting point in the comparison between experimental and simulated values. The value is then adjusted by PEST, a new simulation is run, another comparison between experimental and adjusted values is made, parameters are adjusted again, etc. This process is continued until adjusting the parameter values does not result in a better fit anymore.

The 'surface' of the objective function phi used to assess the quality of the fit is bound to contain several minima, and maxima. There may also be some relatively flat parts where changing parameter values hardly has any effect on the quality of the fit. The aim of the estimation procedure is to find the combination of parameter values that results in the 'deepest' minimum in the function surface, further called the 'global minimum'.

There is, however, a chance of hitting a 'local minimum', i.e. the fit does not seem to improve upon slight changes of the parameter values, and a larger change of parameter values is necessary to 'jump out of' the local minimum and continue the search for the true minimum. However, the user has little insight and control over the adjustment of parameter values that PEST uses during optimisation, and there is a distinct risk that PEST ends up in a local minimum.

To circumvent this pitfall, it is common practice to perform the optimisation runs several times, each time using a different combination of initial values for the parameters to be estimated. If the initial values are spaced sufficiently wide, chances that the entire function surface is sampled during at least one of the optimisation runs are greatly improved, and hence the chances of finding the global minimum of the function surface are equally improved, resulting in a much better chance of finding the best combination of parameter values.

For all cosm studies used in this report, the concentrations in the water used in the optimisation procedure correspond to the total concentration in the water layer, i.e. dissolved plus sorbed to suspended solids, because in the cosm studies used the water samples were not filtered before analysis. As stated earlier, in this report, only concentrations in water were used in the optimisation procedure, even for studies, in which data on concentrations in sediment were available.

The following criteria were used to assess the quality of the optimisation, i.e. the goodness of fit:
• Visual correspondence between the simulated and measured concentrations in water, as a function of time;
• Visual assessment of the residuals (simulated- minus measured data), as a function of time, in order to reveal patterns of over- or under prediction;
• Chi-Square (χ^2) test to assess the deviations between simulated and measured values, relative to the uncertainty of the measurements;
• The confidence interval for the estimates of $DegT_{50, photo,ref}$ and the first loading.

These criteria were derived from FOCUS (2006). FOCUS (2006) was not able to identify a statistical method that provided an objective framework for evaluating the goodness of fit of an individual model and to compare two different models. Therefore, visual assessment, as stated in the first two criteria above, continues to play a major role in evaluating the goodness of fit. This should be used in combination with a χ^2-test to compare the goodness of fit of two different kinetics and a t-test (or confidence intervals) to evaluate the confidence in the parameter estimates.

For the visual assessment of the goodness of fit, measured and optimised data must always be presented graphically. Measured concentrations and the simulated curve should be plotted versus time. A second plot should be made of simulated minus measured data (residuals). In this way, patterns of over- or under prediction may be revealed. For an exact fit, all residuals are zero. If negative and positive residuals are not randomly scattered around zero, systematic deviations may have occurred.

FOCUS (2006) proposed the use of the χ^2-test as a supplementary tool for assessment of the goodness of fit of an individual model. The χ^2-test considers the deviations between observed and predicted values, relative to the uncertainty of the measurements.

$$\chi^2 = \sum \frac{(C-O)^2}{(err/100 \; x \; \bar{O})^2} \tag{8.7}$$

Where
C	= calculated value
O	= observed value
$\bar{O}$	= mean of all observed values (element of scale in error term)
err	= measurement error percentage (element of proportionality in error term)

The calculated χ^2 for a specific fit may be compared to tabulated $\chi^2_{m,\alpha}$ values,
where
m	= degrees of freedom, i.e. number of measurements (after averaging of replicates) minus number of model parameters that are fitted
a	= probability that one may obtain the given or higher χ^2 by chance (FOCUS, 2006).

Tabulated values are given in Table 6-5 of FOCUS (2006). Alternatively, they can be calculated in Excel using the CHINV (a, m) function.

To simplify the test, FOCUS (2006) proposed a pragmatic solution to address the uncertainty of the measurements, and to restrict the computation of χ^2 to using the calculated mean and observed mean values. In this way, the test evaluates the goodness of fit of the model fit and not the variation in replicate values. They stress however, that the true replicate values should be used for the kinetic fit with, in this case, the TOXSWA model.

The χ^2 Significance Test indicates whether the hypothesis of no relationship between measured and calculated values is valid, i.e. that the model is not appropriate. Often a significance of a=0.05 is used, and a value of χ^2 greater than $\chi^2_{m,0.05}$ indicates that the hypothesis is valid and the model is not appropriate. To use the χ^2-test, the percent error should be known (see Eq. 8.7). This is often not the case. Therefore, FOCUS (2006) proposes to calculate the minimum error-% of the error term (error-% /100 * mean observed), at which the test is passed with the aid of Eq. (8.8):

$$err = 100 \sqrt{\frac{1}{\chi^2_{tabulated}} \sum \frac{(C-O)^2}{\bar{O}^2}} \tag{8.8}$$

The test is passed if the calculated value of χ^2 is equal or smaller than the standard tabulated value at the 5% significance level and the given degrees of freedom. In this context, the 5% significance level corresponds with the 95th percentile of the χ^2 distribution. Furthermore, a large value of χ^2 means that the deviations are large (see Eq. 8.7). Passing the test means that the χ^2 is smaller than the 95th percentile of its distribution. A consequence of this is that a lower significance level leads to a less

strict test, which is counterintuitive. E.g. for six degrees of freedom, the tabulated χ^2 is 12.6 for $a = 0.05$ and it is 16.8 for $a = 0.01$ (FOCUS, 2006, p. 91). Therefore, a significance level of 1% would have generated lower *err* values than the chosen level of 5%.

Field data, such as the (mostly outdoor) cosm data in this report, will be inherently more variable than laboratory data generated under controlled conditions. Therefore, for field studies, the error percentages, at which the χ^2-test is passed will generally be larger than for laboratory studies. FOCUS (2006) suggests that a minimum error-% value of 15% is acceptable for field studies. The minimum error-% to pass the test can be calculated explicitly with Eq. 8.8 using the appropriate χ^2_{tab} values, as well as the observed and predicted values.

The uncertainty in the estimated model parameters can also be assessed by performing a *t*-test or by specifying confidence intervals (FOCUS 2006). This helps to assess whether the optimised parameters, especially the photochemical degradation rate, differ significantly from zero at the chosen significance level. PEST generates confidence intervals and, therefore, it was used in this report (at 95% significance) to assess whether the intervals for the $DegT_{50, photo,ref}$ (and the first loading) did not include zero, i.e. the parameters differed significantly from zero.

The correlation coefficient between the first loading and $DegT_{50, photo,ref}$ was calculated by PEST and a standard part of the output given by the fitting procedure. Since a higher value of the first loading should result in a faster degradation rate constant, and hence, in a smaller value for $DegT_{50, photo,ref}$, the value of the correlation coefficient between $DegT_{50, photo,ref}$ and the first loading should be negative. Checking its value may serve as a very minimal quality check on the correctness of the fitting procedure.

Most papers of the analysed studies gave little or no properties for the sediment and suspended solids in the cosms (bulk density, organic matter content of sediment and suspended solids, porosity). Therefore, default values for use in the optimisations were set at realistic levels.

PEST runs were performed for 49 different sets of initial values of the optimisation parameters to check the uniqueness of their optimised values. All possible combinations of the values given in Table 8.1 below result in 49 sets of initial values for $DegT_{50, photo,ref}$ and the loading.

Table 8.1   *Initial values for DegT$_{50, photo,ref}$ and the loading. Combining these values result in 49 unique sets of initial values.*

$DegT_{50,photo,ref}$ (d)	0.1	0.5	1	2	5	10	50
Loading (mg m^{-2})	50	100	300	500	1000	1500	3000

Lower and upper parameter bounds for $DegT_{50, photo,ref}$ were set to resp. 0.1 and 100 d. Lower and upper parameter bounds for the loading were set to resp. 1 and 10 000 mg/m^2.

9 Analysis of cosm studies

9.1 Introduction

The estimation procedure for the photochemical degradation rate in water was based upon the inverse modelling of the cosm study by TOXSWA, coupled to the optimisation tool, PEST. Below, we first summarise the procedure for one optimisation run. In the remainder of this chapter we describe how we performed the estimation procedure for the eight cosms of this report.

In brief, preparing and running one PEST_TOXSWA optimisation for a cosm consists of the following steps:

a. Parameterise the TOXSWA model, as well as possible for the specified cosm, on the basis of the study description;

b. Use the TOXWSA input file (*.txw) to prepare the PEST template file (*.tpl);

c. Run the TOXSWA model and prepare, based on the output of the simulated concentrations in the TOXSWA output file and the concentrations measured in the cosm study, the instruction file(s) (*.ins) and pest control file (*.pst) for PEST;

d. Start a PEST optimisation. PEST will adjust the TOXSWA input parameters (i) photochemical degradation half-life in water, $DegT_{50, photo,ref}$ and (ii) the first loading. On the basis of the correspondence between simulated and measured concentrations the TOXSWA model is re-run with different values for the two input parameters until a pre-defined stop criterion is met.

e. Consider whether the quality of the fit is acceptable. If yes, extract the optimised photochemical degradation half-live in water, $DegT_{50, photo,ref}$.

If more than one satisfactory, optimised value of the $DegT_{50, photo,ref}$ has been obtained for the same cosm study we take the geometric mean of the obtained satisfactory values. This follows the guidance of the FOCUS Degradation Kinetics Working group (FOCUS, 2006) for averaging degradation rates or half-lives, because the geometric mean method has the advantage that geomeans of half-lives correspond to the geomeans of degradation rates.

If cosms of the same study are comparable, data may be pooled. It is then possible to perform steps 1-5 only once by scaling all measured concentration-time profiles from 0 to 1 and comparing these to the (scaled) simulated concentration-time profile (see Section 9.3). Cosms may be considered to be comparable if (i) they can be represented by one set of inputs for the TOXSWA model, which implies that input parameters, such as water depth, are (approximately) similar and (ii) the degradation rates in water of the compound seem to be similar, which can be seen best by plotting the aqueous concentrations on a logarithmic scale to see if the slopes are (approximately) similar.

9.2 Parameterisation for PEST-TOXSWA for all cosm studies

Each cosm was parameterised for the TOXSWA model. Only two parameters were optimised: $DegT_{50, photo,ref, water}$ and the first loading. All other input parameters were fixed values during the optimisation. Some of the fixed input parameters, such as water depth, were chosen to reflect the conditions as measured in the cosms. Others were not measured and had to be estimated in another way. Pesticide properties were taken from the Pesticides Properties DataBase (PPDB[5]). A protocol was used to select the most appropriate values from the Pesticides Properties DataBase (See Annex 2 in Deneer et al. 2015 and Adriaanse et al. 2017). Although the calculations in this report were performed using data from the Pesticides Properties DataBase, calculations for authorisation purposes should, obviously, be

---

[5] https://sitem.herts.ac.uk/aeru/ppdb/en/index.htm (Website last entered on 20 May 2020).

performed using data from the authorisation dossier. All input that was cosm-specific is mentioned in the annex belonging to the study, e.g. Annex 4 for the metribuzin cosm studies. In addition, compound-specific properties appear in the appendices. Other input parameters, such as sediment properties, were defined in the same way for all cosm studies.

Input parameters that were equal for all cosm simulations include: (i) the concentration of suspended solids and their organic matter content, (ii) the sediment properties and the sediment depth, (iii) compound properties, such as molar enthalpies of vaporisation, dissolution and degradation, and the degradation half-life in sediment (Table 9.1).

Table 9.1   *Process-related parameter values and their origin, used in all cosm study simulations.*

Property	Value	Origin
Molar enthalpy of vaporisation (kJ/mol)	95	FOCUS (2001)
Molar enthalpy of dissolution (kJ/mol)	27	FOCUS (2001)
Molar enthalpy of degradation (kJ/mol)	65.4	EFSA (2007)
Degradation half-life in sediment (d)	1000	FOCUS Degradation Kinetics (2006) and section 2.3 2nd paragraph

The photochemical degradation half-life in water does not depend on the temperature of the water. Furthermore, no degradation was assumed to occur in the sediment by fixing the corresponding half-life to 1000 d (Table 9.1). So the temperature played no role in the fitting procedure.

The values for the input parameters of suspended solids and sediment for water-sediment cosms are presented in Table 9.2. The values in Table 9.2 were derived from FOCUS (2001) and based on their bulk density and organic matter content, but fulfilled the requirements of Eq. (9.1) which states that the volume fractions of water, organic matter and mineral parts sum up to 1:

$$\varepsilon + \frac{\rho_{sed}}{\rho_{om}} f_{om,sed} + \frac{(1 - f_{om,sed}) \rho_{sed}}{\rho_{min}} = 1 \tag{9.1}$$

where ρ_{om} (kg L^{-1}) is the phase density of organic matter and ρ_{min} (kg L^{-1}) is the phase density of mineral matter. Using the values of 1.40 kg L^{-1} for ρ_{om} and 2.65 kg L^{-1} for ρ_{min}, the porosity ε (-) for given values of the sediment bulk density ρ_{sed} (kg L^{-1}) and the sediment organic matter content $f_{om,sed}$ (-) can be calculated with Eq. (9.1). For the sediment with $\rho_{sed} = 0.8$ kg.L^{-1} and $f_{om,sed} = 0.09$ (Table 9.2), $\varepsilon = 0.67$ was obtained. The tortuosity λ (-) was calculated according to the empirical equation (Boudreau, 1996):

$$\lambda = \frac{1}{[1 - ln(\varepsilon^2)]} \tag{9.2}$$

Table 9.2   *Values of suspended solids and sediment parameters used in TOXSWA for the cosm study simulations.*

Parameter	Default value
Suspended solids	
Concentration in water (mg/L)	15
Organic matter content (mass fraction, %)	9
Sediment	*(0-10 cm)*
Bulk density (kg/L)	0.8
Organic matter content (mass fraction, %)	9
Porosity (volume fraction, -)	0.67
Tortuosity (-)	0.56
Total sediment depth (cm)	10
Degradation half-life in sediment (d)	1000

TOXSWA requires the daily actual UV-VitD radiation as input. Section 3.3 has given a description how these data were obtained from the TEMIS data base and next, converted from daily clear-sky dose with the aid of cloud cover data of the Copernicus climate data store and a calculated attenuation factor into actual UV-VitD radiation values. Section 3.3. and Annex 3 present further details on the exact locations, years and grid cells used. Next, the TOXSWA model reads the daily actual UV-VitD radiation doses and converts these into hourly values using astronomical functions. These values are distributed over the hours in the day that the sun remains above the horizon (section 8.2.2).

The optimisation procedure requires initial estimates. As described in section 8.3, for each cosm study 49 PEST runs were done and each run was performed using a different set of initial values of the optimisation parameters (see Table 8.1). Initial values of the photochemical degradation rate in water, $DegT_{50, photo,ref}$, were loosely based on estimates of the decline rate in water and were found to be roughly between 1 and 5 days. The range of initial values selected was between a factor 10 lower than 1 day (0.1 day) and a factor 10 higher than 5 days (50 days).

To determine plausible ranges for the loading in mg m^{-2} as input for the inverse modelling a calculation needs to be done to determine the loading needed to reach a certain desired peak concentration. This calculation is explained in section 9.3. Initial values of the first loading for all cosms ranged roughly from 100 to about 1000 mg m^{-2}. A somewhat wider range of initial values was used in the optimisation, e.g. 50 – 3000 mg m^{-2} (see also Table 8.1).

9.3 Scaling of multiple data sets from a single study

In most of the studies used, there were replicates (i.e. physically-separate systems treated at the same concentration) at each treatment level. Whereas some studies report only average concentrations for each treatment level, others report concentrations for each of the replicates separately, thus providing more detailed data.

When data for each replicate are available, analysis can be performed for each of the replicates separately. This provides an estimate of $DegT_{50, photo,ref}$ for each of the replicates, which can then be combined by calculating e.g. the geometric mean value.

Alternatively, when combining all available data for a treatment level into a single analysis, a single estimate of $DegT_{50, photo,ref}$ can be obtained. Data from systems with different treatment levels can be also be combined to estimate one value of the $DegT_{50, photo,ref}$. For the latter case normalisation of concentrations is required before simultaneous analysis of data sets is possible. This can be achieved by dividing, for each replicate separately, all concentrations of a replicate by the highest aqueous concentration (in mg/L) observed in that replicate. Thus, aqueous concentrations are normalised to values of 0 – 1 mg/L for each replicate in a similar manner, which ensures that aqueous concentrations in the combined data set also range from 0 – 1 mg/L. Although in theory not necessary we also used scaled concentrations for data of replicates with identical treatments levels.

Note, however that combining data from systems with different treatment levels should only be done if initial inspection of concentration – time curves indicates that $DegT_{50, photo,ref}$ is not dependent on initial aqueous concentration, i.e. similar dissipation rates are observed for the various treatment levels.

Combining systems by scaling is not possible for systems with repeated applications, in case the loadings of systems differ. Similarly, systems with clearly different water depths or temperatures cannot be simulated by a single TOXSWA run, because only a single value for these parameters can be used in a TOXSWA run.

For all inverse modelling cases described in this report, next to the $DegT_{50, photo,ref}$ the (first) loading into the system was optimised as well. The dimensionless scaled concentrations used as observations in the inverse modelling will be compared to concentrations in g m^{-3} simulated by TOXSWA. The input of the loading in TOXSWA is in mg m^{-2}. To determine plausible ranges for the loading in mg m^{-2} as

input for the inverse modelling, a calculation needs to be done to determine the loading needed to reach a certain desired peak concentration (e.g. the measured, scaled water concentration at t=0, fixed at 1 g m^{-3}). The loading (m_{load} in mg m^{-2}) needed to reach the desired peak concentration is calculated as follows:

$$m_{load} = 1000 \frac{C_{peak,w}V}{wL} \qquad (9.3)$$

where
V =   the volume of water in the cosm (m^3)
w =   the width of the water surface (m)
L =   the length of the cosm (m)

9.4 Value of Freundlich sorption coefficient K_{om} and use of scaled concentrations

Sorption to sediment and suspended solids is described in TOXSWA through a non-linear Freundlich sorption isotherm, using a reference concentration of 1 mg L^{-1}, i.e. the concentration at which the Freundlich sorption coefficient K_{om} and Freundlich exponent N have been determined. When dealing with non-linear sorption the use of scaled concentrations requires calculation of an 'adjusted' organic matter partition coefficient (K_{om}). The Freundlich isotherm equation assumes that the K_{om} is specified for a reference concentration of 1 mg L^{-1} and therefore scaling of concentrations may result in the use of an erroneous value for K_{om}.

So, in situations where data sets from multiple cosms are combined and scaling was necessary to adjust the concentrations in all cosms to a common 0 – 1 range, a new Freundlich sorption coefficient needs to be calculated. TOXSWA uses g m^{-3} (= mg L^{-1}) as the unit of the concentration in the surface water. So in the fitting procedure it is assumed that a measured concentration of 1 equals 1 mg L^{-1}. Use of the Freundlich isotherm implies that the partitioning between solid and liquid phase depends on the concentration. So the K_{om} in the TOXSWA *.txw file has to be adjusted in such a way that the partitioning after scaling is equal to the partitioning before scaling. The procedure is as follows. We define the Freundlich isotherm as:

$$X = m_{om} K_{om} \ C_{ref}\left(C/C_{ref}\right)^N \qquad (9.4)$$

where X is the content sorbed (mg kg^{-1}), m_{om} is mass fraction of organic matter (-), C_{ref} is the reference concentration of 1 mg L^{-1}, C is the concentration in liquid phase (mg L^{-1}), and N is the Freundlich exponent (-). For the adjustment of the K_{om} we require that the partitioning between solid and liquid phase at the start of a study before and after scaling is the same. The partitioning is given by the ratio X/C; so we require that $X_{org}/C_{org} = X_{new}/C_{new}$ where 'org' refers to the original initial C and 'new' refers to the scaled initial C, so $C_{new} = 1$ mg L^{-1}. We have now two Freundlich equations:

$$X_{org} = m_{om} K_{om,org} \ C_{ref}\left(C_{org}/C_{ref}\right)^N \qquad (9.5)$$

$$X_{new} = m_{om} K_{om,new} \ C_{ref}\left(C_{new}/C_{ref}\right)^N \qquad (9.6)$$

Using these equations in combination with $X_{org}/C_{org} = X_{new}/C_{new}$ gives then:

$$K_{om,new} = K_{om,org} \ \left(C_{new}/C_{org}\right)^{1-N} \qquad (9.7)$$

Eqn (9.7) indicates that $K_{om,new}$ and $K_{om,org}$ are equal for a linear isotherm as 1-N then is zero. (Note that this equation differs from the ones mentioned by Deneer et al. (2015) and Adriaanse et al. (2017) who mentioned C_{ref} in the numerator instead of C_{new}. As both parameters equal 1 mg L^{-1}, their resulting $K_{om,new}$ is still correct.)

Data sets from multiple cosms have different initial concentrations; we recommend to use the geomean of the initial concentrations of the different datasets to estimate C_{org}. If scaling is applied to a single data set, we recommend to use the initial concentration of this data set as C_{org}.

For the inverse modelling described in this report we used scaled concentrations for all cosms. Also, instead of initial concentrations, loadings were optimised. Therefore, it is needed to clearly specify 'initial concentration'. We interpreted this as being the first concentration in a set of observations (of one observation group) used for the optimisation with PEST. The unscaled concentration at this time point is used for the correction of the K_{om}.

As an example, the values used for the initial concentrations of metribuzin in the study by Arts et al. (2006) were the concentrations measured at t =0.08 (i.e. ditch 7: 1.4 µg L^{-1}; ditch 4: 7.67 µg L^{-1}; ditch 1: 1.65 µg L^{-1}; ditch 12: 1.44 µg L^{-1}; ditch 6: 6.99 µg L^{-1}; ditch 9: 7.05 µg L^{-1}). The geomean of these values was used to calculate C_{org} resulting in 3.29×10^{-3} mg L^{-1}. The original value of the K_{om} (22 L kg^{-1}) was adjusted for non-linearity of the sorption isotherm using Eqn 9.7 and N =1.08. This resulted in $K_{om,new}$ = 13.92 L kg^{-1}. In the simulations with the scaled concentrations this adjusted value of $K_{om,new}$ equal to 13.92 L kg^{-1} was used, together with N = 1.08 for the sediment and the suspended solids.

9.5 Checking of consistency of degradation rates between higher and lower tiers

Boesten et al. (2014) proposed guidance on how to proceed if several different $DegT_{50}$ values are available for use in exposure calculations for authorisation purposes. They devised a hierarchical system for the use of information gathered in different types of studies (hydrolysis and photolysis studies, and studies that inherently combine various routes of degradation). The stepped approach adheres to the generally-accepted rationale that going from simple to more complex studies should result in more realistic results, giving less conservative estimates of degradation rates.

Their scheme is reproduced in Figure 9.1. The first step is the $DegT_{50}$ that results from hydrolysis. In the second tier, both degradation rate studies with fresh surface water in the dark and photolysis studies in buffered pure water are considered. The three different estimates of $DegT_{50}$ are usually available in authorisation dossiers, and if available, the data taken from a second-tier study are considered more favourable. The third step results in a $DegT_{50}$ from more sophisticated studies, such as photolysis studies with fresh surface water, indoor- and outdoor studies with algae and possibly macrophytes. Data generated in this step represent increased realistic conditions. However, guidance on how to combine $DegT_{50,water}$ values from different steps for use in the authorisation procedure is beyond the scope of this report.

Boesten et al. (2014) pointed out that there is no guidance on how to standardise data influenced by photolysis to standard irradiation fluxes, which makes data from Boxes 2.4, 2.6, 2.7 and 2.8 very difficult to interpret. Hence, in their guidance, they proposed not to use such data. Comparison between lower and higher tiers is, therefore, limited to data from Boxes 2.2, 2.3, 2.5 and 2.9.

The focus of the present investigation was on data belonging to the third step, here step 2.9. This allowed verification of the assumption that more realism will result in less conservative results, i.e. that the $DegT_{50, water}$ estimated from outdoor cosm data will indicate faster degradation than data from lower tiers, such as hydrolysis and water-sediment studies. So in Chapters 11, 12 and 13, which discuss estimates for $DegT_{50,water}$ for metribuzin, imidacloprid and metamitron, dissipation data from lower-tier studies and the currently estimated $DegT_{50, water}$ values from higher-tier outdoor cosm studies will be compared.
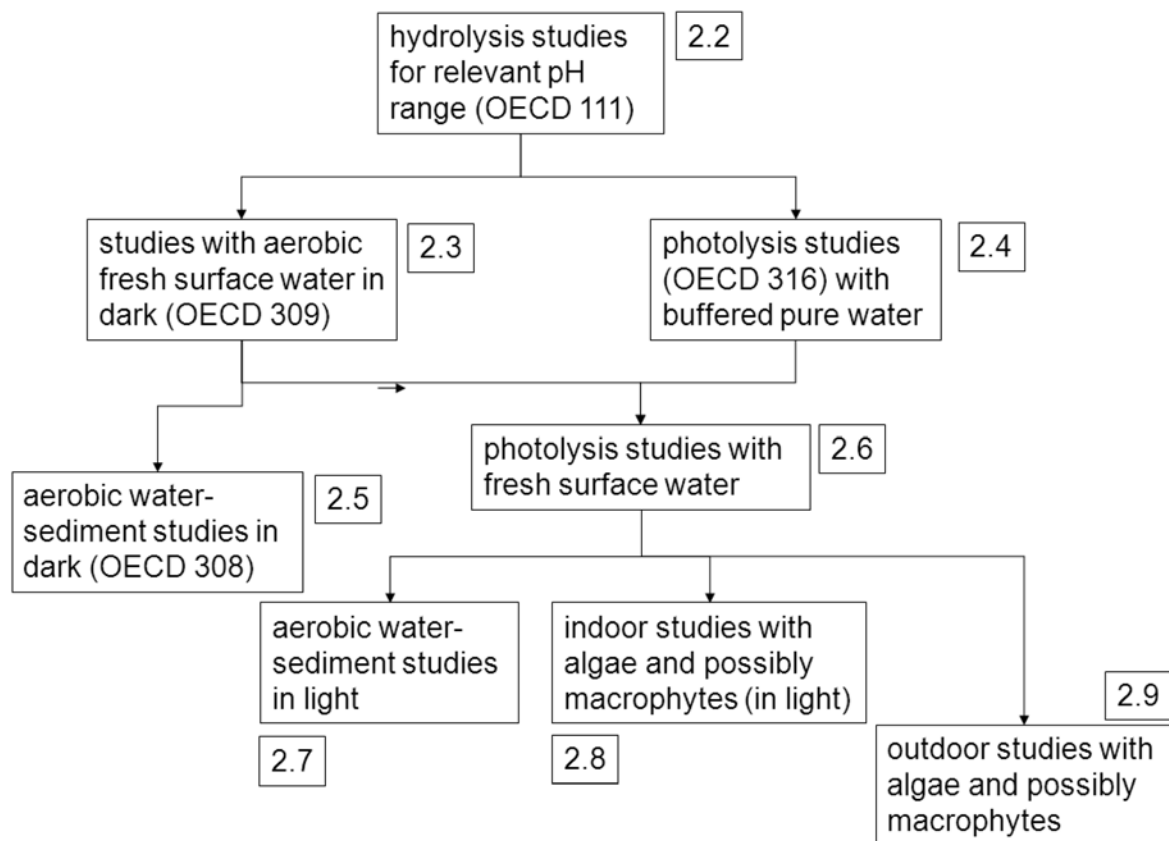
Figure 9.1 *Stepped approach for estimating DegT$_{50}$ values for surface water, taken from Boesten et al. (2014).*

10 Selection and properties of example compounds

10.1 Introduction

To be able to test the proposed methodology we need a number of compounds where degradation is the main dissipation process in the water layer ánd degradation is dominated by photochemical degradation. Moreover, we would like to have at least three outdoor cosm studies for each compound to be able to study the effect of the relevant environmental factors mentioned before, i.e. water depth, water surface area coverage percentage and skyview factor, in addition to the amount of the actual daily UV-VitD radiation. The studies should be reported into sufficient detail to enable the inverse modelling by the TOXSWA model.

So, the aim of the analysis of the compound-cosm studies is to establish whether the difference in actual daily UV-VitD radiation explains the difference in optimised $DegT_{50,photo}$ (after standardisation to the 3 other relevant environmental factors, mentioned above). Or, alternatively: are the standardised $DegT_{50,photo}$ values of the analysed studies approximately equal to the same reference photodegradation half-life?

10.2 Selection of compounds and cosm studies

Deneer et al. (2015) already made a selection and prioritisation of compounds and studies suitable for inverse modelling by TOXSWA. This implied that at least five aqueous concentrations as a function of time, and the water depth were available in at least three studies. Deneer et al. (2015) also established for which compounds photolysis was the main dissipation process and in the water layer. This resulted in the selection of the compounds metribuzin, imidacloprid and metamitron. Table 10.1 gives an overview of their main physico-chemical properties as mentioned in the PPDB database (https://sitem.herts.ac.uk/aeru/ppdb/en/atoz.htm).

Table 10.1 *Main physico-chemical properties of the three selected compounds, that are photodegradable (PPDB database).*

Compound	DT_{50} water-sediment (d)	DT_{50} photolysis (d)	Log K_{ow} (-)	K_{oc} (L kg^{-1})	Saturated vapour pressure at 25 °C (mPa)	pK_a (-)
Imidacloprid	129	0.2	0.57	225[C]	4.0E-7	-
Metamitron	11.1	0.02	0.85	77.7	0.00074	-
Metribuzin	50	0.2	1.65	37.9[C]	0.121	0.99

[C] K_{foc} is used (K_{oc} not available)

Table 10.2 lists the compounds and the available studies, that have been analysed in Chapters 11, 12 and 13 and the Appendices 4, 5 and 6. Daily radiation data were compiled for the outdoor cosm studies of Table 10.2. To do so, clear sky, UV-vitamin D weighed daily radiation doses were extracted from the TEMIS data and combined with cloud cover data, according to the procedure of Chapter 3.3.1 (see also Annex 3 for more details on the exact procedure).

The optimisation procedure in this report on photodegradation only considers aqueous concentrations of the three selected compounds. Because of their low K_{oc} values (Table 10.1), partitioning between water and sediment is expected to be negligible and not to impact the optimisation procedure. For the compounds of metribuzin and imidacloprid this was checked and confirmed by Deneer et al. (2015) in

their Chapter 8. For metribuzin no measurements of sediment concentrations were available, while for imidacloprid the sediment concentration was measured once at the end of the experiment of Colombo et al. (2013) at day 56. So, there were hardly data to compare the simulated concentrations to, but the TOXSWA simulated maximum percentages of total mass in sediment remained below 3% (organic matter percentage in sediment 9%). So, these percentages were too small to have a significant impact the optimised degradation rates in water.

Table 10.2   *Compounds and available cosm studies with their locations, selected for inverse modelling by TOXSWA-PEST.*

Compound	Study	Location	Period of study
Metribuzin	Fairchild & Sappington, 2002	Columbia, Missouri, USA	22 May 2001[*] + 14 d
	Arts et al., 2006	Renkum, NL	6 May 2002 + 14 d
	Brock et al., 2004	Renkum, NL	5 May 1999 + 56 d
Imidacloprid	Colombo et al., 2013	Berlin, Germany	1 June-1 Aug 2009
	Bayer, 2001	Monheim, Germany	8 May 2000 + 21 d
	Bayer, 2003	Itingen, Switzerland	2 May 2001 + 91 d
Metamitron	Wendt-Rasch et al., 2004	Renkum, NL	6 April 1999 + 28 d
	Brock et al., 2004	Renkum, NL	5 May 1999 + 28 d
	Van Wijngaarden et al., 2004	Indoor[*]	

* Study finally not used as it was performed in indoor cosms.

11 Analysis of cosm experiments with metribuzin

11.1 Introduction

Three studies were inversely modelled by TOXSWA-PEST. The main characteristics of these studies are given in Table 11.1.

Table 11.1 *Main characteristics for studies involving metribuzin (Annex 4).*

Data set analysed	Type of cosm	Water depth (m)	Macrophytes	pH	Location	Period	Light intensity
Fairchild & Sappington (2002)	Outdoor clay-lined pond	0.75	> 80% cov. 40 g/m^2 on day -7, *Najas guadalupensis*, common water nymph or guppy grass, > 100 g/m^2 on day 30	8.1 ± 1.2	Columbia, Missouri, USA	22 May 2001* + 14 days	Day 0 = 22 May, turbidity 4.2 ± 2.6 NTUs
Arts et al. (2006)	Outdoor ditch	0.5 (centre ditch)	Highest treatment: decrease filamentous algae from 40 to 5% coverage	8.45	Renkum, The Netherlands	6 May 2002 + 7 days (1 of the 6 ditches + 14 days)	-
Brock et al. (2004)	Outdoor circular enclosures, diameter 105 cm and rim of 25 cm high	0.5	*Myrophillum* (up to 75% cover), *Sagittaria sagittifolia* (<5%) and *Elodea nuttallii* (<1%) present	variable 7.3-10.5	Renkum, The Netherlands	5 May 1999 + 56 days	-

* Year not given, presumably 2001

Table 11.2 presents the main physico-chemical properties of metribuzin, that were used in the simulations.

Table 11.2 *Main physico-chemical properties of metribuzin used in the simulations (taken from Deneer et al., 2015).*

Metribuzin	
Molar mass (g)	214.29
Saturated vapour pressure (mPa)	0.121 (25 °C)
Solubility (mg L-1)	1165 (20 °C)
Kom (estimated) (L kg-1)	Kom=22, N=1.08[6]
pKa	0.99 (for transition between neutral and positively charged molecule)

---

[6] From https://efsa.onlinelibrary.wiley.com/doi/epdf/10.2903/j.efsa.2006.88r and applying Kom=Koc/1.724

11.2   Cosm study by Fairchild and Sappington (2002)

Fairchild and Sappington (2002) described the results of a mesocosm study with metribuzin in ponds located at Columbia, Missouri, U.S.A. The outdoor clay-lined pond measured 1000 m^2 and had a water depth of 0.75 m. Exposure levels were measured only shortly after application of metribuzin on 22nd May (year not given, presumably 2001). Details on measured concentrations are given in Annex 3. No measurements were performed for concentrations in sediment and in the macrophytes present in the ponds, but the macrophyte composition and biomass was measured at several points in time and reported.

The cosm of Fairchild and Sappington (2002) was inversely modelled and the agreement between measured and simulated aqueous concentrations was optimised with the aid of PEST, according to the procedures presented in Chapters 7 and 9. Forty-nine optimisations were performed, each with its own initial values of $DegT_{50, photo,ref}$ and loading at $t = 0$ and specified lower and upper parameter bounds. The initial values used are the same for all simulations and have already been presented in Table 8.1.

Details of the results are given in Annex 4. From the 49 fits, 30 resulted in a satisfactory agreement between measured and simulated aqueous concentrations. These 30 fits resulted in consistent estimates for the $DegT_{50, photo,ref}$ of 4.8 days with 95% confidence intervals of 2.3 – 7.3 days and consistent estimates of the initial loading of 799 mg m^{-2} with 95% confidence intervals of 655-943 mg m^{-2}. The optimisations passed the $\chi2$-test with error percentages clearly below 10%, which is an acceptable value for field experiments according to FOCUS (2006).

Figure 11.1 presents a satisfactory agreement between scaled optimised and measured water concentrations for one of the optimisations (initial $DegT_{50}$ of 5 days and loading of 1000 mg m^{-2}, fitted DegT50, loading and confidence intervals as stated above and error percentage of 6.8%). The simulated concentration profile shows a wavy pattern, due to the rapid photodegradation during daytime and stagnating photodegradation after sunset. Figure 11.2 presents the distribution of the scaled residuals between model-generated and measured concentrations, as suggested by FOCUS (2006). The graph shows that the residuals are randomly scattered around zero, demonstrating that there is no pattern of under- or over-prediction by the TOXSWA model.

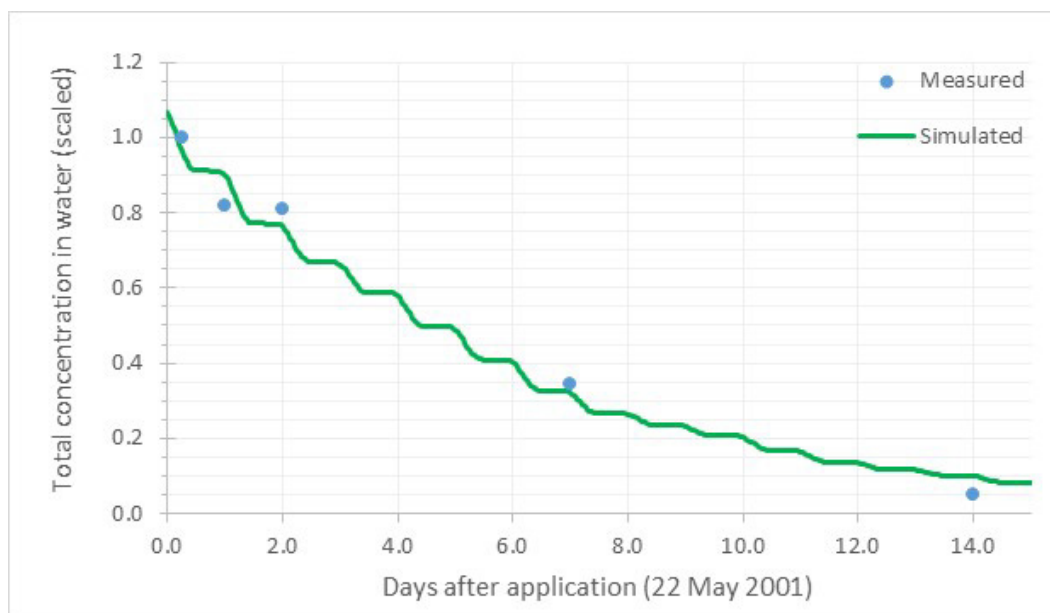**Figure 11.1**   *Simulated and measured total concentration (dissolved+ sorbed to suspended solids, μg.L^{-1}) metribuzin in water as a function of time (d) in the cosm of Fairchild and Sappington (2002). Simulated concentration profile obtained by PEST_TOXSWA optimisation for an initial $DegT_{50,photo,ref}$ = 5 d and an initial loading of 1000 mg m^{-2}.*

Figure 11.2 *Residuals of total concentration (dissolved+ sorbed to suspended solids, µg.L^{-1}) metribuzin in water as a function of time (d) in the cosm of Fairchild and Sappington (2002). Simulated concentration profile obtained by PEST_TOXSWA optimisation for an initial DegT$_{50,photo,ref}$ = 5 d and an initial loading of 1000 mg m^{-2}.*
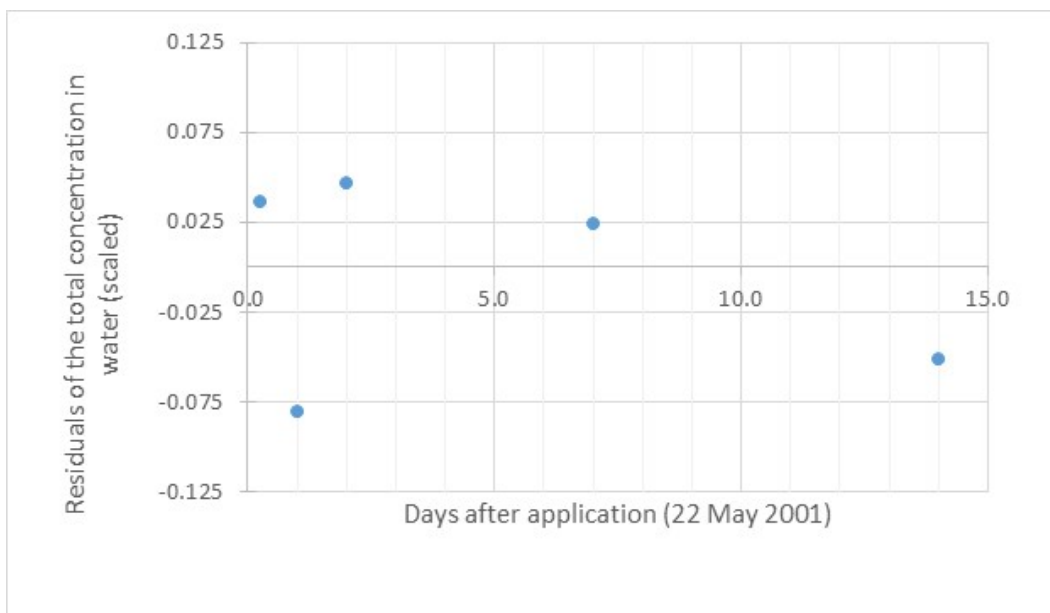
11.3   Cosm study by Arts et al. (2006)

Arts et al. (2006) reported data on the fate of metribuzin in a mesocosm study in outdoor ditches located at Renkum, The Netherlands. Treatment consisted of a single application on 6th May 2002, at three different nominal initial levels, treating three separate ditches at each level. The concentrations in the ditches receiving 1% and 5% of the recommended product use rate were inversely modelled. Water depth in the centre of the ditches was 50 cm, but above the wide side slopes the water depth was less. No measurements of metribuzin in sediments were reported, nor was the organic matter content of the sediment given. The macrophyte composition and biomass was measured at several points in time and reported. Details on concentrations measured in the ditches are given in Annex 3.

The ditches of Arts et al. (2006) were inversely modelled and the agreement between measured and simulated aqueous concentrations (scaled as described in 9.3) was optimised with the aid of PEST, according to the procedures presented in Chapters 7 and 9. Forty-nine optimisations were performed, each with its own initial values of *DegT$_{50, photo,ref}$* and loading at *t* = 0 and specified lower and upper parameter bounds. The initial values used have been presented in Table 8.1.

Details of the results are given in Annex 4. From the 49 fits, 25 resulted in a satisfactory agreement between measured and simulated aqueous concentrations. These 25 fits resulted in consistent estimates for the *DegT$_{50, photo,ref}$* of 1.29 days with 95% confidence intervals of 1.1 – 1.5 days and consistent estimates of the initial loading of 388 mg m^{-2} with 95% confidence intervals of 361-415 mg m^{-2}. The optimisations passed the $\chi2$-test with error percentages below 15%, which is an acceptable value for field experiments according to FOCUS (2006).

Figure 11.3 presents a satisfactory agreement between scaled optimised and measured water concentrations for all six ditches in one of the 25 optimisation sets. Figure 11.4 presents the distribution of the scaled residuals between model-generated and measured concentrations, as suggested by FOCUS (2006). The graph shows that the residuals are reasonably well scattered around zero (only after seven days, the simulation seems to be systematically too low), demonstrating that there is no pattern of under- or over-prediction by the TOXSWA model.

Figure 11.3 *Simulated and measured total concentration (dissolved+ sorbed to suspended solids, µg.L^{-1}) metribuzin in water as a function of time (d) in the ditches of Arts et al. (2006). Simulated concentration profile obtained by PEST_TOXSWA optimisation (fitted DegT$_{50, photo,ref}$ of 1.29 days with 95% confidence intervals of 1.1 – 1.5 days and fitted initial loading of 388 mg m^{-2} for an initial DegT$_{50,photo,ref}$ = 1 d and an initial loading of 500 mg m^{-2}).*

Figure 11.4 *Residuals of total concentration (dissolved+ sorbed to suspended solids, µg.L^{-1}) metribuzin in water as a function of time (d) in the ditches of Arts et al. (2006). The residuals profile was obtained by a PEST_TOXSWA optimisation for an initial DegT$_{50,photo,ref}$ = 1 d and an initial loading of 500 mg m^{-2}.*

11.4   Cosm study by Brock et al. (2004)

The paper by Brock et al. (2004) describes fate data for metribuzin in moderately buffered mesotrophic enclosures (polycarbonate, circular with diameter of 1.05 m and water level 25 cm below the rim, pervious to light, no information on sediment composition is given) in outdoor ditches located

at Renkum, The Netherlands. Enclosures were treated at six different exposure levels on May 5, 1999. Water samples were taken nine or 10 times after the application over a 56 days period. More details on the measured concentrations are given in Annex 3. No analyses in sediment were reported. An initial logarithmic plot of (scaled) concentrations versus time indicated that the dissipation rates in all enclosures were very similar. Assuming that this indicates that the simulated degradation rates were also very similar for all enclosures, it was decided to include only the data for enclosures with the lowest and highest dissipation rates (enclosures 1 and 8, with initial nominal concentrations of 5.6 and 56 µg/L, resp.)

The enclosures of Brock et al. (2004) were inversely modelled and the agreement between measured and simulated aqueous concentrations (scaled as described in 9.3) was optimised with PEST, according to the procedures presented in Chapters 7 and 9. Forty-nine optimisations were performed, each with its own initial values of $DegT_{50, photo, ref}$ and loading at $t = 0$ and specified lower and upper parameter bounds. The initial values used have been presented in Table 8.1.

Details of the results are given in Annex 4. From the 49 fits, 40 resulted in a satisfactory agreement between measured and simulated aqueous concentrations. These 40 fits resulted in consistent estimates for the $DegT_{50, photo, ref}$ of 3.4 days with 95% confidence intervals of 2.7 – 4.1 days and consistent estimates of the initial loading of 468 mg m^{-2} with 95% confidence intervals of 439-498 mg m^{-2}. The optimisations passed the χ^2-test with error percentages around 10%, which is an acceptable value for field experiments according to FOCUS (2006).

Figure 11.5 presents a satisfactory agreement between scaled optimised and measured water concentrations for the two enclosures in one of the optimisation sets. Its initial $DegT_{50}$ was 5 days and loading of 500 mg m^{-2}, the fitted $DegT_{50, photo, ref}$ and initial loading were as mentioned above and the error percentage of 10.4%. Figure 11.5 presents the distribution of the scaled residuals between model-generated and measured concentrations, as suggested by FOCUS (2006). The graph shows that the residuals are reasonably well-scattered around zero, demonstrating that there is no pattern of under- or over-prediction by the TOXSWA model.

Figure 11.5 *Simulated and measured total concentration (dissolved+ sorbed to suspended solids, µg.L^{-1}) metribuzin in water as a function of time (d) in the enclosures of Brock et al. (2004). Simulated concentration profile obtained by PEST_TOXSWA optimisation for an initial $DegT_{50,photo,ref}$ = 5 d and an initial loading of 500 mg m^{-2}.*
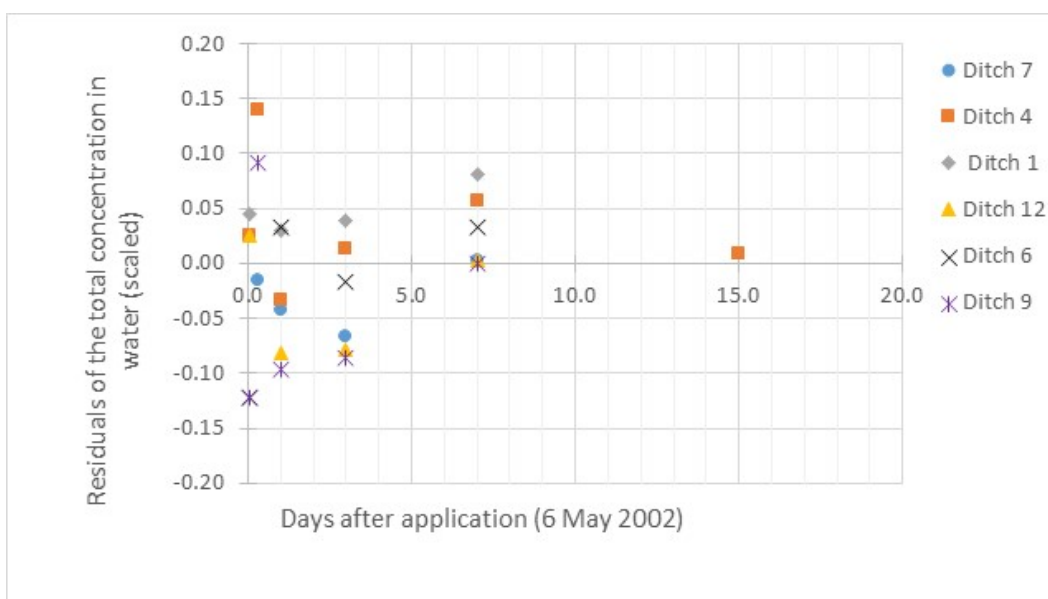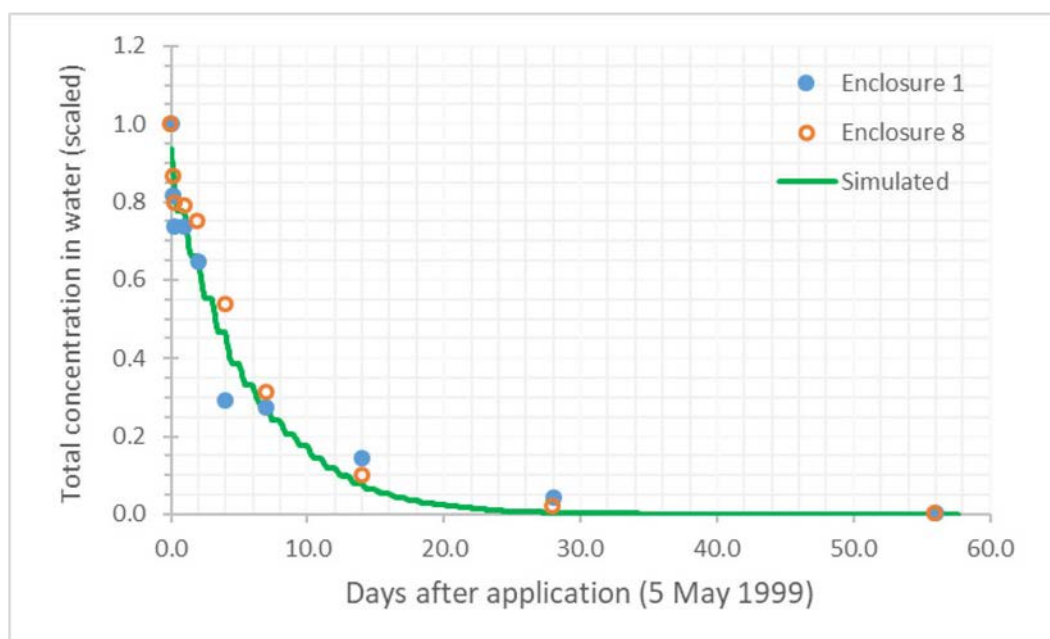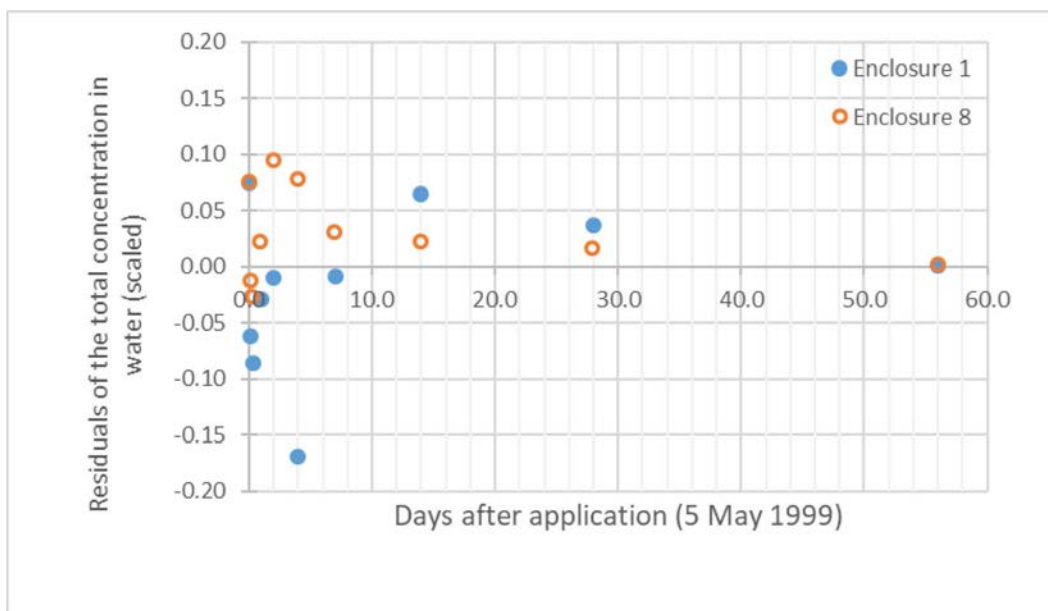
Figure 11.6 *Residuals of total concentration (dissolved+ sorbed to suspended solids, µg.L^{-1}) metribuzin in water as a function of time (d) in the enclosures of Brock et al. (2004). The residuals profile was obtained by a PEST_TOXSWA optimisation for an initial DegT$_{50,photo,ref}$ = 5 d and an initial loading of 500 mg m^{-2}.*

11.5 Comparison with degradation rates from other sources

An overview of the results of the inverse modelling, i.e. the obtained values for the *DegT$_{50,photo,ref}$* in water and the initial loading, is presented in Table 11.3.

Table 11.3 *Estimates of DegT$_{50,photo,ref}$ and initial loading plus their 95% confidence intervals and χ^2 errors for metribuzin in water obtained by inverse modelling by TOXSWA-PEST of the data sets.*

Data set analysed	*DegT$_{50,photo,ref}$* (days)[*] at daily $I_{ref,act,UV-VitD}$ = 5000 J m^{-2}	Initial loading (mg m^{-2})	Approximate χ^2 error (%)
Fairchild and Sappington (2002)	4.8 (2.3-7.3)	799 (655-943)	7%
Arts et al. (2006)	1.29 (1.1-1.5)	388 (361-415)	14%
Brock et al. (2004)	3.4 (2.7-4.1)	468 (439-498)	10%

The influence of water depth of the cosms, their skyview and water surface area coverage by macrophytes on the obtained *DegT$_{50,photo,ref}$* values is considered in Chapter 14 as well as a comparison with the values for the *DegT$_{50}$* values (at the reference temperature of 20 °C) obtained in the report of Deneer et al. (2015).

Table 11.4 gives an overview of data found in several sources on the dissipation of metribuzin in water as a result of hydrolysis, photolysis and microbial degradation in laboratory water-sediment studies. With the aid of these data we here evaluate the consistency of the tiered approach for the *DegT$_{50}$* in water, proposed by Boesten et al. (2014) and also presented in Chapter 9.5.

Table 11.4 *Dissipation half-lives of metribuzin as obtained from different sources.*

Process/system	DT_{50} (days)	Source
Hydrolysis	Stable over 34 days at pH 4, 7 and 9 (25°C) DT_{50} 635 d at pH 9 (25°C)	EU agreed endpoints from EFSA conclusion[7]
Hydrolysis	Stable over 34 days at pH 4 – 9 (25°C)	Footprint database
Photolysis	0.18 d, sterile water, sunlight exposure in quartz cell 0.026 d, River Rhine water, Xenon light exposure in quartz cell (temperature not given, not normalized/ standardized to a latitude)	EU agreed endpoints from EFSA conclusion[1]
Photolysis	0.2 d (pH 7)	Footprint database
Water/sediment	DT_{50} water: 41 and 41 d (n=2) DT_{50} whole system: 47 and 50 d (n=2)	EU agreed endpoints from EFSA conclusion[1]
Water/sediment	DT_{50} water: 41 d DT_{50} whole system: 50 d	Footprint database

Boesten et al. (2014) recommended using the longest DT_{50} in the pH range of 7 – 9.5 for hydrolysis data. This was 635 days at 25°C. Assuming an Arrhenius activation energy of 75 kJ/mol, as proposed by Boesten et al. (2014), this corresponds to a DT_{50} of 1,080 days at 20°C (approximately corresponding to the higher range of temperatures found in the cosms).

Aerobic water-sediment studies indicate a whole-system DT_{50} of 50 days at 20°C.

The *DegT$_{50, water}$* estimated from cosm data was in the range of 1.29? to 4.8 days for a $I_{ref,act,UV-VitD}$ of 5000 J m^{-2} d^{-1}.

Hence, for the data considered, going from lower- to higher-tier data did indeed result in less conservative estimates for the degradation rate of metribuzin.

---

[7] https://efsa.onlinelibrary.wiley.com/doi/epdf/10.2903/j.efsa.2006.88r

12 Analysis of cosm experiments with imidacloprid

12.1 Introduction

Three studies were inversely modelled by TOXSWA-PEST. The main characteristics of each of the studies are given in Table 12.1.

Table 12.1 *Main characteristics for studies involving imidacloprid (Annex 5).*

Data set analysed	Type of cosm	Water depth (m)	Macrophytes	pH	Location	Period	Light intensity
Colombo et al. (2013)	Polypropylene containers in outdoor pond	0.11	None	8-9	Berlin, Germany	Late May, probably 2012 + 56 days	High levels, UVB 2.35/2.78/2.75 µW/cm^2 average after each pulse
Bayer (2001)	Outdoor: 1 round test pond, 1 rectangular tank	Pond 1.0 m; tank 0.3 m	Pond coverage 30%; tank coverage 60%	7.0-8.5 slight increase over time	Monheim, Germany	8 May 2000 + 21 days	No changes in turbidity observed
Bayer (2003)	13 round ponds, 1300 or 1800 L, 1 m water depth	1.0	*Lemna* removed regularly at each sampling date, no other macrophytes observed	Increase from 7.4 on day 0-13 to 9.5 (day 35), then decrease to 7.4 (day 91)	Itingen, Switzerland	1 January 2000 + 77 days (pond 2 and 7), + 91 days (pond 8 and 13)[*]	Sunny weather on day of application, daily sun hours given

[*] Date at pages 128 and 129 of Annex 6, 2 May 2001 was mentioned as application day at page 52 of Chapter 7.

Table 12.2 presents the main physico-chemical properties of imidacloprid, that were used in the simulations.

Table 12.2 *Main physico-chemical properties of imidacloprid used in the simulations (taken from Deneer et al., 2015).*

Imidacloprid	
Molar mass (g)	255.66
Saturated vapour pressure (mPa)	4.0 E-7 (25 °C)
Solubility (mg L^{-1})	610 (20 °C)
Kom (estimated) (L kg^{-1})	Kom=132, N=0.802[8]
pKa	n.a.

12.2 Cosm study by Colombo et al. (2013)

Colombo et al. (2013) reported the results of experiments in small (20 L water) enclosures with shallow water depth (11 cm) located at Berlin, Germany, and containing sediment, where macrozoobenthos was exposed to imidacloprid. The exposure was implemented as three pulses with

---

[8] From https://efsa.onlinelibrary.wiley.com/doi/epdf/10.2903/j.efsa.2008.148r

weekly intervals, allowing for substantial decrease of concentrations between applications. Applications occurred from late May – June 2009 (assuming they were in the year the student report on Colombo was written, 2009). Nominal initial concentrations ranged from 0.6 to 40 µg/L. Although exposure concentrations were measured in all of the cosms, the fate of imidacloprid was studied in more detail in cosms with the nominal concentration of 17.3 µg/L, for which a total of 18 measured concentrations in water were reported. Details on measured concentrations are given in Annex 4. The concentration of imidacloprid in sediment was only measured once, on day 56, at the end of the experiment and the containers did not contain macrophytes.

The results from Colombo et al. (2013) were inversely modelled and the agreement between measured and simulated aqueous concentrations (scaled) was optimised with the aid of PEST, according to the procedures presented in Chapters 7 and 9. Forty-nine optimisations were performed, each with its own initial values of $DegT_{50, water}$ and loading and specified lower and upper parameter bounds. The initial values used have already been presented in Table 8.1.

Details of the results are given in Annex 5. All 49 optimisations resulted in consistent estimates of $DegT_{50,photo,ref}$ of 1.6 days with 95% confidence intervals of 1.3 – 1.9 days and consistent estimates of the loading of 101.7 mg m^{-2} with 95% confidence intervals of 86.3-116.1 mg m^{-2}. Relatively high error percentage just below 15% were found, resulting in just passing the $\chi 2$-test according to FOCUS (2006) for field experiments.

Figure 12.1 presents a satisfactory agreement between scaled optimised and measured water concentrations for one optimisation. Its initial DegT$_{50}$ was 2 days and loading of 100 mg m^{-2}, the fitted the $DegT_{50, photo,ref}$ and loading and their 95% confidence intervals were as mentioned above and the error percentage was 14.2%. Figure 12.2 presents the distribution of the scaled residuals between model-generated and measured concentrations, as suggested by FOCUS (2006). The graph shows that the residuals are randomly scattered around zero, demonstrating that there is no pattern of under- or over-prediction by the TOXSWA model.

Figure 12.1 *Simulated and measured total concentration (dissolved+ sorbed to suspended solids) imidacloprid in water as a function of time in the containers of Colombo et al. (2013). The simulated concentration profile was obtained by a PEST_TOXSWA optimisation for an initial DegT$_{50,photo,ref}$ = 2 d and an initial loading of 100 mg m^{-2}.*

Figure 12.2 *Residuals of total concentration (dissolved+ sorbed to suspended solids) imidacloprid in water as a function of time in the containers of Colombo et al. (2013). The simulated concentration profile was obtained by a PEST_TOXSWA optimisation for an initial DegT$_{50,photo,ref}$ = 2 d and an initial loading of 100 mg m^{-2}.*

12.3 Cosm study by Bayer (2001)

Bayer (2001) reported results of simultaneous experiments in a small pond (diameter 2.0 m, water depth 1.0 m) and a small rectangular tank (0.6 x 1.8 m, water depth 0.3 m) located at Monheim, Germany. The exposure for both systems consisted of a single application on 8th May 2000 at a nominal initial concentration of 6.0 µg a.i./L. Details on measured concentrations are given in Annex 4. The concentration of imidacloprid in sediment was measured eight times over 70 days, but most measurements resulted in values below the limit of quantification. The tank had a much higher coverage with macrophytes (60%) than the pond (approx. 30%) over the first 21 days.

The pond and tank of Bayer (2001) were inversely modelled and the agreement between measured and simulated aqueous concentrations (scaled) was optimised with the aid of PEST, according to the procedures presented in Chapters 7 and 9. The pond and tank data were analysed separately as their water depths were very different (pond 1 m and tank 0.3 m) and therefore photodegradation will play a larger role in the concentration profile of the pond than that of the tank.

Both for the pond and the tank, forty-nine optimisations were performed, each with their own initial values of *DegT$_{50, water}$* and loadings and specified lower and upper parameter bounds. The initial values used have been presented in Table 8.1. Details of the results of inverse modelling are given in Annex 5.

For the **pond** 34 of the 49 fits resulted in a satisfactory agreement between measured and simulated aqueous concentrations (excluding an outlier after 0.16 days which was caused by insufficient mixing of the applied imidacloprid). These 34 fits resulted in consistent estimates for the *DegT$_{50, photo,ref}$* of 8.1 days with 95% confidence intervals of 5.9 – 10.2 days and consistent estimates of the initial loading of 1042 mg m^{-2} with 95% confidence intervals of 919-1164 mg m^{-2}. The optimisations passed the *χ2*-test with error percentages around 6-7%, which are very acceptable values for field experiments according to FOCUS (2006).

Figure 12.3 presents a satisfactory agreement between scaled optimised and measured water concentrations for one optimisation. Its initial DegT$_{50}$ was 10 days and loading of 1000 mg m^{-2}, the fitted the *DegT$_{50, photo,ref}$*, initial loading and their 95% confidence intervals were as mentioned above and the error percentage was 6.5%. Figure 12.4 presents the distribution of the scaled residuals between model-generated and measured concentrations, as suggested by FOCUS (2006). The graph

shows that the residuals are reasonably well-scattered around zero (there is a slight wave-type pattern), demonstrating that there is no clear pattern of under- or over-prediction by the TOXSWA model.

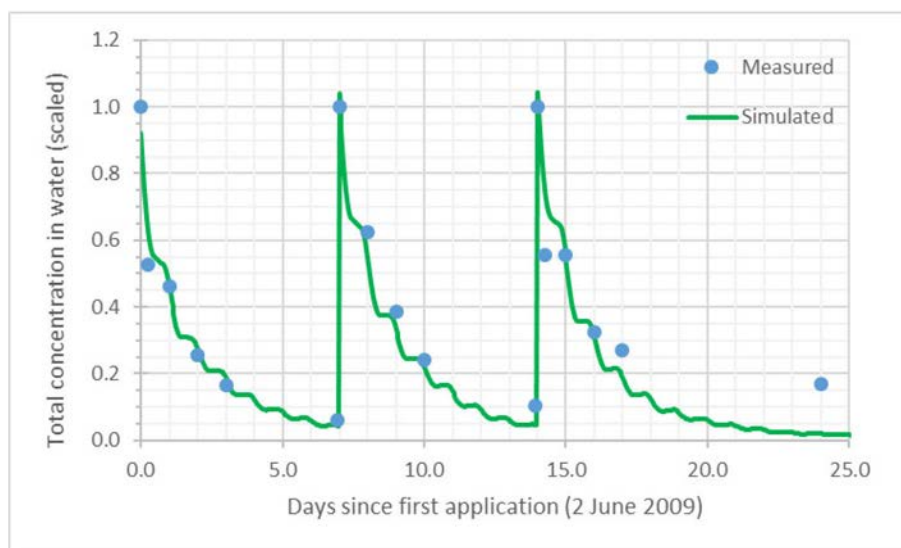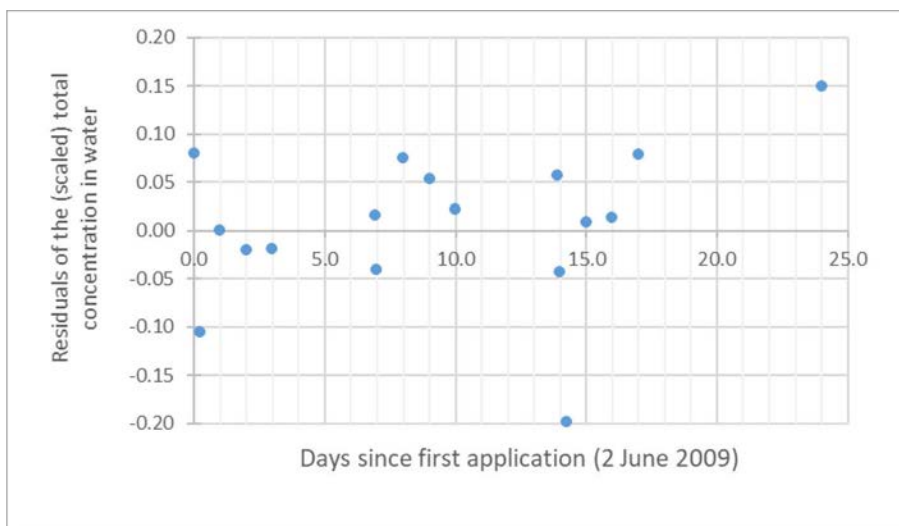**Figure 12.3** *Simulated and measured total concentration (dissolved+ sorbed to suspended solids) imidacloprid in water as a function of time in the pond of Bayer (2001). The simulated concentration profile was obtained by a PEST_TOXSWA optimisation for an initial DegT$_{50,photo,ref}$ = 10 d and an initial loading of 1000 mg m^{-2} (excluding the outlier at t=0.16 d).*

Figure 12.4 *Residuals of total concentration (dissolved+ sorbed to suspended solids) imidacloprid in water as a function of time in the pond of Bayer (2001). The simulated concentration profile was obtained by a PEST_TOXSWA optimisation for an initial DegT$_{50,photo,ref}$ = 10 d and an initial loading of 1000 mg m^{-2} (excluding the outlier at t=0.16 d).*

For the **tank** 37 of the 49 fits resulted in a satisfactory agreement between measured and simulated aqueous concentrations. These 37 fits resulted in consistent estimates for the *DegT$_{50, photo,ref}$* of 6.5 days with 95% confidence intervals of 4.5 – 8.4 days and consistent estimates of the initial loading of 290 mg m^{-2} with 95% confidence intervals of 259-321 mg m^{-2}. The optimisations passed the $\chi 2$-test with error percentages around 7-8%, which are very acceptable values for field experiments according to FOCUS (2006).

Figure 12.5 presents a satisfactory agreement between scaled optimised and measured water concentrations for one optimisation. Its initial $DegT_{50}$ was 5 days and loading of 300 mg m^{-2}, the fitted the $DegT_{50, photo,ref}$, initial loading and their 95% confidence intervals were as mentioned above and the error percentage was 7.7%. Figure 12.6 presents the distribution of the scaled residuals between model-generated and measured concentrations, as suggested by FOCUS (2006). The graph shows that the residuals are reasonably well-scattered around zero (there is again a slight wave-type pattern), demonstrating that there is no clear pattern of under- or over-prediction by the TOXSWA model.
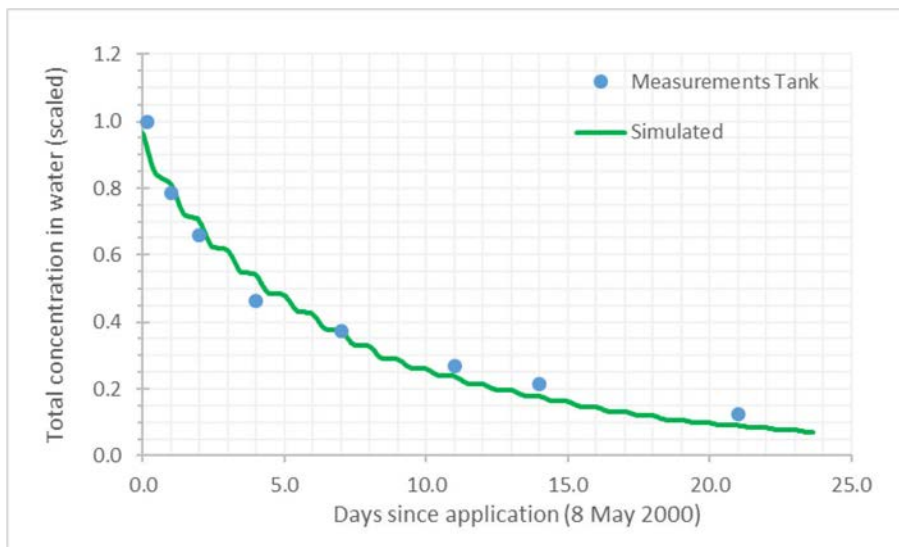
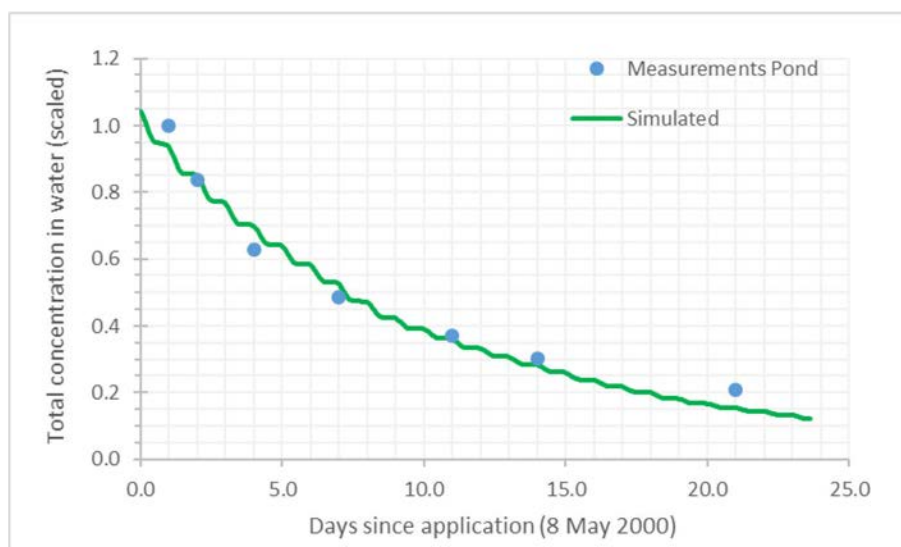**Figure 12.5** *Simulated and measured total concentration (dissolved+ sorbed to suspended solids) imidacloprid in water as a function of time in the tank of Bayer (2001). The simulated concentration profile was obtained by a PEST_TOXSWA optimisation for an initial DegT$_{50,photo,ref}$ = 5 d and an initial loading of 300 mg m^{-2}.*
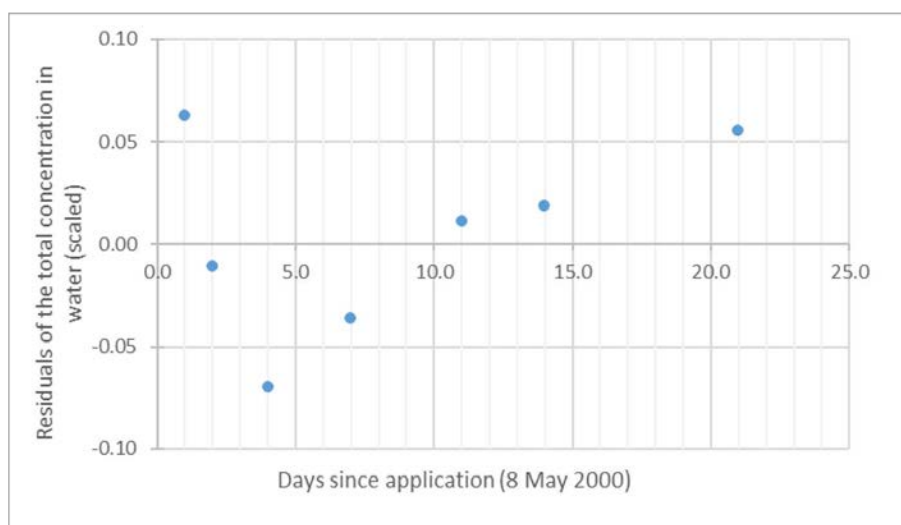

Figure 12.6 *Residuals of total concentration (dissolved+ sorbed to suspended solids) imidacloprid in water as a function of time in the tank of Bayer (2001). The simulated concentration profile was obtained by a PEST_TOXSWA optimisation for an initial DegT$_{50,photo,ref}$ = 5 d and an initial loading of 300 mg m^{-2}.*

12.4   Cosm study by Bayer (2003)

Bayer (2003) described a study in 13 outdoor ponds located at Itingen, Switzerland. The test substance was applied twice, on 2nd May and 23rd May 2001. There was no deliberate mixing of the ponds after application and there was no or only slight wind during the applications on both dates. Water samples (14 or 15) were taken from each of the ponds up to 77 or 91 days after the first application. Details on measured concentrations and dosages applied are given in Annex 4. The report mentions that floating plants of *Lemna* were removed from the ponds at each sampling date and that perifyton algae were present on the tank wall and water surface. This lead to low percentages (1.6 to 4.1%) surface water area coverage for the 4 ponds with the two highest treatments of 9.4 and 23.5 μg/L.

Each of these four ponds (nrs 7 and 13 with 23.5 μg/L, and nrs 2 and 8 with 9.4 μg/L) were inversely modelled and the agreement between measured and simulated aqueous concentrations (scaled) was optimised with the aid of PEST, according to the procedures presented in Chapters 7 and 9.

So, estimation of $DegT_{50, water}$ was performed for each of the ponds separately. The systems could not be merged in the calculations, because of repeated dosing of the test substance causing different 'loadings' to be used for the second application (TOXSWA cannot simultaneously perform calculations with systems needing different 'loadings' on the same day). For each pond, forty-nine optimisations were performed, each with the initial values of $DegT_{50, water}$ and first loading and specified lower and upper parameter bounds. The initial values used have been given in Table 8.1. Details on the results of inverse modelling are given in Annex 5.

For **pond 2**, all 49 optimisations resulted in a satisfactory estimations of $DegT_{50, photo,ref}$ and loading at $t = 0$. Consistent estimates for the $DegT_{50, photo,ref}$ of 7.3 days with 95% confidence intervals of 5.9 – 8.8 days were obtained as well as consistent estimates of the initial loading of 873 mg m^{-2} with 95% confidence intervals of 760-985 mg m^{-2}. The optimisations passed the $\chi2$-test with the acceptable error percentages of around 13-14%, i.e. below 15%, the acceptable value for field experiments according to FOCUS (2006).

For one optimisation set Figure 12.7 presents the scaled optimised and measured water concentrations. The agreement is good except at the time of the loadings, where the measured concentrations are clearly higher than the simulated ones. The first loading was included in the optimisation, the second not. This is explained by Bayer (2003), who noted that the measured concentrations were clearly higher than the nominal concentrations calculated on the basis of the test doses (126-150% for the first application and 123-148% for the second application). They attributed this to the fact that the dosing solution had not been homogeneously distributed over the water column. The optimisation of Figure 12.7 had an initial DegT$_{50}$ of 5 days and initial loading of 1000 mg m^{-2}, the fitted $DegT_{50, photo,ref}$, initial loading and their 95% confidence intervals were as mentioned above and the error percentage was 13.6%. Figure 12.8 presents the distribution of the scaled residuals between model-generated and measured concentrations, as suggested by FOCUS (2006). The graph shows that, except for the two loadings (see explanation above), the residuals are reasonably well-scattered around zero, demonstrating that there is no significant pattern of under- or over-prediction by the TOXSWA model.
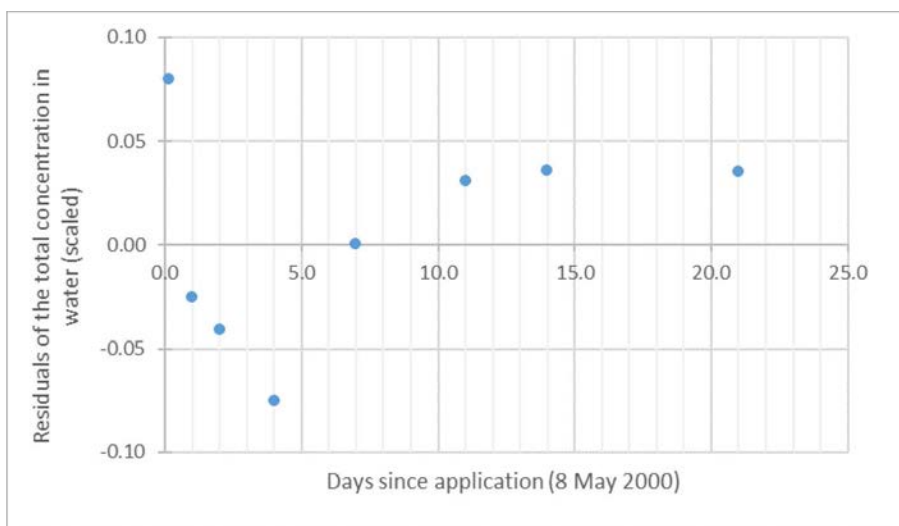
Figure 12.7 *Simulated and measured total concentration (dissolved+ sorbed to suspended solids, scaled concentrations) imidacloprid in water as a function of time after first measurement (d) for pond 2 in the data set of Bayer (2003). Simulated concentration profiles obtained by PEST_TOXSWA optimisation for DegT$_{50,photo,ref}$ = 5 d and an initial loading at t = 0 d of 1000 mg m^{-2}.*

Figure 12.8 *Residuals of total concentration (dissolved+ sorbed to suspended solids, scaled concentration) imidacloprid in water as a function of time after first measurement (d) for pond 2 in the data set of Bayer (2003). Simulated concentration profiles obtained by PEST_TOXSWA optimisation for DegT$_{50,photo,ref}$ = 5 d and an initial loading at t = 0 d of 1000 mg m^{-2}.*

For **pond 7**, 48 of the 49 optimisations resulted in a satisfactory estimations of $DegT_{50, photo,ref}$ and loading at t = 0. Consistent estimates for the $DegT_{50, photo,ref}$ of 7.2 days with 95% confidence intervals of 5.6 – 8.8 days were obtained as well as consistent estimates of the initial loading of 879 mg m^{-2} with 95% confidence intervals of 753-1006 mg m^{-2}. The optimisations with error percentages just above 15% did not pass the $\chi 2$-test, as 15% is the acceptable value for field experiments according to FOCUS (2006).

For one optimisation set Figure 12.9 presents the scaled optimised and measured water concentrations. The agreement is good except at the time of the loadings, where the measured concentrations are again clearly higher than the simulated ones. The first loading is fitted, the second not. As explained above Bayer (2003) attributed the too high measured concentrations at the time of the loadings to the fact that the dosing solution had not been homogeneously distributed over the water column. The optimisation of Figure 12.9 had an initial DegT$_{50}$ of 5 days and initial loading of 1000 mg m^{-2}, the fitted $DegT_{50, photo,ref}$,

initial loading and their 95% confidence intervals were as mentioned above and the error percentage was 15.6%. Figure 12.10 presents the distribution of the scaled residuals between model-generated and measured concentrations, as suggested by FOCUS (2006). The graph shows that, except for the two loadings (see explanation above), the residuals are reasonably well-scattered around zero, demonstrating that there is no significant pattern of under- or over-prediction by the TOXSWA model.
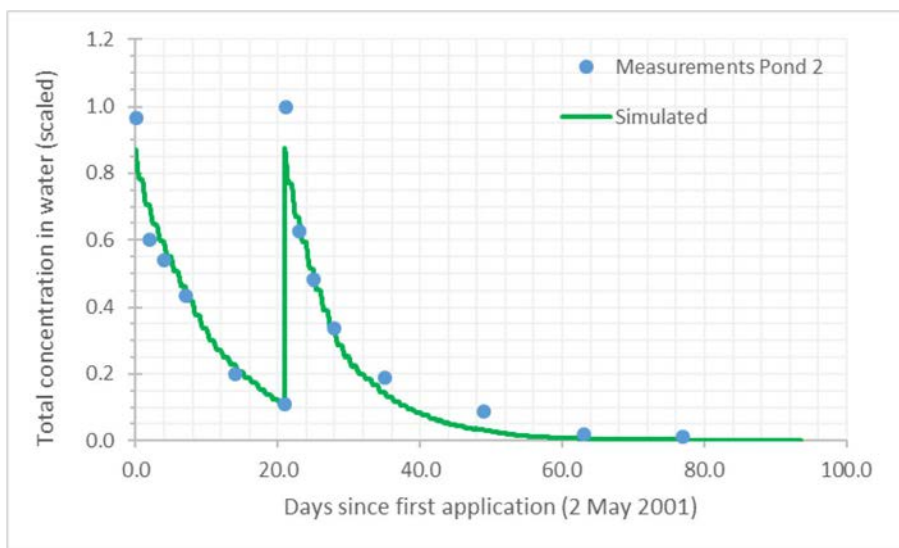

Figure 12.9 *Simulated and measured total concentration (dissolved+ sorbed to suspended solids, scaled concentrations) imidacloprid in water as a function of time after first measurement (d) for pond 7 in the data set of Bayer (2003). Simulated concentration profiles obtained by PEST_TOXSWA optimisation for $DegT_{50,photo,ref}$ = 5 d and an initial loading at t = 0 d of 1000 mg m^{-2}.*

Figure 12.10 *Residuals of total concentration (dissolved+ sorbed to suspended solids, scaled concentration) imidacloprid in water as a function of time after first measurement (d) for pond 7 in the data set of Bayer (2003). Simulated concentration profiles obtained by PEST_TOXSWA optimisation for $DegT_{50,photo,ref}$ = 5 d and an initial loading at t = 0 d of 1000 mg m^{-2}.*
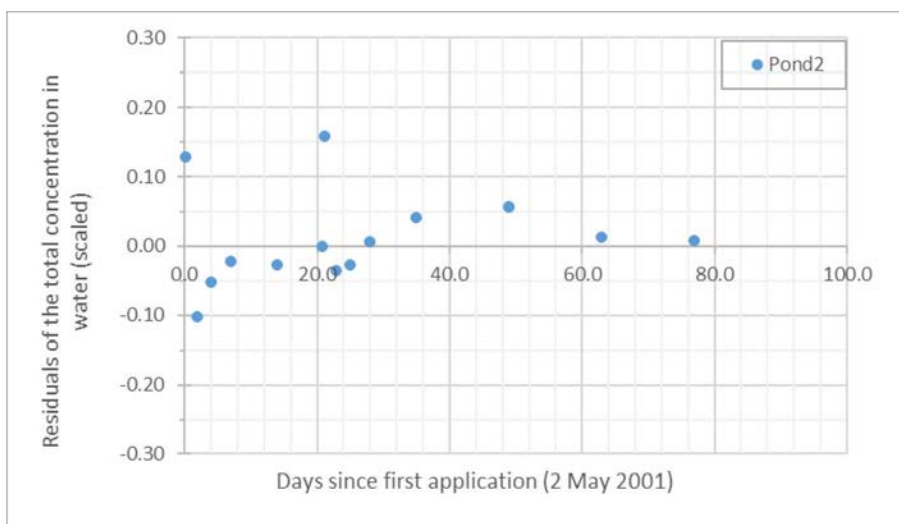
For **pond 8**, 48 of the 49 optimisations resulted in a satisfactory estimations of $DegT_{50, photo,ref}$ and loading at t = 0. Consistent estimates for the $DegT_{50, photo,ref}$ of 6.7 days with 95% confidence intervals of 5.7 – 7.8 days were obtained as well as consistent estimates of the initial loading of 939 mg m^{-2} with 95% confidence intervals of 847-1030 mg m^{-2}. The optimisations passed the $\chi2$-test with the acceptable error percentages of around 11-12%, i.e. below 15%, the acceptable value for field experiments according to FOCUS (2006).

For one optimisation set Figure 12.11 presents the scaled optimised and measured water concentrations. The agreement is good except at the time of the loadings, where the measured concentrations are again clearly higher than the simulated ones. The first loading is fitted, the second not. As explained above Bayer (2003) attributed the too high measured concentrations at the time of the loadings to the fact that the dosing solution had not been homogeneously distributed over the water column. The optimisation of Figure 12.11 had an initial $DegT_{50}$ of 5 days and initial loading of 1000 mg m^{-2}, the fitted $DegT_{50, photo,ref}$, initial loading and their 95% confidence intervals were as mentioned above and the error percentage was 11.5%. Figure 12.12 presents the distribution of the scaled residuals between model-generated and measured concentrations, as suggested by FOCUS (2006). The graph shows that, except for the two loadings (see explanation above), the residuals are reasonably well-scattered around zero, demonstrating that there is no significant pattern of under- or over-prediction by the TOXSWA model.
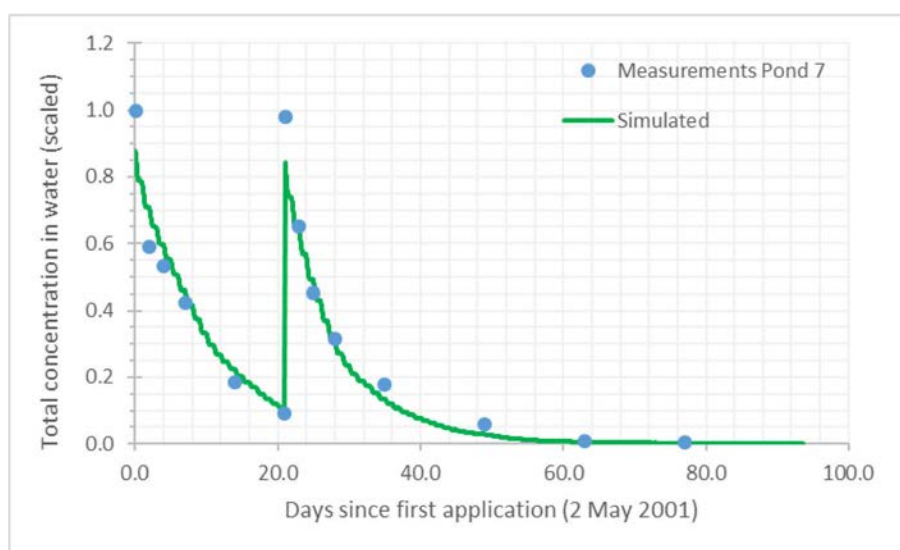

Figure 12.11 *Simulated and measured total concentration (dissolved+ sorbed to suspended solids, scaled concentrations) imidacloprid in water as a function of time after first measurement (d) for pond 8 in the data set of Bayer (2003). Simulated concentration profiles obtained by PEST_TOXSWA optimisation for $DegT_{50,photo,ref}$ = 5 d and an initial loading at t = 0 d of 1000 mg m^{-2}.*

Figure 12.12 *Residuals of total concentration (dissolved+ sorbed to suspended solids, scaled concentration) imidacloprid in water as a function of time after first measurement (d) for pond 8 in the data set of Bayer (2003). Simulated concentration profiles obtained by PEST_TOXSWA optimisation for $DegT_{50,photo,ref}$ = 5 d and an initial loading at t = 0 d of 1000 mg m^{-2}.*
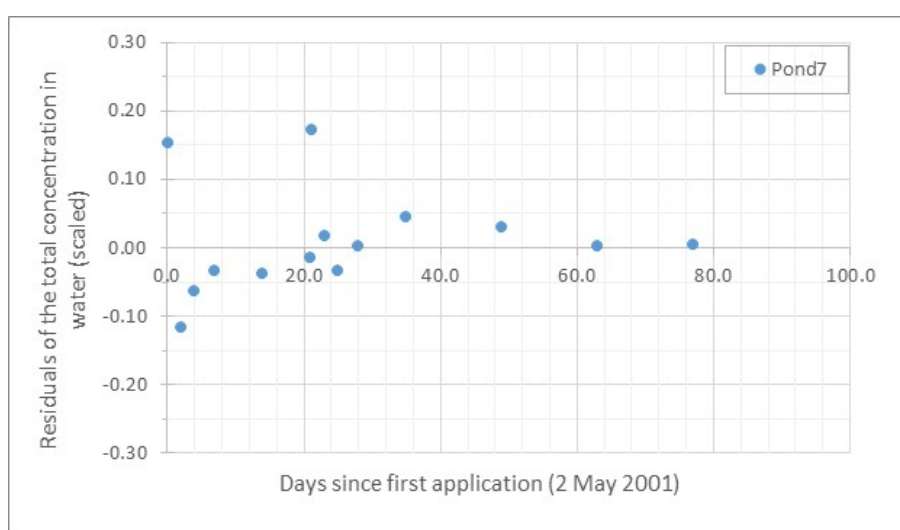
For **pond 13**, all 49 optimisations resulted in a satisfactory estimations of $DegT_{50, photo,ref}$ and loading at $t = 0$. Consistent estimates for the $DegT_{50, photo,ref}$ of 7.0 days with 95% confidence intervals of 5.1-8.8 days were obtained as well as consistent estimates of the initial loading of 876 mg m^{-2} with 95% confidence intervals of 728-1024 mg m^{-2}. The optimisations with error percentages of around 20-21%, did not pass the $\chi 2$-test, as 15% is the acceptable value for field experiments according to FOCUS (2006).

For one optimisation set Figure 12.13 presents the scaled optimised and measured water concentrations. The agreement is good except at the time of the loadings, where the measured concentrations are again clearly higher than the simulated ones. The first loading is fitted, the second not. As explained above Bayer (2003) attributed the too high measured concentrations at the time of the loadings to the fact that the dosing solution had not been homogeneously distributed over the water column. The optimisation of Figure 12.13 had an initial $DegT_{50}$ of 5 days and initial loading of 1000 mg m^{-2}; the fitted $DegT_{50, photo,ref}$, was 7.0 days and its 95% confidence interval was 5.1-8.8 days, the fitted initial loading was 875 mg m^{-2} and its 95% confidence intervals was 728-1024 mg m^{-2}. The error percentage was 20.6%. Figure 12.14 presents the distribution of the scaled residuals between model-generated and measured concentrations, as suggested by FOCUS (2006). The graph shows that, except for the two loadings (see explanation above), the residuals are reasonably well-scattered around zero, demonstrating that there is no significant pattern of under- or over-prediction by the TOXSWA model.
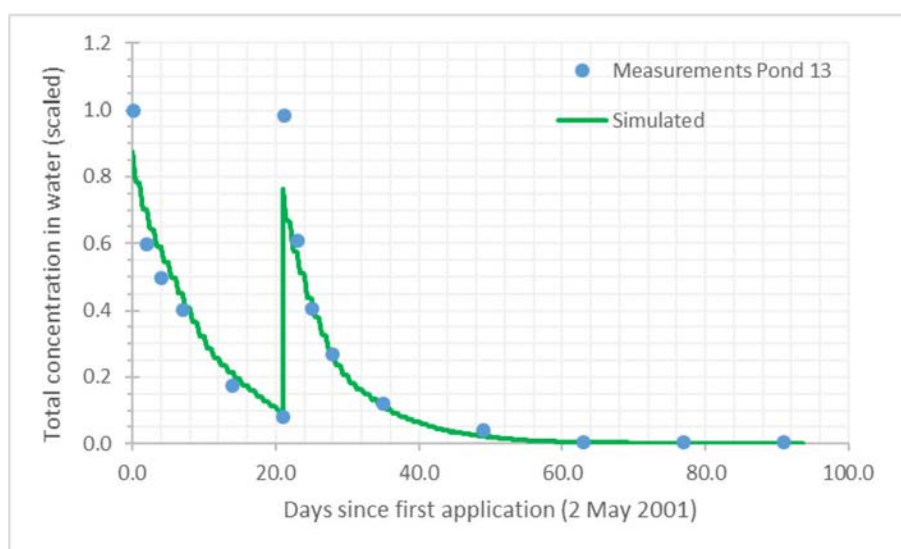
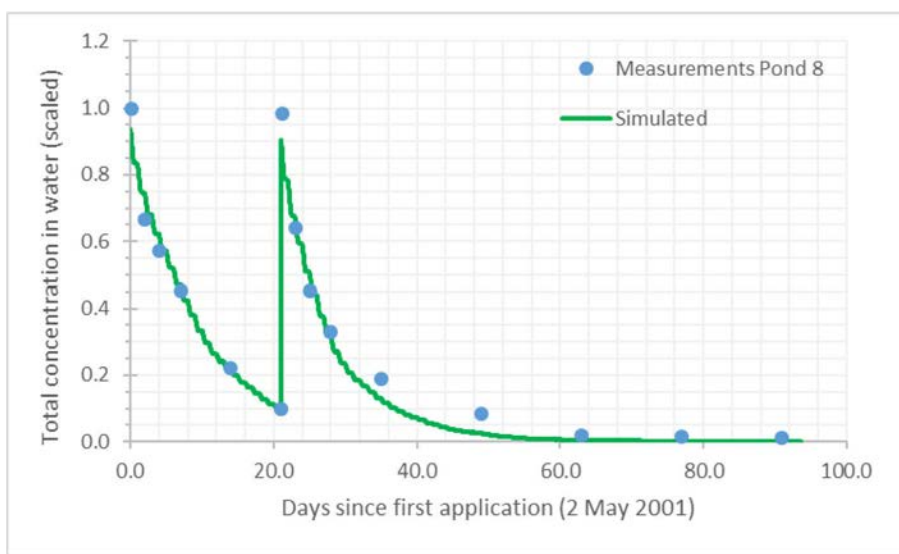**Figure 12.13** *Simulated and measured total concentration (dissolved+ sorbed to suspended solids, scaled concentrations) imidacloprid in water as a function of time after first measurement (d) for pond 13 in the data set of Bayer (2003). Simulated concentration profiles obtained by PEST_TOXSWA optimisation for $DegT_{50,photo,ref}$ = 5 d and an initial loading at t = 0 d of 1000 mg m^{-2}.*
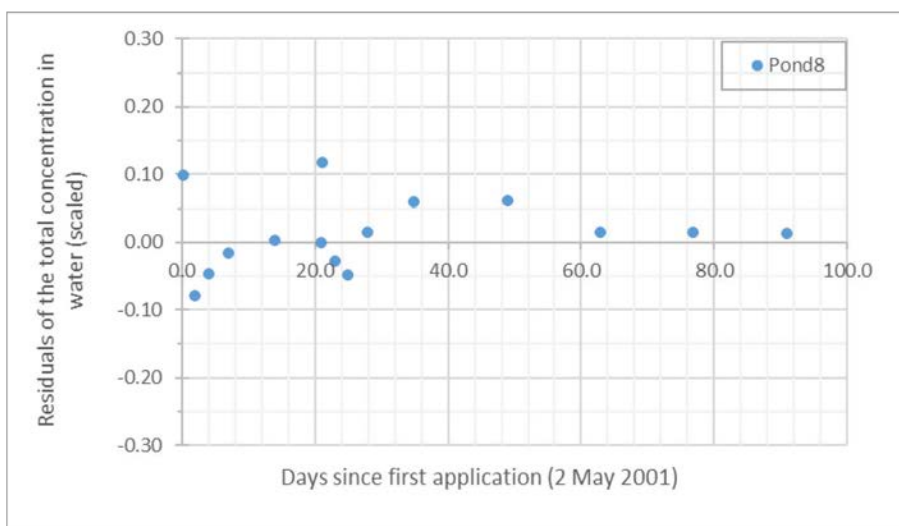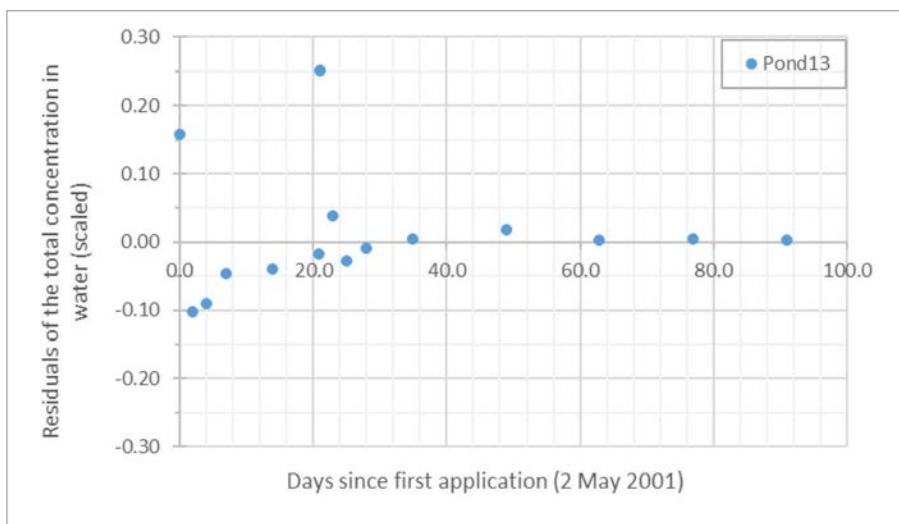
Figure 12.14 *Residuals of total concentration (dissolved+ sorbed to suspended solids, scaled concentration) imidacloprid in water as a function of time after first measurement (d) for pond 13 in the data set of Bayer (2003). Simulated concentration profiles obtained by PEST_TOXSWA optimisation for DegT$_{50,photo,ref}$ = 5 d and an initial loading at t = 0 d of 1000 mg m^{-2}.*

12.5 Comparison with degradation rates from other sources

An overview of the results of the inverse modelling, i.e. the obtained values for the *DegT$_{50,photo,ref}$* of imidacloprid in the cosm water and the initial loading, is presented in Table 12.3.

Table 12.3 *Estimates of DegT$_{50,photo,ref}$ and initial loading plus their 95% confidence intervals and χ^2 errors for imidacloprid in water obtained by inverse modelling by TOXSWA-PEST of the data sets.*

Data set analysed	DegT$_{50,photo,ref}$ (days) at $I_{ref,act,UV-VitD}$ = 5000 J m^{-2}	Initial loading (mg m^{-2})	Approximate χ^2 error (%)
Colombo et al. (2013)	1.6 (1.3-1.9)	101.7 (86.3-116.1)	14-<15%
Bayer (2001)	Pond** 8.1 (5.9-10.2)	1042 (919-1164)	6-7%
	Tank 6.5 (4.5-8.4)	290 (259-321)	7-8%
Bayer (2003)	Pond 2 7.3 (5.9-8.8)	873 (760-985)	13-14%
	Pond 7 7.2 (5.6-8.8)	879 (753-1006)	15-16%
	Pond 8 6.7 (5.7-7.8)	939 (847-1030)	11-12%
	Pond 13 7.0 (5.1-8.8)	876 (728-1024)	20-21%

The influence of water depth of the cosms, their skyview and water surface area coverage by macrophytes on the obtained *DegT$_{50,photo,ref}$* values is considered in Chapter 14 as well as a comparison with the *DegT$_{50}$* values (at the reference temperature of 20 °C) obtained in the report of Deneer et al. (2015).

Table 12.4 gives an overview of data found in several sources on the dissipation of imidacloprid in water as a result of hydrolysis, photolysis and microbial degradation in laboratory water-sediment studies. With the aid of these data we here evaluate the consistency of the tiered approach for the *DegT$_{50}$* in water, proposed by Boesten et al. (2014) and also presented in Chapter 9.5.

Table 12.4   *Dissipation half-lives of **imidacloprid** as obtained from different sources.*

Process	DT$_{50}$ (days)	Source
Hydrolysis	DT$_{50}$ > 1 year at pH 5 and 7; DT$_{50}$ 1 year at pH 9 (25°C)	EU agreed endpoints from EFSA conclusion [9]
Hydrolysis	20.0 d (pH 10.8), 2.85 d (pH 11.8)	Zheng and Liu, 1999
Hydrolysis	Stable at acidic and neutral conditions, increased hydrolysis in alkaline solutions	Liu et al., 2006
Photolysis	Study 1 Suntest, sterile water, normalized results: - 50° latitude (GCSOLAR): 0.24 d spring, 0.17 d summer - 10° longitude, 50° latitude (Frank & Klöpffer): April-summer 0.4-0.28 d, Nov-Dec 3.1-6.73 d *Other photolysis studies are available in the LoEP but were not aimed at the derivation of a DT50 but merely at identifying metabolites*	EU agreed endpoints from EFSA conclusion
Photolysis	Slightly over 3 h, pH 2.8	Banić et al., 2014
Photolysis	5 – 18 min. (25°C)	Liu et al., 2006
Photolysis	43 min. a.i., 126 min. formulated product Confidor (temperature not specified)	Wamhoff and Schneider (1999)
Water/sediment	DT$_{50}$ water: > 30 d, 14.2 d, 109 d DT$_{50}$ whole system: 129 d, 30 d, 150 d	EU agreed endpoints from EFSA conclusion

For hydrolysis data, the longest DT$_{50}$ in the pH range of 7 – 9.5 was 1 year at 25°C. Assuming an Arrhenius activation energy of 75 kJ/mol, as proposed by Boesten et al. (2014), this corresponds to a DT$_{50}$ of 620 days at 20°C, which was the approximate temperature in all cosms of the three studies.

Aerobic water-sediment studies indicate a whole-system DT$_{50}$ of 30 – 150 days (geometric mean: 83 days) at 20°C.

The *DegT$_{50, water}$* estimated from cosm data was in the range of 1.6 – 8.1 days for a *I$_{ref,act,UV-VitD}$* of 5000 J m^{-2} d^{-1}. As imidacloprid is not a strongly sorbing compound, it is unlikely that water-sediment studies with a *DegT$_{50, water}$* of e.g. 7 d would result in whole-system DT$_{50}$ values of 30 – 150 days.

Hence, for the data considered going from lower- to higher-tier data does indeed result in less conservative estimates for the degradation rate of imidacloprid.

---

[9] https://efsa.onlinelibrary.wiley.com/doi/epdf/10.2903/j.efsa.2008.148r

13 Analysis of cosm experiments with metamitron

13.1 Introduction

Three sufficiently detailed papers were found, all describing cosm studies involving metamitron.

In the first study (van Wijngaarden et al., 2004) metamitron was applied twice to a number of indoor microcosm systems with a water volume of approx. 600 L, containing a 10 cm sediment layer and a 50 cm water layer. The light conditions were specified: artificial daylight provided by Philips HPI-T 400 W high-pressure halide lamp. Daily photoperiod of 14 h and temperature was 20 ± 1ºC. Dissipation half-lives in water (first-order kinetics) were calculated to be 2.3 d (0.5% treatment level) and 3.0 d (range 2.9-3.1 d, 5% treatment level) in the publication.
As the study was performed indoor and it was not easily possible to transcribe the radiation of the used halide lamp into radiation within the UV-VitD action spectrum, it was finally decided not to include this study in the inverse modelling exercise.

So, finally only two studies with metamitron in outdoor cosms were analysed using the inverse modelling by TOXSWA coupled to PEST. The main characteristics of the two studies of Wendt-Rasch et al. (2004) and Brock et al. (2004) have been summarized in Table 13.1.

Table 13.1 *Data on cosm studies with metamitron.*

Property	Wendt-Rasch et al., 2004	Brock et al., 2004
Type of system	Outdoor microcosms, concrete tanks, Sinderhoeve Renkum, NL	Outdoor cosms, polycarbonate enclosures in experimental ditches Sinderhoeve, Renkum, NL
Dimensions system	1.2 x 1.4 x 1.2 m, approx. 0.5 m^3 water	Cylinders, diameter 1.05 m, height 0.9 m, approx. 433 L water
Depth water layer	30 cm	50 cm
Macrophytes info	Two types of system, either *Elodea nuttallii* dominated, or *Lemna* dominated; both types also contained 3 pots with 5 g *Myriophillum spicatum* each (on the bottom)	No macrophytes present in enclosures
pH	Variable over time and different between systems, range 6.2 – 9.3	In most systems 8.5 – 9.5, only at highest treatment 7 – 8.5 during first 14 days, 8.5 – 9.5 on later days
Application number	1	1
Nominal initial concentration	11.7 µg/L	14, 70, 280, 1120, 4480 µg/L
Date of the applications	4 May 1999	5 May 1999

Table 13.2 presents the main physico-chemical properties of metamitron, that were used in the simulations.

Table 13.2 *Main physico-chemical properties of metamitron used in the simulations (PPDB and Ctgb).*

Metamitron	
Molar mass (g)	202.21
Saturated vapour pressure (mPa)	7.44 10^{-4} (20 °C)
Solubility (mg L^{-1})	1770 (20 °C)
Kom (estimated) (L kg^{-1})	Kom=50.1, N=0.78
pKa	n.a.

13.2   Cosm study by Wendt-Rasch et al. (2004)

The study (Wendt-Rasch et al., 2004) gives fate data for metamitron in outdoor microcosms at the Sinderhoeve experimental station in Renkum, The Netherlands (concrete tanks containing approx. 500 L of water and a sediment layer). Only the data for the highest (of 4) treatment levels are given (in a graph), at 5 times after treatment (up to 21 d after the first application). Aqueous concentrations are given both for cosms dominated by submerged macrophytes and cosms with a high *Lemna* coverage, separately. No data on measured concentrations of metamitron in sediments is provided, nor are data on the organic carbon content of the sediment given (two different types of sediment were used for the two types of microcosms). Some data on the coverage of the water surface or the proportion of bottom covered with macrophytes is given. Extensive data on temperature, dissolved oxygen and pH of the water are provided.

The application was done at 4 May 1999. Dissipation half-lives in water (first-order kinetics) were calculated to be 0.67 d (95% confidence intervals: 0.52-0.95 d, 5% treatment level) in the *Elodea*-dominated outdoor microcosms and 1.9 d (95% confidence intervals: 1.6-2.2 d, 5% treatment level) in the *Lemna*-dominated outdoor microcosms in the publication. The water depth in the cosms was 30 cm.

The cosms of Wendt-Rasch et al. (2004) were inversely modelled and the agreement between measured and simulated aqueous concentrations was optimised with the aid of PEST, according to the procedures presented in Chapters 7 and 9. Forty-nine optimisations were performed, each with its own initial values of $DegT_{50, photo,ref}$ and loading at $t = 0$ and specified lower and upper parameter bounds. The initial values used have already been presented in Table 8.1.

Details of the results are given in Annex 6. For the *Elodea* dominated systems, 28 of the 49 fits resulted in a satisfactory agreement between measured and simulated aqueous concentrations. The 28 fits resulted in consistent estimates for the $DegT_{50, photo,ref}$ of 0.60 day with 95% confidence intervals of 0.43 – 0.77 days and consistent estimates of the initial loading of 352 mg m^{-2} with 95% confidence intervals of 308-395 mg m^{-2}. The optimisations passed the $\chi2$-test with error percentages of 6-7%, which is an acceptable value for field experiments according to FOCUS (2006).

For the *Lemna* dominated systems, 26 of the 49 fits resulted in a satisfactory agreement between measured and simulated aqueous concentrations. The 26 fits resulted in consistent estimates for the $DegT_{50, photo,ref}$ of 1.7 days with 95% confidence intervals of 1.3 – 2.1 days and consistent estimates of the initial loading of 319 mg m^{-2} with 95% confidence intervals of 294-343 mg m^{-2}. The optimisations passed the $\chi2$-test with error percentages of 3-4%, which is an acceptable value for field experiments according to FOCUS (2006).

Figures 13.1 and 13.3 present a satisfactory agreement between scaled optimised and measured water concentrations for one of the optimisations of the *Elodea* and *Lemna* dominated systems, respectively (initial DegT$_{50}$ of 1 days and loading of 300 mg m^{-2}, fitted DegT50, loading and confidence intervals as stated above (except the upper boundary of the 95% confidence interval of the loading which was 396 instead of 395 mg m^{-2}) and error percentage of 6.7% for the *Elodea* dominated systems, for the *Lemna* dominated systems these were: initial DegT$_{50}$ of 2 days and loading of 300 mg m^{-2}, fitted DegT50, loading and confidence intervals as stated above and error percentage of 3.4%). The simulated concentration profiles show a wavy pattern, due to the rapid photodegradation during daytime and stagnating photodegradation after sunset. In the *Elodea* dominated systems, the concentration decreases more rapidly than the concentration in the *Lemna* dominated systems. Figures 13.2 and 13.4 present the distribution of the scaled residuals between model-generated and measured concentrations, as suggested by FOCUS (2006). The graphs show that the residuals are randomly scattered around zero, demonstrating that there is no pattern of under- or over-prediction by the TOXSWA model.
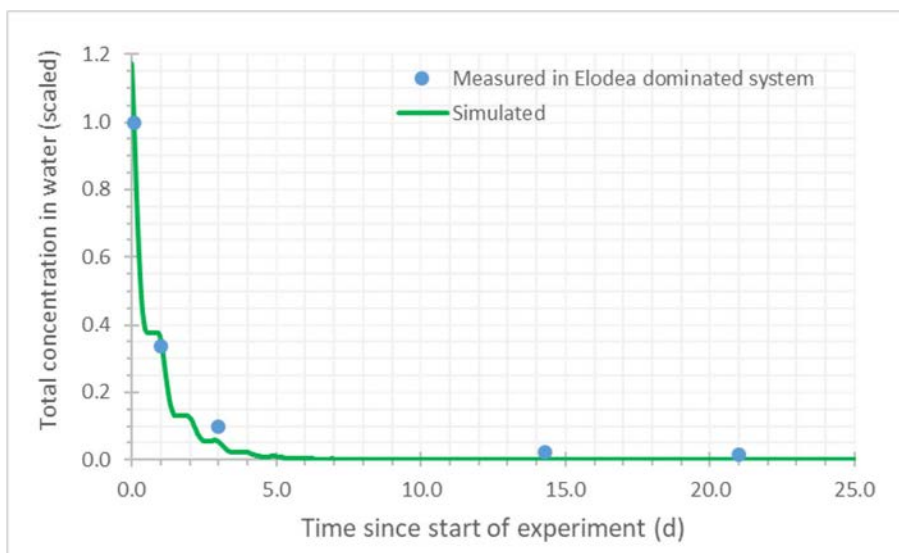
Figure 13.1 *Simulated and measured total concentration (dissolved+ sorbed to suspended solids, µg.L⁻¹) metribuzin in water as a function of time (d) in the Elodea dominated system of Wendt-Rasch et al. (2004). Simulated concentration profile obtained by PEST_TOXSWA optimisation for an initial DegT$_{50,photo,ref}$ = 1 d and an initial loading of 300 mg m⁻².*

Figure 13.2 *Residuals of total concentration (dissolved+ sorbed to suspended solids, µg.L⁻¹) metribuzin in water as a function of time (d) in the Elodea dominated system of Wendt-Rasch et al. (2004). Simulated concentration profile obtained by PEST_TOXSWA optimisation for an initial DegT$_{50,photo,ref}$ = 1 d and an initial loading of 300 mg m⁻².*

Figure 13.3 *Simulated and measured total concentration (dissolved+ sorbed to suspended solids, µg.L^{-1}) metamitron in water as a function of time (d) in the Lemna dominated system of Wendt-Rasch et al. (2004). Simulated concentration profile obtained by PEST_TOXSWA optimisation for an initial DegT$_{50,photo,ref}$ = 2 d and an initial loading of 300 mg m^{-2}.*

Figure 13.4 *Residuals of total concentration (dissolved+ sorbed to suspended solids, µg.L^{-1}) metamitron in water as a function of time (d) in the Lemna dominated system of Wendt-Rasch et al. (2004). Simulated concentration profile obtained by PEST_TOXSWA optimisation for an initial DegT$_{50,photo,ref}$ = 2 d and an initial loading of 300 mg m^{-2}.*

13.3   Cosm study by Brock et al. (2004)

The paper by Brock et al. (2004) describes fate data for metamitron in moderately buffered mesotrophic enclosures (diameter 1.05 m, height 0.90 m, water depth 0.5 m, no information on sediment composition is given) in outdoor ditches. Enclosures were treated at six different exposure levels (0, 14, 70, 280, 1120, 4480 µg/L) of metamitron. The enclosures were made of polycarbonate cylinders, which are pervious to light. The height of the rim of the enclosures above the water level was 25 cm. Water was sampled 8 times after the application over a 14 days period (nine samples over 28 days for the highest treatment level). Concentrations for the metabolite desamino-metamitron measured in water are also reported. No analyses in sediment are reported.

The application was made on 5 May 1999. Dissipation half-lives in water were calculated to be 1.92 d (range = 1.18-3.19 d for 14, 70, 280, 1120, 4480 ug/L treatment) in the publication.

The 10 microcosms of Brock et al. (2004) were inversely modelled as one system with scaled concentrations and the agreement between measured and simulated aqueous concentrations was optimised with the aid of PEST, according to the procedures presented in Chapters 7 and 9. Forty-nine optimisations were performed, each with its own initial values of $DegT_{50, photo,ref}$ and loading at $t = 0$ and specified lower and upper parameter bounds. The initial values used have been presented in Table 8.1.

Details of the results are given in Annex 6. Forty fits of the 49 fits resulted in a satisfactory agreement between measured and simulated aqueous concentrations. These 40 fits resulted in consistent estimates for the $DegT_{50, photo,ref}$ of 1.86 days with 95% confidence intervals of 1.7 – 2.0 days and consistent estimates of the initial loading of 525 mg m^{-2} with 95% confidence intervals of 507-542 mg m^{-2}. The optimisations passed the $\chi2$-test with error percentages clearly below 15%, which is an acceptable value for field experiments according to FOCUS (2006).

Figure 13.5 presents a satisfactory agreement between scaled optimised and measured water concentrations for one of the optimisations (initial $DegT_{50}$ of 2 days and loading of 500 mg m^{-2}, fitted DegT50, loading and confidence intervals as stated above and error percentage of 12.3%). The simulated concentration profile shows a wavy pattern, due to the rapid photodegradation during daytime and stagnating photodegradation after sunset. Figure 13.6 presents the distribution of the scaled residuals between model-generated and measured concentrations, as suggested by FOCUS (2006). The graph shows that the residuals are reasonably randomly scattered around zero, demonstrating that there is no pattern of under- or over-prediction by the TOXSWA model (Figure 13.6). Looking at the different enclosures individually however, for some enclosures the concentration is clearly underestimated (e.g. Enclosure 7) or overestimated (e.g. Enclosure 1).
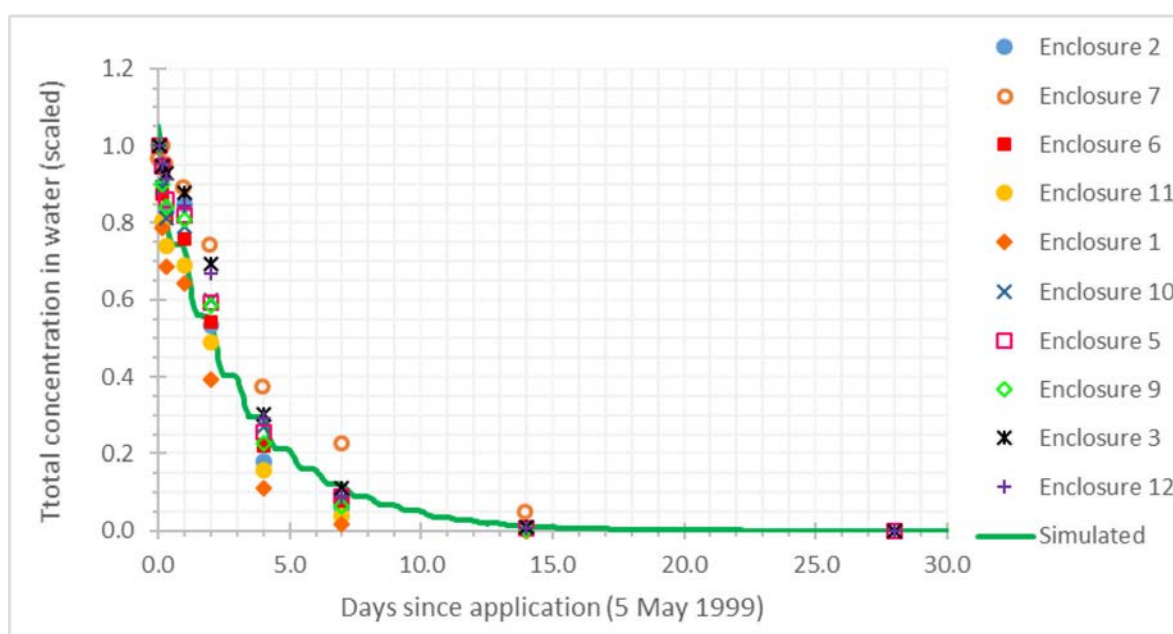
Figure 13.5 *Simulated and measured total concentration (dissolved+ sorbed to suspended solids, µg.L^{-1}) metamitron in water as a function of time (d) in the enclosures of Brock et al. (2004). Simulated concentration profile obtained by PEST TOXSWA optimisation for an initial DegT$_{50,photo,ref}$ = 2 d and an initial loading of 500 mg m^{-2}.*

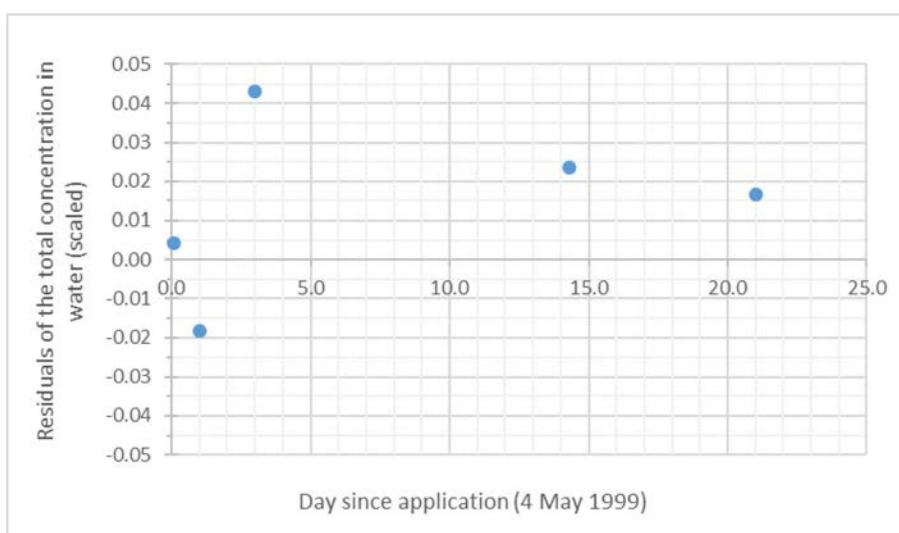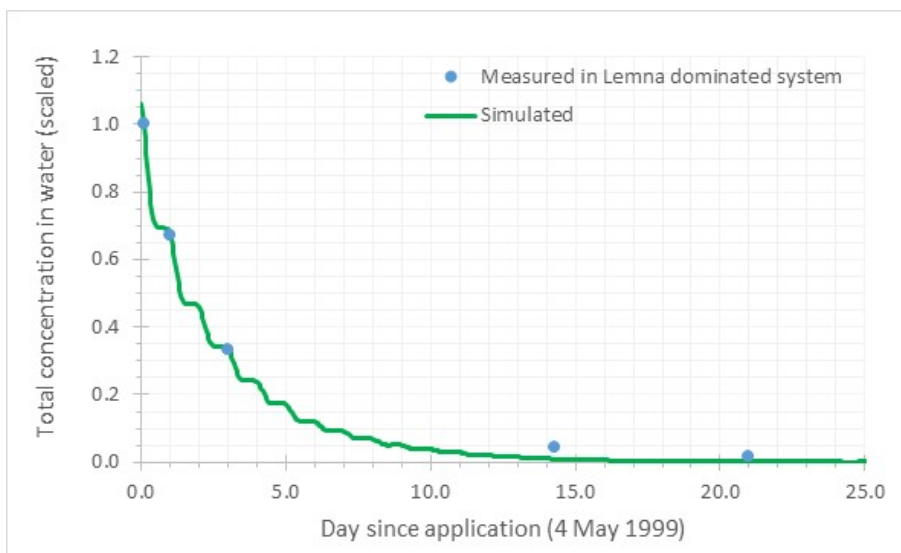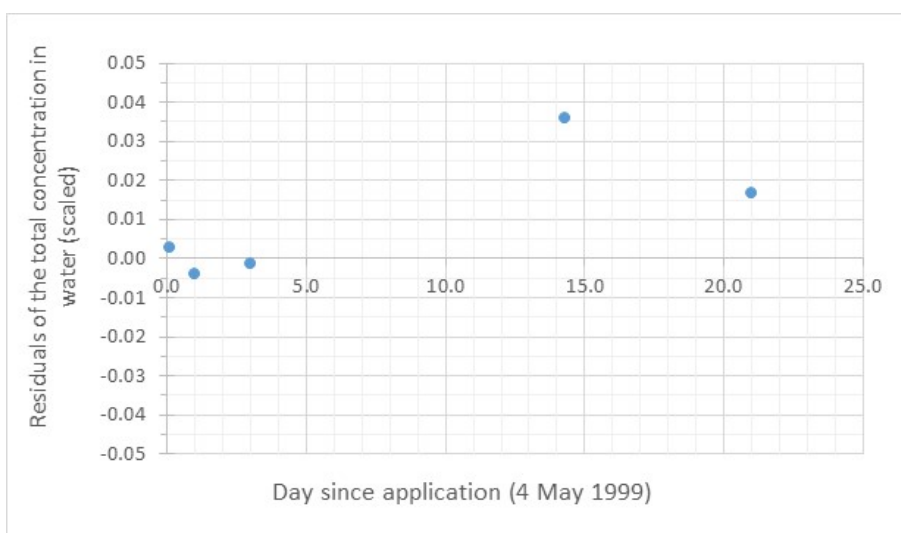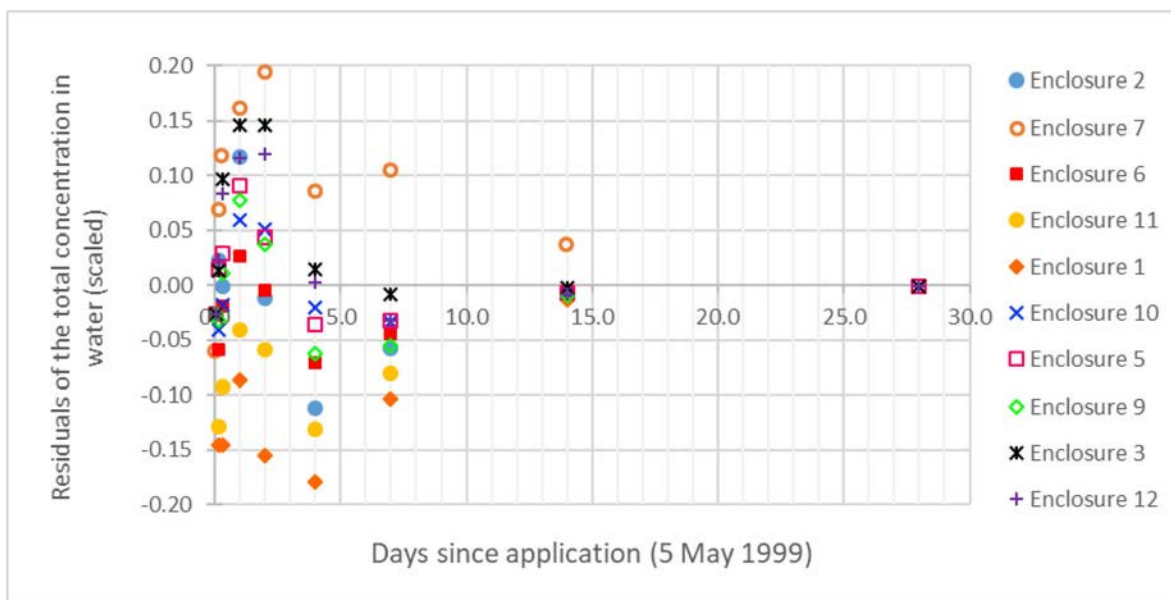**Figure 13.6** *Residuals of total concentration (dissolved+ sorbed to suspended solids, μg.L⁻¹) metamitron in water as a function of time (d) in the enclosures of Brock et al. (2004). Simulated concentration profile obtained by PEST_TOXSWA optimisation for an initial DegT$_{50,photo,ref}$ = 2 d and an initial loading of 500 mg m⁻².*

13.4 Comparison with degradation rates from other sources

An overview of the results of the inverse modelling, i.e. the obtained values for the $DegT_{50,photo,ref}$ in water and the initial loading, is presented in Table 13.3.

Table 13.3 *Estimates of DegT$_{50,photo,ref}$ and initial loading plus their 95% confidence intervals and χ² errors for metamitron in water obtained by inverse modelling by TOXSWA-PEST of the data sets.*

Data set analysed	$DegT_{50,photo,ref}$ (days)* at $I_{ref,act,UV-VitD}$ = 5000 J m⁻² d⁻¹	Initial loading (mg m⁻²)	Approximate χ² error (%)
Wendt-Rasch et al. (2004)			
Elodea dominated systems	0.60 (0.43-0.77)	352 (308-395)	6-7%
Lemna dominated systems	1.7 (1.3-2.1)	319 (294-343)	3-4%
Brock et al. (2004)	1.86 (1.7-2.0)	525 (507-542)	12-13%

* The $DegT_{50,photo,ref}$ obtained from experimental data was corrected for the UV-VitD actual daily radiation, resulting in a value at 5000 J m⁻² d⁻¹ as explained in Chapter 7.1.

A comparison with the values for the DegT$_{50}$ (at the reference temperature of 20 °C) obtained in the report of Deneer et al. (2015) will be made in Chapter 14.

Table 13.4 gives an overview of data found in several sources on the dissipation of metamitron in water as a result of hydrolysis, photolysis and microbial degradation in laboratory water-sediment studies. With the aid of these data we here evaluate the consistency of the tiered approach for the $DegT_{50}$ in water, proposed by Boesten et al. (2014) and also presented in Chapter 9.5.

Table 13.4 *Dissipation half-lives of metamitron as obtained from different sources.*

Process/system	DT50 (days)	Source
Hydrolysis	pH=7: 479.6 d, pH=5: 353.2 d, pH=9: 8.5 d; second study: pH=7: 84 d, pH=4: 65 d; pH=9: 5.3 d (all at 20°C)	EU agreed endpoints from EFSA conclusion[10]
Hydrolysis	480 (pH sensitive, pH=5: 353.2 d, pH=9: 8.5 d, all at 20°C)	Footprint database
Photolysis	1.45 h in river water (xenon lamp); 0.47 h in pure water, 34°C, natural summer light, 50 ° latitude	EU agreed endpoints from EFSA conclusion[3]
Photolysis	0.02 (1.45 h river water, pH 7 and test conditions); 0.5 h, pure water, natural summer light, 50 deg North)	Footprint database
Water/sediment	DT50 water: 9.62 and 11.55 d in 2 different systems, geomean is 10.54 d DT50 whole system: 10.8 and 11.41 d, the latter being used in exposure assessment (geomean is 11.1 d)	EU agreed endpoints from EFSA conclusion[8]
Water/sediment	DT50 water: 10.5 DT50 whole system: 11.1	Footprint database

Boesten et al. (2014) recommended using the longest DT_{50} in the pH range of 7 – 9.5 for hydrolysis data. This was 480 days at 20°C.

Aerobic water-sediment studies indicate a whole-system DT_{50} of 11 days at 20°C.

The *DegT$_{50,photo,ref}$* estimated from cosm data was in the range of 0.60 to 1.86 days for a *I$_{ref,act,UV-VitD}$* of 5000 J m^{-2} d^{-1}.

Hence, for the data considered, going from lower- to higher-tier data did indeed result in clearly less conservative estimates for the degradation rate of metamitron.

---

[10] https://efsa.onlinelibrary.wiley.com/doi/epdf/10.2903/j.efsa.2008.185r

14 Further standardisation of *DegT$_{50,photo,ref}$* estimated for the outdoor cosms

14.1 Overview

The optimisation of the degradation rate in the outdoor cosms as a function of radiation by PEST-TOXSWA results in half-lives, *DegT$_{50,photo,ref}$*, at a reference daily UV-VitD radiation of 5000 J m^{-2}, i.e. approximately an average value for the Central Zone of the EU for the period April-October, when most pesticide applications are done. However, water depth, skyview (i.e. actual exposure of the water surface to the overlying sky) and coverage of the water surface area by water plants vary between the cosms, thus the amount of radiation available for degradation within the water column varies, due to extinction of the UV-VitD radiation with depth and shading effects by the rim of the cosm and by water plants. In an attempt to eliminate the effect of variable water depth, skyview and coverage we standardized the optimised *DegT$_{50,photo,ref}$* further and next compared the obtained values for each substance. Our expectation was that these standardization leads to a smaller range in the half-lives of the optimised cosms.

For water depths of more than 30 cm we standardize the *DegT$_{50,water,ref}$* to a standard water depth of 30 cm, as explained in the conclusion in Chapter 5.3:

$$DegT_{50,photo,ref,30cm} = (30/h_{cosm}) * DegT_{50,photo,ref} \qquad \text{Eq 14.1}$$

With
DegT$_{50,photo,ref}$ = degradation half-life in cosm by photolytic degradation standardized at a reference daily UV-VitD radiation of 5000 J m^{-2} (d);
DegT$_{50,photo,ref,30cm}$ = degradation half-life in cosm by photolytic degradation standardized at a reference daily UV-VitD radiation of 5000 J m^{-2} and a water depth of 30 cm (d), and
h$_{cosm}$ = water depth of cosm (cm).

Considering the skyview we standardize the *DegT$_{50,photo,ref}$* to a full skyview, i.e. the water surface area of the cosm is entirely exposed to the overlying sky, as explained in the conclusion in Chapter 7.3:

$$DegT_{50,photo,ref,full\_skyview} = f_{skyview} * DegT_{50,photo,ref} \qquad \text{Eq 14.2}$$

With
DegT$_{50,photo,ref,full\_skyview}$ = degradation half-life in cosm by photolytic degradation standardized at a reference daily UV-VitD radiation of 5000 J m^{-2} and a full skyview, i.e. skyview factor of 1 (d), and
f$_{skyview}$ = skyview factor of cosm (-).

Note that the skyview factor has been calculated for the water surface area of the cosm, while the photolytic degradation occurs in the underlying water column. So, by applying the skyview factor in Eq 14.2 we assume that this factor approximates the UV-VitD radiation in the entire water column.

Considering the coverage of the water surface area by water plants we standardize the *DegT$_{50,photo,ref}$* to no coverage by Eq. 14.3. The underlying assumption here is that photolysis is proportional to the intensity of radiation entering the water column. So, no photolysis occurs in that part of the water column that is located in the shade of the water plants that cover the corresponding part of the water surface area.

$$DegT_{50,photo,ref,nocov} = ((100-\%coverage)/100) * DegT_{50,photo,ref} \qquad \text{Eq 14.3}$$

With:

$DegT_{50,photo,ref,nocov}$ = degradation half-life in cosm by photolytic degradation standardized at a reference daily UV-VitD radiation of 5000 J m^{-2} and no coverage of the water surface of the cosm by water plants (d), and

$\%coverage$ = percentage of water surface area of cosm covered by water plants (-).

14.2 Coverage by macrophytes

Below we determine the coverage percentage for each mesocosm used for determining a $DegT_{50,photo,ref,nocov}$. As explained in Chapter 7.2, in the ecotoxicological literature the coverage is related to the percentage of macrophytes covering the bottom of the cosm generally without mentioning where in the water column the macrophytes are present, while we are interested in the percentage of the water surface area that is covered by macrophytes. Therefore, we deduced the surface area coverage percentage from the type of macrophytes, the amount and month of the experiment (determining the growth stage of the macrophytes). This was done for the period immediately after the application of the pesticide up to approximately 3 times the dissipation half-life later, when most of the pesticide mass has dissipated.

Cosms with metribuzin
A total of 6 ditches with the two highest treatment levels were inversely modelled of the so-called 'potatotox' experiment of Arts et al. (2006), executed at the 'Sinderhoeve' experimental station in Renkum, the Netherlands: ditches 1, 7 and 12 which received 1% of the recommended product use rate and ditches 4, 6 and 9 which received 5%. The water depth in all ditches was approximately 50 cm. The herbicide metribuzin was applied only once at 22 April 2002, two weeks after the first application (of prosulfocarb) in the experiment. The dissipation half-life from water was estimated at 1.7 day for metribuzin and thus we are interested in the coverage from approximately 14 to 19 days after the start of the experiment. Macrophyte cover, abundance and structure (height) was monitored every 6 to 7 weeks, in total 6 times during the experiment. The aquatic vegetation in the ditches was dominated by *Chara globularis* ssp. *Virgata* (average of 6 ditches at day 0 was 22.0% and at day 45 45.1% bottom cover). Other abundant macrophytes were *Elodea nuttallii* (average of 6 ditches at day 0 was 24.2% and at day 45 17.3% bottom cover) and *Sagittaria sagittifolia* (average of 6 ditches at day 0 was 0.4% and at day 45 10.5% bottom cover), only the latter is an emergent macrophyte, the others being submerged species. Locally, submerged and floating algal beds were abundant. Table 10 of Arts et al. (2006) specifies the coverage percentage of floating filamentous algae at day 0 and day 45 of the experiment, respectively 10.42 and 9.56 for the 1% treatment level and 0.83 and 2.19 for the 5% treatment level. This leads to estimated coverages of 10% and 1.5% for the 1 and 5% treatment levels, respectively, and an overall average of 6% (all ditches were inversely modelled as one by scaling, see Deneer et al., 2015). The only emergent macrophyte *Sagittaria sagittifolia* remains below 5% bottom cover between day 14 and 19, so we assume that the plant had hardly emerged from the water. So, the overall coverage at the water surface remains at the estimated 6% by the floating filamentous algae for the optimised $DegT_{50,water,photo}$.

Two enclosures were selected from the semi-field experiment of Brock et al. (2004) for the inverse modelling. These enclosures (1 and 8) had the lowest and highest dissipation rate of the 10 treated enclosures, all having very similar dissipation rates (Deneer et al., 2015). The two enclosures received a single application of metribuzin at 5 May 1999 with initial nominal concentrations of 5.6 and 56 µg/L. The enclosures had a water depth of approximately 50 cm and were located in the same ditch at the 'Sinderhoeve' experimental station in Renkum, the Netherlands. The mean dissipation half-life from water for all enclosures was calculated at 7.1 day and thus we are interested in the coverage from day zero up to approximately 14 to 21 days after the start of the experiment. The percentage bottom cover by macrophytes in the enclosures was estimated on the sampling dates: -7, 7, 22, 35 and 49 days post-application. Only 2 species of macrophytes were found near the water surface in the enclosures: *Myriophyllum spicatum* (submerged species) and *Sagittaria sagittifolia* (emergent species). Bottom cover at deeper water layers could not be estimated reliably because of the turbidity of the water, which was caused by high phytoplankton concentrations. The average (mean of 2 enclosures that received the same treatment) cover near the surface was specified separately for

the 2 macrophyte species, for *M. spicatum*, it was 7, 15 and 62% and for *S. sagittifolia* it was 0, 0 and 2% at day -7, 7 and 22 for the enclosure with the 5.6 µg/L initial nominal concentration, while for the enclosure with the 56 µg/L initial nominal concentration the numbers were 15, 25 and 5% for *M. spicatum* and three times zero for *S. sagittifolia*. As *Myriophyllum spicatum* is a submerged species it is not considered in the estimation of the surface coverage. So based on *Sagittaria sagittifolia* we concluded to a surface coverage of 1% and 0% for the enclosures with the 5.6 and 56 µg/L initial nominal concentrations, respectively.

One of the two high-treatment ponds (nominal concentration of 75 µg/L) of Fairchild & Sappington (2002) was inversely modelled with the PEST_TOXSWA models. The outdoor clay-lined pond was located in Columbia (MO, USA) and measured 1000 m^2 with a water depth of 0.75 m. It was treated once with metribuzin on May 22 (probably 2001). The calculated half-life of dissipation in water was 5 d, so we are interested in the coverage rate of the pond from application up to approximately 15 d later. Macrophytes were sampled on day -7, 20 and 30 post-treatment and the species composition (either *Najas guadalupensis* or *Chara* sp.) was visually assessed. Measured mean biomass for both species at day -7 and 20 for the two ponds with 75 µg/L treatment was 46 and 67 g/m^2, respectively, composed of 74.5 and 25.5% at day -7 and 86.6 and 13.3% at day 20 post-treatment for *Najas* and *Chara*. Both *Najas* and *Chara* are submerged plants, having slender stems and thin leaves/branches. So, we quantify the coverage at the water surface of the pond to be zero.

Cosms with imidacloprid
The study of Colombo et al. (2013) was performed in 20-L polypropylene containers (45.5 x 30 x 21 cm) with an 11-cm water layer overlying 0.55 cm sediment. The microcosms contained no macrophytes, so coverage is zero.

Bayer (2001) studied the fate of imidacloprid in two outdoor cosms: a cylindrical steel pond (diameter 2.0 m, 1.5 m depth with 1.0 m water depth) and a rectangular steel tank (length 1.77 m, width 0.58 m, depth 0.55 m and 0.30 m water depth). Imidacloprid was applied once at 8 May 2000 at a nominal concentration of 6.0 µg/L and the calculated dissipation half-life in water was 5.6 d in the pond and 5.7 d in the tank. So, we are interested in the coverage of the pond and the tank during approximately the first 18 d of the experiment. During the study the abundance of macrophytes was assessed visually. In the pond *Callitriche* sp. (submerged and floating) and *Elodea canadensis* (submerged) were identified, while in the tank *Potamogeton pusillus*, *Potamogeton crispus* (both submerged) and *Elodea canadensis* were observed. The percentages bottom cover were estimated at 15, 20, 30 and 35 for the pond and 5, 60, 70 and 60 for the tank at days 2, 10, 15 and 22 post-application, respectively. In the pond only the water starwort (*Callitriche* sp) may be floating at the water surface; given the relatively low cover percentages, we estimate the coverage at water surface area to be on average 10% during the first 18 d post-application. In the tank all the species are submerged, however the cover is relatively high, the water depth is only 30 cm and *Potamogeton crispus* has broad leaves that easily float on the water surface. Therefore we estimate the coverage of the tank at water surface level to be 10%.

Bayer (2003) studied the fate and effects of imidacloprid in thirteen artificial microcosms, representing shallow mesotrophic ponds. The artificial ponds consisted of cylindrical glass-fibre reinforced polyester tanks, impervious for UV radiation. They had a diameter of 2.0 or 2.2 m, their water depth was approximately 1.0 m and a natural sediment layer was 10 cm deep. Imidacloprid was applied twice, on 2 and 23 May 2001 by spray application on the pond surface at initial nominal concentrations of 0.6, 1.5, 3.8, 9.4 and 23.5 µg/L, in duplicate. The four ponds with the two highest initial nominal concentrations were inversely modelled and the average DT50 (first order kinetics) over the two applications was 7.1 d (for the ponds 13 and 7 with 23.5 µg/L) and 8.2 d (for the ponds 8 and 2 with 9.4 µg/L). So, we are interested in the coverage of these four ponds by macrophytes from 2 May up to approximately 24 days after 23 May, i.e. 16 June, so from day 0 to 45 days post-application. Except for duck weed, *Lemna minor*, no other macrophytes were observed during the entire study. These floating macrophytes were removed at each sampling date. For the four inversely modelled ponds this equalled 3 *Lemna* plants at 25 May in pond 8 (9.4 µg/L), 5, 5 and 2 *Lemna* plants at 23, 25 and 27 May in pond 13 (23.5 µg/L) up to 16 June. At all other dates in these four ponds there were no *Lemna* plants reported to be removed (Table 105 of Bayer, 2003). So, the coverage by *Lemna* can be

neglected for our purpose. In addition to *Lemna* the presence of periphyton algae with intense growth on the tank walls and on the water surface was reported. From day 14 onwards their cover area on the water surface was estimated. The average surface coverage of the periphyton from day 1 to 45 days post-application was approximately 500, 1300, 800 and 600 cm^2 for the ponds 2, 8, 7 and 13, respectively (derived from Figure 77 and Table 104 of Bayer, 2003), corresponding to coverage percentages of 1.6, 4.1, 2.5 and 1.6, respectively. So we used these percentages.

Cosms with metamitron

The fate of metamitron (Wendt-Rasch et al., 2004) was inversely modelled in four of the 20 outdoor microcosms of the experiment. The microcosms consisted of a concrete tank (length 1.2 m, width 1.4 m, height 1.2 m), having 30 cm water above the sediment (depth not measured, but consisting of neutral sand first and on top the wished type of sediment, resulting in a rim of the cosms of approximately 20 to 40 cm). They were located at the 'Sinderhoeve' experimental station in Renkum, the Netherlands. Two of the inversely modelled cosms simulated mesotrophic aquatic systems dominated by submerged macrophytes (*Elodea*) and two others simulated eutrophic ecosystems with a high *Lemna* coverage. Metamitron was applied once at day 28 of the experiment, day 0 being 6 April 1999. The average calculated nominal concentrations of the inversely modelled cosms were 11.79 μg/L for the *Eleodea* dominated cosms and 11.92 μg/L for the *Lemna* dominated cosms (Crum, pers. comm. 27 May 2019). The mean dissipation half-life was 0.67 d for the *Elodea* dominated cosms and 1.9 d for the *Lemna* dominated cosms (Wendt-Rasch et al., 2004), so we are interested in the surface coverage during the first 3 to 6 days after application, i.e. from day 28 to day 31 or 34. However, the proportion of bottom covered by submerged vegetation (*Elodea* sp.) and the proportion of the water surface covered with filamentous algae and *Lemna* sp. was visually estimated at day 64 only. At the start of the experiment *Elodea nuttalli* shoots were introduced in the *Elodea* dominated cosms (other cosms not mentioned in Wendt-Rasch et al., 2004) and there was an acclimatization period of unreported length. The two *Elodea* dominated cosms (T4 treatment level) were both clear, the *Lemna* and filamentous algae coverage was 0% and the *Elodea* coverage was 65% and 90%. As *Elodea* is a submerged species, the estimated surface coverage for these two cosms is 0%. Of the two *Lemna* dominated cosms (T4 treatment level) one was turbid and the other clear, the *Elodea* coverage was not visible for the turbid one and 3% for the clear cosm; the *Lemna* coverage was 75 and 15 and % filamentous algae was 3 and 70 for the two cosms. So, the average surface coverage of the *Lemna* dominated cosms is 83% at day 64. Assuming a more or less linear increase in coverage we finally estimate the surface coverage for the *Lemna* dominated systems to be 40% during the period from day 28 to day 31 or 34.

Ten enclosures were selected from the semi-field experiment of Brock et al. (2004) for the inverse modelling. These enclosures (nrs 2+7, 6+11, 1+10, 5+9 and 3+12) received a single application of metribuzin at 5 May 1999 with initial nominal concentrations of 14, 70, 280, 1120 and 4480 μg/L, respectively. The enclosures had a water depth of approximately 50 cm and were located in the same ditch at the 'Sinderhoeve' experimental station in Renkum, the Netherlands. The mean dissipation half-life from water for all enclosures was calculated at 1.92 day and thus we are interested in the coverage from day zero up to approximately 6 days after the start of the experiment. The percentage bottom cover by macrophytes in the enclosures was estimated on the sampling dates: -7, 7 and 22 days post-application. Only 2 species of macrophytes were found near the water surface in the enclosures: *Myriophyllum spicatum* (submerged species) and *Sagittaria sagittifolia* (emergent species). *Elodea nuttallii* and some *Chara* sp were also present in deeper water layers. Bottom cover at deeper water layers could not be estimated reliably because of the turbidity of the water, which was caused by high phytoplankton concentrations. The average (mean of 2 enclosures that received the same treatment) cover near the surface was specified separately for the 2 macrophyte species, but as only *Sagittaria sagittifolia* is an emergent species we only consider this species. However, its water surface coverage was 0 at day -7d as well as at day 7 for all enclosures. So we assumed no surface coverage.

14.3 Skyview factor

Applying the procedures described in Chapter 7.3 the skyview factors were calculated for all inversely modelled cosms. Table 14.1 below presents the results.

Table 14.1 *Skyview factors for the studied cosms.*

Length (cm)	Width (cm)	Height of rim (cm)	Skyview factor (-)	Reference
45.5	30	10	0.59	Colombo et al., 2013
177	58	25	0.63	Bayer, 2001
140	120	20-30-40	0.70-0.62-0.55	Wendt-Rasch et al., 2004
105		25	0.58	Brock et al., 2004
200 (minimum)		50	0.57	Bayer, 2001
220 (maximum)		50	0.59	Bayer, 2001
200		40	0.62	Bayer, 2003
220		30	0.70	Bayer, 2003

The outdoor pond of Fairchild and Sappington (2002) had a skyview of 1.0, i.e. the hemisphere could be seen from the entire water surface area.

The skyview factor for the outdoor ditches of Arts et al. (2006) with their water surface width of 3.3 m, side slope of 2/3 and bank of 0.4 m above the water surface had been calculated before at 0.90.

Bayer (2001) reported that the diameter of their pond was 200 cm but their Figure 1 showed that the top part of the pond had a wider diameter (estimated to be 220 cm from this figure). The diameter at the level of the water surface was estimated to be about 210 cm, so we propose to use the average value of 200 and 220 cm, i.e. 0.58.

We finally summarized the skyview factors and the percentages of water surface areas covered by macrophytes in Table 14.2 below. These factors are used to standardize the $DegT_{50,photo,ref}$ further for the effects of skyview, coverage by macrophytes and water depth.

Table 14.2 *Percentage of water surface areas covered by macrophytes and skyview factors used in the inversely modelled cosms calculations.*

Substance/authors	Cosms modelled	Surface coverage by macrophytes (%)	Skyview factor (-)	Remarks
Metribuzin				
Fairchild & Sappington (2002)	1 pond	0	1.0	
Arts et al. (2006)	6 ditches as one system	6	0.90	
Brock et al. (2004)	5.6 µg/L enclosure	1	0.58	
	56 µg/L enclosure	0	0.58	
Imidacloprid				
Colombo et al. (2013)	Average of 7 replicates, so one system	0	0.59	
Bayer (2001)	Pond (1.0 m water)	10	0.58	
	Tank (0.3 m water)	10	0.63	
Bayer (2003)	Pond 13 (diameter 2.2 m)	1.6	0.70	
	Pond 7 (diameter 2.0 m)	2.5	0.62	
	Pond 8 (diameter 2.0 m)	4.1	0.62	
	Pond 2 (diameter 2.0 m)	1.6	0.62	
Metamitron				
Wendt-Rasch (2004)	Average of 2 *Elodea* dominated cosms	0	0.62	Average factor for rims of 20, 30 and 40 cm with factors of 0.70, 0.62 and 0.55
	Average of 2 *Lemna* dominated cosms	40	0.62	
Brock et al. (2004)	10 enclosures as one system	0	0.58	

14.4   Calculations to standardize the $DegT_{50,photo,ref}$ further

To obtain the degradation rate that characterises best the degradation of the compound as observed in the various cosms we calculate the geomean value of the $DegT_{50,photo,ref}$ for each of the studied compounds, which is a good measure because a lognormal distribution excludes negative values of the individual cosm $DegT_{50,photo,ref}$ values (based on FOCUS, 2006, taking the geomean of half-lives has become the standard procedure in the EU risk assessment procedures). To evaluate the range in individual cosm $DegT_{50,photo,ref}$ values we calculate the standard deviation of the logarithmic transformed values of the individual cosm $DegT_{50,photo}$. So, by considering the calculated standard deviations we can assess whether the standardization leads to a smaller range in the half-lives of the optimised cosms, as expected.

Note that for 3 cosms we calculate the geomean as:

$$geomean = \sqrt[3]{(DegT_{50,cosm1} * DegT_{50,cosm2} * DegT_{50,cosm3})} = e^{((lnDegT_{50,cosm1} + lnDegT_{50,cosm2} + lnDegT_{50,cosm3})/3)} \quad \text{Eq 14.4}$$

and the standard deviation, using the 'n-1 method' for the logarithmic transformed values of the individual cosm $DegT_{50,photo,ref}$ as:

$$standard\ deviation = \sqrt{\frac{\sum(lnDegT_{50,cosmn} - Ave)^2}{(n-1)}} \quad \text{Eq 14.5}$$

with *Ave* being the arithmetic mean of the logarithmic transformed values of the individual cosm $DegT_{50,photo,ref}$ and *n* equals the number of cosm studies for the compound (here 3 or 2). The geomean is expressed in days, similar to the $DegT_{50,photo}$ values, while the standard deviation is dimensionless. (Note that the standard deviation is dimensionless, because *Ave* is also a logarithmic value and thus the numerator of Eq. 14.5 is of the type lnA-lnB=ln(A/B), which is dimensionless.)

So, we first calculated the geomean and its standard deviation for the $DegT_{50,photo,ref}$ values obtained by inverse modelling. Next, we standardized the $DegT_{50,photo,ref}$ for skyview, water depth and %coverage separately, and all three factors together and calculated again the geomean and its standard deviation of the standardized $DegT_{50,photo,ref}$ values. We did so for all three compounds, i.e. metribuzin (Table 14.3), imidacloprid (Table 14.4) and metamitron (Table 14.5).

Table 14.3 *Outdoor cosm studies for metribuzin and standardized $DegT_{50,photo}$ for UV-VitD daily radiation of 5000 J m^{-2}, a water depth of 30 cm, full skyview and no coverage of the water surface area by water plants.*

Study	$DegT_{50,photo,ref}$		Water depth	% coverage	Skyview factor	$DegT_{50,photo,ref}$ standardized for			
	Deneer et al., 2015	This study				Water depth	% coverage	skyview	All 3
	day, average	day, average, (95% confidence intervals)	cm	-	-				
Fairchild & Sappington	4.04	4.8 (2.3-7.3)	75	0	1	1.9	4.8	4.8	1.9
Arts et al	1.05	1.3 (1.1-1.5)	50[11]	6	0.9	0.82	1.21	1.16	0.69
Brock et al	3.11	3.4 (2.7-4.1)	50	0.5	0.58	2.0	3.4	2.0	1.2
Geomean	2.4	2.8				1.4	2.7	2.2	1.2
s.d.[@]	0.71	0.68				0.51	0.72	0.72	0.51

[@] standard deviation of logarithmic transformed values of the individual cosm $DegT_{50}$.

The results of the standardization for the three cosm studies of metribuzin are presented in Table 14.3. Standardization to a 30 cm water depth lowers the geomean $DegT_{50,photo}$ for a daily UV-VitD radiation of 5000 J m^{-2} from 2.8 to 1.4 d and reduces the standard deviation (s.d.) from 0.68 to 0.51. However, the s.d. increases from 0.68 to 0.72 for the standardization to no coverage by water plants, as well as for full skyview. Standardization to all three factors (water depth of 30 cm, no coverage by water plants and full skyview) results in a geomean $DegT_{50,photo}$ for a daily UV-VitD radiation of 5000 J m^{-2} of 1.2 d with a s.d. of 0.51. So, the standardization to all three factors leads to a clearly lower geomean $DegT_{50,photo}$ (especially by standardizing to the 30 cm water depth). Thus, this demonstrates that these cosms clearly differed from the standard conditions (water depth of 30 cm, no coverage by macrophytes and full skyview). The standardization results into a lower s.d. for metribuzin (from 0.68 to 0.51) but the variability of the standardized $DegT_{50,photo,ref}$ values still remains considerable in view of their s.d. of 0.51 and their range from 0.69 to 1.9 d.

When we compare our results to those from Deneer et al. (2015) with their geomean $DegT_{50,water}$ of 2.4 d (vs our final result of 1.2 d) and s.d. of 0.71 (vs our 0.51) we conclude that, with respect to the variation in the finally obtained $DegT_{50,water}$, our correction for UV-VitD radiation (i.e. without correction for water temperature, as photolytic degradation is independent of temperature) seems to be more important than the correction for the water temperature of Deneer et al. (2015) in this case of metribuzin.

---

[11] The experimental ditches have a bottom width of 1.60 m and a side slope of 3:2 (hor:vert); this implies that not all water volume had a water depth of 50 cm, as part of it is situated above the side slopes. We calculated that 1.60 + 2*0.30 = 2.20 m width had a water depth exceeding 30 cm for which a water depth correction factor applies. The average water depth of the water volume was 0.473 m. Therefore the 50 cm water depth in Table 14.3 was replaced by 47.3 cm for the calculation of the tabulated $DegT_{50,photo,ref}$ according to Eq. (14.1).

Table 14.4 *Outdoor cosm studies for imidacloprid and standardized DegT$_{50,photo}$ for UV-VitD daily radiation of 5000 J m^{-2}, a water depth of 30 cm, full skyview and no coverage of the water surface area by water plants.*

| Study | DegT$_{50,photo,ref}$ | | Water depth | % coverage | Skyview factor | DegT$_{50,photo,ref}$ standardized for | | | |
| | Deneer et al., 2015 | This study | | | | Water depth | % coverage | Skyview | All 3 |
	day, average	day, average, (95% confidence intervals)	cm	-	-				
Colombo et al	1.01	1.6 (1.3-1.9)	11	0	0.59	-	1.6	0.94	0.94
Bayer	5.54	8.1 (5.9-10.2)	100 (pond)	10	0.58	2.4	7.3	4.7	1.3
	4.26	6.5 (4.5-8.4)	30 (tank)	10	0.63	6.5	5.9	4.1	3.7
Bayer	5.57	7.3 (5.9-8.8)	100 (pond 2)	1.6	0.62	2.2	7.2	4.5	1.3
	5.45	7.2 (5.6-8.8)	100 (pond 7)	2.5	0.62	2.2	7.0	4.5	1.3
	5.22	6.7 (5.7-7.8)	100 (pond 8)	4.1	0.62	2.0	6.5	4.2	1.2
	5.28	7.0 (5.1-8.8)	100 (pond 13)	1.6	0.7	2.1	6.7	4.9	1.4
Geomean	4.1	5.7				2.6	5.5	3.8	1.4
s.d.[@]	0.63	0.57				0.45	0.55	0.59	0.43

[@] standard deviation of logarithmic transformed values of the individual cosm *DegT$_{50}$*.

The results of the standardization for the three cosm studies of imidacloprid are presented in Table 14.4. Standardization to a 30 cm water depth lowers the geomean *DegT$_{50,photo}$* for a daily UV-VitD radiation of 5000 J m^{-2} from 5.7 to 2.6 d and reduces the standard deviation (s.d.) from 0.57 to 0.45. For the standardization to no coverage by water plants the s.d. decreases less, from 0.57 to 0.55, while the s.d. increases from 0.57 to 0.59 for full skyview. Standardization to all three factors (water depth of 30 cm, no coverage by water plants and full skyview) results in a geomean *DegT$_{50,photo}$* for a daily UV-VitD radiation of 5000 J m^{-2} of 1.4 d with a s.d. of 0.43. So, the standardization to all three factors leads to a clearly lower geomean *DegT$_{50,photo}$* (especially by standardizing to the 30 cm water depth and to a lesser extent to full skyview). Thus, this demonstrates that these cosms clearly differed from the standard conditions (water depth of 30 cm, no coverage by macrophytes and full skyview). The standardization results into a lower s.d. (from 0.57 to 0.43), thus the standardization to the three factors does improve the estimation of the geomean *DegT$_{50,photo,ref}$* for imidacloprid as well.

When we compare our results to those from Deneer et al. (2015) with their geomean *DegT$_{50,water}$* of 4.1 d (vs our final result of 1.4 d) and s.d. of 0.63 (vs our 0.43) we conclude that in this case of imidacloprid the correction for the water temperature of Deneer et al. (2015) seems to be less important than our correction for UV-VitD radiation with respect to the variation in the finally obtained *DegT$_{50,water}$*.

Table 14.5 *Outdoor cosm studies for metamitron and standardized DegT$_{50,photo}$ for UV-VitD daily radiation of 5000 J m^{-2}, a water depth of 30 cm, full skyview and no coverage of the water surface area by water plants.*

| Study | DegT$_{50,photo,ref}$ | Water depth | % coverage | Skyview factor | DegT$_{50,photo,ref}$ standardized for | | | |
	day, average, (95% confidence intervals)	cm	-	-	Water depth	% coverage	skyview	All 3
Wendt-Rasch	0.60 (0.43-0.77)	30	0	0.62	0.60	0.60	0.37	0.37
	1.7 (1.3-2.1)	30	40	0.62	1.69	1.01	1.05	0.63
Brock et al	1.86 (1.7-2.0)	50	0	0.58	1.12	1.86	1.08	0.65
Geomean	1.2				1.0	1.0	0.75	0.53
s.d.[@]	0.63				0.52	0.57	0.61	0.31

[@] standard deviation of logarithmic transformed values of the individual cosm *DegT$_{50}$*.

The results of the standardization for the two cosm studies of metamitron are presented in Table 14.5. Standardization to a 30 cm water depth lowers the geomean $DegT_{50,photo}$ for a daily UV-VitD radiation of 5000 J m^{-2} from 1.2 to 1.0 d and reduces the standard deviation (s.d.) from 0.63 to 0.52. For the standardization to no coverage by water plants the s.d. decreases from 0.63 to 0.57, while the s.d. decreases from 0.63 to 0.61 for full skyview. So, all three factors contribute individually to lowering the s.d. and thus obtaining a better geomean $DegT_{50,photo}$ for a daily UV-VitD radiation of 5000 J m^{-2}. Standardization to all three factors (water depth of 30 cm, no coverage by water plants and full skyview) results in a geomean $DegT_{50,photo}$ for a daily UV-VitD radiation of 5000 J m^{-2} of 0.53 d. So, the standardization to all three factors leads to a lower geomean $DegT_{50,photo}$. Thus, this demonstrates that for cosms that clearly differ from the standard conditions (water depth of 30 cm, no coverage by macrophytes and full skyview) the $DegT_{50,photo,ref}$ can be better estimated. Moreover, the standardization to all three factors leads to a clearly lower s.d. (from 0.63 to 0.31) and thus the standardization is successful.

Deneer et al. (2015) did not analyze the cosms with metamitron, so no comparison can be made with their results.

14.5 Variation of UV-VitD radiation sums between the cosm experiments

The results for the three compounds showed that the standard deviations of the geomean $DegT_{50,photo,ref}$ were quite high (0.57-0.68) and only slightly lower than those obtained by Deneer et al. (2015). A possible explanation for this would be that there was little variation between the radiation sums of the different cosm studies. So we investigated this as follows. For the cosm studies analysed in this report we calculated the daily average UV-VitD radiation sum over the period from the first application up to around 3* $DegT_{50,photo,ref}$ after the last application to get an impression of the difference of average daily radiation sums from the reference daily radiation sum of 5000 J m^{-2} over various locations (Table 14.6). The daily average radiation sum varied between 85 to 122% of the reference radiation sum so the differences between the cosms were indeed quite small. The reason is probably that all experiments were conducted in May-June at latitudes that were close to each other (mostly Netherlands and Germany).

For the four ponds of Bayer (2003) the average daily radiation sum was 119% of the reference sum and thus the photolytic degradation half-life in the cosm was somewhat shorter than the photolytic degradation half-life at the reference radiation sum, e.g. for pond 2 the average daily radiation sum is 5925 J m^{-2}, (119%) of the reference 5000 J m^{-2}, and thus the average photolytic degradation half-life in this pond is 6.1 d over the considered period of 43 days, instead of the 7.3 d at the reference daily radiation (See Eq. 7.2). This example demonstrates how a correction for actual radiation at locations of surface water scenarios used in the regulatory risk assessment may influence the PEC_{sw} and thus the aquatic risk assessment.

Table 14.6 *UV-VitD radiation sums over specified time interval for the indicated studies, the interval ranges from the time of first loading up to 3*DegT$_{50photo,ref}$ after the last loading, i.e. when the large majority of the pesticide mass has degraded in the cosms. (N.B. Unless indicated otherwise only one loading took place.)*

Cosm	Fitted DegT$_{50photo,ref}$ (days)	Time interval (first loading -3*DegT$_{50}$ after last loading	Duration [for checking]	Daily average UV–VitD radiation sum over interval (J m^{-2} d^{-1})	Percentage of reference daily radiation sum of 5000 J m^{-2}d^{-1} (%)
metribuzin					
Fairchild & Sappington (2002)	4.8	22 May 2001 9:00 h – 5 June 2001 19:00 h	14.4 d= 346 h	6095	122
Arts et al. (2006)	1.3	6 May 2002 9:00 h – 10 May 2002 6:00 h	3.87 d = 93 h	4919	98
Brock et al. (2004)	3.4	5 May 1999 9:00 h – 15 May 1999 14:00 h	10.2 d = 245 h	4254	85
imidacloprid					
Colombo et al. (2013)	1.6	2 June 2009 11:00 h** – 21 June 2009 6:00 h	18.8 d = 451 h	5806	116
Bayer (2001)		8 May 2000 9:00 h -			
Pond	8.1	- 1 June 2000 16:00 h	24.3 d = 583 h	5323	106
Tank	6.5	- 27 May 2000 21:00 h	19.5 d = 468 h	5356	107
Bayer (2003)		2 May 2001 9:00 h*** -			
Pond 2	7.3	- 14 June 2001 10:00 h	43.06 d = 1033 h	5925	119
Pond 7	7.2*	- 14 June 2001 3:00 h	42.76 d = 1026 h	5932	119
Pond 8	6.7	- 12 June 2001 15:00 h	41.26 d = 990 h	5939	119
Pond 13	7.0*	- 13 June 2001 13:00 h	42.16 d = 1012 h	5943	119
metamitron					
Wendt-Rash et al. (2004)		4 May 1999 9:00 h -			
Elodea dominated	0.60	- 6 May 1999 4:00 h	1.8 d = 43 h	5194	104
Lemna dominated	1.7	- 9 May 1999 11:00 h	5.1 d = 122 h	4474	89
Brock et al. (2004)	1.86	5 May 1999 9:00 h – 10 May 1999 23:00 h	5.58 d = 134 h	4445	89

* χ² error above 15%

** three loadings, timing of third loading is 16 June 2009 11:00 h

*** two loadings, timing of second loading is 23 May 2010 13:00 h

14.6   Conclusions

The main results are summarized in Table 14.7.

Table 14.7 *Overview of optimised geomean DegT50,water and their standard deviations.*

Compound	DegT$_{50,photo,ref}$	DegT$_{50,photo,ref}$ standardized to water depth of 30 cm, no coverage and full skyview	Deneer et al. (2015)
Metribuzin (*n*=3)			
geomean (d)	2.8	1.2	2.4
s.d. (-) [@]	0.68	0.51	0.71
Imidacloprid (*n*=3)			
geomean (d)	5.7	1.4	4.1
s.d. (-)	0.57	0.43	0.63
Metamitron (*n*=2)			
geomean (d)	1.2	0.53	n.a.
s.d. (-)	0.63	0.31	n.a.

[@] standard deviation of logarithmic transformed values of the individual cosm *DegT$_{50}$*.

The analysis of the photodegradation rate of the three compounds in the outdoor cosms and their successive standardization to water depth, no coverage of the water surface by plants and full skyview leads to the following overall conclusions:

1. For two compounds the new photodegradation methodology resulted in a lower variation of the standardized $DegT_{50,water}$, in the cosms than the variation found by Deneer et al. (2015), which assumed an overall degradation rate in water that was a function of water temperature.
   For metribuzin the standard deviation of the geomean $DegT_{50,water}$ decreased from 0.69 (Deneer et al., 2015) down to 0.51. For imidacloprid the standard deviation of the geomean $DegT_{50,water}$ decreased from 0.63 (Deneer et al., 2015) down to 0.43. For metamitron the standard deviation of the geomean $DegT_{50,water}$ decreased from 0.63 (standardized to daily UV-VitD radiation of 5000 J m^{-2}) down to 0.31 and no comparison to results of Deneer et al. (2015) could be made.
   (Note that the s.d. was calculated of the logarithmic transformed values of the individual cosm $DegT_{50,water}$).

2. Comparison of the values of the geomean $DegT_{50,photo,ref}$ to those after standardization to a water depth of 30 cm, no coverage by water plants and full skyview demonstrates that this standardization leads to significantly lower estimates of the $DegT_{50,photo,ref}$ for standard water bodies for all three compounds. Thus, for waterbodies with conditions differing from a water depth of 30 cm, no coverage by water plants and full skyview the overall $DegT_{50,photo,ref}$ can be better estimated by taking these three factors into account. This knowledge can be used in the calculation of the PECs in surface water scenarios, that may differ from these reference conditions and that are used in the regulatory process of pesticides in the Netherlands as well as at the EU level.

So, the approach appears to be promising, although the standard deviation of the geomean $DegT_{50,water}$ value is larger than we had expected and the efforts needed to obtain the improved estimates are considerable.

15 Proposed flow chart to decide upon estimation of higher-tier photochemical degradation rate

15.1 Introduction

In this section it is explained how to decide whether it is useful to estimate a more realistic $DegT_{50,water}$ from outdoor cosms. If yes, the flow chart of Figure 15.1 needs to be followed, to decide whether it is useful to apply the method developed in this report to estimate a higher-tier $DegT_{50,photo,ref}$ from outdoor cosm experiments.

So, a first step is to determine whether it is useful to perform a higher tier exposure assessment with the aid of a more realistic $DegT_{50,water}$ value, so to estimate a faster degradation in water. The question to answer is then whether the maximum PEC_{sw} is sensitive to the used $DegT_{50,water}$. This can be the case when multiple applications are done in watercourses having a low flow velocity, which may lead to stacking of the loadings in the watercourse. Alternatively, stacking of loadings and concentrations may occur by the combination of drainage/runoff entries of spray drift deposition events. The PEC_{sw} may also be sensitive to the $DegT_{50,water}$ when time weighed average values are determined. If the maximum PEC_{sw} is not sensitive to the $DegT_{50,water}$ value, there is no use of estimating a more realistic degradation rate, thus there is no need to go through the flow chart below.

So, only if the PEC_{sw} is sensitive to the used $DegT_{50,water}$ value, it is useful to perform an inverse modelling exercise of the outdoor cosm with PEST_TOXSWA and to obtain a more realistic $DegT_{50,water}$. Once the $DegT_{50,water}$ and the ratio of mass lost by degradation to all dissipated mass from the water layer has been estimated ($F_{M,deg-water}$ at a point in time of approx. 3* the $DegT_{50,water}$ after the last application, Eq 15.1) it is useful to enter the flow chart to determine whether photolysis is the dominant degradation process in the cosm water.

15.2 Flow chart to determine whether photodegradation is the dominant degradation process

The flow chart below has been developed to help risk assessors decide whether it is useful to determine a higher-tier, more realistic degradation rate caused by photolysis by using the inverse modelling methodology for outdoor cosm experiments of this report. So, only when the flow chart ends in one of the two green boxes at the end of the flow chart (photolysis is dominant process) the optimization of the $DegT_{50,photo, ref}$ as a function of UV-VitD radiation is useful. The flow chart can be applied by risk assessors for the compound review in The Netherlands, the three regulatory zones as well as the EU.

Note that the minimal requirements for outdoor cosms to be suitable for the inverse modelling exercise is that at least five measured concentrations in the water phase as a function of time, as well as the water depth are available (see also Deneer et al., 2015). Before entering the flow chart it is necessary to estimate the $DegT_{50,water}$ of the considered compound in the cosm, because this value (called A) is needed in the flow chart. This value can be estimated by plotting the natural logarithm of the aqueous concentrations as a function of the time after the first application and drawing the best fitting straight line through the plotted points; assuming first order kinetics, the degradation rate k then equals the slope of the line and the $DegT_{50,water}$ is equal to ln2/k.

The $F_{M,deg-water}$ factor of box 1 of the flow chart is defined by:

$$F_{M,deg-water} = \frac{\int_{i=0}^{i=n} M_{deg-wat} di}{\int_{i=0}^{i=n} M_{diss-wat} di}$$
Eq 15.1

With:

$F_{M,deg-water}$ = fraction of mass degraded in the water layer to the overall mass dissipated from the water layer (-),

$M_{deg-wat}$ = mass degraded in the water layer for hour i (g),

$M_{diss-wat}$ = mass dissipated from the water layer by e.g. volatilisation, transport to sediment or degradation for hour i (g).

However, the value of $F_{M,deg-water}$ can only be determined with the aid of TOXSWA calculations, i.e. after the optimisation, while the flow chart is designed to determine whether the optimisation by PEST-TOXSWA is useful to perform, i.e. before the optimisation calculations. Therefore we propose to first estimate whether degradation is the main dissipation process in the water layer, and not volatilisation or sorption to sediment. To do so, we propose to consider the saturated vapour pressure and the K_{oc}/K_{om} value of the compound. If the saturated vapour pressure at 20-25 °C is smaller than approximately 1 mPa ánd the K_{oc} value smaller than approximately 500 L/kg, the $F_{M,deg-water}$ value is very probably larger than 50% and thus the answer in Box 1 would be 'Yes'. After the optimisation the answer can be confirmed by the TOXSWA output.

Some additional comments to the flow chart are:

\#   In case of photolytic degradation the $DegT_{50,water}$ is often in the order of a few days;

\#   Often the laboratory water-sediment study (generally performed in the dark) is no good predictor of the $DegT_{50,water}$ in the cosm, even when photolytic degradation is not the main degradation process (see e.g. Adriaanse et al. (2012), who found a $DegT_{50,water}$ of prosulfocarb in outdoor ditches of 2.9 d while water-sediment studies resulted in a $DegT_{50,water}$ of 214 d), and

\#   The used phrase 'is approx. equal to' in the flow chart has been defined as representing the interval of 0.5*$DegT_{50,water}$ to 2* $DegT_{50,water}$.
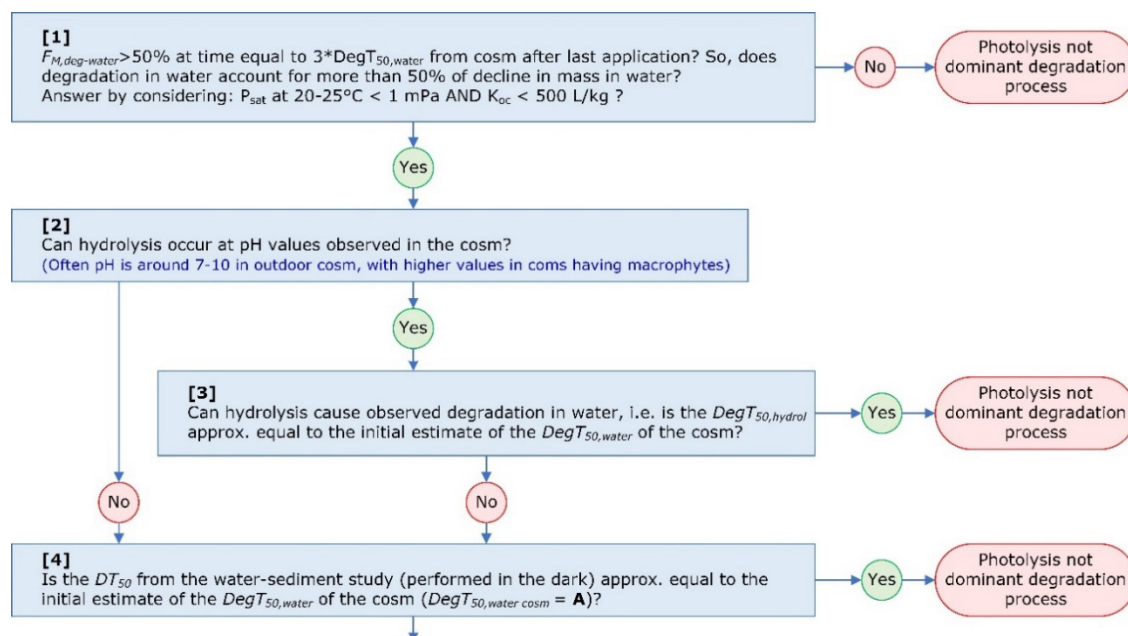
Figure 15.1   *Flow chart to determine whether photolysis is the dominant degradation process in the outdoor cosm- Part 1.*
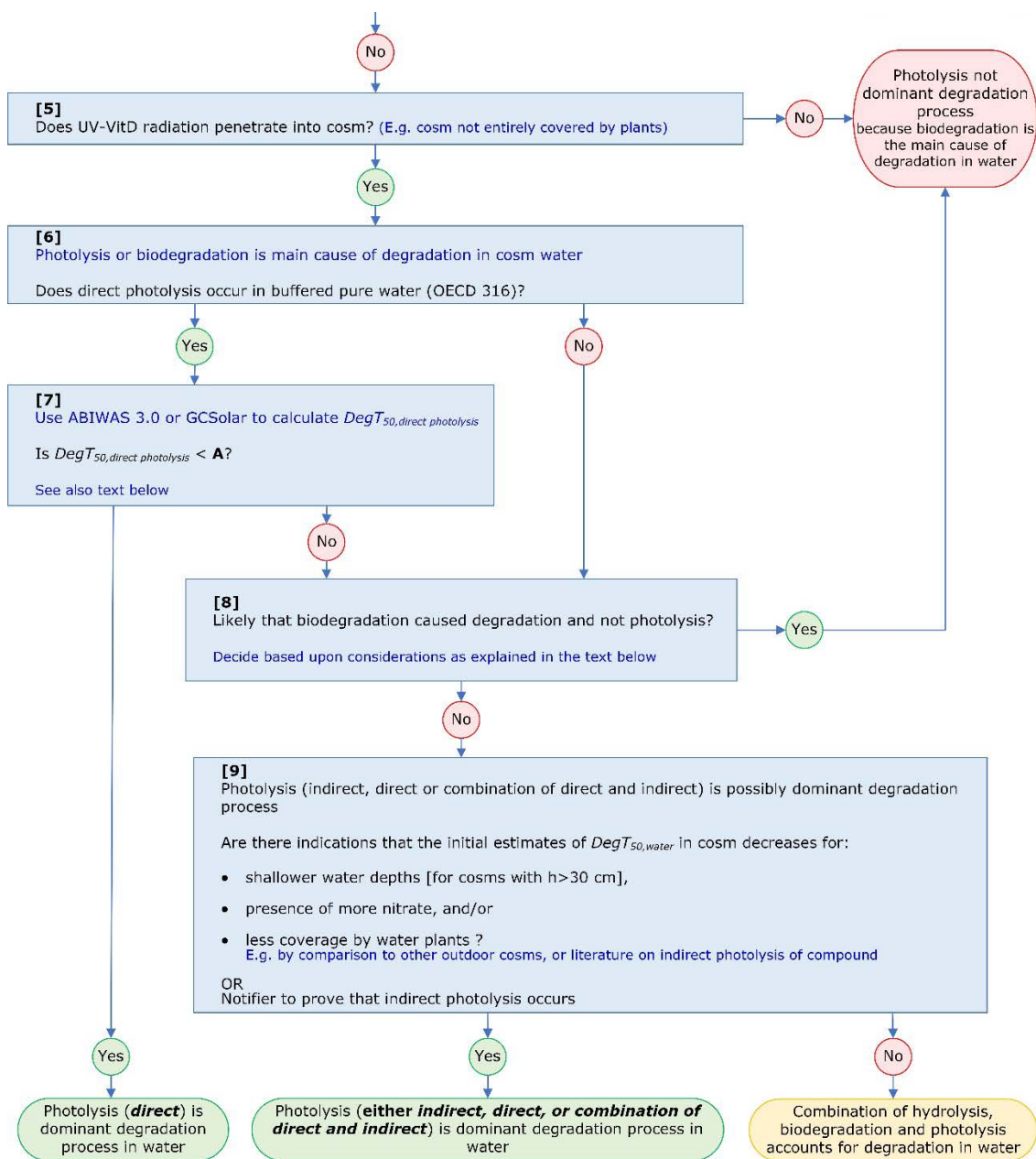
Figure 15.2 *Flow chart to determine whether photolysis is the dominant degradation process in the outdoor cosm- Part 2.*

With respect to box [7]: both ABIWAS and GCSOLAR (Annex 2) may be used to determine $DegT_{50, direct photolysis}$ for the risk assessment. In case of agreed endpoints it should be checked whether the calculated direct photolysis rates are relevant, i.e. whether the conditions for which the endpoints have been calculated apply to those of the cosm (water depth, light attenuation, season and latitude). If not, the $DegT_{50, direct photolysis}$ should be recalculated for the relevant conditions of the cosm.

With respect to box [8]: the likelihood that biodegradation is the main degradation process in water and not photolysis can be assessed considering:
Dossier data on direct and indirect photolysis, ready biodegradability, biodegradation in natural surface water (OECD (309), (irradiated) water-sediment studies;
Literature on biodegradation or photolysis of the compound;
Studies on indirect photolysis; e.g. according to OPPTS 835.5270 (EPA, 1998b) but including several levels of nitrate as this may accelerate photolysis (Lam et al., 2003).

The flow chart has been tested by applying it to the three compounds analysed in this report: metribuzin, imidacloprid and metamitron. Annex 7 details the steps taken for each of the compounds and demonstrates that the flow chart functions well.

16 Discussion, conclusions and recommendations

Discussion

This report presents a new method to estimate a degradation half-life from outdoor coms, where degradation is dominated by photolysis. It is demonstrated that the estimated photolytic degradation rate represents reality better than the standard laboratory studies on degradation, such as the direct photolysis studies in buffered pure water, the hydrolysis studies, and the water-sediment studies in the dark. A flow chart indicates for which compounds photolytic degradation is likely to be the dominant degradation process in the water layer, and thus for which compounds it is useful to apply the developed method of optimising the $DegT_{50,photo,ref}$ by inverse modelling by PEST-TOXSWA.

Such a higher-tier degradation rate may be useful when the predicted exposure concentration, PEC_{sw}, for assessment of risks for the aquatic ecosystem in the regulatory procedure depends on the degradation rate in the water layer. This may happen in case of multiple applications with spray drift deposition on slowly moving watercourses, resulting in stacking of deposited mass, when a spray drift deposition falls on top of a runoff or drainage entry in a slowly moving watercourse, or when time weighed average concentrations are used in the ecotoxicological risk assessment. The higher-tier degradation rate will then result in a PEC_{sw} that is lower, than the PEC_{sw} calculated on basis of the lower-tier longer $DegT_{50,water}$.

The use of a higher-tier degradation rate may be an alternative to other higher-tier options in the regulatory procedure, e.g. a refined estimation of the spray drift deposition or runoff or drainage entries. At present, nor in the Netherlands, neither at EU level a tiered approach is available which gives a clear, systematic and coherent overview of all possibilities for refinement of the exposure assessment in surface water for regulatory purposes. For the Netherlands such tiered approaches are currently being developed for scenarios with arable crops, as well as for fruit orchards and lane trees. At EU level the so-called EU FOCUS surface water scenarios have been 'repaired' from 2017 to 2020, but without explicit consideration of a systematic overall tiered approach, replacing the current Steps 1-2-3-4.

The developed estimation method of this report needs hourly data on actual UV radiation for the location of the outdoor cosm experiments and for the scenario locations. Over the years, and even in the course of this project, more and better reprocessed data on e.g. the measurement data portals of TEMIS and WOUDC (Chapter 2.2.3) have become available, which makes it increasingly easy to obtain the necessary data at the wished spatial and temporal resolution. We now used a spatial resolution of approximately 11*11 km and a temporal resolution of 6 hours for the cloud cover in Europe and 25*25 km with a 1-hourly resolution for the USA (Chapter 3.3.1). To obtain improved actual radiation data it would be helpful to reduce the current temporal resolution of 6 h in Europe.

Conclusions

We developed an inverse modelling method with PEST-TOXSWA to optimise the $DegT_{50,photo,ref}$ for a reference daily UV-VitD filtered radiation dose to obtain a degradation rate in water for compounds with dominant photolytic degradation. This allows for an improved, more realistic estimation of the degradation in outdoor surface water with known UV-VitD radiation sums. We selected the radiation in the 250 to 335 nm wavelength range for the Vitamin D action spectrum as the radiation that determines best photolytic degradation of pesticides (Chapter 3.2.3).

In addition to the correction for UV-VitD radiation immediately above the water surface we developed a standardization method for the radiation within the water column by correcting for water depth, surface are coverage by macrophytes and skyview of the water surface.

The inverse modelling method with PEST-TOXSWA should only be applied for compounds with photolysis (direct and/or indirect) as the dominant degradation process in water. The flow chart of

Chapter 15 should be used to determine whether the compound under consideration is such a compound.

Daily doses of the actual UV-VitD radiation, $I_{act,UV-VitD}$, have a much larger variation from day to day than their variation across locations in the Netherlands. This means that the whole of the Netherlands can be represented by the temporal population of $I_{act,UV-VitD}$ daily doses at one location (e.g. De Bilt). Furthermore, variation of three-day sums of this radiation in early June was limited to about a factor of three for the whole of Europe. So probably the EU is relatively well represented by the temporal population of $I_{act,UV-VitD}$ at the 10 EU FOCUS surface water locations (Chapter 4.3 and 4.4).

The developed method has been applied to three example compounds and compared to the results of a former study by Deneer et al. (2015), where degradation was a function of water temperature Table 16.1). The analysis of the photodegradation rate in the outdoor cosms of the three compounds metribuzin, imidacloprid and metamitron and their successive standardization to water depth, no coverage of the water surface area by water plants and full skyview leads to the following conclusions (Table 16.1): (1) for two compounds the variation between the standardised photolysis half-lives was less than when standardised based on water temperature, (2) for the third compound this comparison was impossible but the resulting variation between the standardised photolysis half-lives was lower than for the other two compounds, (3) the standardization to water depth, no coverage and skyview appeared for all three compounds to be more important than the standardisation to $I_{act,UV-VitD}$ because the variation of $I_{act,UV-VitD}$ between cosms was comparatively small. So, the approach appears to be promising, although the variation between the standardized photolysis half-lives is still larger than we had expected and the efforts needed to obtain the improved estimates are considerable.

Given the importance of the water depth, plant surface coverage and skyview, it seems also necessary to include these factors in the calculation of the PECs in surface water scenarios that are used in the regulatory process of pesticides in the Netherlands as well as at the EU level. Note that daily UV-VitD radiation sums for the 15 or 20 scenario years have already been gathered for this purpose in this study and are available upon request (Annex 3).

Table 16.1 *Overview of optimised geomean DegT$_{50,water}$ and their standard deviations.*

Compound	DegT$_{50,photo,ref}$	DegT$_{50,photo,ref}$ standardized for water depth of 30 cm, no coverage and full skyview	Deneer et al. (2015)
Metribuzin (*n*=3)			
geomean (d) 2.8	1.2	2.4	
s.d. (-) [@] 0.68	0.51	0.71	
Imidacloprid (*n*=3)			
geomean (d) 5.7	1.4	4.1	
s.d. (-) 0.57	0.43	0.63	
Metamitron (*n*=2)			
geomean (d) 1.2	0.53	n.a.	
s.d. (-) 0.63	0.31	n.a.	

[@] standard deviation of logarithmic transformed values of the individual cosm DegT$_{50}$.

Recommendations

We recommend to test the developed estimation method for the *DegT$_{50,photo,ref}$* for a number of additional photolytically degradable compounds and outdoor cosm studies to confirm or detail the conclusions of this report, that are based upon the analysis of three compounds only.

We also recommend to have a critical look at the value of the *DegT$_{50,sediment}$*, here set at 1000 d. The reason is that for some compounds the laboratory water-sediment studies may suggest that this value is not realistic and that the compound does degrade in the sediment, e.g. when for a relatively strongly sorbing compound the majority of the mass has entered the sediment after a couple of days

and the overall $DegT_{50}$ of the water-sediment systems is much lower than 1000 d. In such a case the overall $DegT_{50}$ value seems a better estimate for the $DegT_{50,sediment}$ than the default value of 1000 d. This may lead to an improved correspondence between simulated and measured values in the sediment (as well as in the water) and thus an improved estimation of $DegT_{50, photo,ref}$. For the three studies compounds here (metribuzin, imidacloprid and metamitron), their K_{om} value was below 150 L kg^{-1}, so few mass entered the sediment and using the default value of 1000 d is appropriate.

We recommend to develop a protocol for an experiment to estimate the (direct +indirect) photolysis rates under outdoor known radiation conditions. The best starting point for this protocol with respect to indirect photolysis would be the OPPTS 835.5270 of the US-EPA (1998b), which we described in Chapter 6.4. We there concluded that it would be necessary to cover the range of environmental conditions in the EU and to include the measurements of nitrate concentrations in the outdoor systems.

In order to improve the UV radiation data used in for scenario calculations we recommend to reduce the spatial and temporal resolution (currently approximately 11*11 km and 6 hours for the cloud cover data).

The standardization of the cosm studies to the UV-VitD radiation, water depth, coverage and skyview aims to estimate the course of the UV-VitD radiation with depth in the water column. As there are still considerable inaccuracies in this estimation procedure (reflected in the still large variability of $DT_{50,photo,standard}$), it seems advisable to measure in future cosm studies the UV-radiation as a function of depth on an hourly basis. Relatively simple and cheap UV sensors for outdoor under-water conditions exist, that offer the option to select a wished band of radiation (see e.g. Figure 16.1). So, we recommend the use of such devices during outdoor cosm experiments for compounds that are likely to exhibit photolytic degradation.
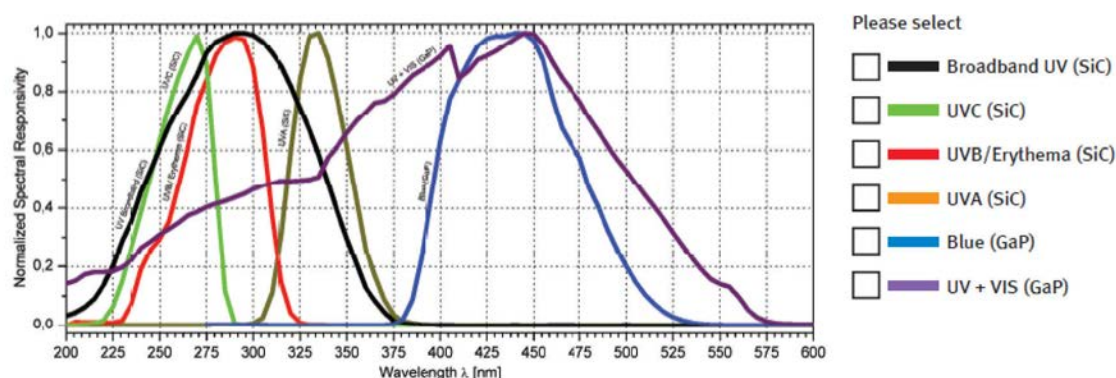
Figure 16.1 *Example of possible wave bands for measurements of radiation at the location of an outdoor cosm experiment.*

For outdoor cosm experiments we recommend to document the exact timing of all applications (in view of the determination of the number of day light hours during the first day after application, as photolytic degradation half-lives may be quite fast, e.g. in the order of hours only).

We also recommend to document the water surface area coverage by water plants during the experiment, especially during the period from the first application up to three times the estimated $DT_{50,water}$ of the experiment, as this is the period of approximately 90% mass dissipation. So, in addition to the bottom coverage, which generally is currently measured by ecotoxicologists, also the coverage at the water surface should be measured.

We recommend to include the daily UV-VitD radiation doses in the characterisation of surface water scenarios used in the regulatory procedure in The Netherlands as well as at EU level to enable the correction of the photolytic degradation rate for the ambient radiation conditions of the scenarios. In this way more realistic degradation rates and thus PEC_{sw} may be calculated.

In order to be consistently implemented in the regulatory risk assessment procedure we recommend to develop guidance for a higher-tier exposure assessment, including photochemical degradation, e.g. in the form of a well structured, comprehensive tiered approach for the estimation of the PEC_{sw}.

We recommend to develop a more user-friendly way of performing the inverse modelling by PEST-TOXSWA and successive data processing to obtain a geomean $DegT_{50,photo,ref}$ in order to facilitate its implementation in the regulatory procedure. Before doing so, we also recommend to perform an analysis of registered products over the last e.g. 10 years, to assess whether the estimate of a higher-tier $DegT_{50,photo,standard}$ value would have led to other conclusions concerning the acceptability of the ecotoxicological risk of the compound considered.

References

Adriaanse, P.I. 1996. Fate of pesticides in field ditches: the TOXSWA simulation model. Winand Staring Centre report 90, Wageningen, The Netherlands.

Adriaanse, P.I. 1997. Exposure assessment of pesticides in field ditches: The TOXSWA model. Pest. Sci. 49, 210 – 212.

Adriaanse, P.I., Boesten J.J.T.I., Crum S.J.H. 2012. Estimating degradation rates in outdoor stagnant water by inverse modelling with TOXSWA: a case study with prosulfocarb. Pest Manag. Sci. 69, 755 – 676.

Adriaanse, P.I., J.W. Deneer, J.J.T.I. Boesten and C. van Griethuysen, 2017. Estimation of degradation rates in water of outdoor cosms with measured concentrations in water and sediment. Guidance for inverse modelling using TOXSWA. Report 2859. Wageningen Environmental Research, Wageningen University & Research, 149 pp.

Adam, M. E. N. (2015). Determination of daily total ultraviolet-B in a subtropical region (Upper Egypt): An empirical approach. Atmospheric Research, 153, 1-9.

Allaart, M., van Weele, M., Fortuin, P., and Kelder, H., 2004. An empirical model to predict the UV-index based on solar zenith angles and total ozone, Meteorol. Appl., 11, 59–65.

American Meteorological Society, 2016, AMS Glossary of Meteorology. http://glossary.ametsoc.org/wiki/Main_Page. Accessed 2 November 2016. Search terms: shortwave radiation, solar radiation, global radiation, direct solar radiation, diffuse solar radiation, longwave radiation, terrestrial radiation.

Apell, J.N., N.C. Pflug and K. McNeill, 2019. Photodegradation of fludioxonil and other pyrroles: the importance of indirect photodegradation for understanding environmental fate and photoproduct formation. Environ. Sci. Technol. 53:11240-11250.

Arts, G.H.P., L.L. Buijse – Bogdan, D.M. Belgers, C.H. van Rhenen – Kersten, R.P.A. van Wijngaarden, I. Roessink, S.J. Maund, P.J. van den Brink, T.C.M. Brock. 2006. Ecological impact in ditch mesocosms of simulated spray drift from a crop protection program for potatoes. Integrated Environmental Assessment and Management 2, 105 – 125.

Attri, P., Y.H. Kim, D.H. Park et al., 2015. Generation mechanism of hydroxyl radical species and its lifetime prediction during the plasma-initiated ultraviolet (UV) photolysis. Sci. Rep. 5, 9332; DOI:10.1038/srep09332.

Bayer AG, Crop Protection, 2001. Fate of Imidacloprid SL 200 in outdoor microcosms. Study report no. HBF/Mt 11, Laboratory project ID: E 413 1819 – 7, Leverkusen, Germany. Study report date 2001 – 02 – 20.

Bayer AG, Crop Protection 2003. Biological effects and fate of imidacloprid SL 200 in outdoor microcosm ponds. Study report no. 811776, Leverkusen, Germany.

Beltman, W.H.J., H.M. Mulder, M.M.S. ter Horst and E.L. Wipfler, 2015. Transformation by photolysis in water in the pesticide model TOXSWA; Implementation report. Wageningen, Alterra Wageningen UR (University & Research centre), Alterra report 2649. 48 pp.; 10 fig.; 6 tab.; 12 ref.

Bernhard, G. and Seckmeyer, G., 1997. Measurements of spectral solar UV irradiance in tropical Australia, J. Geophys. Res., 102, 8719–8730.

Bodesa, J. and Van Weele, M., 2002. Effects of aerosols on UV-index. Scientific Report WR-2002-07, KNMI, De Bilt, The Netherlands.

Boesten J.J.T.I, P.I. Adriaanse, M.M.S. ter Horst, A. Tiktak and A.M.A. van der Linden, 2015. Guidance proposal for using available DegT50 values for estimation of degradation rates of plant protection products in Dutch surface water and sediment. Wettelijke Onderzoekstaken Natuur en Milieu, Document 284.

Boesten J.J.T.I., 2017. Conceptual considerations on exposure assessment goals for aquatic pesticide risks at EU level. Pest Management Science 74: 264-274, doi: 10.1002/ps.4701.

Bordewijk, J. A., H. Slaper, H. A. J. M. Reinen, and E. Schlamann (1995). Total solar radiation and the influence of clouds and aerosols on the biologically effective UV. Geophys. Res. Lett., 22, 2151–2154.

Brock, T.C.M., S.J.H. Crum, J.W. Deneer, F. Heimbach, R.M.M. Roijackers, J.A. Sinkeldam. 2004. Comparing aquatic risk assessment methods for the photosynthesis-inhibiting herbicides metribuzin and metamitron. Environ. Poll. 130, 403 – 426.

Burrows, H.D., M. Canle, J.A. Santaballa, S. Steenken, 2002. Reaction pathways and mechanism of photodegradation of pesticides. J. of Photochemistry and Photobiology B: Biology 67(2), 71-108.

Calbo, J., & González, J. A. (2005). Empirical studies of cloud effects on UV radiation: A review. Reviews of Geophysics, 43(2).

Colombo, V. Diplomarbeit on the determination of the impact of repeated application of imidacloprid on an indigenous invertebrate-community; field-based microcosm experiment. 2009. Berlin.

Colombo, V., S. Mohr, R. Berghahn, V.J. Pettigrov. 2013. Structural changes in a macrozoobenthos assemblage after imidacloprid pulses in aquatic field-based microcosms. Arch. Environ. Contam. Toxicol. 65, 683 – 692.

Deneer, J.W., P.I. Adriaanse, C. van Griethuysen and J.J.T.I. Boesten, 2015, Estimation of degradation rates in cosm water. Guidance for inverse modelling using TOXSWA. Alterra report 2679, Alterra, Wageningen UR, 151 pp.

Den Outer, P. N., Slaper, H., & Tax, R. B. (2005). UV radiation in the Netherlands: Assessing long-term variability and trends in relation to ozone and clouds. Journal of Geophysical Research: Atmospheres, 110(D2).

Den Outer, P. N., Slaper, H., Kaurola, J., Lindfors, A., Kazantzidis, A., Bais, A. F., ... & Josefsson, W. (2010). Reconstructing of erythemal ultraviolet radiation levels in Europe for the past 4 decades. Journal of Geophysical Research: Atmospheres, 115(D10).

EFSA PPR Panel (EFSA Panel on Plant Protection Products and their Residues), 2013a. Guidance on tiered risk assessment for plant protection products for aquatic organisms in edge-of-field surface waters. EFSA Journal 2013; 11(7):3290, 268 pp. doi: 10.2903/j.efsa.2013.3290.

European Food Safety Authority, 2013b. EFSA Guidance Document on the risk assessment of plant protection products on bees (*Apis mellifera*, *Bombus* spp. and solitary bees). EFSA Journal 2013; 11(7):3295, 268 pp doi: 10.2903/j.efsa.2013.3295.

EFSA (European Food Safety Authority), 2015. EFSA Guidance Document for predicting environmental concentrations of active substances of plant protection products and transformation products of these active substances in soil. EFSA Journal 2015; 13(4):4093, 102 pp. doi: 10.2903/j.efsa.2015.4093.

EFSA Scientific Committee, 2016. Guidance to develop specific protection goals options for environmental risk assessment at EFSA, in relation to biodiversity and ecosystem services. EFSA Journal 2016; 14(6):4499, 50 pp. doi:10.2903/j.efsa.2016.4499.

EFSA (European Food Safety Authority), Paulien Adriaanse, Arnaud Boivin, Michael Klein, Nick Jarvis and Michael Stemmer, Gabriella Fait and WG chair Mark Egsmose, 2020. Scientific report of EFSA on the 'repair action' of the FOCUS surface water scenarios. EFSA Journal 2020;18(6):6119, 301 pp. https://doi.org/10.2903/j.efsa.2020.6119.

EPA (1998a) OPPTS 835.2210 Direct photolysis rate in water by sunlight. EPA, Washington, USA, 35 pp.

EPA (1998b) OPPTS 835.5270 Indirect photolysis screening test. EPA, Washington, USA, 22 pp.

Fairchild, J.F., L.C. Sappington. 2002. Fate and effects of the triazinone herbicide metribuzin in experiment pond mesocosms. Arch. Environ. Contam. Toxicol. 43, 198 – 202.

Fioletov V.E., L.J.B. McArthur, T.W. Mathews and L. Marrett, 2009. On the relationship between erythemal and vitamin D action spectrum weighted ultraviolet radiation. Journal of Photochemistry and Photobiology B: Biology, 95, 9-16.

Fioletov, V. E., Kerr, J. B., & Fergusson, A. (2010). The UV index: definition, distribution and factors affecting it. Can J Public Health, 101(4), 5-9.

FOCUS, 2001. FOCUS Surface Water Scenarios in the EU Evaluation Process under 91/414/EEC. Report of the FOCUS Working Group on Surface Water Scenarios, EC Document Reference SANCO/4802/2001-rev.2, 245 pp.

FOCUS, 2006. Guidance Document on Estimating Persistence and Degradation Kinetics from Environmental Fate Studies on Pesticides in EU Registration. Report of the FOCUS Work Group on Degradation Kinetics, EC Document Reference Sanco/10058/2005 version 2.0, 434 pp.

Frederick, J. E., Snell, H. E., & Haywood, E. K. (1989). Solar ultraviolet radiation at the earth's surface. Photochemistry and Photobiology, 50(4), 443-450.

Goudriaan, J. (1977). Crop micrometeorology: a simulation study (No. 551.5 G688). Centre for Agricultural Publishing and Documentation, Wageningen.

Holick, M., Bouillon, R., Eisman, J., Garabedian, M., Kleinschmidt, J., Suda, T., Terenetskaya, I., and Webb, A., 2005. Action spectrum for production of previtamin D3 in human skin. Tech. Rep. final draft report of September 2005, CIE Technical Committee 6-54, 2005.

Katagi, T. 2018. Direct photolysis mechanism of pesticides in water. J. Pestic. Sci. 43(2), 57-72

Klein, J., M. Klein, M. Muller, 2019. ABIWAS 3.0. Calculation of the abiotic degradation of chemicals in water. Fraunhofer Institute for Molecular Biology and Applied Ecology IME, Schmallenberg, Germany.

Jacobs, C.M.J., P.I. Adriaanse and J. Deneer, 2010. Modelling water temperature in TOXSWA. Wageningen, Alterra report 2099.

Lam, M.W., K. Tantuco, S.A. Mabury, 2003. PhotoFate: a new approach in accounting for the contribution of indirect photolysis of pesticides and pharmaceuticals in surface waters. Environ. Sci. Technol. 37: 899-907.

McKinlay, A. F. and B. L. Diffey (1987). A reference action spectrum for ultraviolet induced erythemal in human skin. CIE Journal. 6, 17–22.

Mensink, B.J.W.G., M. Montforts, L. Wijkhuizen-Máslankiewicz, H. Tibosch, J.B.H.J. Linders (1995). Manual for summarising and evaluating the environmental aspects of pesticides. Report no. 679101022, National Institute of Public Health and Environmental Protection, RIVM, Bilthoven, The Netherlands, 117 pp.

Monteith, J., & Unsworth, M. (2013). Principles of environmental physics: plants, animals, and the atmosphere. Academic Press.

Nann, S. and Riordan, C., 1991. Solar spectral irradiance under clear and cloudy skies: Measurements and a semiempirical model. Journal of Applied Meteorology, 30(4), pp.447-462.

NTP, National Toxicology Program (2000). Background Document for Ultraviolet Radiation and UVA, and UVB, and UVC. http://ntp.niehs.nih.gov/ntp/newhomeroc/roc10/uv_no_appendices_508.pdf

Oke, T. R. (1987). Boundary layer climates, 2nd Ed. Routledge London, New York.

Pesticide Properties DataBase, University of hertfordshire, UK. www.herts.ac.uk/aeru/ppdb

Remucal, C.K., 2014. The role of indirect photochemical degradation in the environmental fate of pesticides: a review. Environ. Sci.: Processes Impacts 16: 628-653.

Setlow, R. B., 1974. The wavelengths in sunlight effective in producing skin cancer: a theoretical analysis. P. Natl. Acad. Sci. USA, 71, 3363–3366.

Stull, R.B., 1988. An introduction to boundary layer meteorology. Kluwer Academic Publishers, Dordrecht, Boston, London.

Van Geffen, J., van der A, R., van Weele, M., Allaart, M., and Eskes, H., 2005. Surface UV radiation monitoring based on GOME and SCIAMACHY. In: Proceedings of the ENVISAT & ERS Symposium, 6–10 September 2004, Salzburg, Austria. SP 572, ESA, Paris.

Van Geffen, J., Van Weele, M., Allaart, M. and Van der A, R., 2017. TEMIS UV index and UV dose MSR-2 data products, version 2. Dataset. Royal Netherlands Meteorological Institute (KNMI). doi.org/10.21944/temis-uv-msr2-v2.

Van Wijngaarden, R.P.A., J.G.M. Cuppen, G.H.P. Arts, S.J.H. Crum, M.W. van den Hoorn, P.J. van den Brink, T.C.M. Brink (2004). Aquatic risk assessment of a realistic exposure to pesticides used in bulb crops: a microcosm study. Environ. Toxicol. Chem. 23, 1479 – 1498.

Vione, D., V. Maurino, C. Minero, E. Pelizzetti, 2005. Reactions induced in natural waters by irradiation of nitrate and nitrite ions. In Boule P. (Ed.) Handbook of Environmental Photochemistry, p. 221-253. Springer, Berlin.

Wang, L., Gong, W., Li, J., Ma, Y., & Hu, B. (2014). Empirical studies of cloud effects on ultraviolet radiation in Central China. International Journal of Climatology, 34(7), 2218-2228.

Watanabe, H., Takagi, K., & Vu, S. H. (2006). Simulation of mefenacet concentrations in paddy fields by an improved PCPF-1 model. Pest management science, 62(1), 20-29.

Wendt – Rasch, L., P.J. van den Brink, S.J.H. Crum, P. Woin (2004). The effects of a pesticide mixture on aquatic ecosystems differing in trophic status: responses of the macrophyte *Myriophyllum spicatum* and the periphytic algal community. Ecotoxicol. Environ. Saf. 57, 383 – 398.

Wiegant, E., (2016). Improving satellite-based estimations of UV index and dose and first assessment of UV in a world-avoided. KNMI Scientific Report WR-2016-01. KNMI, De Bilt.

WMO (World Meteorological Organization), (2006). Instruments to Measure Solar Ultraviolet Radiation, Part 2: Broadband Instruments Measuring Erythemally Weighted Solar Irradiance. WMO TD No. 1289, WMO/GAW No. 164. WMO/GAW, Geneva, Switzerland.

Zempila, M.-M., van Geffen, J.H.G.M., Taylor, M., Fountoulakis, I., Koukouli, M.-E., Van Weele, M., Van Der A, R.J., Bais, A., Meleti, C., Balis, D., 2017. TEMIS UV product validation using NILU-UV ground-based measurements in Thessaloniki, Greece. Atmospheric Chemistry and Physics 17, 7157-7174.

Annex 1 Computing UV radiation intensities from solar radiation

Outline of the method

Den Outer et al. (2005) tested several relationships between CMF_{UV} and CMF_{TS} against observations in Bilthoven (the Netherlands) and found the following relationship to be adequate to estimate daily, erythemally weighted, surface-level UV radiation doses from total solar radiation:

$$I_{actual,UV} = I_{clear,UV} \frac{1 - (1 + pCMF_{TS})^{-0.27}}{1 - (1 + p)^{-0.27}} \qquad \text{[A1.1a]}$$

which is equivalent to

$$CMF_{UV} = \frac{1 - (1 + pCMF_{TS})^{-0.27}}{1 - (1 + p)^{-0.27}} \qquad \text{[A1.1b]}$$

where p is a coefficient, taken to be a function of the maximum solar elevation on a specific day and which therefore depends on the season. The maximum solar elevation is expressed in terms of the so-called solar zenith angle, that is, the angle between the center of the solar disc and the zenith (an imaginary point directly above an observer or location on a line perpendicular to the Earth's surface). Thus, the minimum zenith angle (Θ) on a specific day at a specific location coincides with the maximum solar elevation at that day and location. It will be smaller in summer (high maximum elevation of the sun, so a smaller angle with the zenith) than in winter (low maximum elevation of the sun, so a larger angle with the zenith). Table A1.1 gives the recommended values of p as a function of Θ (Den Outer et al., 2005). For an illustration of the function that describes the erythemal action spectrum the reader is referred to Figure A1.9.

Eqs [A1.1a]-[A1.1b] allow the intensity or daily dose of UV radiation to be estimated using measured solar radiation as follows.

First, the clear-sky intensities of both radiation quantities ($I_{clear,X}$) are computed for each day of the year (DOY), using standard astronomical computations and assuming a standard atmospheric composition. Since these computations require the solar elevation or zenith angle Θ to be known they are also used to establish p for each DOY, for later use in Eq. A1, via "lookup" Table A1.1.

Second, the observed total solar radiation intensity $I_{actual,TS}$ is divided by clear-sky value $I_{clear,TS}$ to compute the cloud modification factor for total solar radiation, CMF_{TS}.

Third, using Eq. [A1.1a] with CMF_{TS} from the second step and p from the first step $I_{actual,UV}$ is computed. Obviously, the corresponding effect of clouds on UV radiation, quantified via CMF_{UV}, can be determined from [A1.1b] as well, but this step is not strictly required in the proposed procedure.

Table A1.1 *Values of coefficient p in [A1.1] as a function of solar zenith angle (Θ) (Den Outer et al., 2005).*

cos(Θ)	Θ	P
0.75-0.90	25.8-41.4	0.383
0.60-0.75	41.4-53.1	1.07
0.45-0.60	53.1-63.3	1.94
0.30-0.45	63.3-72.5	3.03
0.15-0.30	72.5-81.4	4.40
<0.15	>81.4	6.13

Using the *p*-values from Table A1.1, this method can formally be applied to erythemally weighted UV intensities only (see Eq. A1.3 and Figure A1.9 for the weighing function), since the *p*-values were derived for this action spectrum. Because of the dependency of absorption and scattering on wavelength it may be expected that other action spectra would need other *p*-values. However, for the time being we assume that the values from Table A1.1 can be applied to other action spectra as well, as long as these are broadband weighing functions.

Implementation: a first example

In this section, the method briefly outlined above will be detailed further and illustrated with sample calculations for The Netherlands, using solar radiation data observed in Wageningen. Furthermore, a radiation transfer model (kindly made available by the National Institute for Public Health and the Environment, RIVM, Bilthoven, Netherlands) has been used to compute clear sky radiation intensities $I_{clear,X}$, using the default settings of the model. This includes an assumed ozone column depth of 300 DU (Dobson Units) and the subsequent wavelength-specific effect on atmospheric UV absorption. No radiation intensity weighing via any action spectrum is applied at this stage. Furthermore, for the UV calculations we concentrate on the UVB spectrum between 280 and 320 nm.

Estimation of $I_{actual,UV}$ from total solar radiation requires the following steps.

1. Estimation of solar zenith angle and clear-sky total solar radiation

Clear-sky total solar radiation at the surface can be estimated with reasonable accuracy using astronomical formulae that compute solar elevation as a function of position on the Earth's surface, season and time of day, and assuming standard atmospheric conditions. Estimation methods range from simple parameterizations like the one implemented in TOXSWA (Jacobs et al., 2010) to more sophisticated radiation transfer models like the one used here. Per location the computation of daily clear-sky radiation needs to be performed only once, allowing lookup tables to be created. So, the computational burden of using a somewhat more accurate radiation transfer model is considered not to be a critical issue. Since all methods to determine $I_{clear,TS}$ require the solar elevation or solar zenith angle Θ to be known these computations are also used to determine the values of p (see Eq. 4) as a function of DOY for a specific location, for later use in Step 4. This can be achieved by means of a lookup-table based on Table 1. However, it may be more practical to use a continuous function. In this example we choose to stick to the original methodology of Den Outer et al. (2005) as closely as possible. Furthermore, in our sample computations we will ignore leap-years.
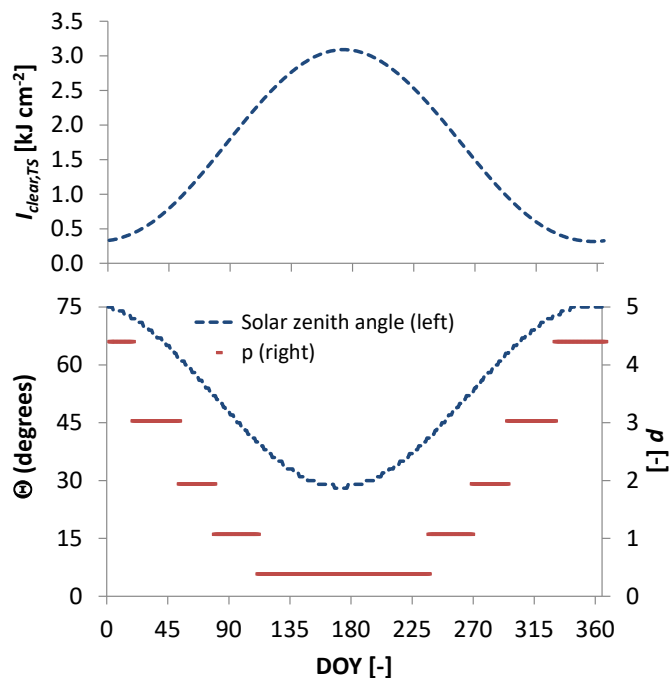

Figure A1.1 *Example of computed clear sky total solar radiation, $I_{clear,TS}$ (upper panel), solar zenith angle Θ and coefficient p (lower panel, derived from Table A1.1) for central Netherlands.*

The upper panel of Figure A1.1 shows the computed $I_{clear,TS}$ for a location in the center of the Netherlands as a function of DOY. The underlying minimum Θ on each day and the corresponding values of p are shown in the lower panel of the figure. Obviously, maximum clear-sky intensities are reached around 21 June (DOY=172), when the sun reaches is highest elevation and the Θ therefore reaches its minimum. In the Netherlands Θ remains below about 75 degrees, so that the maximum value of p listed in Table A1.1 is never reached.

2. Estimation of clear-sky UV radiation

The estimation of $I_{clear,UV}$ can to some extent also be considered as a preprocessor step. This is the case if we assume the depth of the ozone column to be constant, like we will do in these sample calculations. Since the result is influenced by this depth, one could also consider including observed ozone depth from satellite observations. In the RIVM model used here, this would require an update of the wavelength-specific UV absorption characteristics on each specific day and this would imply year-to-year variations as well. For the time being, the assumption of an ozone column depth of 300 DU is considered sufficiently accurate.

The resulting clear-sky UVB radiation intensity at the surface is shown in Figure A1.2. At first sight, the annual course shows a pattern similar to the one for total solar radiation, but obviously with much lower intensity levels. However, the ratio between the summer maximum and winter minimum in the case of UVB (measuring the 'relative amplitude of the wave') is much higher than in the case of total solar radiation: 7.4/0.23=32.2 for UVB versus 3.1/0.32=9.8 for total solar radiation. This implies that the portion of UVB expressed as a fraction of solar radiation shows a seasonal variation. We come back to this issue below.
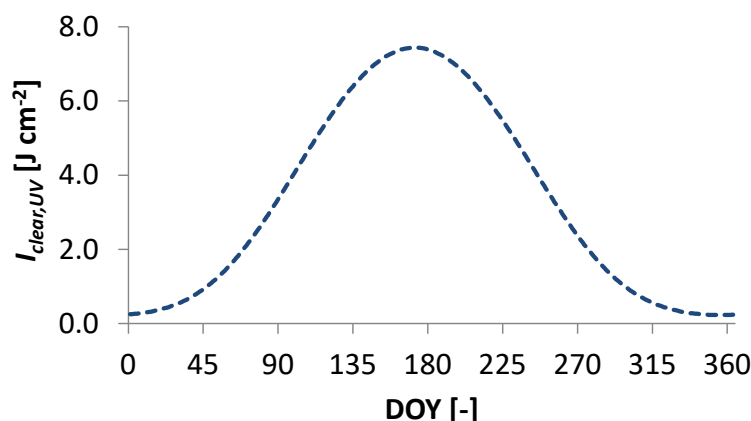

Figure A1.2 *Example of computed clear sky UVB radiation intensity, $I_{clear,UV}$ for central Netherlands.*

3. Estimation of CMF$_{TS}$ using observed total solar radiation

In the third step CMF$_{TS}$ is estimated by dividing observed total solar radiation at the surface by the clear-sky estimate obtained in Step 1. Observed total solar radiation is also called global radiation and is available from observations at the main meteorological stations in The Netherlands and in a growing number of other countries as well. Here, we compute CMF$_{TS}$ from solar radiation observations performed at the Veenkampen meteorological station in Wageningen, run by the Meteorology and Air Quality group of Wageningen University & Research. The example uses observations from the years 2013-2015. The observations are shown in the upper panels of Figure A1.3, the corresponding CMF$_{TS}$ values are shown in the lower panels. While the main seasonal pattern in the data follows the clear-sky values, the effect of clouds can clearly be distinguished. On the one hand the clear sky estimate may be slightly too low on some days. However, forward scattering sometimes causes CMF values larger than 1 as well. Minimum CMF values of less than 0.1 occur on some days. Although there are large differences between years on a specific DOY, the general characteristics like seasonal patterns and monthly to annual sums are roughly similar for the years considered here.
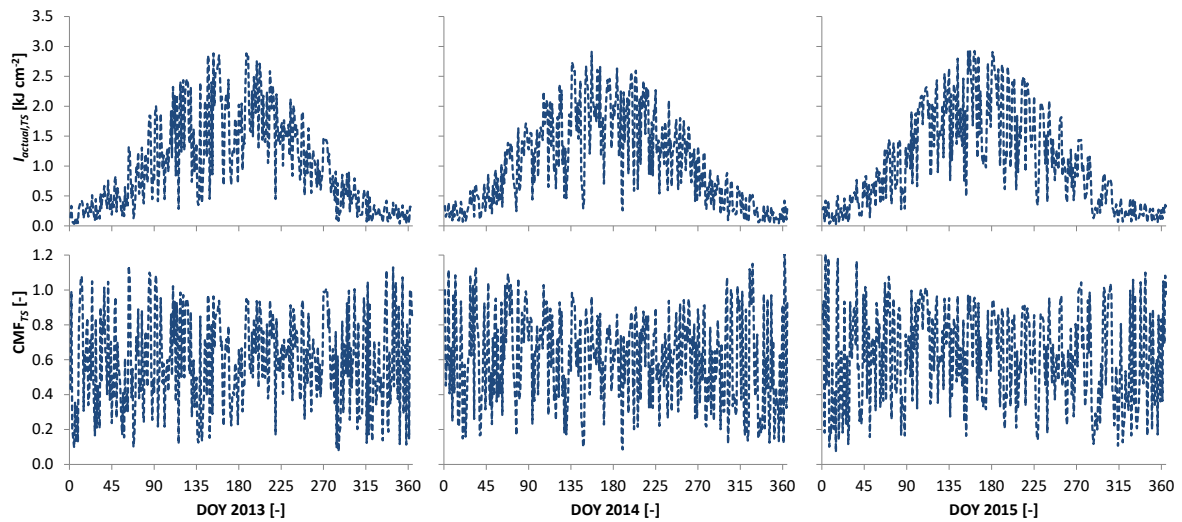
Figure A1.3 *Observed total solar radiation, $I_{ACTUAL,TS}$, at the Veenkampen weather station in Wageningen Netherlands (2013-2015, upper panels), and CMFTS values estimate from the observations and the clear sky values (lower panels).*

4. Estimation of actual UV radiation intensity at the surface

Using CMF_{TS} from the previous step $I_{actual,UV}$ can now be determined using Eq. [A1.1a]. The result is shown in the upper panels of Figure A1.4. The annual course of the corresponding CMF_{UV} is shown in the lower panels. Like expected from [A1.1], CMF_{UV} is on average larger than CMF_{TS}, 0.686 versus 0.591. Also, the variability seems to be somewhat smaller. The standard deviation is 0.225 for CMF_{UV} versus 0.264 for CMF_{TS}. Again, it can be seen that the ratio between summer and winter values is higher than in the case of total solar radiation (cf. Figure A1.3).
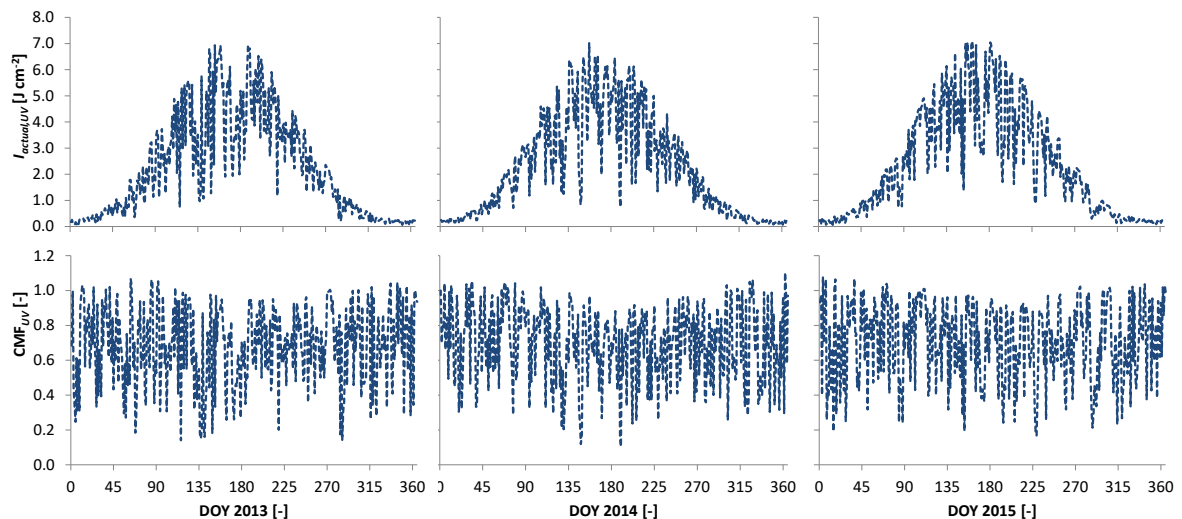
Figure A1.4 *Estimated actual UV radiation intensity at the surface, $I_{actual,TS}$, (upper panels) and corresponding CMF_{UV} values (lower panels) for the years 2013-2015 in Wageningen, The Netherlands.*

Uncertainties

The method described in this annex uses cloud modification factors for UVB that are in fact designed to compute an erythemally weighted UV dose. Since we apply no action spectrum, we implicitly assume that the CMF values represent the effect of clouds on the non-weighted UVB. This is not necessarily the case (Nann and Riordan, 1991). Nevertheless, the procedure is assumed to give better correction factors for photolysis rates and degradation times than the assumption of a constant *ratio* between UVB and total solar radiation. It is likely that clouds are the most important atmospheric

factor disturbing a linear relation between the intensity of solar and UV radiation at the surface, except perhaps for very low solar elevations. However, in the present context daily totals will be used and radiation at low solar elevation will in most regions of the world not contribute much in terms of total daily energy received at the Earth's surface.

The effect of the depth of the ozone column on absorption of UVB probably represents a much larger uncertainty. UVB is partly absorbed by ozone in the stratosphere (the 'ozone layer', of which the depth is expressed in Dobson Units, DU). The absorption is wavelength-dependent, with the absorption being much stronger for the shorter wavelengths in the UVB band. UVA is nearly independent of absorption by ozone (Allaart et al., 2004). The absorption also depends on the solar zenith angle. This is illustrated in Figure A1.5 which depicts instantaneous values of the clear-sky UVB irradiance at the surface as a function of wavelength between 285 and 320 nm, for an ozone column depth of 300 and 400 DU and solar zenith angles of 30° and 70°, respectively. This range represents typical temporal and spatial variations over Europe (see below). The figure is constructed using results from computations with a sophisticated model, performed by the World Meteorological Organization (WMO, 2006). It can clearly be seen that more UVB is absorbed in the case of the thicker layer (400 DU).

The dependence of the absorption on wavelength is also illustrated in the figure. The dotted red line gives the ratio of the irradiance at the surface for 400 DU to that at 300 DU. Thus, for each wavelength it simply gives the ratio of the value given displayed by the green dashed curve at 400 DU (@400 DU) and the value at 300 DU (@300 DU) shown by means of the purple line. A low ratio thus expresses a relatively strong absorption at 400 DU, compared to the one at 300 DU. The lower ratios at shorter wavelengths thus indicate a much stronger absorption than at longer wavelengths. However, only little energy is received at the surface for through the shorter wavelengths. Over 95% of the energy in the UVB band is contained in wavelengths > 305 nm.
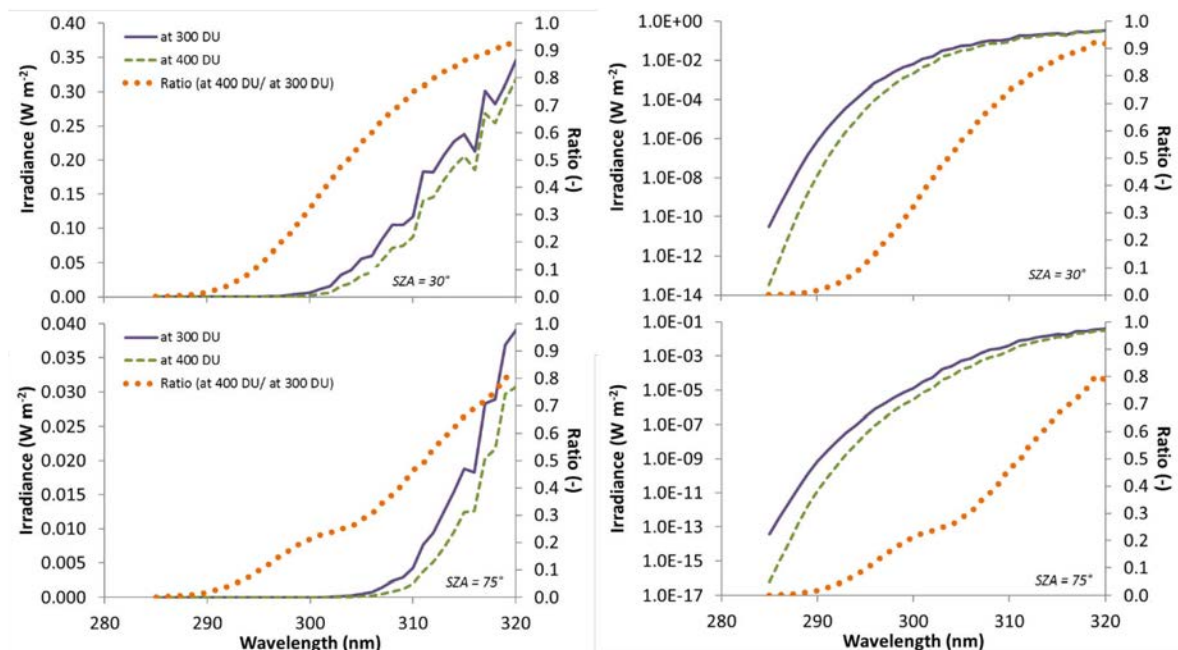
Figure A1.5   *Clear-sky irradiance of UVB at the Earth's surface as a function of wavelength (left axis), for two ozone column depths (300 and 400 DU) and two solar zenith angles (SZA=30°, upper; SZA= 75°, lower). Also shown is the ratio of irradiance for the two ozone column depths (right axis), also as a function of wavelength. The left and right panels contain the same information, but the scaling of the left vertical axis is linear and logarithmic, respectively.*

The reduction in the total UVB irradiance due to the deeper ozone column (400 versus 300 DU) can be obtained by summing the contribution from each wavelength considered, between 285 and 320 nm. At a solar zenith angle of 30° (high solar elevation), the atmospheric path is relatively short and in total 18% less UVB is received at the surface if the depth of the ozone column increases from 300 to

400 DU. At the higher solar zenith angle of 75° (low solar elevation), the atmospheric path is longer and more UVB is absorbed. The total amount of energy received at the surface is 30% less in if the depth of the ozone column would increase from 300 to 400 DU.

Figure A1.6 shows two examples of the spatial distribution of the ozone column depth over the Northern Hemisphere. The figures are based on satellite observations and are available from www.temis.nl. Two examples are shown: the ozone column depth on 1 December and 1 June 2012, respectively. It can be seen that the depth varies between about 225 and 475 DU for the case in December, and between about 275 and 425 DU in June. The large-scale spatial patterns are connected with weather patterns, including stratospheric patterns. Depending on the large-scale meteorological conditions and the condition of the ozone column the aforementioned range of values could occur within Europe as well. See www.temis.nl for more examples.
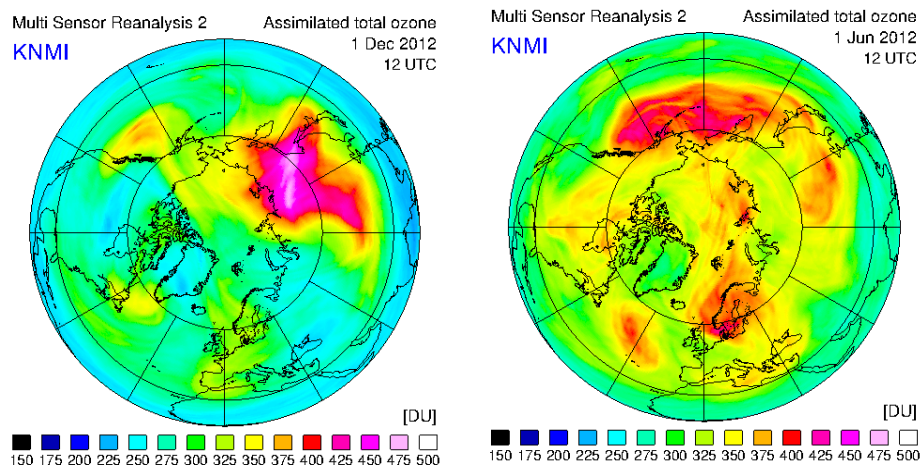
Figure A1.6 *Examples of ozone column depth variation over the Northern Hemisphere: 1 December 2012 (left) and 1 June 2012 (right). The colours express the depth in Dobson Units. Figures were obtained from www.temis.nl.*

Figure A1.7 gives an impression of the temporal variation in ozone column depth from observations at two specific locations: Diekirch in Luxemburg and Kishinev in Moldova. The data were obtained from the World Ozone and Ultraviolet radiation Data Centre (WOUDC, www.woudc.org) and cover the years 2006-2010. When on a specific day no ozone observation was available the value of the previous day was repeated. In spite of the gaps a good impression is obtained of the temporal variations of ozone column depth. Although for specific days the differences are considerable, the seasonal to annual patterns show some similarity, with a maximum depth of around 400 DU in early spring and a minimum depth of about 300 DU in late autumn. Typical variations remain between those values but larger values up to 500 DU and smaller values down to 250 DU occur as well. This is largely consistent with the examples of the spatial patterns given in Figure A1.6.
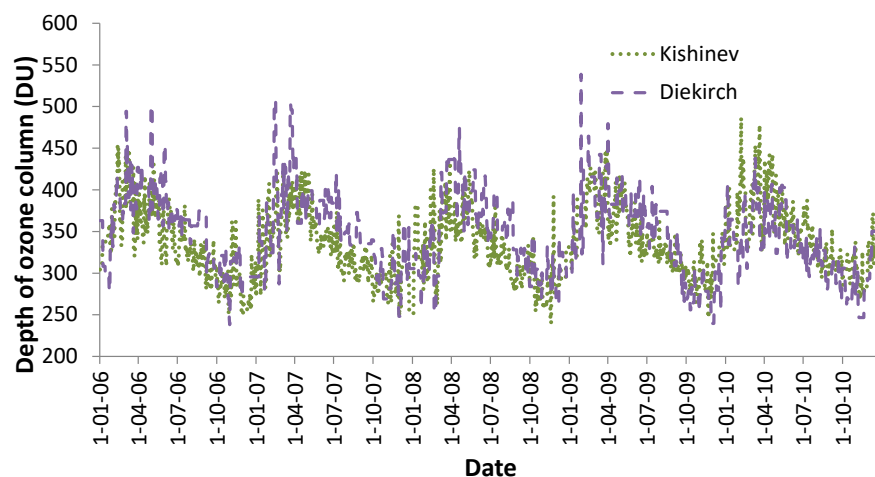
Figure A1.7 *Ground-based observations of total ozone column depth over Kishinev in Moldova and Diekirch in Luxemburg, from 1 January 2006 – 31 December 2010. See www.woudc.org for more information on the observations.*

Another factor influencing the ratio of UVB to solar radiation is the spectral shift caused by infrared absorption by oxygen and water vapor. However, as can be seen in Figure 2.1, this contribution and in particular the variability in the contribution that may affect the proportion of UV in solar radiation is expected to be (much) less than 10%.

In addition to the effect of atmospheric properties on the proportion of UVB light in the solar radiation, the actual exposure of the surface to the overlying sky, the skyview, will play an important role. For a specific location, the skyview factor Ψ_s is defined as the fraction of the overlying hemisphere occupied

by the sky. For an *isotropically* radiating hemisphere it equals the ratio of the radiation received by a planar surface from the sky to the radiation emitted from the entire hemisphere, so that $I_0 = \Psi_s I_S$ with I_0 the irradiance at the surface and I_S the radiation emitted from the total hemisphere. Elements that block the view on the hemisphere, like houses and trees, will also block direct radiation, that is, will provide shade.

Figure A1.8 *Two-dimensional illustration of the skyview factor, Ψ_s. The left hand side schematically depicts a ditch of which the water surface (blue dashed line) is exactly at the ground surface (thick green line), the right hand side a lower-lying ditch where part of the he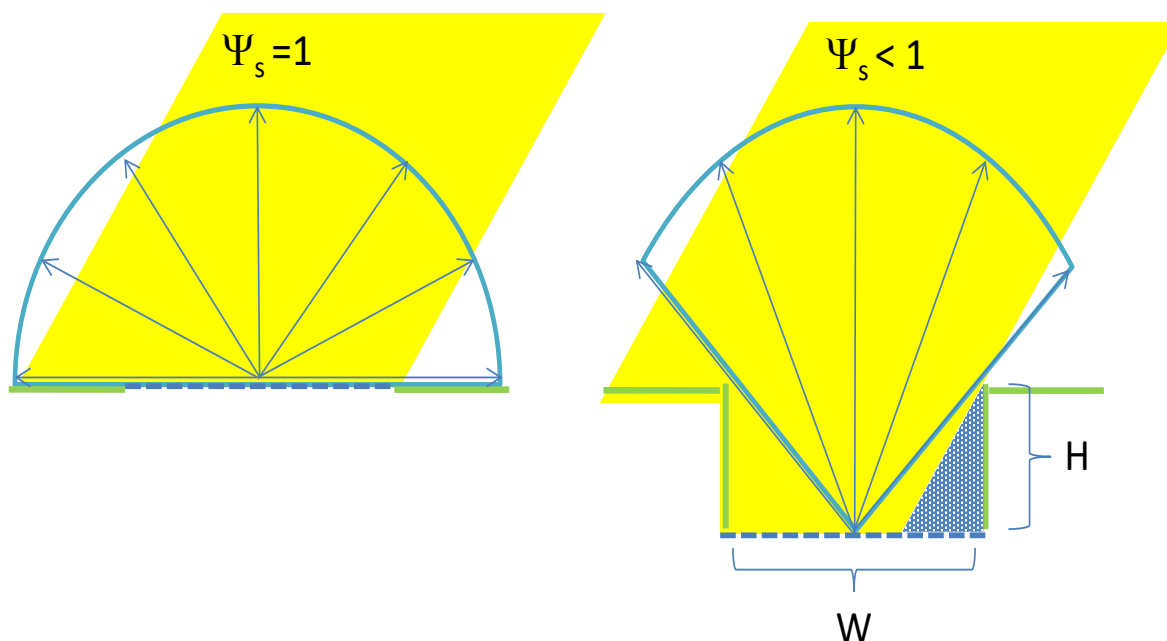misphere is blocked by the ditch walls. The hemisphere is symbolized by means of the blue circle parts ('pies'), the skyview by means of the arrows. The tilted yellow surface symbolizes the direct radiation received at the surface, with the blue triangle indicating the shading due to the ditch wall.*

A two-dimensional illustration of the skyview factor is given in Figure A1.8. From a location in the middle of a ditch with the water surface at the level of the ground surface the entire hemisphere can be observed, so that $\Psi_s = 1$. The water surface will be fully exposed to sunlight, direct as well as diffuse. For a ditch with the water surface below the ground surface part of the hemisphere is blocked by the ditch walls so that $\Psi_s < 1$.

Diffuse radiation at the surface with limited skyview is reduced by a fraction Ψ_s. In addition, part of the water surface may be shaded depending on the position of the sun. In the case of a straight ditch of infinite length Ψ_s can be expressed as a function of the height (H) to width (W) ratio. In other cases, for example when trees and single houses block the skyview, determination of Ψ_s may become more complicated.

Because of the strong dependence of Rayleigh scattering on wavelength, it may be expected that the ratio of diffuse to direct radiation is different for UV radiation and total solar radiation. In partly overcast to clear-sky conditions, the part of the sky representing the apparent source of solar or UV light at the surface may differ. Since most of the UV radiation at the surface is diffuse, shading elements will have a much smaller effect on UV radiation than on other parts of the solar spectrum in sunny conditions. Trees, houses or simply the walls of a ditch may considerably affect the skyview at a given surface location. Differences in skyview between different locations are therefore expected to lead to different 'source-receptor' relationships for the radiation (Oke, 1987) and thus to differing ratios between UV light an total solar radiation.

Test of the method for two locations in Europe
The method was tested for two locations in Europe outside The Netherlands. For both locations broadband UVB observations are made available via WOUDC (www.woudc.org). We selected UVB observations from Diekirch (Luxemburg; 49.87N, 6.17E) and Kishinev (Moldova; 47.0N, 28.82E) for the years 2006-2010.

At Diekirch broadband UVB irradiance is measured for wavelengths between 280 and 320 nm, using the UV-Biometer, 501A radiometer (manufacturer *Solar Light*). At Kishinev irradiance is measured for

wavelengths between 280 en 315 nm, using the UVS-B-C radiometer (manufacturer *Kipp & Zn.*) Both radiometers provide so-called CIE weighted irradiances that take into account for the erythemal action spectrum (see Figure A1.9). The total output (E_w) is given by (WMO 2006):

$$E_w = \int E(\lambda)W(\lambda)d\lambda \tag{A1.2}$$

Where λ (nm) is the wavelength, $E(\lambda)$ (W m^{-2} nm^{-1}) is the unweighted wavelength dependent irradiance and $W(\lambda)$ (-) is the wavelength dependent weighting function or so-called action spectrum. The internationally accepted CIE erythemal action spectrum weighing function reads (McKinlay and Diffey, 1987):

$$
\begin{aligned}
W(\lambda) \quad &= 1 \text{ for } 250 < \lambda \le 298 \text{ nm} \\
&= 10^{(0.094(298-\lambda))} \text{ for } 298 < \lambda \le 328 \text{ nm} \\
&= 10^{(0.015(139-\lambda))} \text{ for } 328 < \lambda \le 400 \text{ nm}
\end{aligned} \tag{A1.3}
$$

This function is illustrated in Figure A1.9 for the UVB wavelengths between 280 and 320 nm. In order to compare the results of our method with the observations, the function is applied to the clear-sky UVB irradiance values estimated in the second step of the method described above (computation of clear-sky UV radiation values). Since the weights are small for wavelengths containing most of the energy and the reverse, the difference between the unweighted and weighted integrated irradiance is large, about a factor of 20-35 over the complete UVB range.
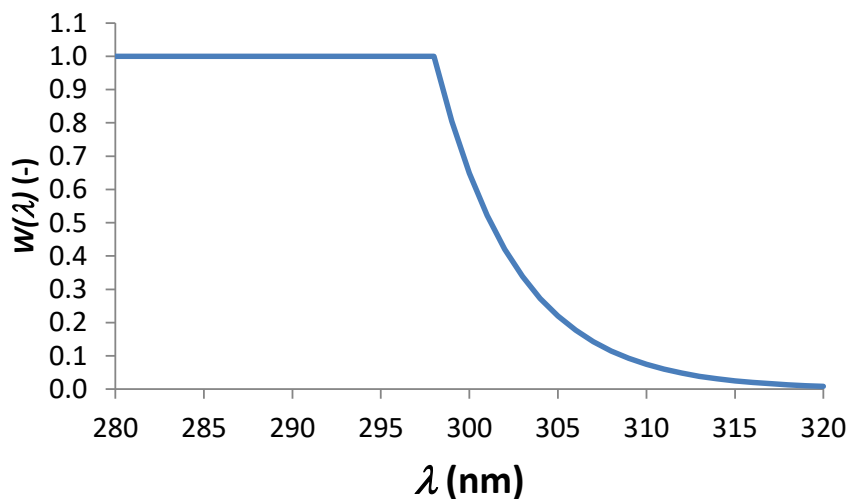
Figure A1.9 *CIE-1987 erythemal action spectrum for the UVB wavelength bands (McKinlay and Diffey, 1987).*

Total solar radiation data were obtained from the World Radiation Data Centre (WRDC, http://wrdc.mgo.rssi.ru/). For Diekirch, measurements were obtained from a nearby station in Germany (Trier; 49.75°N, 6.67°E). In the case of Kishinev, total solar radiation observations were collocated with the UVB measurements.

Figure A1.10 compares the resulting time series of the daily radiation sum for Diekirch and Kishinev with the observed CIE-weighted UVB time series. Figure A1.11 shows a scatterplot of computed versus observed radiation sums, with a regression line forced through the origin.

It can be seen that the radiation intensities for Diekirch are estimated rather well and that annual and daily variations are largely reproduced. This is confirmed in the scatterplot, which shows that there is hardly any bias (slope of the regression line is close to 1) and the explained variance is about 95% (r^2=0.9472). However, the estimates for Kishinev seem to be too low by a factor of about two (slope of the regression line is about 0.5). However, the daily to annual variability (scaled) is reproduced well (r^2=0.9505). This is rather unexpected since the average difference in daily radiation intensities is

expected to be small because the latitude of both stations is similar (around 48°N). Differences in ozone concentration are not expected to be systematic either. Indeed, ozone column thickness varies between –typically- 300 DU and 400 DU at both stations (Figure A1.7). According to WMO (2006), instrumental errors related to the response function of the instrument in combination with the applied CIE weighting function (Figure A1.9) can be quite large, up to more than a factor of two, but there is no proof that such errors would explain the difference for Kishinev here.

In this test the action spectrum given by Eq. A1.3 has been applied. For other purposes other action spectra could be applied as well. For example, the computations could be limited to smaller wavelength bands, down to the model's resolution of the wavelength spectrum. At present the model resolution is 0.1 nm. In this way, the model can be applied for the wavelength band that is actually responsible for photochemical degradation. However, because the value of p in Eq. A1.1 has been fitted to represent the erythemal action spectrum, such a weighing function could introduce a large uncertainty. The p-value in Eq. A1.1 for another weighing of the UV spectrum will likely deviate from the ones given in Table A1.1 and used here in the tests, since the scattering and absorption characteristics and therefore the cloud modification factors are highly dependent upon wavelength.

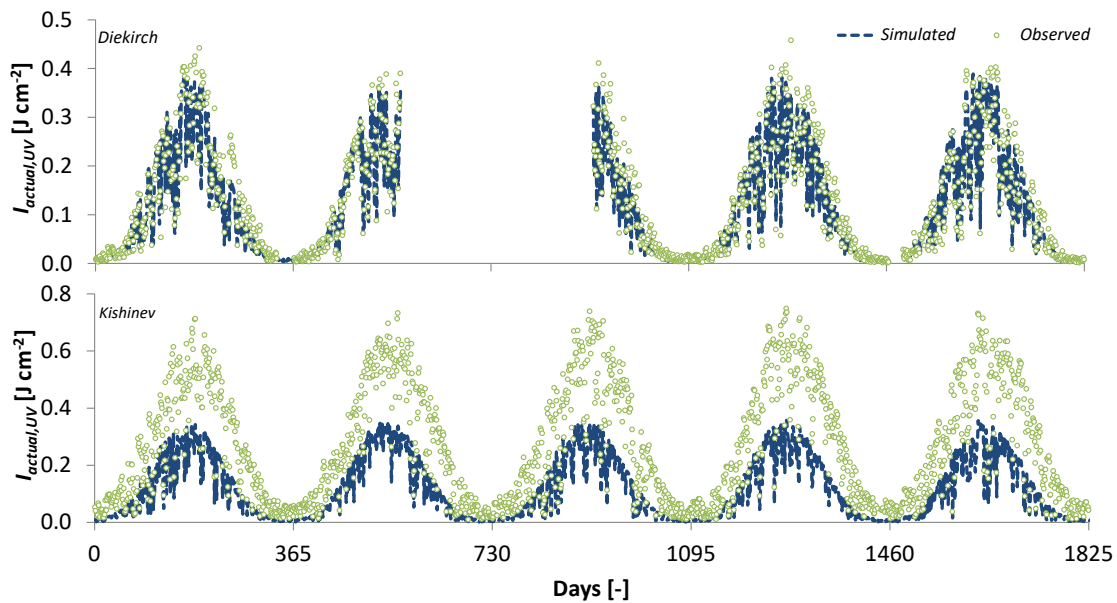**Figure A1.10** *Time series of simulated and observed daily UVB radiation sums for Diekirch (upper panel) and Kishinev (lower panel).*
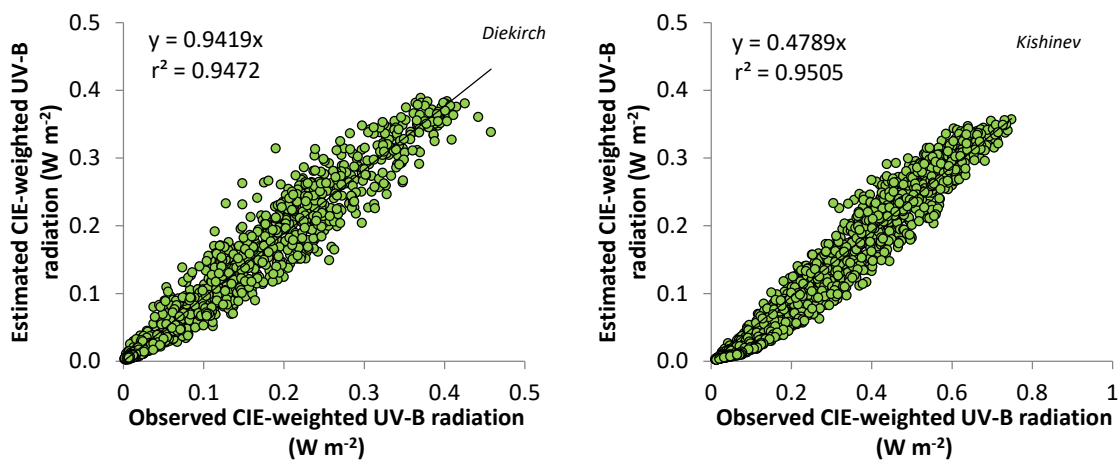

Figure A1.11 *Scatterplot of simulated versus observed daily UVB radiation sums for Diekirch (left panel) and Kishinev (right panel). The regression line has been forced through the origin. Note the difference is scale of the x-axis between the graph for Diekirch and Kishinev.*

Annex 2   ABIWAS 3.0 and GCSOLAR to calculate abiotic degradation by direct photolysis in surface waters

ABIWAS

The software program ABIWAS 3.0 calculates abiotic degradation in water (Klein J., M. Klein and M. Muller, 2019). It is the reimplementation of ABIWAS 2.0 implemented by M. Muller in 2002. In OECD 316 (2008) the program ABIWAS is mentioned "to estimate direct photolysis rates and half-life for the test chemical applicable to any types of surface waters (defined by depth and light attenuation), seasons and latitudes of interest". It can be obtained from the site of the Fraunhofer Institute in Germany:

(https://www.ime.fraunhofer.de/en/Research_Divisions/business_fields_AE_BR/Businessareas_AE/Software_E/ABIWAS.html)
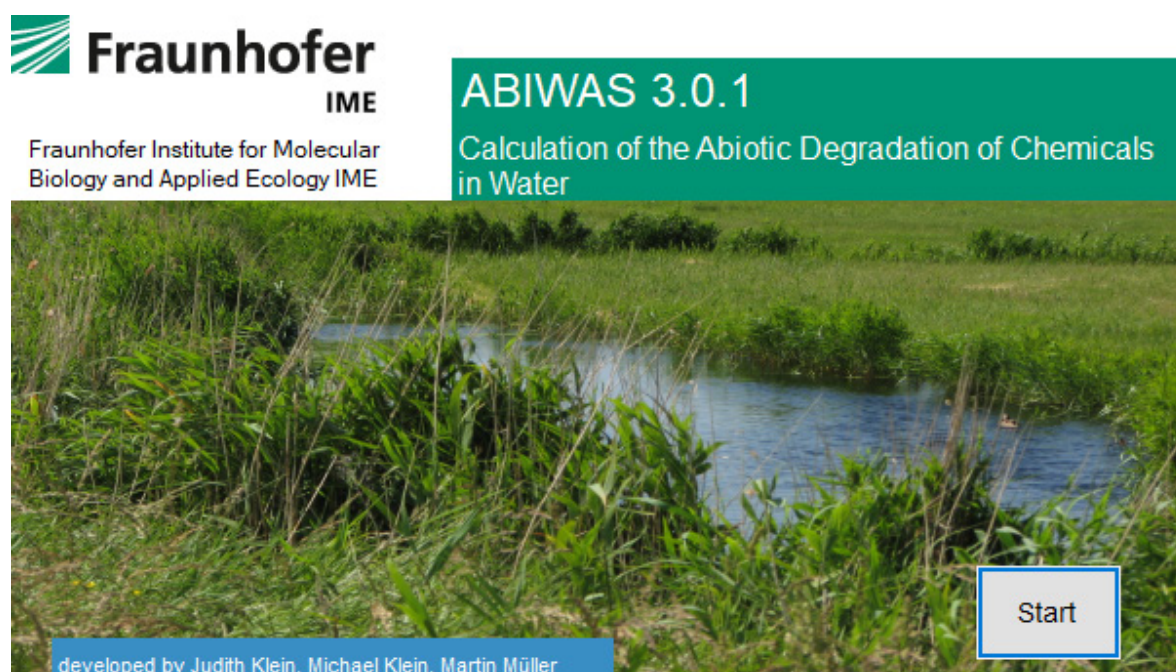
The software calculates the abiotic degradation in water based upon the concentration of the chemical in mol/L, the extinction of the chemical at wavelength and the quantum yield of substance at wave length. The input can be derived according to OECD (2008). The endpoints of the calculation are the half time values (DegT50,min, DegT50 and DegT50,max) and the corresponding photolysis rates for the 12 months of the year.

There is one standard scenario implemented, with radiation data based on central Europe (55° N). The water layer of 10 cm depth can be without absorption (extinction equal to zero) or equal to the extinction of distilled water. ABIWAS 3.0.1 allows the user to select other water depths.

GCSOLAR

GCSOLAR is a program of the United States Environmental Protection Agency, that computes direct photolysis rates and half-lives of pollutants in the aquatic environment. It is based upon the publication 'Rates of direct photolysis in aquatic environment' by R.G. Zepp and D.M. Cline in Environmental Science and Technology, 11:4, pp 359-366 (1977). Similar to ABIWAS it is mentioned

in OECD 316 (2008) "to estimate direct photolysis rates and half-life for the test chemical applicable to any types of surface waters (defined by depth and light attenuation), seasons and latitudes of interest". The July 2018 release of the GCSOLAR program differs from earlier versions of the program in that it is written in C#, whereas the previous versions were written in FORTRAN. Release notes, and a user's manual are available at the site. This version also permits the user to interact with the application using graphical user interface. It can be obtained from the site: (https://www.epa.gov/ceam/gcsolar).

HomePage — □ ×

GCSolar Options   GCSolar User Guide PDF Document

   ○ View Current Values of all the Parameters Associated with the Simulation

   ○ Modify Values of Parameters Associated with Simulations

   ◉ Compute Direct Photolysis Rates as a Function of Time-of-Day

                  [Proceed]   [Close]
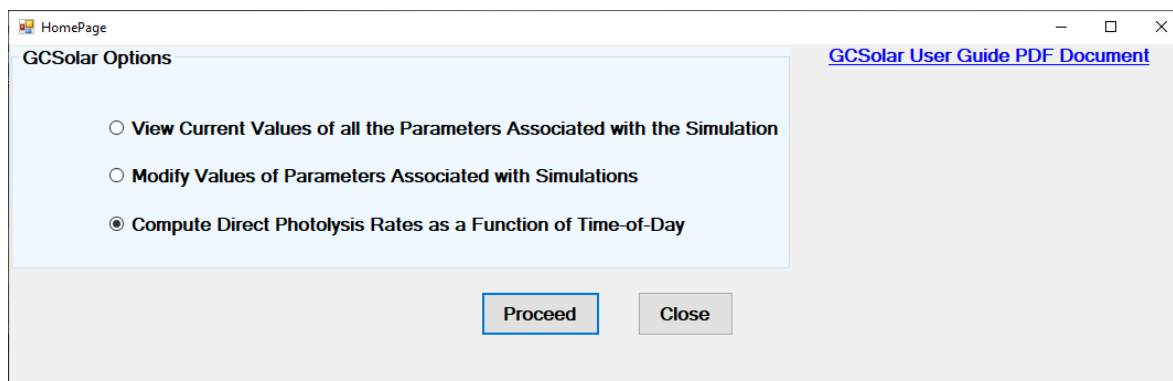
The half-lives are calculated as a function of season, latitude, time-of-day, depth in water bodies and ozone layer thickness.

There is one standard scenario implemented for methoxyclor in pure water, assuming a quantum yield of 0.32, and specifying the Water Absorption Coefficients (m**-1) and Chemical Absorption Coefficients (L(mole cm) as a function of the wavelength 297.5 to 330 nm (see Appendix I of the user's manual). The input of e.g. longitude, latitude, season, water depth, ozone layer depth and quantum yield may be changed by the user. The output consists of a plot presenting the photolysis rate (s-1) as a function of the time-of-day for the selected input.

Annex 3 Overview of used grid cells and their exact locations for the compiled radiation and cloud cover data sets of the selected locations

Section 3.3 describes the procedure and databases used to derive hourly doses for $UV_{actual,UV-VitD}$ radiation data. In this annex we document the grid cells, including their exact locations, which were used from the data bases of TEMIS and cloud cover (Table A3.1).

Table A3.1   *Overview of locations and used data bases to derive $UV_{actual,UV-VitD}$ radiation data.*

FOCUS or NL scenario / cosm	Location	Longitude (decimal notation)	Latitude (decimal notation)	TEMIS-X	TEMIS-Y	TEMIS cell centre Lon	TEMIS cell centre Lat	Cloud cover - X	Cloud cover - Y	Cloud cover cell centre X	Cloud cover cell centre Y	Cloud cover cell centre Lon	Cloud cover cell centre Lat
FOCUS D1	Lanna (S)	13.050	58.333	772	126	13.125	58.375	309	186	297029	1163844	13.001	58.320
FOCUS D2	Brimstone (UK)	-1.633	51.650	713	153	-1.625	51.625	222	251	-659971	448844	-1.572	51.654
FOCUS D3	Vredepeel (NL)	5.867	51.533	743	153	5.875	51.625	269	256	-142971	393844	5.937	51.523
FOCUS D4	Skousbo (DK)	12.083	55.617	768	137	12.125	55.625	306	214	264029	855844	12.173	55.608
FOCUS D5	La Jailliere (F)	0.967	47.450	723	170	0.875	47.375	234	295	-527971	-35156	0.967	47.467
FOCUS D6	Thiva (GR)	23.100	38.383	812	206	23.125	38.375	402	378	1320029	-948156	23.031	38.356
FOCUS R1	Weiherbach (D)	8.667	49.000	754	164	8.625	48.875	286	282	44029	107844	8.603	48.968
FOCUS R2	Porto (P)	-8.631*	41.096*	685	195	-8.625	41.125	155	348	-1396971	-618156	-8.683	41.093
FOCUS R3	Bologna (I)	11.400	44.500	765	182	11.375	44.375	307	327	275029	-387156	11.460	44.465
FOCUS R4	Roujan (F)	3.317	43.500	733	186	3.375	43.375	248	336	-373971	-486156	3.372	43.532
NL	De Bilt (NL)	5.180	52.100	740	151	5.125	52.125	264	250	-197971	459844	5.108	52.098
Cosm	Renkum (NL)	5.754	51.990	743	152	5.875	51.875	268	251	-153971	448844	5.756	52.013
Cosm	Berlijn (D)	13.283	52.493	773	150	13.375	52.375	315	245	363029	514844	13.351	52.511
Cosm	Monheim (D)	6.901	51.074	747	155	6.875	51.125	275	261	-76971	338844	6.900	51.041
Cosm	Itingen (CH)	7.785	47.467	751	170	7.875	47.375	281	297	-10971	-57156	7.854	47.486
Cosm	Columbia (MO, USA)	-92.334	38.952	350	204	-92.375	38.875	1071$	204	not applic	not applic	267.750	39.000

* coordinates of Valdares which is close to R2 scenario (coordinates -8.640, 41.183).

$ grey highlight indicates that another raster has been used (for details, see section 3.3.1).

Radiation data were compiled for the outdoor cosms for which $DegT_{50,water,photo}$ have been determined in this report, as well as for the EU FOCUS surface water scenarios and the meteorological station used in the future Dutch surface water scenarios (Tiktak et al., 2012; Boesten et al., 2018). The acronyms D and R of the FOCUS scenarios refer to drainage, respectively runoff scenarios (FOCUS, 2001).

The outdoor cosms selected for analysis in this report (see section 10.2) have been summarised in Table A3.2 below.

Table A3.2 *Compounds and cosm studies for which DegT$_{50,water,photo}$ have been obtained by inverse modelling with PEST_TOXSWA.*

Compound	Study	Location	Period of study
Metribuzin	Fairchild & Sappington, 2002	Columbia, Missouri, USA	22 May 2001[*] + 14 d
	Arts et al., 2006	Renkum, NL	6 May 2002 + 14 d
	Brock et al., 2004	Renkum, NL	5 May 1999 + 56 d
Imidacloprid	Colombo et al., 2013	Berlin, Germany	1 June-1 Aug 2009
	Bayer, 2001	Monheim, Germany	8 May 2000 + 21 d
	Bayer, 2003	Itingen, Switzerland	2 May 2001 + 91 d
Metamitron	Wendt-Rasch et al., 2004	Renkum, NL	6 April 1999 + 28 d
	Brock et al., 2004	Renkum, NL	5 May 1999 + 28 d

[*] Year not given, presumably 2001.

The TEMIS data were used to extract the clear sky, UV-vitamin D weighed daily radiation doses from hdf-files. TEMIS-X and TEMIS-Y are the cell index numbers of the used raster, in which the selected location is found. Numbering of the cells is from LeftAbove to RightBelow and <X,Y> is there <0,0> and <1339, 719> and the total raster counts 1440 to 720 cells. Cell size is 0.25 degrees in both directions, resulting in 360 * 180 degrees (with X, longitude, representing the total earth round and Y, latitude, from pole to pole). Based upon the cell index the coordinates can be calculated for the cell, the corners as well as the centre. E.g. the longitude and latitude of the Monheim cell: Lon = ((747+0.5)*0.25) − 180 = 6.875 and Lat = 90 − ((155+0.5)*0.25) = 51.125.

The cloud cover data refer to the raster used in the grib files. Cloud cover-X and Cloud cover-Y are the indices for the used points of the raster. These have been converted to the centre of the used cells, with their longitude and latitude (conversion not described here). Note that for all locations, except Columbia in the USA, the data were based upon the Copernicus climate data store, while for Columbia of the USA another data base was used (for details, see section 3.3).

Note that the time indicates in the obtained .meth and .csv files are in hours UTC (so, excluding time zones or summer time).

Annex 4 Details of the assessment of the photolytic degradation rate of metribuzin in cosm water

The main characteristics of the studies with metribuzin (cosm studies of Fairchild & Sappington (2002), Arts et al. (2006) and Brock et al. (2004) have been summarized in tables 4.1 and 4.2 in Annex 4 in Deneer et al. (2015). The tables given in the Deneer et al. (2015) are repeated in this section and where necessary data is corrected and additional data necessary for the inverse modelling approach described in this report is provided.

Table A4.1   *Data on cosm studies with metribuzin (taken from Deneer et al. 2015 and corrected).*

Label in data file	MetrCosm1	MetrCosm2	MetrCosm3
Reference	Fairchild & Sappington (2002)	Arts et al. (2006)	Brock et al. (2004)
Compound	Metribuzin (technical grade)	Metribuzin	Metribuzin
Type of system	Outdoor clay-lined pond	Outdoor ditch	Polycarbonate enclosures in outdoor ditch, outdoor (ditch, enclosure)
Dimensions system	1000 m^2, 1.5 m depth, 750 m^3 water volume	Length=40 m, bottom width=1.6-3.3 m, water depth=0.5 m, volume=55 m^3	Diameter 1.05 m, height 0.9 m, water depth 0.5 m
Side slope (hor/vert)	0	3/2	0
Depth water layer (m)	0.75 m	No measurements, M&M states 'each with a water depth of 0.5 m'	0.5
Depth sediment (cm)	-	25	25
Sediment om%	3.2 oc-5.5 om	-, (sandy loam)	-
Sediment bulk density	-	-	-
Sediment porosity	-	-	-
Macrophytes info	> 80% cov. 40 g/m2 on day -7, *Najas guadalupensis*, common water nymph or guppy grass, > 100 g/m2 day 30	Highest treatment: decrease filamentous algae from 40 to 5% coverage	*Myrophillum* (up to 75% cover), *Sagittaria sagittifolia* (<5%) and *Elodea nuttallii* (<1%) present
pH	Hourly, 8.1 ± 1.2	low conc: 7.3 – 9.7 (8.5 avg); high conc 7.4 – 9.8 (8.4 avg)	10 cm below water surface: 5.6 µg/L: 7.3 – 10.0; 56 µg/L: 7.4 – 10.2
Temperature	Hourly, 19 ± 4°C	low conc: 17.5^{o}C average, high conc: 17.3^{o}C average	Surface (presumably 10 cm below water surface), in the morning: encl. 1 (5.6 ug/L): 16.1^{o}C, encl. 8 (56 ug/L): 17.0^{o}C; average temp of 16.55^{o}C used in calculations average
Light intensity	Day 0 = May 22, turbidity 4.2 ± 2.6 NTU's	-	-
Application number	1	1	1
Application interval	-	-	-
Nominal initial application	75 µg/L	1.6 / 8.2 µg/L	5.6 (encl. 1) and 56 (encl. 8) µg/L. Other concentrations (1.8/18/180 ug/L) used in the study as well, all concentrations in duplicate, but only 2 enclosures included in the analysis
Date and timing of the applications	22 May 2001; 9:00*	2 May 2002; 9:00*	5 May 1999; 9:00*

* The exact timing of the application is unknown. 9:00 is assumed for the following reason: WENR staff performing these type of cosm experiments indicated that they usually start the dosing around 9:00 because standard after 8 hours a measurements is taken and that is preferably done near the end of a working day (i.e. 17:00).

In the table below the input values on the physico-chemical properties of metribuzin and the cosm-specific input, such as e.g. the water depth are summarized.

Table A4.2 *Parameter values used in the simulations with metribuzin (taken from Deneer et al. 2015, system dimensions added and side slope Arts et al. slightly changed).*

Cosm label	MetrCosm1	MetrCosm2	MetrCosm3
Reference	Fairchild & Sappington (2002)	Arts et al. (2006)	Brock et al. (2004)
Molar mass (g)		214.29	
Saturated vapour pressure (mPa)		0.121 (25°C)	
Solubility (mg/L)		1165 (20°C)	
Kom (estimated) (L/kg)		Kom=22, 1/n=1.08[12]	
pKa		0.99 (strong acid)	
		in our view: weak base)	
Water depth (m)	0.75	0.5	0.5
Bottom width (m)	1	1.6	1
Length (m)	1	40	1
Side slope (hor/vert, -)	0	1.5	0
Temperature ($^\circ$C)	19 (estimated by us)	17.4	16.55
Measurements in sediment	No	No	No

MetrCosm1: Fairchild & Sappington (2002)

Table 4.3 in Annex 4 in Deneer et al. (2015) gives the measured concentrations in water (in $\mu g\ L^{-1}$ and scaled concentrations) as a function of time in the cosm study of Fairchild and Sappington (2002). The values have been read by Deneer et al. (2015) from a figure in the publication and they represent the total concentration in water, as the water was not filtered before extraction. Similar to Deneer et al. (2015) the scaled concentrations[13], which are repeated in Table A4.3, are used as observations in the inverse modelling.

Table A4.3 *Scaled concentrations in water as a function of time (d) for the cosm study with metribuzin by Fairchild and Sappington (2002).*

Number	Time (hours)	Time in TOXSWA	Scaled concentration in water
1	0.25 h	0 days	1.0000
2	1 d	1	0.8184
3	2 d	2	0.8089
4	7 d	7	0.3455
5	14 d	14	0.0495

As scaled concentrations were used in the optimisation procedure, the Freundlich sorption coefficient, K_{om}, was corrected according the guidance given in Chapter 9.4. The $c_{t=0,\ geo}$ was set to the unscaled concentration at t = 0.25 h in the measured dataset (7.38E^{-2} mg L^{-1}). The corrected K_{om} value used in the optimisation was 17.86 L kg^{-1}.

The cosm of Fairchild and Sappington (2002) was inversely modelled and the agreement between measured and simulated aqueous concentrations (scaled) was optimised with the aid of the PEST, running TOXSWA many times, according to the procedures presented in Chapter 9. The $DegT_{50,photo,ref}$ and the loading in to the ditch at 22 May 2001 09:00[14] were optimised. In total 49 optimisations were

---

[12] From https://efsa.onlinelibrary.wiley.com/doi/epdf/10.2903/j.efsa.2006.88r and applying Kom=Koc/1.724

[13] The scaling method is explained in Chapter 9.4 of this report.

[14] Deneer et al. (2015) reported that the year in which the experiment was performed was unknown. Similar to Deneer et al. (2015) we presume that the experiment took place in 2001.

performed, each with its own initial values of $DegT_{50,photo,ref}$ and the loading at t=0 (mg m^{-2})[15] (varying between 0.1 and 50 d for $DegT_{50,photo,ref}$ and 50 to 3000 mg m^{-2} for the loading at t=0[16]). For all optimisations the same lower and upper parameter bounds were used: 0.1 – 100 d for the $DegT_{50,photo,ref}$ and 1.0 – 10 000 mg m^{-2} for the loading.

From the 49 optimisations, 19 fits resulted in to an unsatisfactory estimation of $DegT_{50,photo,ref}$ and the loading at t=0. All other optimisations resulted in consistent estimates of $DegT_{50,photo,ref}$ of 4.8 days with 95% confidence intervals of 2.3 – 7.3 days and consistent estimates of the loading of 799 mg m^{-2} with 95% confidence intervals of 655 - 943 mg m^{-2}.

Table A4.4 gives estimates of the optimized $DegT_{50,photo,ref}$ and loading for the optimisation with initial values of resp. 5 days and 1000 mg m^{-2}. It also specifies the value of the objective function phi (i.e. the sum of squared differences between model-generated and measured aqueous concentrations), the error percentage of the $\chi2$-test and the number of times TOXSWA has been run by PEST. Note that the $\chi2$-test is explained into more detail in section 2.3 of Deneer et al. (2015). FOCUS (2006) suggests that a minimum error percentage value of 15% is acceptable for field studies.

The error percentage of 6.8% is an acceptable value for field experiments according to FOCUS (2006), so the optimisation did pass the $\chi2$-test.

Table A4.4   *Optimisation results for one of the 30 satisfactory optimisations for the Fairchild and Sappington cosm (2002) with metribuzin.*

Initial $DegT_{50,photo,ref}$ (d)	Initial loading (mg m^{-2})	Fitted $DegT_{50,photo,ref}$ (d)	Fitted loading (mg m^{-2})	Phi (-)	Err%	TOXSWA iterations
5	1000	4.8 (2.3 – 7.3)	799 (655 - 943)	0.013	6.8%	42

The simulated concentration as function of time presented in Figure A3.1 shows a wavy pattern. This is caused by more rapid degradation due to photolysis during daytime and stagnating degradation once the sun sets and UV radiation becomes zero.

The visual agreement between scaled optimised and measured water concentrations presented in Figure A4.1 is judged to be satisfactory.

In addition the residuals are randomly scattered around zero (only after seven days, the simulation seems to be systematically too low), demonstrating that there is no clear pattern of under- or over-prediction by the TOXSWA model (Figure A4.2).

---

[15] All possible combinations of the values given in the matrix below result in 49 sets of $DegT_{50,photo,ref}$ and the loading.

$DegT_{50,photo,ref}$ (d)	0.1	0.5	1	2	5	10	50
Loading (mg m^{-2})	50	100	300	500	1000	1500	3000

[16] Although the scaled concentrations used as observations in the inverse modelling are dimensionless, they will be compared with concentrations simulated by TOXSWA which are in g m^3. The input of the pesticide loading in TOXSWA is in mg m^{-2}. To determine plausible ranges for the loading in mg m^{-2} as input for the inverse modelling a calculation needs to be done to determine the loading needed to reach a certain desired peak concentration (e.g. the measured, scaled water concentration at t=0). Suppose that the desired peak concentration in water ($c_{peak,w}$) is 1 g m^{-3} (1000 mg m^{-3}). The loading needed to reach this peak concentration is:

$$c_{peak,w} \cdot V/(w \cdot L)$$

where is V = the volume of water in the cosm (m^3), w = the width of the water surface (m) and L is the length of the cosm (m). For the study of Fairchild and Sappington (2002) where the system has a water depth of 0.75 m, a side slope of 0, a width of 1.0 m and a length of 1.0 m, the water volume, V, is 0.75 m^3 and the width of the water surface is 1.0 m. Supposing $c_{peak,w}$ is 1000 mg m^{-3} a loading of 1000·0.75/1·1 = 750 mg/m^2 is needed to reach this peak concentration in the water of the ditch.

Figure A.4.1 *Simulated and measured total concentration (dissolved+ sorbed to suspended solids, µg.L⁻¹) metribuzin in water as a function of time (d) in the cosm of Fairchild and Sappington (2002). Simulated concentration profile obtained by PEST_TOXSWA optimisation for an initial DegT$_{50,photo,ref}$ = 5 d and an initial loading of 1000 mg m⁻².*
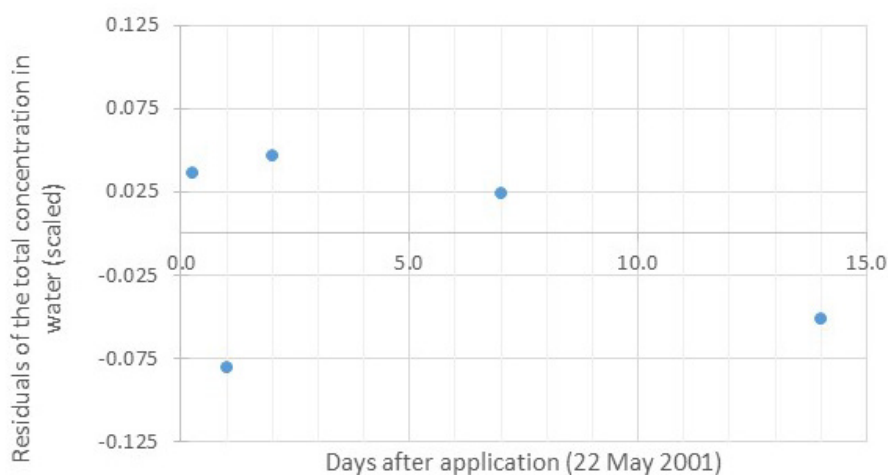

Figure A.4.2 *Residuals of total concentration (dissolved+ sorbed to suspended solids, µg.L⁻¹) metribuzin in water as a function of time (d) in the cosm of Fairchild and Sappington (2002). Simulated concentration profile obtained by PEST_TOXSWA optimisation for an initial DegT$_{50,photo,ref}$ = 5 d and an initial loading of 1000 mg m⁻².*

MetrCosm2: Arts et al. (2006)

Table 4.5 in Deneer et al. (2015) gives measured concentration in water (µg/L and scaled) as a function of time (d) for the ditch study with metribuzin by Arts et al. (2006). The raw data were provided to Deneer et al. (2015) by the author Arts of the publication and they represent the total concentration in water; i.e. the water was not filtered. Two initial nominal concentrations were used in the experiment, corresponding to 1% and 5% spray drift deposition (application rate of 0.35 kg/ha): ditches 1, 7 and 12 were treated with a nominal initial concentration of 1.6 µg/L; ditches 4, 6 and 9 were treated with a nominal initial concentration of 8.2 µg/L. To combine all data of the different treatment levels in to one optimisation, in which both *DegT$_{50,photo,ref}$* and the loading at t=0 (mg m⁻²) are optimised, some form of normalisation is required. The scaling method given in Chapter 4 of Deneer et al. (2015) (and Chapter 9.3 of this report) was applied by Deneer et al. (2015) and the resulting scaled concentrations are repeated in Table A4.5 and used as observations in the inverse modelling described here below.

For the inverse modelling the scaled concentrations are used and presented in the Table A3.4. Concentrations at time = 0 (6 May 2002 09:00) are not used as observations for the inverse modelling

as they were not measured shortly after application of the compound in the ditch, but calculated from residue measurements in the spray solution, the amounts of solution sprayed, and the estimated amount of water (55 m³).

As scaled concentrations were used in the optimisation procedure, the Freundlich sorption coefficient, K_{om}, was corrected according the guidance given in Chapter 9.4. The unscaled concentrations measured at t =0.08 (i.e. ditch 7: 1.4 µg L⁻¹; ditch 4: 7.67 µg L⁻¹; ditch 1: 1.65 µg L⁻¹; ditch 12: 1.44 µg L⁻¹; ditch 6: 6.99 µg L⁻¹; ditch 9: 7.05 µg L⁻¹) were used to calculate $c_{t=0, geo}$, resulting in a $c_{t=0, geo}$ of 3.29E⁻³ mg L⁻¹. The corrected K_{om} value used in the optimisation was 13.92 L kg⁻¹.

The ditches of Arts et al. (2006) were inversely modelled and the agreement between measured and simulated aqueous concentrations (scaled) was optimised with the aid of the PEST, running TOXSWA many times, according to the procedures presented in Chapter 9. The $DegT_{50,photo,ref}$ and the loading in to the ditch at 6 May 2002 09:00 were optimised. In total 49 optimisations were performed, each with its own initial values of $DegT_{50,photo,ref}$ and the loading at t=0 (mg m⁻²)[17] (varying between 0.1 and 50 d for $DegT_{50,photo,ref}$ and 50 to 3000 mg m⁻² for the loading at t=0[18]). For all optimisations the same lower and upper parameter bounds were used: 0.1 – 100 d for the $DegT_{50,photo,ref}$ and 1.0 – 10 000 mg m⁻² for the loading.

From the 49 optimisations, only two fits resulted in to an unsatisfactory estimation of $DegT_{50,photo,ref}$ and the loading at t=0. All other optimisations resulted in consistent estimates of $DegT_{50,photo,ref}$ of 1.29 days with 95% confidence intervals of 1.1 – 1.5 days and consistent estimates of the loading of 388 mg m⁻² with 95% confidence intervals of 361 – 415 days.

---

[17] All possible combinations of the values given in the matrix below result in 49 sets of $DegT_{50,photo,ref}$ and the loading.

$DegT_{50,photo,ref}$ (d)	0.1	0.5	1	2	5	10	50
Loading (mg m⁻²)	50	100	300	500	1000	1500	3000

Although the scaled concentrations used as observations in the inverse modelling are dimensionless, they will be compared with concentrations simulated by TOXSWA which are in g m³. The input of the pesticide loading in TOXSWA is in mg m⁻². To determine plausible ranges for the loading in mg m⁻² as input for the inverse modelling a calculation needs to be done to determine the loading needed to reach a certain desired peak concentration (e.g. the measured, scaled water concentration at t=0). Suppose that the desired peak concentration in water ($c_{peak,w}$) is 1 g m⁻³ (1000 mg m⁻³). The loading needed to reach this peak concentration is:

$$c_{peak,w} \cdot V/(w \cdot L)$$

where is V = the volume of water in the ditch (m³), w = the width of the water surface (m) and L is the length of the ditch (m). For the study of Arts et al. (2006) where the ditch has a water depth of 0.5 m, a side slope of 1.5, a bottom width of 1.6 m and a length of 40 m, the water volume, V, is 47 m³ and the width of the water surface is 3.1 m. Supposing $c_{peak,w}$ is 1000 mg m⁻³ a loading of 1000·47/3.1·40 = 379 mg/m² is needed to reach this peak concentration in the water of the ditch.

Note that the 47 m3 calculated here differs from the 55 m³ used by Arts et al. to calculate the initial concentrations. As this loading corresponds to the wished initial concentration and we optimise the initial loading anyhow, this difference does not influence our results with respect to the optimised $DegT_{50,photo,ref}$.

Table A4.5 Measured concentrations in water (scaled) as a function of time (d) for the ditch study with metribuzin by Arts et al. (2006). Values are taken from Table 4.5 in Annex 4 (p100) in Deneer et al., 2015).

Time (d)	Exact time	Time of calculated concentration in output file TOXSWA (i.e. ConSysWaLay: momentaneous total concentration in water)	Scaled concentration in water					
			Ditch 7 obs group 1	Ditch 4 obs group 2	Ditch 1 obs group 3	Ditch 12 obs group 4	Ditch 6 obs group 5	Ditch 9 obs group 6
0	06/05/2002 09:00	06-May-2002-09h00	Loading into the enclosure at this time is fitted					
0.08	06/05/2002 10:55	06-May-2002-11h00	NA	0.9808	1	0.9796	0.8321	0.8333
0.33	06/05/2002 16:55	06-May-2002-17h00	0.9396	0.8414	NA	NA	0.9107	0.7931
1	07/05/2002 09:00	07-May-2002-09h00	0.5705	0.5793	0.642	0.5306	0.6464	0.5166
3	09/05/2002 09:00	09-May-2002-09h00	0.1477	0.2276	0.2531	0.1361	0.1976	0.1277
7	13/05/2002 09:00	13-May-2002-09h00	0.0336	0.087	0.1111	0.034	0.0631	0.0307
15	21/05/2002 09:00	21-May-2002-09h00	NA	0.009	NA	NA	NA	NA

Table A4.6 gives estimates of the optimized $DegT_{50,photo,ref}$ and loading for the optimisation with initial values of resp. 1 day and 500 mg m^{-2}. It also specifies the value of the objective function phi (i.e. the sum of squared differences between model-generated and measured aqueous concentrations), the error percentage of the $\chi2$-test and the number of times TOXSWA has been run by PEST. Note that the $\chi2$-test is explained into more detail in section 2.3 of Deneer et al. (2015). FOCUS (2006) suggests that a minimum error percentage value of 15% is acceptable for field studies.

The error percentage of 13.6% is an acceptable value for field experiments according to FOCUS (2006), so the optimisation passed the $\chi2$-test.

Table A4.6 Optimisation results for one of the 47 satisfactory optimisations for the Arts et al. (2006) ditches with metribuzin

Initial $DegT_{50,photo,ref}$ (d)	Initial loading (mg m^{-2})	Fitted $DegT_{50,photo,ref}$ (d)	Fitted loading (mg m^{-2})	Phi (–)	Err%	TOXSWA iterations
1	500	1.29 (1.1 – 1.15)	388 (361 – 415)	0.16	13.6%	28

Figure A4.3 presents a satisfactory agreement between scaled optimised and measured water concentrations for all six ditches in one optimisation set, while Figure A4.4 presents the distribution of the scaled residual between model-generated and measured concentrations, as suggested by FOCUS (2006). The graph shows that the residuals are reasonably well scattered around zero, demonstrating that there is no clear pattern of under- or over-prediction by the TOXSWA model.

Figure A.4.3 *Simulated and measured total concentration (dissolved+ sorbed to suspended solids, µg.L^{-1}) metribuzin in water as a function of time (d) in the ditches of Arts et al. (2006). Simulated concentration profile obtained by PEST_TOXSWA optimisation for an initial DegT$_{50,photo,ref}$ = 1 d and an initial loading of 500 mg m^{-2}.*
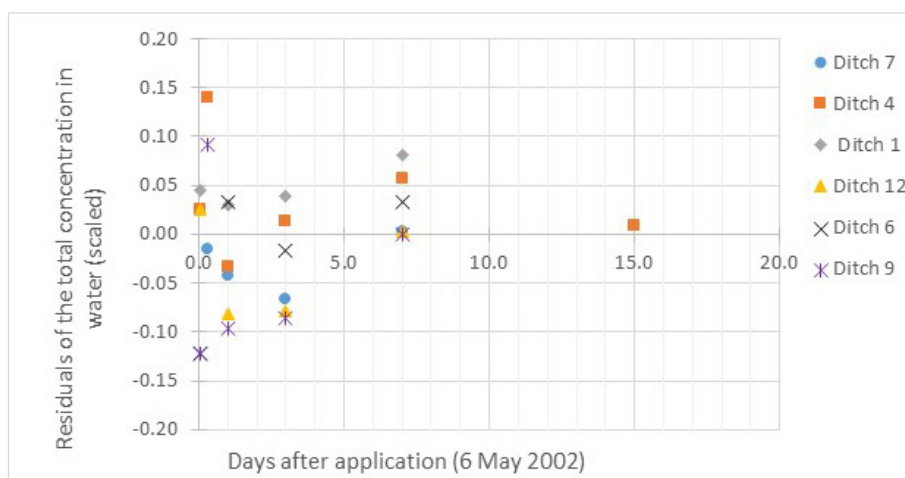
Figure A.4.4 *Residuals of total concentration (dissolved+ sorbed to suspended solids, µg.L^{-1}) metribuzin in water as a function of time (d) in the ditches of Arts et al. (2006). The residuals profile was obtained by a PEST_TOXSWA optimisation for an initial DegT$_{50,photo,ref}$ = 1 d and an initial loading of 500 mg m^{-2}.*

MetrCosm3: Brock et al. (2004)

Table 4.7 in Deneer et al. (2015) gives measured concentration in water (µg/L and scaled) as a function of time (d) for the ditch study with metribuzin by Brock et al. (2004). The raw data were provided to Deneer et al. (2015) by the authors of the publication and they represent the total concentration in water; i.e. the water was not filtered. The optimisation was done for two exposure levels: enclosures 1 and 8, treated with a nominal initial concentration of 5.6 µg/L and 56 µg/L resp.

To combine all data of the different treatment levels in to one optimisation, in which both $DegT_{50,photo,ref}$ and the loading at t=0 (mg m^{-2}) are optimised, some form of normalisation is required. The scaling method given in Chapter 4 of Deneer et al. (2015) was applied by Deneer et al. (2015) and the resulting scaled concentrations are repeated in Table A4.7 and used as observations in the inverse modelling described here.

It was assumed that application of the compound in to the cosms took place at 5 May 1999 09:00 and therefore the loading in to the cosms at 5 May 1999 09:00 was optimised.

Table A4.7   *Measured concentrations in water (scaled) as a function of time (d) for the ditch study with metribuzin by Brock et al. (2004). Values are taken from Table 4.7 in Annex 4 (p103) in Deneer et al., 2015).*

| Time (d) | Exact time | Time of calculated concentration in output file TOXSWA (i.e. ConSysWatLay: momentaneous total concentration in water) | Scaled concentration in water | |
			Enclosure 1	Enclosure 2
0	05/05/1999 09:00	05-May-1999-09h00	Loading into the enclosure at this time is fitted	
0.042	05/05/1999 10:00	05-May-1999-10h00	1.000000	1.000000
0.17	05/05/1999 13:04	05-May-1999-13h00	0.815380	0.864640
0.3	05/05/1999 16:12	05-May-1999-16h00	0.738460	0.796950
1	06/05/1999 09:00	06-May-1999-09h00	0.738460	0.790190
2	07/05/1999 09:00	07-May-1999-009h0	0.646150	0.749580
4	09/05/1999 09:00	09-May-1999-09h00	0.292310	0.538070
7	12/05/1999 09:00	12-May-1999-09h00	0.273850	0.313030
14	19/05/1999 09:00	19-May-1999-09h00	0.143080	0.099830
28	02/06/1999 09:00	02-Jun-1999-09h00	0.041540	0.021150
56	30/06/1999 09:00	30-Jun-1999-09h00	0.007690	0.001690

As scaled concentrations were used in the optimisation procedure, the Freundlich sorption coefficient, K_{om}, was corrected according the guidance given in Chapter 9.4. The $c_{t=0, geo}$ was calculated using the unscaled concentrations at t = 0.04 in the measured dataset (6.5 and 59.1 µg L^{-1} for respectively enclosure 1 and enclosure 2). This resulted in a $c_{t=0, geo}$ of 0.0196 mg L^{-1}.The corrected K_{om} value used in the optimisation was 16.06 L kg^{-1}.

The enclosures of Brock et al. (2004) were inversely modelled and the agreement between measured and simulated aqueous concentrations (scaled) was optimised with the aid of the PEST, running TOXSWA many times, according to the procedures presented Chapters 7 and 9.

In total 49 optimisations were performed, each with its own initial values of $DegT_{50,photo,ref}$ and the loading at t=0 (mg m^{-2})[19] (varying between 0.1 and 50 d for $DegT_{50,photo,ref}$ and 50 to 3000 mg m^{-2} for the loading at t=0[20]). For all optimisations the same lower and upper parameter bounds were used: 0.1 – 100 d for the $DegT_{50,photo,ref}$ and 1.0 – 10 000 mg m^{-2} for the loading.

From the 49 optimisations, 9 fits resulted in to an unsatisfactory estimation of $DegT_{50,photo,ref}$ and the loading at t=0. All other optimisations resulted in consistent estimates of $DegT_{50,photo,ref}$ of 3.4 days with 95% confidence intervals of 2.7 – 4.1 days and consistent estimates of the loading of 468 mg m^{-2} with 95% confidence intervals of 439 - 498 days.

Table A4.8 gives estimates of the optimized $DegT_{50,photo,ref}$ and loading for the optimisation with initial values of resp. 5 day and 500 mg m^{-2}. It also specifies the value of the objective function phi (i.e. the sum of squared differences between model-generated and measured aqueous concentrations), the error percentage of the $\chi2$-test and the number of times TOXSWA has been run by PEST. Note that the $\chi2$-test is explained into more detail in section 2.3 of Deneer et al. (2015). FOCUS (2006) suggests that a minimum error percentage value of 15% is acceptable for field studies. The error percentage of 10.6% is an acceptable value for field experiments according to FOCUS (2006), so the optimisation passed the $\chi2$-test.

Table A4.8 *Optimisation results for one of the 40 satisfactory optimisations for the Brock et al. (2004) ditches with metribuzin.*

Initial $DegT_{50,photo,ref}$ (d)	Initial loading (mg m^{-2})	Fitted $DegT_{50,photo,ref}$ (d)	Fitted loading (mg m^{-2})	Phi (-)	Err%	TOXSWA iterations
5	500	3.4 (2.7 – 4.1)	468 (439 - 498)	0.073	10.4%	32

Figure A4.5 presents the agreement between scaled optimised and measured water concentrations for the two enclosures in one optimisation set. Figure A.4.6 presents the distribution of the scaled residual between model-generated and measured concentrations, as suggested by FOCUS (2006). The graph shows that the residuals are reasonably well scattered around zero, demonstrating that there seems to be no clear pattern of under- or over-prediction by the TOXSWA model.

---

[19] All possible combinations of the values given in the matrix below result in 49 sets of $DegT_{50,photo,ref}$ and the loading.

$DegT_{50,photo,ref}$ (d)	0.1	0.5	1	2	5	10	50
Loading (mg m^{-2})	50	100	300	500	1000	1500	3000

[20] Although the scaled concentrations used as observations in the inverse modelling are dimensionless, they will be compared with concentrations simulated by TOXSWA which are in g m^3. The input of the pesticide loading in TOXSWA is in mg m^{-2}. To determine plausible ranges for the loading in mg m^{-2} as input for the inverse modelling a calculation needs to be done to determine the loading needed to reach a certain desired peak concentration (e.g. the measured, scaled water concentration at t=0). Suppose that the desired peak concentration in water ($c_{peak,w}$) is 1 g m^{-3} (1000 mg m^{-3}). The loading needed to reach this peak concentration is:

$$c_{peak,w} \cdot V/(w \cdot L)$$

where is V = the volume of water in the enclosure (m^3), w = the width of the water surface (m) and L is the length of the enclosure (m). For the study of Brock et al. (2004) where the enclosure has a water depth of 0.5 m, a width of 1.0 m, a side slope of 0 and a length of 1 m, the water volume, V, is 0.5 m^3. Supposing $c_{peak,w}$ is 1000 mg m^{-3} a loading of 1000·0.5/1.0·1.0 = 500 mg/m^2 is needed to reach this peak concentration in the water of the enclosure. We assumed that the enclosures were square in our calculations above, although the cosm was round. So, the calculated loading is not correct. However, this does not influence the outcome of the $DegT_{50,photo,ref}$ as (i) the loading corresponds to the wished initial concentration and (ii) it is optimised in our procedure.
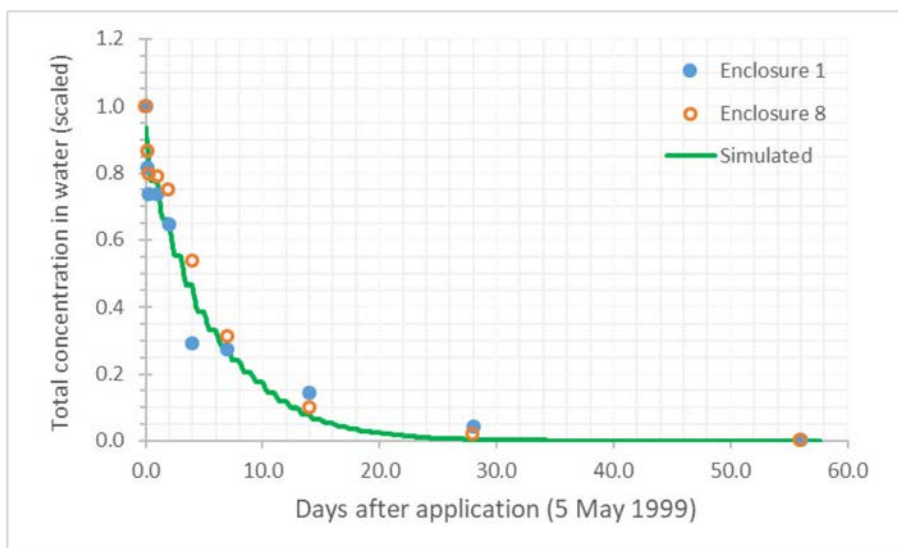
Figure A.4.5 *Simulated and measured total concentration (dissolved+ sorbed to suspended solids, µg.L^{-1}) metribuzin in water as a function of time (d) in the enclosures of Brock et al. (2004). Simulated concentration profile obtained by PEST_TOXSWA optimisation for an initial DegT$_{50,photo,ref}$ = 5 d and an initial loading of 500 mg m^{-2}.*
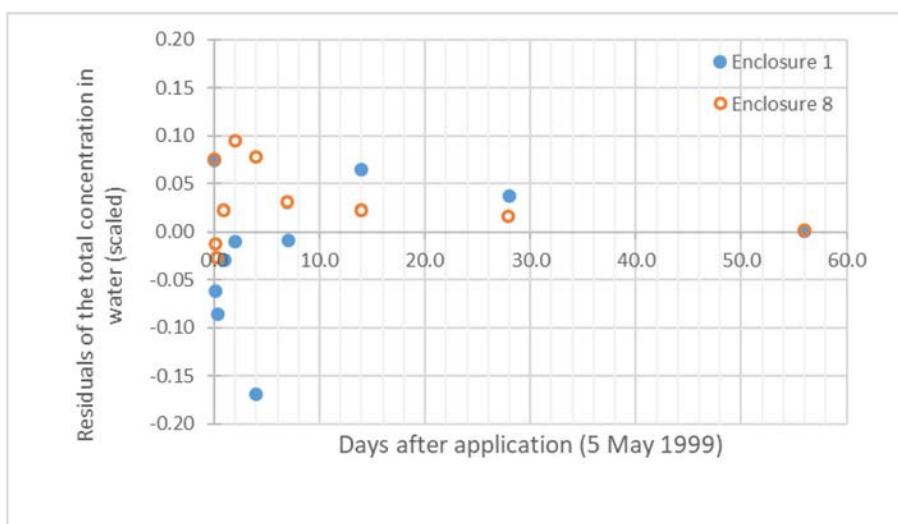

Figure A.4.6 *Residuals of total concentration (dissolved+ sorbed to suspended solids, µg.L^{-1}) metribuzin in water as a function of time (d) in the enclosures of Brock et al. (2004). The residuals profile was obtained by a PEST_TOXSWA optimisation for an initial DegT$_{50,photo,ref}$ = 5 d and an initial loading of 500 mg m^{-2}.*

Annex 5   Details of the assessment of the photolytic degradation rate of imidacloprid in cosm water

The main characteristics of the studies with imidacloprid (cosm studies of Colombo et al. (2013), Bayer (2001) and Bayer (2003) have been summarized in tables 6.1 and 6.2 of Annex 6 in Deneer et al. (2015). The tables given in the Deneer et al. (2015) are repeated in this section and where necessary additional data needed for the inverse modelling approach described in this report is provided.

Table A5.1   *Data on cosm studies with imidacloprid (taken from Deneer et al. 2015).*

Label in data file	ImiCosm1	ImiCosm2	ImiCosm3
Reference	Colombo et al. (2013)	Bayer (2001)	Bayer (2003)
Compound	Imidacloprid (type of material not specified)	Imidacloprid (type of material not specified)	Imidacloprid SL200 formulation, 17.3% w/w imidacloprid
Type of system	Polypropylene containers in outdoor pond	A circular pond and a rectangular tank, both outdoor	13 circular ponds
Dimensions system	45.5 x 30 x 21 cm (20 Liters total volume, 15 L of water, 0.55 cm sediment)	Diameter 2.0 m (water depth 1.0 m) and 0.6 x 1.8 m (water depth 0.3 m)	Water depth 1.0 m, 3100 L (3.1 m^2) or (ponds 11 and 13) 3800 L (3.8 m^2)
Side slope (hor/vert)	0	0	0
Depth water layer	Calculated: 45.5 x 30 cm, 15 Liters of water --> 11.0 cm	Pond 1.0 m, tank 0.3 m (calculations for merged data set used 0.65 m)	All ponds 1.0 m
Depth sediment	0.55 cm	pond: 12 – 15 cm, tank: 12 cm; sediment contained in trays on bottom of pond/tank	10 cm
Sediment om%	3% om silt and clay loam	4.1% oc --> 7.05% om	3.4% oc --> 5.9% om
Sediment bulk density	-	-	
Sediment porosity	-	-	
Macrophytes info	None, no turbidity, no colored substances	Pond coverage 30%, tank coverage 60%	*Lemna* were removed regularly, other macrophytes not mentioned and assumed absent
pH	8-9	7.0 – 8.5, slight increase over time	pH increased from aprox. 7.4 on day 0 – 13 to approx. 9.5 (average value on day 35) and then decreased to approx. 7.4 (average value on day 91). Values taken from Figure 91.
Temperature	10 (night) – 24 (day), average value not given	Average air temp in May estimated: 16.7°C	Average water temp days 0 – 191 estimated from graph: 19°C
Light intensity	High levels, UVB 2.35/2.78/2.75 µW/cm^2 average after each pulse	No changes in turbidity were observed	Sunny weather on days of application, daily sun hours given
Application number	3	1	2: May 02 and May 23, 2001
Application interval	7 days	-	21 days
Nominal initial application	17.3 µg/L (other conc not monitored often enough)	6.0 µg/L	23.5 and 9.3 µg/L (ponds with initial nominal 3.8, 1.5 and 0.6 ug/L not used for estimation of DegT$_{50,photo}$)
Date and timing of the applications	2 June 2009; 11:00	8 May 2000; 9:00*	2 May 2001; 9:00*

* The exact timing of the application is unknown. 9:00 h is assumed for the following reason: WENR staff performing these type of cosm experiments indicated that they usually start the dosing around 9:00 h, because standardly after 8 hours a measurements is taken and that is preferably done near the end of a working day (i.e. 17:00 h).

In Table A5.2 the input values on the physico-chemical properties of imidacloprid and the cosm-specific input, such as e.g. the water depth are summarized.

Table A5.2   *Parameter values used in the simulations with imidacloprid (taken from Deneer et al. 2015, system dimensions added).*

Cosm label	ImiCosm1	ImiCosm2	ImiCosm3
Reference	Colombo et al. (2013)	Bayer (2001)	Bayer (2003)
Molar mass (g)	255.66		
Saturated vapour pressure (mPa)	4.0 E-7 (25˚C)		
Solubility (mg/L)	610 (20˚C)		
Kom (estimated) (L/kg)	Kom = 132, 1/n = 0.802[21]		
pKa	n.a.		
Water depth (m)	0.11	pond 1.0 and tank 0.30	1.0
Bottom width (m)	1	1	1
Length (m)	1	1	1
Side slope (hor/vert, -)	0	0	0
Temperature (˚C)	17°C (average of 10 and 24)[22]	16.7°C (average air temp in May)	19°C (average water temp over 191 days, estimated from graph)
Measurements in sediment	No, only a single measurement at end of experiment	No, only a single measurement at end of experiment	Yes, but not used in present analysis

ImiCosm1: Colombo et al. (2013)

Table 6.3 in Annex 6 in Deneer et al. (2015) gives the measured concentrations in water as a function of time in the outdoor containers in the study of Colombo et al. (2013). The values have been read by Deneer et al. (2015) from a figure in the publication. The exact timing of the loadings however was not given in the publication but necessary for the inverse modelling in this report. Therefore the authors of the publication were contacted and the student report (Colombo, 2009) which was the basis for the publication was kindly provided by Silvia Mohr from the UBA.

Table A5.3 gives measured concentrations in water (µg/L and scaled) as a function of time (d) in the microcosms spiked with 17.3 µg L^{-1} of the study with imidacloprid by Colombo et al. (2013). The values are averages for 7 replicates, values for single systems are not reported; they represent the total concentration in water (incl. suspended solids), as the water was not filtered before extraction.

Loadings of the second and third application were calculated assuming that the three treatments consisted of dosing with equal concentrations of imidacloprid, which corresponded to 17.3 µg/L (volume is 15 Litres of water, i.e. 15 * 17.3 µg = 260 µg were dosed. Area of container: 45.5 x 30 cm = 1365 cm^2; loading = 260 / 1365 µg/cm^2 or 1.89 mg/m^2). The scaled loading was calculated to be 1.89*1000/17.3 = 109.88 mg m^{-2} for both the second and the third application.

---

[21] From https://efsa.onlinelibrary.wiley.com/doi/epdf/10.2903/j.efsa.2008.148r

[22] The student report (Colombo, 2009) containing all raw data of the experiment including a graph of the daytime air temperatures during the experiment shows that an estimate of 17 °C is justified.

Table A5.3 *Measured concentrations in water (µg L⁻¹ and scaled) as a function of time (d) for the study with imidacloprid by Colombo et al. (2013). Values are taken from the student report (Colombo, 2009) which was the basis for the publication of Colombo et al. (2013) and which was kindly provided by Silvia Mohr from the UBA.*

Time (d)	Exact time	Concentration in water (µg L⁻¹)	scaled concentrations	
0	02/06/2009 11:00	17.3000	1.000000	nominal concentration
0.25	02/06/2009 17:00	9.0800	0.524855	
1	03/06/2009 11:00	7.9600	0.460116	
2	04/06/2009 11:00	4.4500	0.257225	
3	05/06/2009 11:00	2.8700	0.165896	
6.917	09/06/2009 09:00	1.0300	0.059538	
7	09/06/2009 11:00	17.3000	1.000000	nominal concentration
8	10/06/2009 11:00	10.8000	0.624277	
9	11/06/2009 11:00	6.6800	0.386127	
10	12/06/2009 11:00	4.1700	0.241040	
13.917	16/06/2009 09:00	1.8000	0.104046	
14	16/06/2009 11:00	17.3000	1.000000	nominal concentration
14.25	16/06/2009 17:00	9.5800	0.553757	
15	17/06/2009 11:00	9.6400	0.557225	
16	18/06/2009 11:00	5.6100	0.324277	
17	19/06/2009 11:00	4.6700	0.269942	
24	26/06/2009 11:00	2.92	0.168786	

As scaled concentrations were used in the optimisation procedure, the Freundlich sorption coefficient, K_{om}, was corrected according the guidance given in Chapter 9.4. The $c_{t=0, geo}$ was set to the unscaled concentration at t = 0 in the measured dataset (see Table A5.3). The corrected K_{om} value used in the optimisation was 294.74 L kg⁻¹.

The containers of Colombo et al. (2013) were inversely modelled and the agreement between measured and simulated aqueous concentrations (scaled) was optimised with the aid of the PEST, running TOXSWA many times, according to the procedures presented in Chapter 9. Note, that contrary to the other fits in this report, the scaled concentrations at t=0, 7 and 14 days used as observations in the inverse modelling are based on the nominal concentrations (and not on the concentration of the first measurement after the dosing). This was done because the time between the dosing and the first measurement was quite long, six hours; the period in which most of the photolytic degradation occurs.

In total 49 optimisations were performed, each with its own initial values of $DegT_{50,photo,ref}$ and the loading at t=0 (mg m⁻²)[23] (varying between 0.1 and 50 d for $DegT_{50,photo,ref}$ and 50 to 3000 mg m⁻² for the loading at t=0). For all optimisations the same lower and upper parameter bounds were used: 0.1 – 100 d for the $DegT_{50,photo,ref}$ and 1.0 – 10 000 mg m⁻² for the loading.

All 49 optimisations resulted in consistent estimates of $DegT_{50,photo,ref}$ of 1.6 days with 95% confidence intervals of 1.3 – 1.9 days and consistent estimates of the loading of 101.7 mg m⁻² with 95% confidence intervals of 86.3 – 116.1 mg m⁻².

Table A5.4 gives estimates of the optimized $DegT_{50,photo,ref}$ and loading for the optimisation with initial values of resp. 2 days and 100 mg m⁻². It also specifies the value of the objective function phi (i.e. the sum of squared differences between model-generated and measured aqueous concentrations), the error percentage of the $\chi2$-test and the number of times TOXSWA has been run by PEST. Note that the $\chi2$-test is explained into more detail in section 2.3 of Deneer et al. (2015). FOCUS (2006) suggests that a minimum error percentage value of 15% is acceptable for field studies.

---

[23] All possible combinations of the values given in the matrix below result in 49 sets of $DegT_{50,photo,ref}$ and the loading.

$DegT_{50,photo,ref}$ (d)	0.1	0.5	1	2	5	10	50
Loading (mg m⁻²)	50	100	300	500	1000	1500	3000

The error percentage of 14.2% is an acceptable value for field experiments according to FOCUS (2006), so the optimisation passed the $\chi2$-test.

Table A5.4 *Optimisation results for one of the 49 satisfactory optimisations (out of 49) for the containers of Colombo et al. (2013) for imidacloprid.*

Initial $DegT_{50,photo,ref}$ (d)	Initial loading (mg m^{-2})	Fitted $DegT_{50,photo,ref}$ (d)	Fitted loading (mg m^{-2})	Phi (-)	Err%	TOXSWA iterations
2	100	1.6 (1.3 – 1.9)	101.7 (86.3 – 116.1)	0.1	14.2%	19

Figure A5.1 presents the agreement between optimised and measured scaled water concentrations for one optimisation, while Figure A5.2 presents the distribution of the scaled residuals between model-generated and measured concentrations, as suggested by FOCUS (2006). The graph shows that the residuals are randomly scattered around zero, demonstrating that there is no pattern of under- or over-prediction by the TOXSWA model.
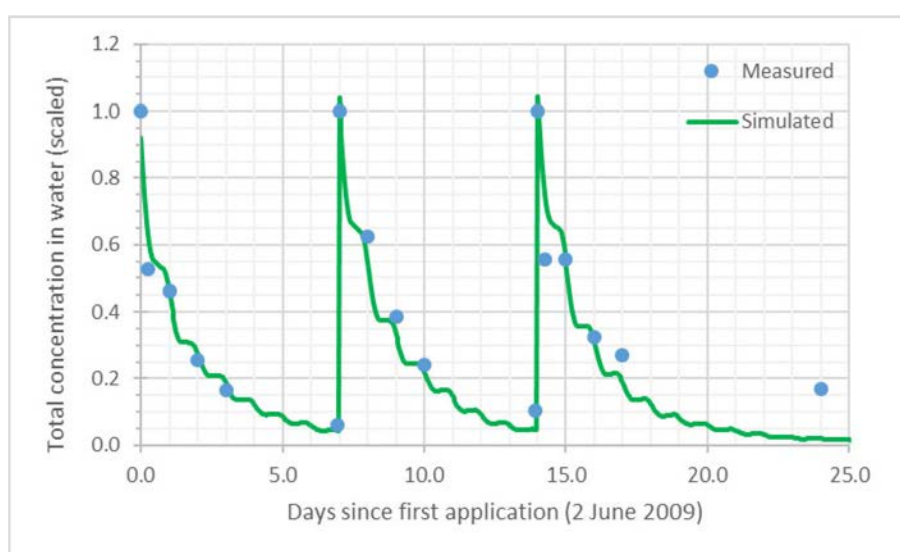

Figure A5.1 *Simulated and measured total concentration (dissolved+ sorbed to suspended solids) imidacloprid in water as a function of time in the containers of Colombo et al. (2013). The simulated concentration profile was obtained by a PEST_TOXSWA optimisation for an initial DegT$_{50,photo,ref}$ = 2 d and an initial loading of 100 mg m^{-2}.*
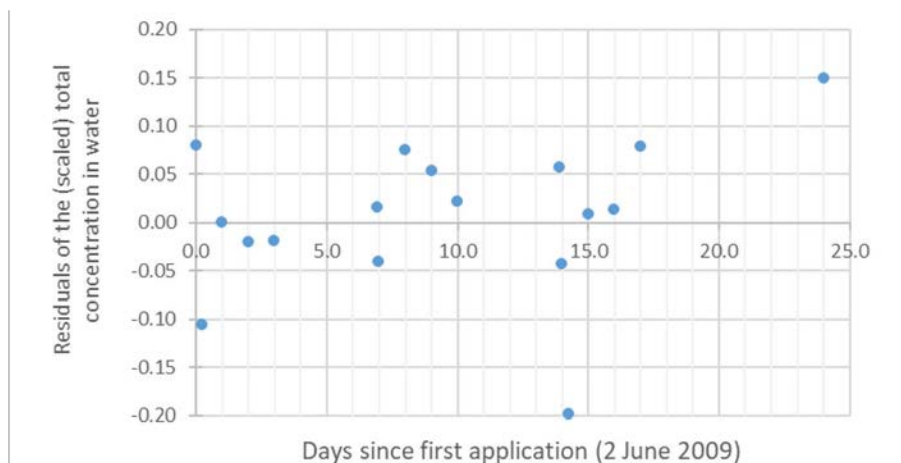
Figure A5.2 *Residuals of total concentration (dissolved+ sorbed to suspended solids) imidacloprid in water as a function of time in the containers of Colombo et al. (2013). The simulated concentration profile was obtained by a PEST_TOXSWA optimisation for an initial DegT$_{50,photo,ref}$ = 2 d and an initial loading of 100 mg m^{-2}.*

ImiCosm2: Bayer (2001)

Table 6.5 in Deneer et al. (2015) gives measured concentrations in water (μg/L and scaled) as a function of time (d) in a pond and a tank system for the study with imidacloprid by Bayer (2001). According to Deneer et al. (2015) no mention is made of filtering the sampled water before extraction, so, it was assumed that the total concentration including suspended solids was measured. Both the pond and the tank were treated at 6.0 μg/L nominal initial concentration.

As in the other optimisations normalisation of the measured aqueous concentrations was done. The scaling method given in Chapter 4 of Deneer et al. (2015) was applied by Deneer et al. (2015) and the resulting scaled concentrations are repeated in Table A5.5 and used as observations in the inverse modelling described here.

It was assumed that application of the compound in to the cosms took place at 8 May 2000 09:00 h and therefore the loading in to the systems at 8 May 2000 09:00 h was optimised.

Table A5.5 *Measured concentrations in water (scaled) as a function of time (d) for the study with imidacloprid by Bayer (2001). Values are taken from Table 6.5 in Annex 6 (p121) in Deneer et al., 2015).*

Time (d)	Exact time	Time of calculated concentration in output file TOXSWA (i.e. ConSysWatLay: momentaneous total concentration in water)	Scaled concentration in water	
			Pond	Tank
0	08/05/2000 09:00	08-May-2000-09h00	Loading into the enclosure at this time is fitted	
0.16	08/05/2000 12:50	08-May-2000-13h00	0.7209	1
1	09/05/2000 09:00	09-May-2000-09h00	1	0.7857
2	10/05/2000 09:00	10-May-2000-09h00	0.8372	0.6607
4	12/05/2000 09:00	12-May-2000-09h00	0.6279	0.4643
7	15/05/2000 09:00	15-May-2000-09h00	0.4883	0.375
11	19/05/2000 09:00	19-May-2000-09h00		0.2679
14	22/05/2000 09:00	22-May-2000-09h00	0.3023	0.2143
21	29/05/2000 09:00	29-May-2000-09h00	0.2093	1.25E-01

As scaled concentrations were used in the optimisation procedure, the Freundlich sorption coefficient, K_{om}, was corrected according the guidance given in Chapter 9.4. The $c_{t=0, geo}$ was set to the unscaled concentration at t = 1 in the measured dataset of the pond (4.3 μg L^{-1}; note that this is the first

measurement used in the optimisation, as the measurement at t = 0.16 was considered to be an outlier and omitted) and to the unscaled concentration at t = 0.16 in the measured dataset of the tank (5.6 µg L^{-1}). The corrected K_{om} value used in the optimisation were 388.28 and 368.5 L kg^{-1} for respectively the pond and the tank.

The pond and tank of Bayer (2001) were inversely modelled and the agreement between measured and simulated aqueous concentrations (scaled) was optimised with the aid of the PEST, running TOXSWA many times, according to the procedures presented in Chapter 9.

The pond and tank data were analysed separately i.e. inverse modelling was separately done for the two systems. For the pond system the first measurement (Table A5.5) was omitted. As explained by Deneer et al. (2015) it was indicated by the authors that this first measured concentration was probably low due to insufficient mixing of the aqueous phase during the first few hours after application.

In total 49 optimisations were performed, each with its own initial values of $DegT_{50,photo,ref}$ and the loading at t=0 (mg m^{-2})[24] (varying between 0.1 and 50 d for $DegT_{50,photo,ref}$ and 50 to 3000 mg m^{-2} for the loading at t=0[25]). For all optimisations the same lower and upper parameter bounds were used: 0.1 – 100 d for the $DegT_{50,photo,ref}$ and 1.0 – 10 000 mg m^{-2} for the loading.

Results pond system

For the pond system 15 fits from the 49 optimisations resulted in an unsatisfactory estimation of $DegT_{50,photo,ref}$ and the loading at t=0. All other optimisations resulted in consistent estimates of $DegT_{50,photo,ref}$ of 8.1 days with 95% confidence intervals of 5.9 – 10.2 days and consistent estimated of the loading of 1042 mg m^{-2} with 95% confidence intervals of 919 – 1164 mg m^{-2}.

Table A5.6 gives estimates of the optimized $DegT_{50,photo,ref}$ and loading for the optimisation with initial values of resp. 10 day and 1000 mg m^{-2}. It also specifies the value of the objective function phi (i.e. the sum of squared differences between model-generated and measured aqueous concentrations), the error percentage of the $\chi 2$-test and the number of times TOXSWA has been run by PEST. Note that the $\chi 2$-test is explained into more detail in section 2.3 of Deneer et al. (2015). FOCUS (2006) suggests that a minimum error percentage value of 15% is acceptable for field studies.

The error percentage of 6.5% is an acceptable value for field experiments according to FOCUS (2006), so the optimisation passed the $\chi 2$-test.

Table A5.6 *Optimisation results for one of the 34 satisfactory optimisations (out of 49) for the pond data of Bayer (2001) for imidacloprid.*

Initial $DegT_{50,photo,ref}$ (d)	Initial loading (mg m^{-2})	Fitted $DegT_{50,photo,ref}$ (d)	Fitted loading (mg m^{-2})	Phi (-)	Err%	TOXSWA iterations
10	1000	8.1 (5.9 – 10.2)	1042 (919 - 1164)	0.014	6.5%	32

---

[24] All possible combinations of the values given in the matrix below result in 49 sets of $DegT_{50,photo,ref}$ and the loading.

$DegT_{50,photo,ref}$ (d)	0.1	0.5	1	2	5	10	50
Loading (mg m^{-2})	50	100	300	500	1000	1500	3000

[25] Although the scaled concentrations used as observations in the inverse modelling are dimensionless, they will be compared with concentrations simulated by TOXSWA which are in g m^3. The input of the pesticide loading in TOXSWA is in mg m^{-2}. To determine plausible ranges for the loading in mg m^{-2} as input for the inverse modelling a calculation needs to be done to determine the loading needed to reach a certain desired peak concentration (e.g. the measured, scaled water concentration at t=0). Suppose that the desired peak concentration in water ($c_{peak,w}$) is 1 g m^{-3} (1000 mg m^{-3}). The loading needed to reach this peak concentration is:

$$c_{peak,w} \cdot V/(w \cdot L)$$

where is V = the volume of water in the merged system (m^3), w = the width of the water surface (m) and L is the length of the system (m). For the study of Bayer (2001) where the (average) water depth of the merged system is assumed to be 0.65 m, a width of 1.0 m, a side slope of 0 and a length of 1 m, the water volume, V, is 0.65 m^3. Supposing $c_{peak,w}$ is 1000 mg m^{-3} a loading of 1000·0.65/1.0·1.0 = 650 mg/m^2 is needed to reach this peak concentration in the water of the enclosure.

Figure A5.3. presents a satisfactory agreement between optimised and measured scaled water concentrations for one optimisation, excluding the first measurement that was too low, as concluded by Deneer et al. (2015). The graph of the residuals in Figure A.5.4. confirms that the agreement is sufficient as the residues are neatly scattered around zero (although there is aslight wave-type pattern). This leads to the conclusion that there is no clear pattern of under- or overprediction by the TOXSWA model.
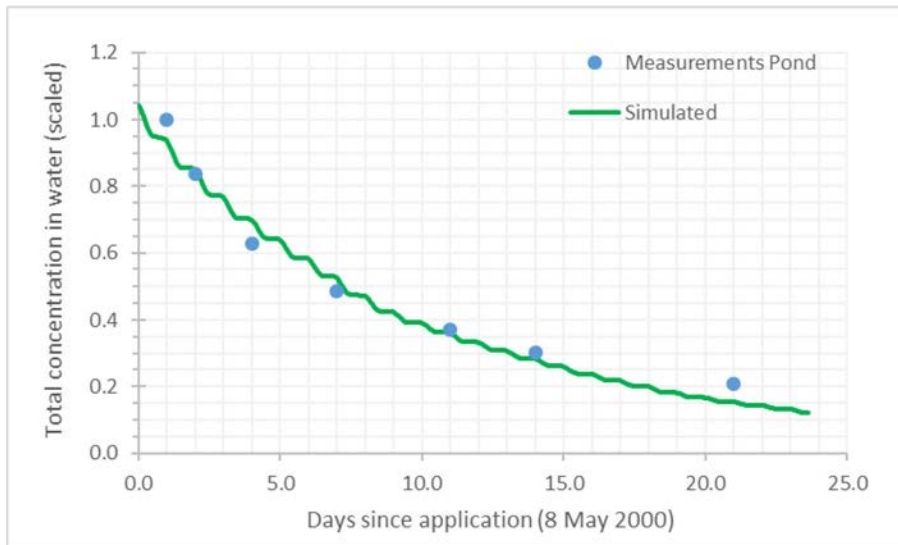

Figure A5.3 *Simulated and measured total concentration (dissolved+ sorbed to suspended solids) imidacloprid in water as a function of time in the pond of Bayer (2001). The simulated concentration profile was obtained by a PEST_TOXSWA optimisation for an initial DegT$_{50,photo,ref}$ = 10 d and an initial loading of 1000 mg m^{-2} and excluding the first measurement at t=0.16 d.*
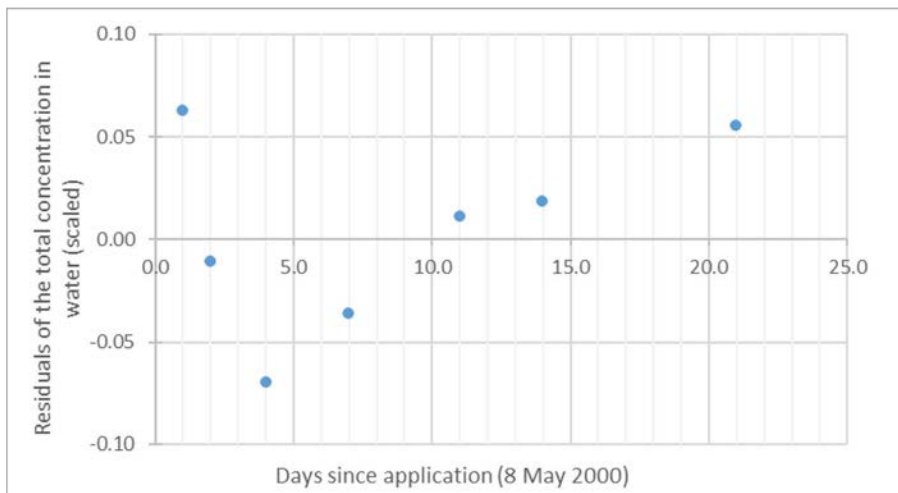

Figure A5.4 *Residuals of total concentration (dissolved+ sorbed to suspended solids) imidacloprid in water as a function of time in the pond of Bayer (2001). The simulated concentration profile was obtained by a PEST_TOXSWA optimisation for an initial DegT$_{50,photo,ref}$ = 10 d and an initial loading of 1000 mg m^{-2} and excluding the first measurement at t=0.16 d.*

Results tank system

For the tank system 12 fits from the 49 optimisations resulted in to an unsatisfactory estimation of DegT$_{50,photo,ref}$ and the loading at t=0. All other optimisations resulted in consistent estimates of DegT$_{50,photo,ref}$ of 6.5 days with 95% confidence intervals of 4.5 – 8.4 days and consistent estimated of the loading of 290 mg m^{-2} with 95% confidence intervals of 259 - 321 mg m^{-2}.

Table A5.7 gives estimates of the optimized $DegT_{50,photo,ref}$ and loading for the optimisation with initial values of resp. 5 days and 300 mg m^{-2}. It also specifies the value of the objective function phi (i.e. the sum of squared differences between model-generated and measured aqueous concentrations), the error percentage of the $\chi2$-test and the number of times TOXSWA has been run by PEST. Note that the $\chi2$-test is explained into more detail in section 2.3 of Deneer et al. (2015). FOCUS (2006) suggests that a minimum error percentage value of 15% is acceptable for field studies.

The error percentage of 7.7% is an acceptable value for field experiments according to FOCUS (2006), so the optimisation passed the $\chi2$-test.

Table A5.7 *Optimisation results for one of the 39 satisfactory optimisations (out of 49) for the tank data of Bayer (2001) for imidacloprid.*

Initial $DegT_{50,photo,ref}$ (d)	Initial loading (mg m^{-2})	Fitted $DegT_{50,photo,ref}$ (d)	Fitted loading (mg m^{-2})	Phi (-)	Err%	TOXSWA iterations
5	300	6.5 (4.5 – 8.4)	290 (259 - 321)	0.017	7.7%	32

Figure A5.5 presents a satisfactory agreement between optimised and measured scaled water concentrations for the optimisation of Table A5.7. Figure A5.6 presents the distribution of the scaled residuals between simulated and measured concentrations. The residuals as a function of time are not really randomly scattered around zero, but are wave-shaped, indicating that the estimate of the $DegT_{50,photo,ref}$ first seems slightly under-predicted and later on slightly over-predicted by the single $DegT_{50,photo,ref}$ value. However, the overall conclusion is drawn that no clearly significant pattern of under- or overprediction by the TOXSWA model.
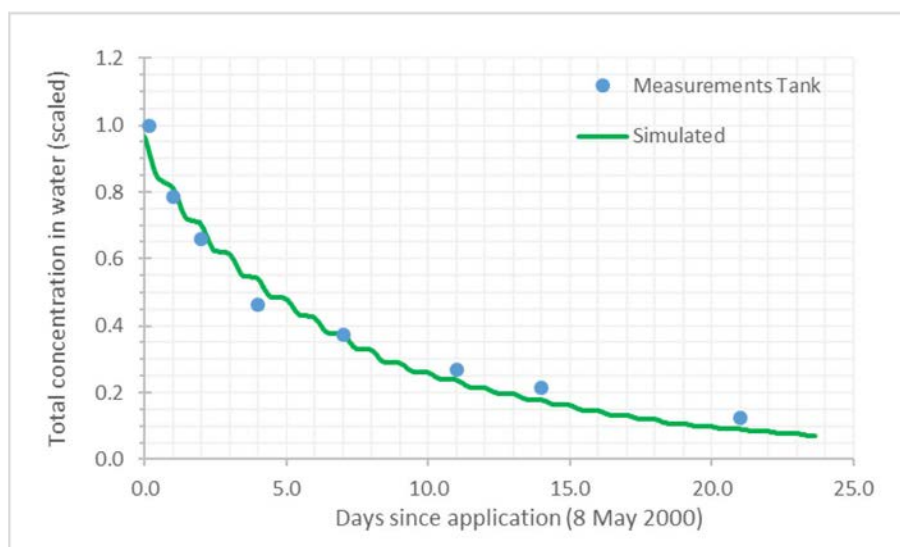

Figure A5.5 *Simulated and measured total concentration (dissolved+ sorbed to suspended solids) imidacloprid in water as a function of time in the tank of Bayer (2001). The simulated concentration profile was obtained by a PEST_TOXSWA optimisation for an initial $DegT_{50,photo,ref}$ = 5 d and an initial loading of 300 mg m^{-2}.*
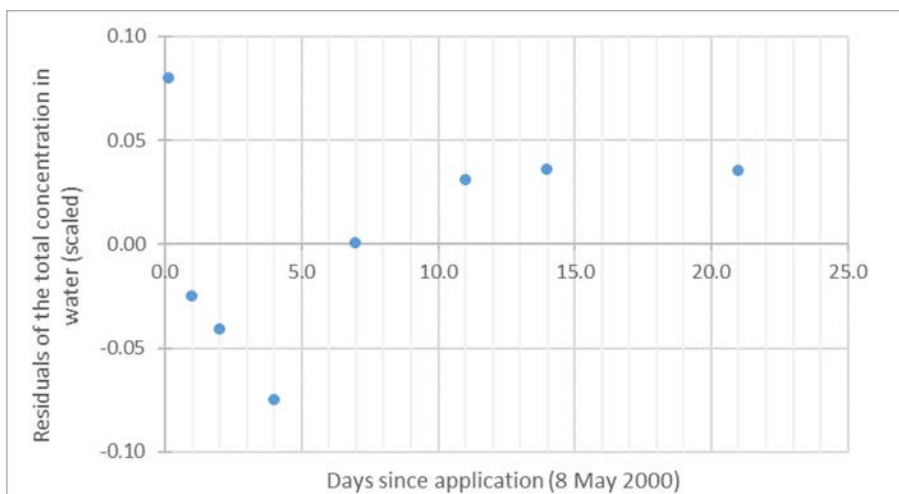
Figure A5.6 *Residuals of total concentration (dissolved+ sorbed to suspended solids) imidacloprid in water as a function of time in the tank of Bayer (2001). The simulated concentration profile was obtained by a PEST_TOXSWA optimisation for an initial DegT$_{50,photo,ref}$ = 5 d and an initial loading of 300 mg m^{-2}.*

ImiCosm3: Bayer (2003)

Table 6.10 up to 6.15 in Deneer et al. (2015) gives measured concentration in water (µg/L and scaled) as a function of time (d) in the study with imidacloprid by Bayer (2003). According to Deneer et al. (2015) no mention is made of filtering the sampled water before extraction, so, it was assumed that the total concentration including suspended solids was measured. Although data of several systems with different treatments levels are available, like Deneer et al. (2015) we used only the systems with the two highest treatment levels, ponds 7, 13, 8 and 2 for the estimation of *DegT$_{50,photo,ref}$*.

Imidacloprid was applied twice on 2 May and 23 May 2001. Two inverse modelling strategies are possible: 1) fitting the loading of the first application and fixing the loading of the second application and 2) fitting the loadings of both applications. For the first option scaling of the loading of the second application is necessary when using scaled concentrations.

The authors have provided Deneer et al. (2015) with measured concentrations in dosing solutions and the amount of dosing solution applied to each of the systems. These loadings (in mg/system) were converted into loadings/m^2 by taking into account the dimensions of the system (water depth of 1 meter, volumes of each of the systems given as 3100 L and therefore an area of 3.1 m^2, except for pond 13 which has a volume of 3800 L and therefore an area of 3.8 m^2). Scaled loadings were calculated by dividing the loading (in mg/m^2) by the highest aqueous concentration (in mg/L), analogous to the scaling of aqueous concentrations (see Table 6.10 and 6.11 in Annex 6 of Deneer et al., 2015).

For the inverse modelling the scaled concentrations as presented in Table A5.8 were used as observations in the fitting procedure and scaled loadings of the second application as presented in A5.9 were used as fixed input in the TOXSWA model. As the scaled loading of the second application varies considerably between the four systems, each system had to be optimised separately.

Table A5.8 *Measured concentrations in water (scaled) as a function of time (d) for the study with imidacloprid by Bayer (2003). Values are taken from tables 6.10 and 6.11 in Annex 6 of Deneer et al. (2015).*

Time (d)	Exact time	Time of calculated concentration in output file TOXSWA (i.e. ConSysWatLay: momentaneous total concentration in water)	Scaled concentration in water			
			Pond2	Pond7	Pond8	Pond13
0	02/05/2001 09:00	02-May-2001-09h00	Loading into the pond at this time is fitted			
0.16	02/05/2001 12:50	02-May-2001-13h00	0.9677	1.0000	1.0000	1.0000
2	04/05/2001 09:00	04-May-2001-09h00	0.6008	0.5901	0.6644	0.5977
4	06/05/2001 09:00	06-May-2001-09h00	0.5411	0.5311	0.5712	0.4958
7	09/05/2001 09:00	09-May-2001-09h00	0.4363	0.4255	0.4527	0.4023
14	16/05/2001 09:00	16-May-2001-09h00	0.2000	0.1848	0.2212	0.1731
20.95	23/05/2001 07:48	23-May-2001-08h00	0.1089	0.0910	0.0975	0.0810
21.16	23/05/2001 12:50	23-May-2001-13h00	1.0000	0.9814	0.9831	0.9830
23	25/05/2001 09:00	25-May-2000-09h00	0.6274	0.6522	0.6407	0.6091
25	27/05/2001 09:00	27-May-2001-09h00	0.4831	0.4534	0.4544	0.4051
28	30/05/2001 09:00	30-May-2001-09h00	0.3371	0.3168	0.3297	0.2671
35	06/06/2001 09:00	06-Jun-2001-09h00	0.1871	0.1792	0.1881	0.1207
49	20/06/2001 09:00	20-Jun-2001-09h00	0.0871	0.0581	0.0856	0.0402
63	04/07/2001 09:00	04-Jul-2001-09h00	0.0177	0.0080	0.0180	0.0056
77	18/07/2001 09:00	18-Jul-2001-09h00	0.0104	0.0062	0.0162	0.0053
91	01/08/2001 09:00	01-Aug-2001-09h00	NA	NA	0.0135	0.0029

Table A5.9 *Measured loadings of the second application on 23 May 2001 (mg/system, mg m^{-2} and scaled) as a function of time (d) for the study with imidacloprid by Bayer (2003). Values are taken from tables 6.10 and 6.11 in Annex 6 of Deneer et al. (2015).*

System	Loading (mg/system)	Loading (mg m^{-2})	Scaled loading
Pond 2	29.52	9.52	767.7
Pond7	73.79	23.801	739.13
Pond8	29.52	9.52	806.8
Pond13	89.29	23.50	665.7

Scaled concentrations were used in the optimisation procedure, and thus the Freundlich sorption coefficient, K_{om}, was corrected according the guidance given in Chapter 9.4. For each pond a corrected K_{om} value was calculated. Therefore the value of the first measurement in the set of observations (at t = 0.16) was used as $c_{t=0, geo}$ (Pond 2: 0.012 mg L^{-1}; Pond 7: 0.0322 mg L^{-1}; Pond 8: 0.0118 mg L^{-1}; Pond 13: 0.0353 mg L^{-1}). The corrected K_{om} values in the optimisations were 316.88 L kg^{-1} for Pond 2, 260.63 L kg^{-1} for Pond 7, 317.94 L kg^{-1} for Pond 8 and 255.93 L kg^{-1} for Pond 13.

In total 49 optimisations were performed for each of the four ponds, each with its own initial values of $DegT_{50,photo,ref}$ and the loading at t=0 (mg m^{-2})[26] (varying between 0.1 and 50 d for $DegT_{50,photo,ref}$ and 50 to 3000 mg m^{-2} for the loading at t=0). For all optimisations the same lower and upper parameter bounds were used: 0.1 – 100 d for the $DegT_{50,photo,ref}$ and 1.0 – 10 000 mg m^{-2} for the loading.

Results Pond 2
For Pond 2, all 49 optimisations resulted in a satisfactory estimation of $DegT_{50,photo,ref}$ and the loading at t=0. Consistent estimates of $DegT_{50,photo,ref}$ of 7.3 days with 95% confidence intervals of 5.9 – 8.8 days were obtained as well as consistent estimates of the loading of 873 mg m^{-2} with 95% confidence intervals of 760 - 985 mg m^{-2}.

---

[26] All possible combinations of the values given in the matrix below result in 49 sets of $DegT_{50,photo,ref}$ and the loading.

$DegT_{50,photo,ref}$ (d)	0.1	0.5	1	2	5	10	50
Loading (mg m^{-2})	50	100	300	500	1000	1500	3000

Table A5.10 gives estimates of the optimized $DegT_{50,photo,ref}$ and loading for the optimisation with initial values of resp. 5 days and 1000 mg m^{-2}. It also specifies the value of the objective function phi (i.e. the sum of squared differences between model-generated and measured aqueous concentrations), the error percentage of the $\chi2$-test and the number of times TOXSWA has been run by PEST. Note that the $\chi2$-test is explained into more detail in section 2.3 of Deneer et al. (2015). FOCUS (2006) suggests that a minimum error percentage value of 15% is acceptable for field studies.

The error percentage of 13.6% is an acceptable value for field experiments according to FOCUS (2006), so the optimisation passed the $\chi2$-test.

Table A5.10 *Optimisation results for one of the 49 satisfactory optimisations (out of 49) for pond 2 of the study with imidacloprid by Bayer (2003).*

Initial $DegT_{50,photo,ref}$ (d)	Initial loading (mg m^{-2})	Fitted $DegT_{50,photo,ref}$ (d)	Fitted loading (mg m^{-2})	Phi (-)	Err%	TOXSWA iterations
5	1000	7.3 (5.9 – 8.8)	873 (760 - 985)	0.063	13.6%	29

Figure A5.7 presents the agreement between scaled optimised and measured water concentrations for pond 2. It can be seen that the simulated concentrations are lower than the measured concentrations around the timing of application. The first loading is fitted, however the second loading is fixed (see Table A4.10) based upon nominal concentrations used by Bayer (2003). Bayer (2003) also noted that measured concentrations were higher than the nominal test concentrations used (126-150% for the first application and 123 – 148% for the second application). They provided the following explanation. Recoveries exceeding 100% of the concentration measured shortly after the first application were presumably caused by the fact that the formulation was not homogeneously distributed in the water columns shortly after the overspray application, especially due to the slight wind during and after the application time. The higher than expected concentrations measured shortly after the second application were caused by the application of the test item to the remaining concentrations in the water and presumably also by inhomogeneity of the applied test item in the water column. Except for these discrepancies at the time of the loadings, the agreement between simulated and measured scaled concentrations is good.

Figure A5.8 presents the distribution of the scaled residuals between model-generated and measured concentrations. The residuals corresponding to the first and second loading are a bit higher than the other residuals for the reasons explained above. The other residuals are randomly scattered around zero, demonstrating that there is no pattern of under- or over-prediction by the TOXSWA model.
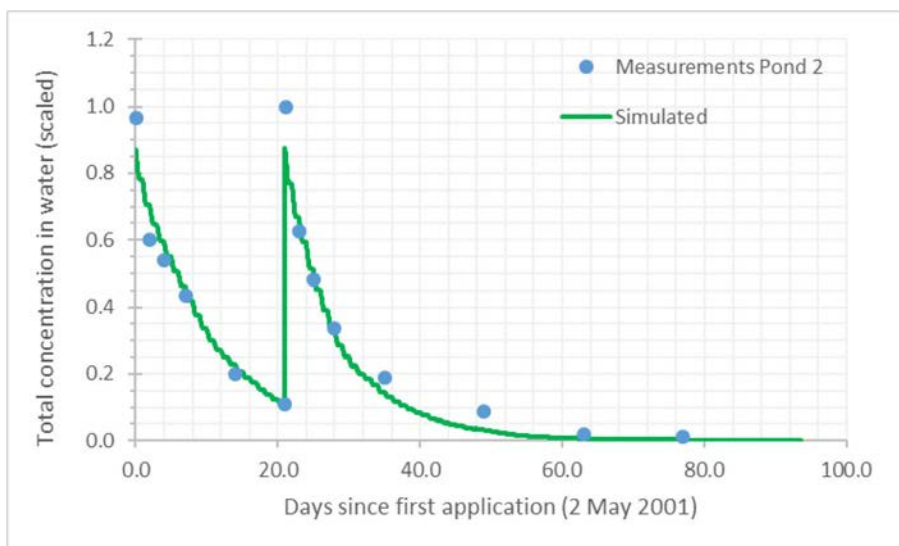
Figure A5.7 *Simulated and measured total concentration (dissolved+ sorbed to suspended solids, scaled concentrations) imidacloprid in water as a function of time after first measurement (d) for pond 2 in the data set of Bayer (2003). Simulated concentration profiles obtained by PEST_TOXSWA optimisation for DegT$_{50,photo,ref}$ = 5 d and an initial loading at t = 0 d of 1000 mg m^{-2}.*
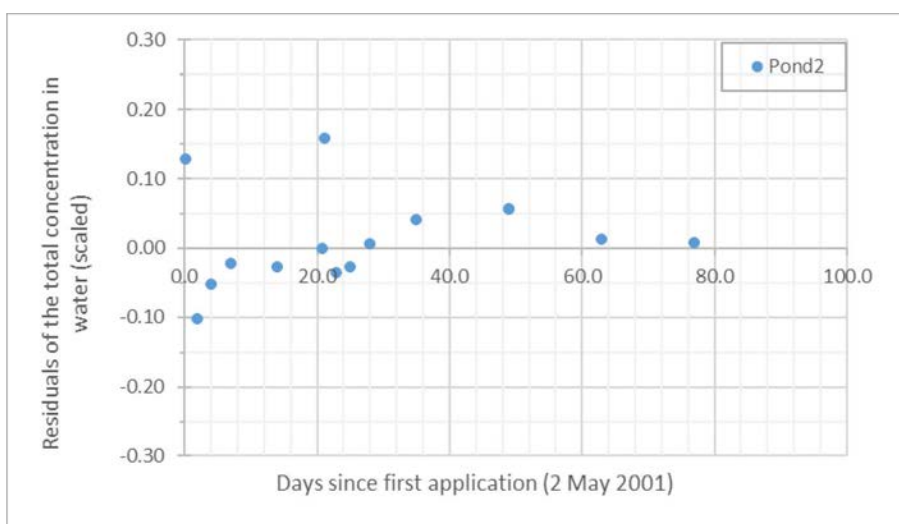

Figure A5.8 *Residuals of total concentration (dissolved+ sorbed to suspended solids, scaled concentration) imidacloprid in water as a function of time after first measurement (d) for pond 2 in the data set of Bayer (2003). Simulated concentration profiles obtained by PEST_TOXSWA optimisation for DegT$_{50,photo,ref}$ = 5 d and an initial loading at t = 0 d of 1000 mg m^{-2}.*

Results Pond 7

For Pond 7 1 fit from the 49 optimisations resulted in to an unsatisfactory estimation of *DegT$_{50,photo,ref}$* and the loading at t=0. All other optimisations resulted in consistent estimates of *DegT$_{50,photo,ref}$* of 7.2 days with 95% confidence intervals of 5.6 – 8.8 days and consistent estimates of the loading of 879 mg m^{-2} with 95% confidence intervals of 753 - 1006 days mg m^{-2}.

Table A5.11 gives estimates of the optimized *DegT$_{50,photo,ref}$* and loading for the optimisation with initial values of resp. 5 days and 1000 mg m^{-2}. It also specifies the value of the objective function phi (i.e. the sum of squared differences between model-generated and measured aqueous concentrations), the error percentage of the *χ2*-test and the number of times TOXSWA has been run by PEST.

The error percentage of 15.6% is an unacceptable value for field experiments according to FOCUS (2006), so the optimisation did not pass the *χ2*-test.

Table A5.11 *Optimisation results for one of the 48 satisfactory optimisations (out of 49) for pond 7 of the study with imidacloprid by Bayer (2003).*

Initial $DegT_{50,photo,ref}$ (d)	Initial loading (mg m^{-2})	Fitted $DegT_{50,photo,ref}$ (d)	Fitted loading (mg m^{-2})	Phi (–)	Err%	TOXSWA iterations
5	1000	7.2 (5.6 – 8.8)	879 (753 – 1006)	0.08	15.6%	30

Figure A5.9 presents the agreement between scaled optimised and measured water concentrations for pond 7. Similar to pond 2, the simulated concentrations shortly after application of the test substance are lower than the measured concentrations. Measured concentrations shortly after application are higher than the nominal test concentrations presumably caused by inhomogeneous distribution of the substance in the water column (for more details, see the section on the results of Pond 2).
Figure A5.10 presents the distribution of the scaled residuals between model-generated and measured concentrations. The residuals corresponding to the first and second loading are a bit higher than the other residuals for the reasons explained above. The other residuals are randomly scattered around zero, demonstrating that there is no pattern of under- or over-prediction by the TOXSWA model.
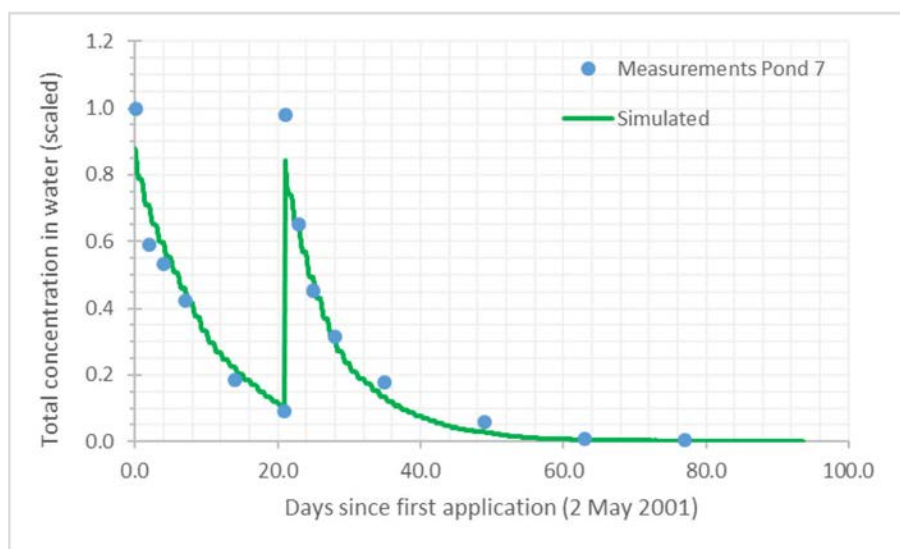

Figure A5.9 *Simulated and measured total concentration (dissolved+ sorbed to suspended solids, scaled concentrations) imidacloprid in water as a function of time after first measurement (d) for pond 7 in the data set of Bayer (2003). Simulated concentration profiles obtained by PEST_TOXSWA optimisation for DegT$_{50,photo,ref}$ = 5 d and an initial loading at t = 0 d of 1000 mg m^{-2}.*
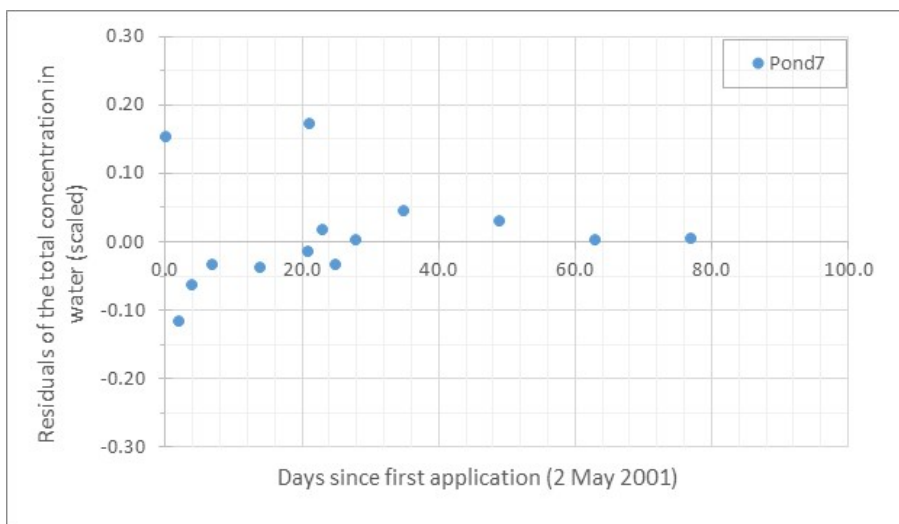
Figure A5.10 *Residuals of total concentration (dissolved+ sorbed to suspended solids, scaled concentration) imidacloprid in water as a function of time after first measurement (d) for pond 7 in the data set of Bayer (2003). Simulated concentration profiles obtained by PEST_TOXSWA optimisation for $DegT_{50,photo,ref}$ = 5 d and an initial loading at t = 0 d of 1000 mg m^{-2}.*

Results Pond 8

For Pond 8 1 fit from the 49 optimisations resulted in to an unsatisfactory estimation of $DegT_{50,photo,ref}$ and the loading at t=0. All other optimisations resulted in consistent estimates of $DegT_{50,photo,ref}$ of 6.7 days with 95% confidence intervals of 5.7 – 7.8 days and consistent estimates of the loading of 939 mg m^{-2} with 95% confidence intervals of 847 - 1030 mg m^{-2}.

Table A5.12 gives estimates of the optimized $DegT_{50,photo,ref}$ and loading for the optimisation with initial values of resp. 5 days and 1000 mg m^{-2}. It also specifies the value of the objective function phi (i.e. the sum of squared differences between model-generated and measured aqueous concentrations), the error percentage of the $\chi2$-test and the number of times TOXSWA has been run by PEST.

The error percentage of 11.5% is an acceptable value for field experiments according to FOCUS (2006), so the optimisation passed the $\chi2$-test.

Table A5.12 *Optimisation results for one of the 48 satisfactory optimisations (out of 49) for pond 8 of the study with imidacloprid by Bayer (2003).*

Initial $DegT_{50,photo,ref}$ (d)	Initial loading (mg m^{-2})	Fitted $DegT_{50,photo,ref}$ (d)	Fitted loading (mg m^{-2})	Phi (-)	Err%	TOXSWA iterations
5	1000	6.7 (5.7 – 7.8)	939 (847 – 1030)	0.046	11.5%	32

Figure A5.11 presents the agreement between scaled optimised and measured water concentrations for pond 8. Similar to pond 2 and pond 7, the simulated concentrations shortly after application of the test substance are lower than the measured concentrations. Measured concentrations shortly after application are higher than the nominal test concentrations presumably caused by inhomogeneous distribution of the substance in the water column (for more details, see the section on the results of Pond 2). Figure A5.12 presents the distribution of the scaled residuals between model-generated and measured concentrations. Although less pronounced than for pond 2 and pond 7, the residuals corresponding to the first and second loadings are somewhat higher than the other residuals for the reasons explained above. The other residuals are randomly scattered around zero, demonstrating that there is no pattern of under- or over-prediction by the TOXSWA model.
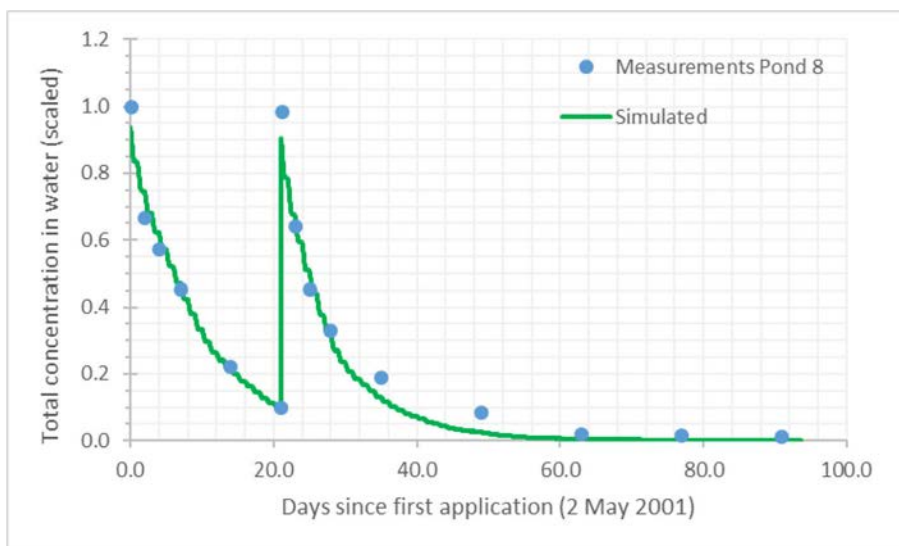
Figure A5.11 *Simulated and measured total concentration (dissolved+ sorbed to suspended solids, scaled concentrations) imidacloprid in water as a function of time after first measurement (d) for pond 8 in the data set of Bayer (2003). Simulated concentration profiles obtained by PEST_TOXSWA optimisation for DegT$_{50,photo,ref}$ = 5 d and an initial loading at t = 0 d of 1000 mg m^{-2}.*
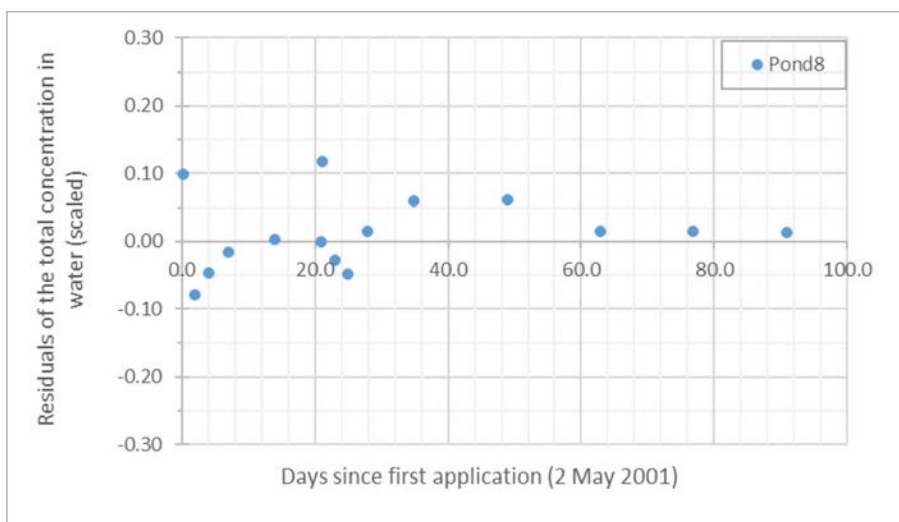

Figure A5.12 *Residuals of total concentration (dissolved+ sorbed to suspended solids, scaled concentration) imidacloprid in water as a function of time after first measurement (d) for pond 8 in the data set of Bayer (2003). Simulated concentration profiles obtained by PEST_TOXSWA optimisation for DegT$_{50,photo,ref}$ = 5 d and an initial loading at t = 0 d of 1000 mg m^{-2}.*

Results Pond 13

For Pond 13, all of the 49 optimisations resulted in to an satisfactory estimation of *DegT$_{50,photo}$* and the loading at t=0. Consistent estimates of *DegT$_{50,photo,ref}$* of 7.0 days with 95% confidence intervals of 5.1–8.8 days and consistent estimates of the loading of 876 mg m^{-2} with 95% confidence intervals of 728-1024 mg m^{-2} were found.

Table A5.13 gives estimates of the optimized *DegT$_{50,photo,ref}$* and loading for the optimisation with initial values of resp. 5 days and 1000 mg m^{-2}. It also specifies the value of the objective function phi (i.e. the sum of squared differences between model-generated and measured aqueous concentrations), the error percentage of the $\chi 2$-test and the number of times TOXSWA has been run by PEST.

The error percentage of 20.6 is an unacceptable value for field experiments according to FOCUS (2006), so the optimisation did not pass the $\chi 2$-test.

Table A5.13 *Optimisation results for one of the 48 satisfactory optimisations (out of 49) for pond 8 of the study with imidacloprid by Bayer (2003).*

Initial $DegT_{50,photo,ref}$ (d)	Initial loading (mg m^{-2})	Fitted $DegT_{50,photo,ref}$ (d)	Fitted loading (mg m^{-2})	Phi (–)	Err%	TOXSWA iterations
5	1000	7.0 (5.1 – 8.8)	873 (728 – 1024)	0.11	20.6%	30

Figure A5.13 presents the agreement between scaled optimised and measured water concentrations for pond 13. Similar to pond 2, pond 7 and pond 8, the simulated concentrations shortly after application of the test substance are lower than the measured concentrations. Measured concentrations shortly after application are higher than the nominal test concentrations presumably caused by inhomogeneous distribution of the substance in the water column (for more details, see the section on the results of Pond 2). Figure A5.14 presents the distribution of the scaled residuals between model-generated and measured concentrations. The residuals corresponding to the first and especially the second loadings are somewhat higher than the other residuals for the reasons explained above. The other residuals are randomly scattered around zero, demonstrating that there is no pattern of under- or over-prediction by the TOXSWA model.
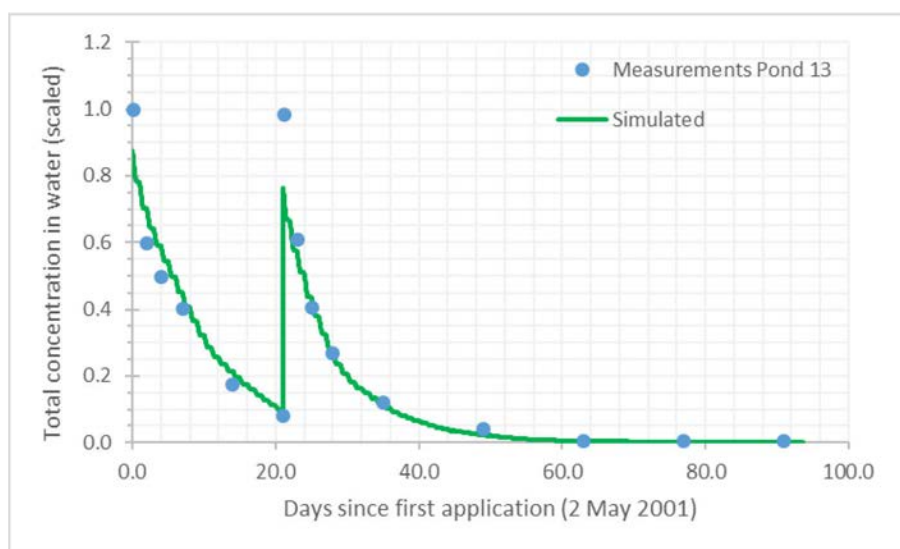

Figure A5.13 *Simulated and measured total concentration (dissolved+ sorbed to suspended solids, scaled concentrations) imidacloprid in water as a function of time after first measurement (d) for pond 13 in the data set of Bayer (2003). Simulated concentration profiles obtained by PEST_TOXSWA optimisation for DegT$_{50,photo,ref}$ = 5 d and an initial loading at t = 0 d of 1000 mg m^{-2}.*
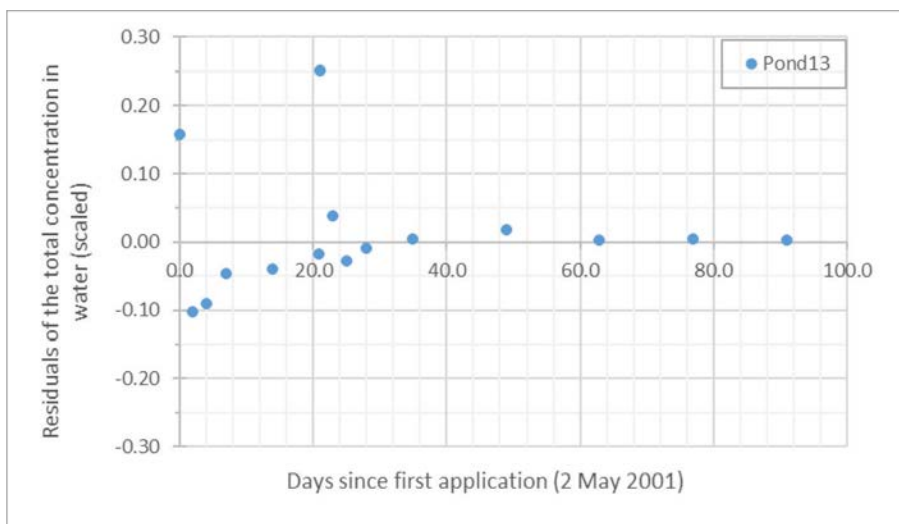
Figure A5.14 *Residuals of total concentration (dissolved+ sorbed to suspended solids, scaled concentration) imidacloprid in water as a function of time after first measurement (d) for pond 13 in the data set of Bayer (2003). Simulated concentration profiles obtained by PEST_TOXSWA optimisation for DegT$_{50,photo,ref}$ = 5 d and an initial loading at t = 0 d of 1000 mg m^{-2}.*

Annex 6 Details of the assessment of the photolytic degradation rate of metamitron in cosm water

The main characteristics of the studies with metamitron in the two cosm studies of Wendt-Rasch et al. (2004) and Brock. et al. (2004) have been summarized in Table A6.1.

Table A6.1 *Data on cosm studies with metamitron.*

Label in data file	MetamitCosm1	MetamitCosm2
Reference	Wendt-Rasch et al., 2004	Brock et al., 2004
Compound	Goltix WG, 70%	Metamitron 700 SC, 690 g/L
Type of system	Outdoor microcosms, concrete tanks, Sinderhoeve Renkum	Outdoor cosms, polycarbonate enclosures in experimental ditches Sinderhoeve, Renkum
Dimensions system	1.2 x 1.4 x 1.2 m, approx. 0.5 m^3 water	Cylinders, diameter 1.05 m, height 0.9 m, approx. 433 L water
Side slope (hor/vert)	0	0
Depth water layer	30 cm	50 cm
Depth sediment	Not specified	15 cm
Sediment om%	Not specified	Not specified
Sediment bulk density	Not specified	Not specified
Sediment porosity	Not specified	Not specified
Macrophytes info	Two types of system, either *Elodea nuttallii* dominated, or *Lemna* dominated; both types also contained 3 pots with 5 g *Myriophillum spicatum* each (on the bottom)	No macrophytes present in enclosures
pH	Variable over time and different between systems, range 6.2 – 9.3	In most systems 8.5 – 9.5, only at highest treatment 7 – 8.5 during first 14 days, 8.5 – 9.5 on later days
Temperature	Not specified, May – June 1999, Renkum	First week post-application: 13-17°C
Light intensity	Not specified, May – June 1999, Renkum	Not specified, May 1999, Renkum
Application number	1	1
Application interval	-	-
Nominal initial application	11.7 µg/L	14, 70, 280, 1120, 4480 µg/L
Date and timing of the applications	4 May 1999; 9:30 h*	5 May 1999; 9:00 h**

* From the data provided was clear that the application of the highest treatment level was at 9:30 h.

** The exact timing of the application is unknown. 9:00 is assumed the following reason WENR staff performing these type of cosm experiments indicated that they usually start the dosing around 9:00 h, because standard after 8 hours a measurements is taken and that is preferably done near the end of a working day (i.e. 17:00 h).

In Table A6.2 below the input values on the physico-chemical properties of metamitron and the cosm-specific input, such as e.g. the water depth are summarized.

Table A6.2   *Parameter values used in the simulations with metamitron.*

Cosm label	MetamitCosm1	MetamitCosm2
Reference	Wendt-Rasch et al., 2004	Brock et al., 2004
Molar mass (g)	202.21	
Saturated vapour pressure (mPa)	$7.44 \cdot 10^{-4}$ (20°C)	
Solubility (mg/L)	1770 (20°C)	
Kom (estimated) (L/kg)	$K_f=1.09$, $K_{foc}=86.4$, Kom = 50.12, N=0.78	
pKa	Not applicable	
Water depth (m)	0.3	0.5
Bottom width (m)	1.2	1
Length (m)	1.4	1
Side slope (hor/vert, -)	0	0
Temperature (°C)	16.55 °C (same value as of study of Brock et al., 2004 taken)	16.55 °C
Measurements in sediment	No	No

MetamitCosm1: Wendt-Rasch et al. (2004)

Table A6.3 presents the measured concentrations in water as a function of time in the study of Wendt-Rasch et al. (2004). No mention is made of filtering the sampled water before extraction and the total concentration including suspended solids appears to be measured. Both the *Elodea* dominated as well as the *Lemna* dominated systems were treated at 11.7 mg/L nominal initial concentration.

Table A6.3   *Concentrations in water (µg/L and scaled) as a function of time (d) for the microcosms treated with metamitron by Wendt-Rasch et al. (2004).*

	Time in TOXSWA (days)	Concentration in water (µg/L)	Scaled concentration
***Elodea* dominated systems**			
	0.00	11.79	-
1	0.08	8.40	1.0000
2	1	2.82	0.3357
3	3	0.82	0.0976
4	14.3	0.20	0.0238
5	21	0.14	0.0167
***Lemna* dominated systems**			
	0.00	11.92	-
1	0.08	10.06	1.0000
2	1	6.75	0.6710
3	3	3.37	0.3350
4	14.3	0.45	0.0447
5	21	0.19	0.0189

Concentrations at t=0.00 are calculated from concentrations measured in dosing solutions. Concentrations given represent averages over two cosms treated at (nearly) the same level. More detailed concentration data for individual cosms are given below.

Concentrations are taken from the original analytical data, which were supplied by Steven Crum on 27 May 2019. All concentrations refer to measured concentrations of metamitron in cosm water. The cosms contained macrophytes, and were characterized as either *Elodea* dominated or *Lemna* dominated systems (10 systems each). Treatments at each treatment level was performed in 4 cosms, 2 *Elodea* dominated and 2 *Lemna* dominated systems.

In the analytical data the measured concentrations are given for each cosm (-number) separately. The information whether a given cosm was *Elodea* or *Lemna* dominated could not be retrieved. However, Figure 2 in the paper by Wendt-Rasch et al. (2004) indicates that for the systems treated at the highest level, concentrations in the *Lemna* dominated systems decreased more slowly than concentrations in the *Elodea* dominated systems. This information was used to assign cosms of the highest treatment level to either the *Elodea* or *Lemna* dominated group of systems. Since no corresponding graphs were available for the lower treatment levels, the concentrations measured for lower treatment levels could not be assigned to *Elodea* or *Lemna* dominated systems and thus this information was not used for the inverse modelling.

Concentrations per cosm and average concentrations over duplicates of the same type of system (*Elodea* or *Lemna* dominated) are given (Table A6.4). The concentrations given for the start of the exposure period (t=0 h) are calculated from concentrations measured in dosing solutions, assuming a water volume of 840 litres, and do not represent concentrations measured in water.

Table A6.4 *Measured aqueous concentrations (in µg/L) of metamitron per cosm; cosms 1 and 8 are Elodea dominated systems, cosms 13 and 18 are Lemna dominated systems.*

Cosm #	t=0h (dosing)	t=2h	t=1d	t=3d	t=14.3d	t=21d
Elodea						
1	11.88	8.10	2.88	0.98	0.20	0.14
8	11.71	8.70	2.76	0.67	-	-
Average	11.79	8.40	2.82	0.82	0.20	0.14
Lemna						
13	11.84	10.35	7.57	4.40	0.45	0.19
18	12.01	9.77	5.93	2.35	-	-
Average	11.92	10.06	6.75	3.37	0.45	0.19

As scaled concentrations were used in the optimisation procedure, the Freundlich sorption coefficient, K_{om}, was corrected according the guidance given in Chapter 9.4. The $c_{t=0, geo}$ was set to the unscaled concentrations at t = 0.08 d in the measured datasets (8.4 and 10.06 µg L^{-1} for respectively the *Elodea* and *Lemna* dominated system). The corrected K_{om} values used in the optimisation were 143.4 and 137.9 L kg^{-1} for respectively the *Elodea* and *Lemna* dominated system.

The data in Table A6.3 was used in the inverse modelling. Inverse modelling was done separately for the two systems: *Elodea* dominated and *Lemna* dominated. Optimisations were done with the aid of the PEST tool, running TOXSWA many times, according to the procedures presented in Chapter 9. The $DegT_{50,photo,ref}$ and the loading in to the system at 4 May 1999, 09:00 h[27] were optimised. In total 49 optimisations were performed, each with its own initial values of $DegT_{50,photo,ref}$ and the loading at t=0 (mg m^{-2})[28] (varying between 0.1 and 50 d for $DegT_{50,photo,ref}$ and 50 to 3000 mg m^{-2} for the loading at t=0[29]). For all optimisations the same lower and upper parameter bounds were used: 0.1 – 100 d for the $DegT_{50,photo,ref}$ and 1.0 – 10 000 mg m^{-2} for the loading.

---

[27] Application of the highest treatment level was at 9:30. However, in TOXSWA applications can only be done on the hour. A choice needs to be made between either a loading at 9:00 or at 10:00. We selected 9:00 because this is from a regulatory point of view the most conservative approach (more early, less initial radiation and more hours for degradation resulting in lower degradation rates).

[28] All possible combinations of the values given in the matrix below result in 49 sets of $DegT_{50,photo,ref}$ and the loading.

$DegT_{50,photo,ref}$ (d)	0.1	0.5	1	2	5	10	50
Loading (mg m^{-2})	50	100	300	500	1000	1500	3000

[29] Although the scaled concentrations used as observations in the inverse modelling are dimensionless, they will be compared with concentrations simulated by TOXSWA which are in g m^{-3}. The input of the pesticide loading in TOXSWA is in mg m^{-2}. To determine plausible ranges for the loading in mg m^{-2} as input for the inverse modelling a calculation needs to be done to determine the loading needed to reach a certain desired peak concentration (e.g. the measured, scaled water concentration at t=0). Suppose that the desired peak concentration in water ($c_{peak,w}$) is 1 g m^{-3} (1000 mg m^{-3}). The loading needed to reach this peak concentration is:

$c_{peak,w} \cdot V/(w \cdot L)$

For the *Elodea* dominated system 21 fits of the 49 optimisations resulted in to an unsatisfactory estimation of $DegT_{50,photo,ref}$ and the loading at t=0 (Note that these are all fits with initial loadings of 1000 and 3000 mg m^{-2}). All other optimisations resulted in consistent estimates of $DegT_{50,photo,ref}$ of 0.60 days with 95% confidence intervals of 0.43 – 0.77 days and consistent estimates of the loading of 352 mg m^{-2} with 95% confidence intervals of 308 - 395 mg m^{-2}.

For the *Lemna* dominated system 23 fits of the 49 optimisations resulted in to an unsatisfactory estimation of $DegT_{50,photo,ref}$ and the loading at t=0 (Note that most these are all fits with initial loadings of 1000 and 3000 mg m^{-2}). All other optimisations resulted in consistent estimates of $DegT_{50,photo,ref}$ of 1.7 days with 95% confidence intervals of 1.3 – 2.1 days and consistent estimates of the loading of 319 mg m^{-2} with 95% confidence intervals of 294 - 343 mg m^{-2}.

Table A6.5 gives estimates for the *Elodea* dominated system of the optimized $DegT_{50,photo,ref}$ and loading for the optimisation with initial values of resp. 1 days and 300 mg m^{-2}.

Table A6.6 gives estimates for the *Lemna* dominated system of the optimized $DegT_{50,photo,ref}$ and loading for the optimisation with initial values of resp. 2 days and 300 mg m^{-2}.

Both tables specify the value of the objective function phi (i.e. the sum of squared differences between model-generated and measured aqueous concentrations), the error percentage of the χ^2-test and the number of times TOXSWA has been run by PEST. Note, that the χ^2-test is explained into more detail in section 2.3 of Deneer et al. (2015). FOCUS (2006) suggests that a minimum error percentage value of 15% is acceptable for field studies.

The error percentages of 6.7% (*Elodea* dominated system) and 3.4% (*Lemna* dominated system) are acceptable values for field experiments according to FOCUS (2006), so both optimisations did pass the χ^2-test.

Table A6.5   *Optimisation results for one of the 28 satisfactory optimisations for the Elodea dominated system of Wendt-Rasch et al. (2004) with metamitron.*

Initial $DegT_{50,photo,ref}$ (d)	Initial loading (mg m^{-2})	Fitted $DegT_{50,photo,ref}$ (d)	Fitted loading (mg m^{-2})	Phi (-)	Err%	TOXSWA iterations
1	300	0.60 (0.43– 0.77)	352 (308 - 396)	0.003	6.7%	36

Table A6.6   *Optimisation results for one of the 26 satisfactory optimisations for the Lemna dominated system of Wendt-Rasch et al. (2004) with metamitron.*

Initial $DegT_{50,photo,ref}$ (d)	Initial loading (mg m^{-2})	Fitted $DegT_{50,photo,ref}$ (d)	Fitted loading (mg m^{-2})	Phi (-)	Err%	TOXSWA iterations
2	300	1.7 (1.3– 2.1)	319 (294 - 343)	0.002	3.4%	29

The simulated concentration as function of time presented in Figures A6.1 and A6.3 shows a wavy pattern. This is caused by more rapid degradation due to photolysis during daytime and stagnating degradation once the sun sets and UV radiation becomes zero. In the *Elodea* dominated system the concentration decreases more rapidly than in the *Lemna* dominated system.

The agreement between scaled optimised and measured water concentrations presented in Figures A6.1 and A6.3 is judged to be satisfactory.

---

where V = the volume of water in the cosm (m^3), w = the width of the water surface (m) and L is the length of the system (m). For the study of Wendt-Rasch et al. (2004) where the system has a water depth of 0.3 m, a side slope of 0, a width of 1.2 m and a length of 1.4 m, the water volume, V, is 0.504 m^3. Supposing $c_{peak,w}$ is 1000 mg m^{-3} a loading of 1000·0.504/1.2·1.4 = 300 mg/m^2 is needed to reach this peak concentration in the water in the system.

Also the residuals seem to be randomly scattered around zero, demonstrating that there is no pattern of under- or over-prediction by the TOXSWA model (Figure A6.2 and Figure A6.4).
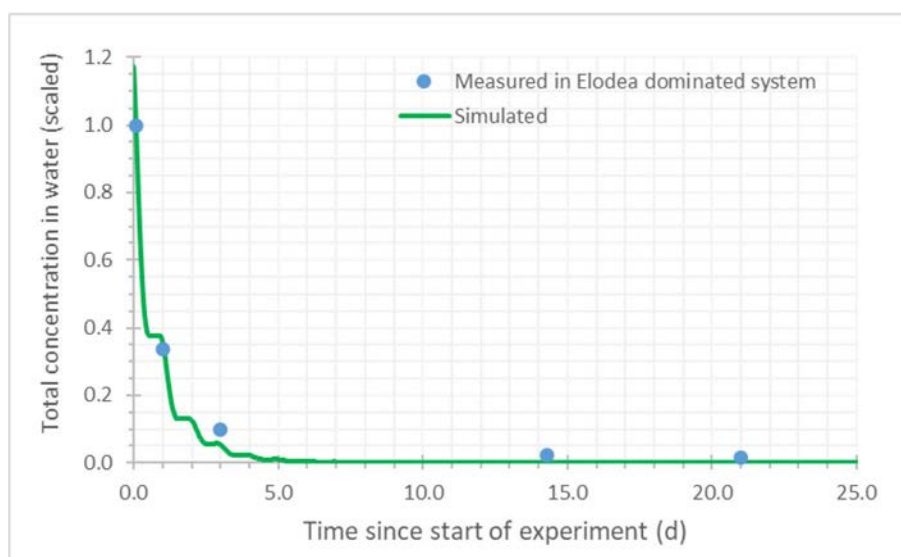

Figure A.6.1 *Simulated and measured total concentration (dissolved+ sorbed to suspended solids, µg.L^{-1}) metribuzin in water as a function of time (d) in the Elodea dominated system of Wendt-Rasch et al. (2004). Simulated concentration profile obtained by PEST_TOXSWA optimisation for an initial DegT$_{50,photo,ref}$ = 1 d and an initial loading of 300 mg m^{-2}.*
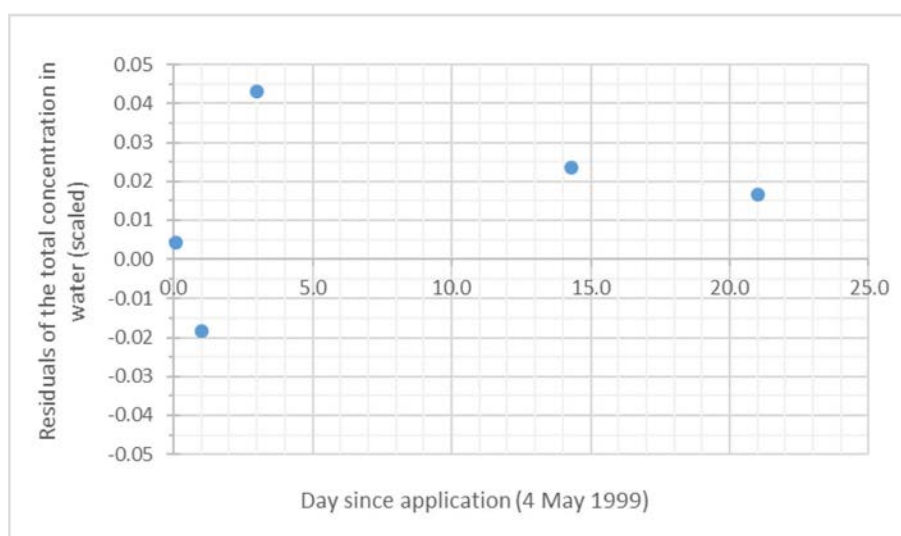

Figure A.6.2 *Residuals of total concentration (dissolved+ sorbed to suspended solids, µg.L^{-1}) metribuzin in water as a function of time (d) in the Elodea dominated system of Wendt-Rasch et al. (2004). Simulated concentration profile obtained by PEST_TOXSWA optimisation for an initial DegT$_{50,photo,ref}$ = 1 d and an initial loading of 300 mg m^{-2}.*
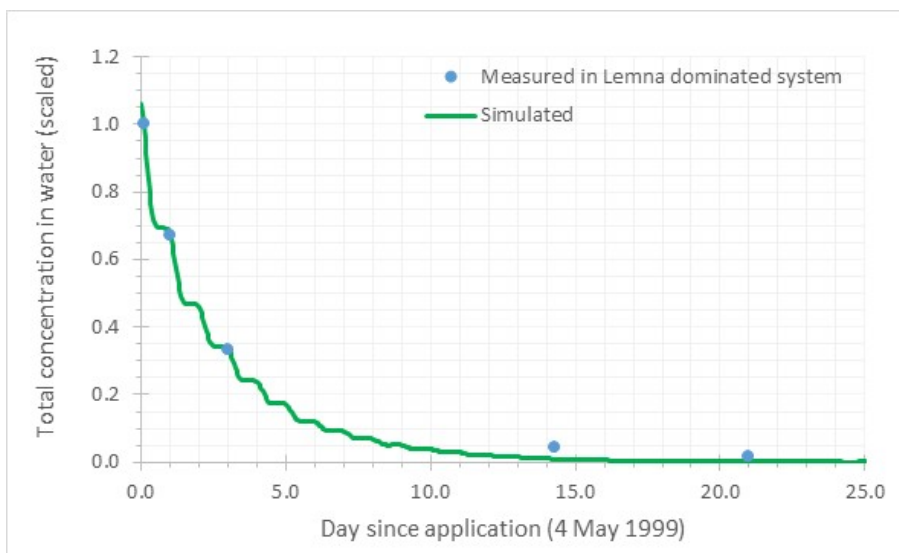
Figure A.6.3 *Simulated and measured total concentration (dissolved+ sorbed to suspended solids, µg.L⁻¹) metamitron in water as a function of time (d) in the Lemna dominated system of Wendt-Rasch et al. (2004). Simulated concentration profile obtained by PEST_TOXSWA optimisation for an initial DegT$_{50,photo,ref}$ = 2 d and an initial loading of 300 mg m⁻².*
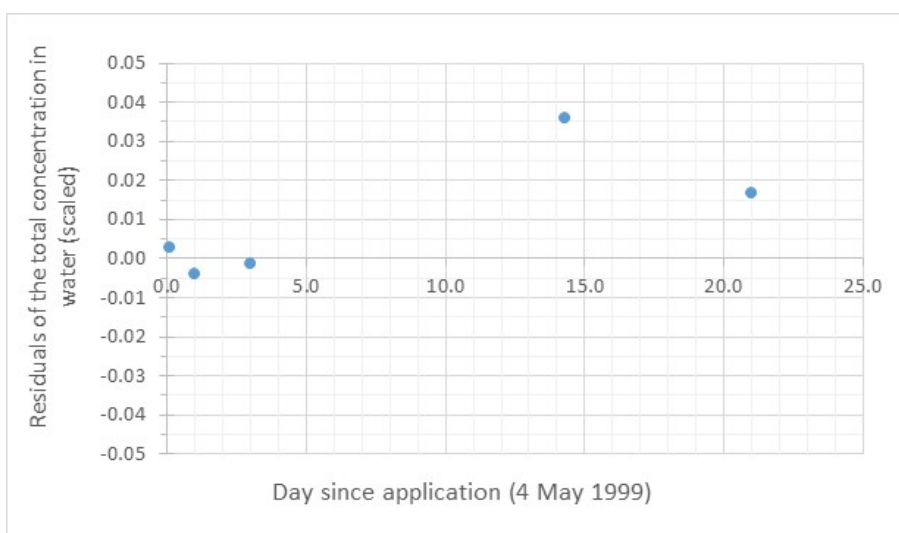

Figure A.6.4 *Residuals of total concentration (dissolved+ sorbed to suspended solids, µg.L⁻¹) metamitron in water as a function of time (d) in the Lemna dominated system of Wendt-Rasch et al. (2004). Simulated concentration profile obtained by PEST_TOXSWA optimisation for an initial DegT$_{50,photo,ref}$ = 2 d and an initial loading of 300 mg m⁻².*

MetamitCosm2: Brock et al. (2004)

Table A6.7 presents the measured concentrations in water as a function of time in the study of Brock et al. (2004). Water was filtered prior to analysis, only the dissolved concentration was measured.

All measurements in Table A6.7 (i.e. 82) are used simultaneously in the fitting procedure. This was considered appropriate as there were no physiological differences between the systems and moreover, no noteworthy differences between the measurements (at similar time) were observed.

Table A6.7 *Concentrations in water (µg/L and scaled) as a function of time (d) for the microcosms treated with metamitron by Brock et al. (2004); concentrations on t=0.00 are calculated from concentrations measured in dosing solutions.*

Number	Time in TOXSWA (days)	Concentration in water (µg/L)	Scaled concentration
Enclosure 2, nominal: 14 ug/L			
	0.00	13.9	-
1	0.04	11.2	1.0000
2	0.17	10.7	0.9554
3	0.3	9.3	0.8304
4	1	9.5	0.8482
5	2	6.0	0.5357
6	4	2.0	0.1786
7	7	0.7	0.0625
	14	< 0.05	-
	28	< 0.05	-
Enclosure 7, nominal: 14 ug/L			
	0.00	13.5	-
9	0.04	11.6	0.9667
10	0.17	12.0	1.0000
11	0.3	11.4	0.9500
12	1	10.7	0.8917
13	2	8.9	0.7417
14	4	4.5	0.3750
15	7	2.7	0.2250
16	14	0.60	0.0500
	28	< 0.2	-
Enclosure 6, Nominal: 70 ug/L			
	0.00	64.8	-
17	0.04	63.0	1.0000
18	0.17	55.0	0.8730
19	0.3	51.2	0.8127
20	1	47.7	0.7571
21	2	34.2	0.5429
22	4	13.8	0.2190
23	7	4.8	0.0762
24	14	0.22	0.0035
	28	< 0.05	-
Enclosure 11, nominal: 70 ug/L			
	0.00	65.5	-
25	0.04	67.2	1.0000
26	0.17	54.0	0.8036
27	0.3	49.7	0.7396
28	1	46.4	0.6905
29	2	32.9	0.4896
30	4	10.7	0.1592
31	7	2.7	0.0402
32	14	0.20	0.0030
	28	< 0.1	-
Enclosure 1, nominal: 280 ug/L			
	0.00	267	-
33	0.04	239	1.0000
34	0.17	188	0.7866
35	0.3	164	0.6862
36	1	154	0.6443
37	2	93.9	0.3929
38	4	26.6	0.1113
39	7	4.1	0.0172
40	14	0.06	0.00025
	28	< 0.2	-

Number	Time in TOXSWA (days)	Concentration in water (µg/L)	Scaled concentration
Enclosure 10, nominal: 280 ug/L			
	0.00	264	-
41	0.04	247	1.0000
42	0.17	220	0.8907
43	0.3	201	0.8138
44	1	195	0.7895
45	2	148	0.5992
46	4	66.7	0.2700
47	7	21.4	0.0866
48	14	1.6	0.0065
	28	< 0.1	-
Enclosure 5, nominal 1120 ug/L			
	0.00	1036	-
49	0.04	916	1.0000
50	0.17	867	0.9465
51	0.3	789	0.8614
52	1	752	0.8210
53	2	542	0.5917
54	4	233	0.2544
55	7	81.4	0.0889
56	14	5.9	0.0064
57	28	0.1	0.0001
Enclosure 9, nominal 1120 ug/L			
	0.00	1013	-
58	0.04	944	1.0000
59	0.17	849	0.8994
60	0.3	796	0.8432
61	1	763	0.8083
62	2	553	0.5858
63	4	215	0.2278
64	7	61.8	0.0655
65	14	3.6	0.0038
	28	< 0.2	-
Enclosure 3, nominal 4480 ug/L			
	0.00	4184	-
66	0.04	3931	1.0000
67	0.17	3718	0.9458
68	0.3	3650	0.9285
69	1	3448	0.8771
70	2	2726	0.6935
71	4	1197	0.3045
72	7	440	0.1119
73	14	43.0	0.0109
74	28	0.47	0.0001
Enclosure 12, nominal 4480 ug/L			
	0.00	4253	-
75	0.04	4166	1.0000
76	0.17	3977	0.9546
77	0.3	3811	0.9148
78	1	3528	0.8469
79	2	2780	0.6673
80	4	1218	0.2924
81	7	369	0.0886
82	14	22.5	0.0054
83	28	0.23	0.0001

As scaled concentrations were used in the optimisation procedure, the Freundlich sorption coefficient, K_{om}, was corrected according the guidance given in Chapter 9.4. Although the concentration levels vary considerably (from approx. 11 to 4000 µg L^{-1}, i.e. a factor of 400), we decided to scale all

experiments into one K_{om} value for simplicity of calculations. The unscaled concentrations measured at t =0.04 d in Table A5.7 were used to calculate $c_{t=0, geo}$, resulting in a $c_{t=0, geo}$ of 0.169 mg L^{-1}. The corrected K_{om} value used in the optimisation was 74.1 L kg^{-1}.

The $DegT_{50,photo,ref}$ and the loading in to the system at 5 May 1999, 09:00 h were optimised. In total 49 optimisations were performed, each with its own initial values of $DegT_{50,photo,ref}$ and the loading at t=0 (mg m^{-2})[30] (varying between 0.1 and 50 d for $DegT_{50,photo,ref}$ and 50 to 3000 mg m^{-2} for the loading at t=0[31]). For all optimisations the same lower and upper parameter bounds were used: 0.1 – 100 d for the $DegT_{50,photo,ref}$ and 1.0 – 10 000 mg m^{-2} for the loading.

From the 49 optimisations, 9 fits resulted in to an unsatisfactory estimation of $DegT_{50,photo,ref}$ and the loading at t=0. All other optimisations resulted in consistent estimates of $DegT_{50,photo,ref}$ of 1.86 days with 95% confidence intervals of 1.7 – 2.0 days and consistent estimates of the loading of 525 mg m^{-2} with 95% confidence intervals of 507 - 542 mg m^{-2}.

Table A6.8 gives estimates of the optimized $DegT_{50,photo,ref}$ and loading for the optimisation with initial values of resp. 2 days and 500 mg m^{-2}.

Table A6.8 specifies the value of the objective function phi (i.e. the sum of squared differences between model-generated and measured aqueous concentrations), the error percentage of the $\chi2$-test and the number of times TOXSWA has been run by PEST. As explained earlier a minimum error percentage value of 15% is acceptable for field studies.

The error percentage of 12.3% is an acceptable value for field experiments according to FOCUS (2006), so the optimisations did pass the $\chi2$-test.

Table A6.8 *Optimisation results for one of the 40 satisfactory optimisations of the inverse modelling exercise using the data of all enclosures of the study of Brock et al. (2004) with metamitron.*

Initial $DegT_{50,photo,ref}$ (d)	Initial loading (mg m^{-2})	Fitted $DegT_{50,photo,ref}$ (d)	Fitted loading (mg m^{-2})	Phi (-)	Err%	TOXSWA iterations
2	500	1.86 (1.7– 2.0)	525 (507 - 542)	0.45	12.3%	19

The simulated concentration as function of time presented in Figure A6.5 shows a wavy pattern. This is caused by more rapid degradation due to photolysis during daytime and stagnating degradation once the sun sets and UV radiation becomes zero.

The agreement between scaled optimised and measured water concentrations presented in Figure A6.5 is quite satisfactory.

Also the residuals are reasonably randomly scattered around zero, demonstrating that there is no pattern of under- or over-prediction by the TOXSWA model (Figure A6.6). Looking at the different

---

[30] All possible combinations of the values given in the matrix below result in 49 sets of $DegT_{50,photo,ref}$ and the loading.

$DegT_{50,photo,ref}$ (d)	0.1	0.5	1	2	5	10	50
Loading (mg m^{-2})	50	100	300	500	1000	1500	3000

[31] Although the scaled concentrations used as observations in the inverse modelling are dimensionless, they will be compared with concentrations simulated by TOXSWA which are in g m^{-3}. The input of the pesticide loading in TOXSWA is in mg m^{-2}. To determine plausible ranges for the loading in mg m^{-2} as input for the inverse modelling a calculation needs to be done to determine the loading needed to reach a certain desired peak concentration (e.g. the measured, scaled water concentration at t=0). Suppose that the desired peak concentration in water ($c_{peak,w}$) is 1 g m^{-3} (1000 mg m^{-3}). The loading needed to reach this peak concentration is:

$c_{peak,w} \cdot V/(w \cdot L)$

where is V = the volume of water in the cosm (m^3), w = the width of the water surface (m) and L is the length of the system (m). For the study of Brock et al. (2004) where the system has a water depth of 0.5 m, a side slope of 0, a width of 1.0 m and a length of 1.0 m, the water volume, V, is 0.5 m^3. Supposing $c_{peak,w}$ is 1000 mg m^{-3} a loading of $1000 \cdot 0.5/1.0 \cdot 1.0 = 500$ mg/m^2 is needed to reach this peak concentration in the water in the system.

enclosures individually however, for some enclosures the concentration is clearly underestimated (e.g. Enclosure 7) or overestimated (e.g. Enclosure 1).
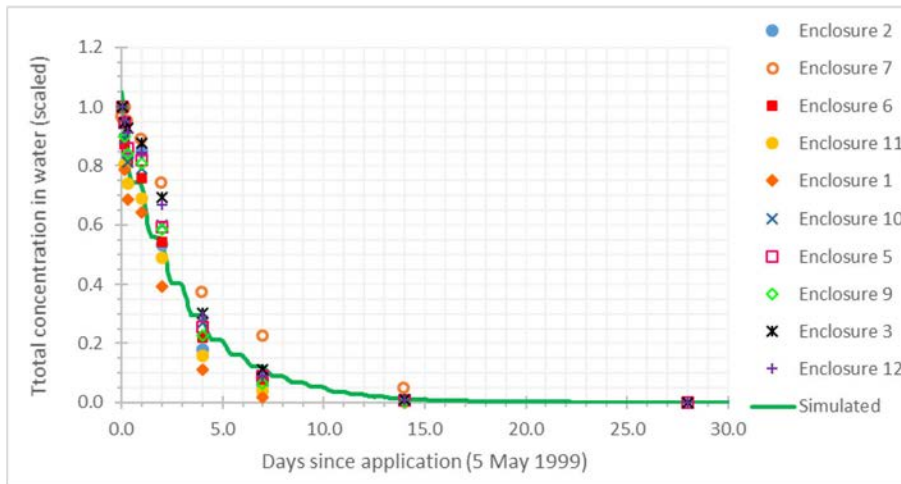

Figure A.6.5 *Simulated and measured total concentration (dissolved+ sorbed to suspended solids, µg.L^{-1}) metamitron in water as a function of time (d) in the enclosures of Brock et al. (2004). Simulated concentration profile obtained by PEST TOXSWA optimisation for an initial DegT$_{50,photo,ref}$ = 2 d and an initial loading of 500 mg m^{-2}.*
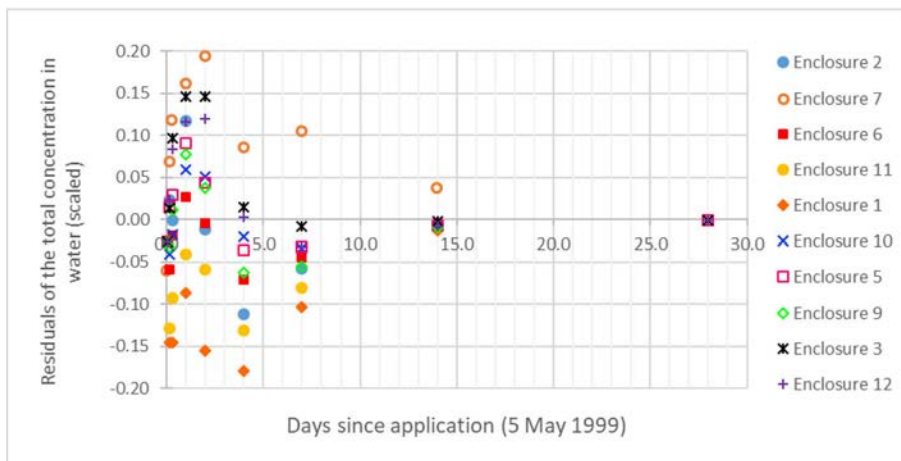

Figure A.6.6 *Residuals of total concentration (dissolved+ sorbed to suspended solids, µg.L^{-1}) metamitron in water as a function of time (d) in the enclosures of Brock et al. (2004). Simulated concentration profile obtained by PEST_TOXSWA optimisation for an initial DegT$_{50,photo,ref}$ = 2 d and an initial loading of 500 mg m^{-2}.*

Annex 7 Application of the flow chart on the usefulness of assessing a photodegradation half-life in water of outdoor cosms for the three example compounds

Application of the flow chart- initial estimate of *DegT$_{50,water}$* in the cosm
The flow chart below has been developed to help risk assessors decide whether it is useful to determine a higher-tier, more realistic degradation rate caused by photolysis by using the inverse modelling methodology for outdoor cosm experiments of this report. So, only when photolysis is the dominant process (flow chart ending in one of the two green boxes at the end of the flow chart of Chapter 15) the optimization of the *DegT$_{50,photo\ ref}$* as a function of UV-VitD radiation is useful.

Before entering the flow chart it is necessary to estimate the *DegT$_{50,water\ cosm}$* of the considered compound in the cosm, because this value (called A) is needed in the flow chart. This value can be estimated by plotting the natural logarithm of the aqueous concentrations as a function of the time after the first application and drawing the best fitting straight line through the plotted points; the degradation rate *k* then equals the slope of the line and the *DegT$_{50,water}$* is equal to ln2/*k*.

Table 1 gives an overview of the initially estimated *DegT$_{50,water\ cosm}$* for the considered compound and cosm, the value A in the flow chart. Note that for metamitron, the fits of the declines of the aqueous concentration showed that the first 70-90% of the dose degraded much faster than the last 10-30%. The flow chart uses the estimated *DegT$_{50,water\ cosm}$* to decide whether the decline could be the result of photolysis. For this purpose it seems more relevant to focus on the decline of the first 70-90%. Therefore we based the estimated *DegT$_{50,water\ cosm}$* for metamitron on the decline of the first 70-90%.

In addition to the requirement that photolysis should be the dominant degradation process in the water layer, at least five measured concentrations in the cosm water as a function of time, as well as the water depth should be available to be able to perform the inverse modelling exercise.

As explained in Chapter 15, the value of $F_{M,deg-water}$ can only be determined with the aid of TOXSWA calculations, i.e. after the optimisation, while the flow chart is designed to determine whether the optimisation by PEST-TOXSWA is useful to perform, i.e. before the optimisation calculations. Therefore we proposed to first estimate whether degradation is the main dissipation process in the water layer, and not volatilisation or sorption to sediment. To do so, consider the saturated vapour pressure and the K_{oc}/K_{om} value of the compound. If the saturated vapour pressure at 20-25 °C is smaller than approximately 1 mPa ánd the K_{oc} value smaller than approximately 500 L/kg, the $F_{M,deg-water}$ value is very probably smaller than 50% and thus the answer in Box 1 would be 'Yes'. After the optimisation the answer can be confirmed by TOXSWA output.

Table A7.1 *Initial estimates of DegT$_{50,water\ cosm}$ to be used for going through the flow chart of Chapter 15.*

Cosm	First estimate of *DegT$_{50,water\ cosm}$* (days)
metribuzin	
Fairchild & Sappington (2002)	3.2
Arts et al. (2006)	1.69
Brock et al. (2004)	6.9
imidacloprid	
Colombo et al. (2013)	2.5
Bayer (2001)	
Pond	9.1
Tank	7.3
Bayer (2003)	
Pond 2	7.7
Pond 7	6.9
Pond 8	8.2
Pond 13	7.0
metamitron	
Wendt-Rasch et al. (2004)	
Elodea dominated	0.9
Lemna dominated	1.9
Brock et al. (2004)	1.82

Application of flow chart to metribuzin

Table A7.2 gives an overview of data found in several sources on the dissipation of metribuzin in water as a result of hydrolysis, photolysis and microbial degradation in laboratory water-sediment studies. These data are used to go through the flow chart presented in Chapter 15. Below we explain step by step how we went through the flow chart for metribuzin.

Table A7.2 *Dissipation half-lives of **metribuzin** as obtained from different sources.*

Process/system	DT$_{50}$ (days)	Source
Hydrolysis	Stable over 34 days at pH 4, 7 and 9 (25°C) DT$_{50}$ 635 d at pH 9 (25°C)	EU agreed endpoints from EFSA conclusion[32]
Hydrolysis	Stable over 34 days at pH 4 – 9 (25°C)	Footprint database
Photolysis	0.18 d, sterile water, sunlight exposure in quartz cell 0.026 d, River Rhine water, Xenon light exposure in quartz cell (temperature not given, not normalized/standardized to a latitude)	EU agreed endpoints from EFSA conclusion[1]
Photolysis	0.2 d (pH 7)	Footprint database
Water/sediment	DT$_{50}$ water: 41 and 41 d (n=2) DT$_{50}$ whole system: 47 and 50 d (n=2)	EU agreed endpoints from EFSA conclusion[1]
Water/sediment	DT$_{50}$ water: 41 d DT$_{50}$ whole system: 50 d	Footprint database

Box 1

For metribuzin, the saturated vapour pressure at 25 °C is 0.121 mPa, so smaller than 1 mPa and the *K$_{foc}$* value is 37.9 L/kg (PPDB, no *K$_{oc}$* value available), so clearly smaller than 500 L/kg. So, we expect that volatilisation and sorption to sediment play a minor role in the mass dissipation in the water layer and that degradation is the main dissipation process. So, the answer to the question in Box 1 is 'yes'.

---

[32] https://efsa.onlinelibrary.wiley.com/doi/epdf/10.2903/j.efsa.2006.88r

Box 2
Hydrolysis is negligible, compound is stable or DT_{50}= 635 d at pH 9 (25°C) (Table A7.2), so the answer is 'no'.

Box 4 (Box 3 is skipped)
The DT_{50} water-sediment equals 41 d (water) and 47 or 50 d (whole system), thus it is not approximately equal to the initially estimated $DegT_{50,water}$ values of the cosms (all estimated to be below 7 d), so the answer is 'no'.

Box 5
UV-VitD radiation does enter the cosm, so the answer is 'yes'.

Box 6
Direct photolysis in quartz cell does occur, it is 0.18 d sterile water for sunlight and 0.026 d in Rhine water for Xenon light (Table A7.2), so the answer is 'yes'.

Box 7
ABIWAS 3.0.1 (based upon the OECD guideline 316 of 2008) could not be used for metribuzin as all photolysis studies for this compound are from an earlier date, so no extinction coefficients and quantum yields as a function of wavelength are available, which is the needed input for ABIWAS 3.0.1. However, on basis of value stated on the list of endpoints of 0.18 day in sterile water (sunlight exposure in quartz cell), it is likely that the answer to the question in Box 7 is 'yes' and thus direct photolysis is a dominant degradation process in water.

For the sake of this example we also continue the flow chart in case the answer might have been 'no'.

Box 8
The photolysis half-lives are significantly shorter than the biodegradation rates of the water-sediment studies (Table A7.2), so the answer to the question is 'no'.

Box 9
The initial estimates of the $DegT_{50,water,cosm}$ decreased for shallower water depths for the study of Arts et al. (2006), but not Brock et al. (2004). It was 3.2 d for the 75 cm water depth of Fairchild & Sappington (2002), 6.9 d for the 50 cm water of Brock et al. (2004) and 1.69 d for the 47.3 cm of Arts et al. (2006). Coverage for water plants was zero to very low for all cosms, so that cannot explain the observed trends. So, it is not convincingly demonstrated that indirect photolysis may be a significant degradation process, so no clear 'yes' or 'no' answer can be given.

Outcome of the flow chart
In any case the left hand green box applies: Photolysis (direct) is the dominant degradation process in water for metribuzin. This outcome corresponds well to the findings of Remucal et al. (2014, Chapter 5.2) who found that metribuzin showed direct photolysis, but could not find information on indirect photolysis. So, the conclusion is that it is useful to perform the inverse modelling by PEST-TOXSWA as a function of the UV-VitD radiation.

Application of flow chart to imidacloprid
Table A7.3 gives an overview of data found in several sources on the dissipation of imidacloprid in water as a result of hydrolysis, photolysis and microbial degradation in laboratory water-sediment studies. These data are used to go through the flow chart presented in Chapter 15. Below we explain step by step how we went through the flow chart for imidacloprid.

Table A7.3   *Dissipation half-lives of imidacloprid as obtained from different sources.*

Process	DT$_{50}$ (days)	Source
Hydrolysis	DT$_{50}$ > 1 year at pH 5 and 7; DT$_{50}$ 1 year at pH 9 (25ºC)	EU agreed endpoints from EFSA conclusion [33]
Hydrolysis	20.0 d (pH 10.8), 2.85 d (pH 11.8)	Zheng and Liu, 1999
Hydrolysis	Stable at acidic and neutral conditions, increased hydrolysis in alkaline solutions	Liu et al., 2006
Photolysis	Study 1 Suntest, sterile water, normalized results: - 50° latitude (GCSOLAR): 0.24 d spring, 0.17 d summer - 10° longitude, 50° latitude (Frank & Klöpffer): April-summer 0.4-0.28 d, Nov-Dec 3.1-6.73 d *Other photolysis studies are available in the LoEP but were not aimed at the derivation of a DT50 but merely at identifying metabolites*	EU agreed endpoints from EFSA conclusion
Photolysis	Slightly over 3 h, pH 2.8	Banić et al., 2014
Photolysis	5 – 18 min. (25ºC)	Liu et al., 2006
Photolysis	43 min. a.i., 126 min. formulated product Confidor (temperature not specified)	Wamhoff and Schneider (1999)
Water/sediment	DT$_{50}$ water: > 30 d, 14.2 d, 109 d DT$_{50}$ whole system: 129 d, 30 d, 150 d	EU agreed endpoints from EFSA conclusion

Box 1

For imidacloprid, the saturated vapour pressure at 25 °C is 4.0 10^{-7} mPa, so very clearly smaller than 1 mPa and the K_{foc} value is 225 L/kg (PPDB, no K_{oc} value available), so smaller than 500 L/kg. So, we expect that volatilisation and sorption to sediment play a minor role in the mass dissipation in the water layer and that degradation is the main dissipation process. So, the answer to the question in Box 1 is 'yes'.

Box 2

Hydrolysis is not likely to have occurred in the studies cosm studies. Only at pH values above 9, hydrolysis occurs (rates of 20.0 d at pH 10.8 and 2.85 d at pH 11.8 were found, Table A7.3). The pH in the study of Colombo et al. (2013) was 8 to 9, for Bayer (2001) the pH was 7.0 to 8.5 and for Bayer it was 7.4 (0-13 d), 9.5 (day 35) and 7.4 (day 91). So, only for the study of Bayer the pH came above 9, but not in the period up to 3*$DegT_{50,water}$ days after application. So, the answer is 'no'.

Box 4 (Box 3 is skipped)

The DT_{50} water-sediment is greater than 30 d, equal to 14.2 or 109 d (water) and 129, 30 or 150 d (whole system), thus it is greater than the initially estimated $DegT_{50,water}$ values of the cosms (all estimated to be below 10 d), so the answer is 'no'.

Box 5

UV-VitD radiation does enter the cosm, so the answer is 'yes'.

Box 6

Direct photolysis does occur, in four studies of Table A7.3 the $DegT_{50}$ value is below 1 d. So, the answer to the question in the box is 'yes'.

Box 7

ABIWAS 3.0.1 (based upon the OECD guideline 316 of 2008) could not be used for imidacloprid as all photolysis studies for this compound are from an earlier date, so no extinction coefficients and quantum yields as a function of wavelength are available, which is the needed input for ABIWAS 3.0.1. However, on basis of value stated on the list of endpoints with all values for spring and summer below

---

[33] https://efsa.onlinelibrary.wiley.com/doi/epdf/10.2903/j.efsa.2008.148r

0.5 d in sterile water (sunlight exposure), it is likely that the answer to the question in Box 7 is 'yes' and thus direct photolysis is a dominant degradation process in water.

For the sake of this exemple we also continue the flow chart in case the answer might have been 'no'.

Box 8
The photolysis half-lives are significantly shorter than the biodegradation rates of the water-sediment studies (Table A7.3), so the answer to the question is 'no'.

Box 9
The initial estimates of the $DegT_{50,water,cosm}$ of the three cosms decreased indeed for shallower water depths. It was 9.1 d in the 100 cm water depth for the pond and 7.3 d for the 30 cm water in the tank of Bayer (2001), 6.9 to 8.2 d in 100 cm water depth of the four ponds of Bayer (2003) and 2.5 d in the 11 cm of Colombo et al. (2013). So, indirect or direct photolysis is a significant degradation process.

So, the answer to the question is 'yes' and thus indirect or direct photolysis is a dominant degradation process in water.

Outcome of the flow chart
Both green boxes are possible: Photolysis (direct OR either indirect or combination of direct and indirect) is the dominant degradation process in water for imidacloprid. This outcome does not contradict the findings of Remucal et al. (2014, Chapter 5.2) who found that imidacloprid showed direct photolysis, but could not find information on indirect photolysis. So, the conclusion is that it is useful to perform the inverse modelling by PEST-TOXSWA as a function of the UV-VitD radiation.

Application of flow chart to metamitron
Table A7.4 gives an overview of data found in several sources on the dissipation of metamitron in water as a result of hydrolysis, photolysis and microbial degradation in laboratory water-sediment studies. These data are used to go through the flow chart presented in Chapter 15. Below we explain step by step how we went through the flow chart for metamitron.

Table A7.4 *Dissipation half-lives of metamitron as obtained from different sources.*

Process/system	DT50 (days)	Source
Hydrolysis	pH=7: 479.6 d, pH=5: 353.2 d, pH=9: 8.5 d; second study: pH=7: 84 d, pH=4: 65 d; pH=9: 5.3 d (all at 20°C)	EU agreed endpoints from EFSA conclusion[34]
Hydrolysis	480 (pH sensitive, pH=5: 353.2 d, pH=9: 8.5 d, all at 20°C)	Footprint database
Photolysis	1.45 h in river water (Xenon lamp); 0.47 h in pure water, 34°C, natural summer light, 50 ° latitude	EU agreed endpoints from EFSA conclusion[3]
Photolysis	0.02 (1.45 h river water, pH 7 and test conditions); 0.5 h, pure water, natural summer light, 50 deg North)	Footprint database
Water/sediment	DT50 water: 9.62 and 11.55 d in 2 different systems, geomean is 10.54 d DT50 whole system: 10.8 and 11.41 d, the latter being used in exposure assessment (geomean is 11.1 d)	EU agreed endpoints from EFSA conclusion[3]
Water/sediment	DT50 water: 10.5 DT50 whole system: 11.1	Footprint database

---

[34] https://efsa.onlinelibrary.wiley.com/doi/epdf/10.2903/j.efsa.2008.185r

Box 1

For metamitron, the saturated vapour pressure at 25 °C is 0.00074 mPa, so clearly smaller than 1 mPa and the K_{foc} value is 77.7 L/kg (PPDB), so smaller than 500 L/kg. So, we expect that volatilisation and sorption to sediment play a minor role in the mass dissipation in the water layer and that degradation is the main dissipation process. So, the answer to the question in Box 1 is 'yes'.

Box 2

The hydrolysis half-lives mentioned are for the first study 479.6 d at a pH of 7, 353.2 d at a pH of 5 and 8.5 d at a pH of 9, while in the second study the half-lives mentioned are 84 d at a pH of 7, 65 d at a pH of 4 and 5.3 d at a pH of 9 (all at 20ºC). The second entry in Table A7.4 repeats the values of the first study. In the study of Wendt-Rasch et al. (2004) the pH was variable over time and different between systems in the range of 6.2-9.3. However, during the first 5 days of their experiment, when most pesticide mass is degraded (initial estimates of $DegT_{50,water}$ were 0.9 and 1.9 d) the pH was around 7 to 7.5, so hydrolysis is negligible then. In the experiment of Brock et al. (2004) the pH in most systems is 8.5 to 9.5, except for the highest treatment where it was 7 to 8.5 during the first 14 days and 8.5 to 9.5 later on. So, in 8 of their 10 ponds inversely modelled hydrolysis might have played a role. So, the answer to the question whether hydrolysis could occur at the pH values observed in the coms is 'yes' for the experiment of Brock et al. (2004) and 'no' for the experiment of Wendt-Rasch et al. (2004).

Box 3

So, for the experiment of Brock et al. (2004) hydrolysis may have played a role. However, at the pond temperature of approximately 15 °C the $DegT_{50}$ by hydrolysis will be approximately 1.5 as large as the ones mentioned above in Table A7.4 for 20ºC, i.e. in the range of 8 to 13 days, while the overall fitted $DegT_{50,photo,ref}$ for the 10 ponds of Brock et al. (2004) was 1.82 days. So, the $DegT_{50,hydrol}$ is not approximately equal to the initially estimated $DegT_{50,water}$ values of the cosms, thus the answer to the question in box 4 is 'no' for the experiment of Brock et al. (2004).

So, both experiments finally end up in Box 4.

Box 4

The DT_{50} water-sediment equals 9.62 and 11.55 d (water, 2 systems) and 10.8 and 11.41 d (whole system), thus these are not approximately equal to the estimated $DegT_{50,water}$ of the cosms (all below 2 d), so the answer is 'no'.

Box 5

UV-VitD radiation does enter the cosm, so the answer is 'yes'.

Box 6

Direct photolysis in quartz cell does occur, it is 0.5 h in pure water under natural summer light at 34°C and 50° latitude and 0.02 d in river water at pH 7 for a Xenon lamp (Table A7.4), so the answer is 'yes'.

Box 7

ABIWAS 3.0.1 (based upon the OECD guideline 316 of 2008) could not be used for metamitron as all photolysis studies for this compound are from an earlier date, so no extinction coefficients and quantum yields as a function of wavelength are available, which is the needed input for ABIWAS 3.0.1. However, on basis of value stated on the list of endpoints with all values below 1 hour in pure water (natural summer sunlight exposure), it is likely that the answer to the question in Box 7 is 'yes' and thus direct photolysis is a dominant degradation process in water.

For the sake of this example we also continue the flow chart in case the answer might have been 'no'.

Box 8

The photolysis half-lives are slightly shorter than the biodegradation rates of the water-sediment studies (Table A7.4), so the answer to the question is 'no'.

The $DegT_{50,water}$ (initial estimates) of the cosms do decrease for shallower water depths. It was 1.82 d for the 50 cm water depth of Brock et al. (2004) and 1.9 (*Lemna* dominated cosms) and 0.9 d (*Elodea* dominated cosms) for the 30 cm of Wendt-Rasch et al. (2004). The *Lemna* dominated systems had approximately 40% surface area coverage, initially, which may have slowed down photolysis, so, this explains that these systems have approximately the same $DegT_{50,cosm}$ as the one of Brock et al. (2004).

So, the answer to the question is 'yes' and thus photolysis is a dominant degradation process in water.

Outcome of the flow chart
Both green boxes are possible: Photolysis (direct OR either indirect or combination of direct and indirect) is the dominant degradation process in water for metamitron. Remucal et al. (2014, Chapter 5.2) found that metamitron showed both direct and indirect photolysis, which is confirmed by the flow chart. The final conclusion is that it is useful to perform the inverse modelling by PEST-TOXSWA as a function of the UV-VitD radiation.

Overview of $F_{M,deg-water}$ values calculated by TOXSWA
Table A7.5 gives an overview of the $F_{M,deg-water}$ values calculated by TOXSWA for the optimised DegT50$_{photo,ref}$ value to check the Box 1 answer for the three compounds given above, on the basis of the compound properties saturated vapour pressure and K_{oc} value. The table demonstrates that for all cosms and compounds the $F_{M,deg-water}$ value is much larger than 50%, so the answer 'yes' given for Box 1 for metribuzin, imidacloprid and metamitron in the text above is confirmed.

Table A7.5 *Percentages of pesticide mass degraded in water layer to pesticide mass dissipated from water layer over specified time interval for the indicated studies, the interval ranges from the time of the first loading up to 3*DegT$_{50photo,ref}$ after the last loading, i.e. when the majority of the pesticide mass has degraded in the cosms. (N.B. Unless indicated only one loading took place.)*

Cosm	Fitted $DegT_{50photo,ref}$ (days)	Time interval (first loading - 3*$DegT_{50}$ after last loading)	Duration [for checking]	Mass degraded / mass dissipated (%)
metribuzin				
Fairchild & Sappington (2002)	4.8	22 May 2001 9:00 h – 5 June 2001 19:00 h	14.4 d= 346 h	98.5
Arts et al. (2006)	1.29	6 May 2002 9:00 h – 10 May 2002 6:00 h	3.87 d = 93 h	99.3
Brock et al. (2004)	3.4	5 May 1999 9:00 h – 15 May 1999 14:00 h	10.2 d = 245 h	98.0
imidacloprid				
Colombo et al. (2013)	1.6	2 June 2009 11:00 h** – 21 June 2009 6:00 h	18.8 d = 451 h	84.4
Bayer (2001)		8 May 2000 9:00 h -		
Pond 8.1		- 1 June 2000 16:00 h	24.3 d = 583 h	94.4
Tank 6.5		- 27 May 2000 21:00 h	19.5 d = 468 h	85.1
Bayer (2003)		2 May 2001 9:00 h*** -		
Pond 2 7.3		- 14 June 2001 10:00 h	43.06 d = 1033 h	95.3
Pond 7 7.2*		- 14 June 2001 3:00 h	42.76 d = 1026 h	95.7
Pond 8 6.7		- 12 June 2001 15:00 h	41.26 d = 990 h	95.5
Pond 13 7.0*		- 13 June 2001 13:00 h	42.16 d = 1012 h	95.8
metamitron				
Wendt-Rasch et al. (2004)		4 May 1999 9:00 h -		
Elodea dominated 0.60		- 6 May 1999 4:00 h	1.8 d = 43 h	97.2
Lemna dominated 1.70		- 9 May 1999 11:00 h	5.1 d = 122 h	94.6
Brock et al. (2004)	1.86	5 May 1999 9:00 h – 10 May 1999 23:00 h	5.58 d = 134 h	97.2

* χ^2 error above 15%

** three loadings, timing of third loading is 16 June 2009 11:00 h

*** two loadings, timing of second loading is 23 May 2010 13:00 h

The mission of Wageningen University & Research is "To explore the potential of nature to improve the quality of life". Under the banner Wageningen University & Research, Wageningen University and the specialised research institutes of the Wageningen Research Foundation have joined forces in contributing to finding solutions to important questions in the domain of healthy food and living environment. With its roughly 30 branches, 6,500 employees (5,500 fte) and 12,500 students, Wageningen University & Research is one of the leading organisations in its domain. The unique Wageningen approach lies in its integrated approach to issues and the collaboration between different disciplines.

To explore
the potential
of nature to
improve the
quality of life

The mission of Wageningen University & Research is "To explore the potential of nature to improve the quality of life". Under the banner Wageningen University & Research, Wageningen University and the specialised research institutes of the Wageningen Research Foundation have joined forces in contributing to inding solutions to important questions in the domain of healthy food and living environment. With its roughly 30 branches, 6,500 employees (5,500 fte) and 12,500 students, Wageningen University & Research is one of the leading organisations in its domain. The unique Wageningen approach lies in its integrated approach to issues and the collaboration between different disciplines.